Intracellular Sodium and the Matching of ATP Supply to Demand in the Heart

O'Brien, Brett Anthony

Awarding institution:
King's College London

Intracellular Sodium and the Matching of ATP Supply to Demand in the Heart

Brett Anthony O'Brien

Thesis undertaken for the degree of Doctor of Philosophy in Cardiac Biochemistry.

Imaging Sciences and Biomedical Engineering Division
&
Cardiovascular Division.

British Heart Foundation Centre of Research Excellence
The Rayne Institute
4th Floor, Lambeth Wing
St Thomas' Hospital
London, SE1 7EH

Submitted - December 2017.

ABSTRACT

There is convincing evidence that myocardial intracellular Na^+ overload ($[Na]_i$) and metabolic derangement are two important and interconnected pathophysiological features of heart failure. Whether $[Na]_i$ elevation plays a causative role in ATP supply-demand mismatching in the heart is unknown. A number of mitochondrial enzymes are stimulated by mitochondrial calcium (Ca_m) during contraction thereby sustaining production of reducing equivalents to maintain ATP supply. It is postulated that this stimulation is perturbed when $[Na]_i$ is high due to increased Ca_m efflux and that this may be linked with derangement in ATP supply-demand matching.

This thesis tests the hypothesis that $[Na]_i$ elevation alters intermediary metabolism and energetics in the isolated perfused heart from healthy rats. $[Na]_i$ elevation was induced by perfusion with the Na^+/K^+ ATPase (NKA) inhibitor, ouabain, and measured in real-time using triple quantum filtered (TQF) ^{23}Na nuclear magnetic resonance (NMR) spectroscopy. Blebbistatin was used to transiently uncouple inotropy to better elucidate $[Na]_i$-dependent from inotropy-dependent effects on metabolism and energetics. Real-time ^{31}P NMR measurements showed a transient increase or decrease in both PCr and P_i that mirrored a transient increase or decrease in inotropy. However PCr levels returned to baseline at the end of the protocol while there was a strong negative correlation between $[Na]_i$ and [ATP] independent of inotropy. End-point metabolomics were assessed using high resolution ^1H NMR and liquid chromatography tandem mass spectrometry (LC-MS/MS). Malate (and more tentatively fumarate) were elevated, suggesting a possible link between $[Na]_m$ and TCA cycle activity in the perfused heart.

Increased ^{13}C incorporation from [U]-^{13}C-glucose inferred higher TCA cycle activity in hearts with $[Na]_i$ overload in the absence of elevated inotropy.

This thesis supports that $[Na]_i$ elevation can cause ATP supply-demand mismatching in the heart and that increased TCA cycle activity is a possible (mal)adaptive response.

ABSTRACTS & PUBLICATIONS

Abstracts and publications arising from this thesis work are as follows:

O'Brien B, Aksentijević D, Eykyn T and Shattock M. (2016a). Intracellular [Na] elevation perturbs cardiac metabolism in the isolated perfused rat heart in the absence of changes in contractility. Gordon Research Conference (Cardiac Regulatory Mechanisms): 'Atoms to Omics- New Approaches to Understand and Treat Cardiac Disease.' (Poster Presentation and Oral Presentation).

O'Brien B, Aksentijević D, Eykyn T and Shattock M. (2016b). Intracellular [Na] elevation perturbs cardiac metabolism in the isolated perfused rat heart in the absence of changes in contractility. Gordon Research Seminar (Cardiac Regulatory Mechanisms): 'Innovative Answers to Classic Cardiac Questions' (Poster Presentation).

O'Brien B, Aksentijević D, Eykyn T and Shattock M. (2016c). Intracellular [Na] elevation perturbs cardiac metabolism in the isolated perfused rat heart in the absence of changes in contractility. Imaging Sciences & Biomedical Engineering Postgraduate Symposium. (Poster Presentation).

O'Brien B, Aksentijević D, Eykyn T and Shattock M. (2016d). $[Na]_i$ elevation perturbs cardiac metabolism in the isolated perfused rat heart in the absence of changes in contractility. British Heart Foundation Postgraduate Symposium. (Oral presentation).

O'Brien B, Aksentijević D, Eykyn T and Shattock M. (2015a). Sodium and Energy Metabolism in the Heart. Imaging Sciences & Biomedical Engineering Postgraduate Symposium. (Award for Best Oral Presentation).

O'Brien B, Aksentijević D, Eykyn T and Shattock M. (2015b). Ouabain induces metabolic changes in the absence of contractile work in the blebbistatin-perfused rat heart. Journal of Molecular and Cellular Cardiology. 86: S1-S78, abstract P-15-18. (poster Presentation).

O'Brien B, Aksentijević D, Eykyn T and Shattock M. (2015c). Ouabain Induces Metabolic Changes in the Non-contracting, Blebbistatin-perfused Rat Heart. British Heart Foundation Postgraduate Symposium. (Poster presentation).

O'Brien B, Aksentijević D, Eykyn T and Shattock M. (2015d). Ouabain induces metabolic changes in the absence of contractile work in the blebbistatin-perfused rat heart. Joint BHF Centres of Research Excellence Imaging Symposium. (Poster presentation).

O'Brien B, Aksentijević D, Eykyn T and Shattock M. (2014). Matching Mitochondrial Energy Production to Supply in the Heart: Role of Intracellular Sodium. British Heart Foundation Postgraduate Symposium (Poster presentation).

ACKNOWLEDGEMENTS

I would like to thank the following people:

- Dr Thomas Eykyn and Professor Michael Shattock for giving me the opportunity to work on this PhD project as well as their untiring 24/7 support and patience over the years. They have transformed the way in which I conduct scientific research which will undoubtedly be invaluable for my future career (in fact, it is already proving invaluable for my new position at GSK!). It has been a true pleasure and privilege to work with them over the years and I wish them both the very best for the future.
- The British Heart Foundation for providing funding for the PhD project.
- Members of the Shattock group, particularly Dr Dunja Aksentijevic for the initial training in heart perfusions and for her kind feedback on my abstracts, posters, presentations and thesis. I am also very grateful to Dr James Winter for his support on electrophysiological measurements and to Dr Sergiy Tokar for carrying out the patch clamp experiments with blebbistatin and ouabain. Receiving feedback during the weekly Shattock group meetings has been crucial in driving the project forward and I am sincerely grateful for the suggestions from all members of the group over the years.
- Dr Sophie Strickfuss and Simon Hamilton (MSD, Hoddesdon) for very kindly permitting access to their LC-MS/MS and for their advice in developing the TCA cycle quantification method.
- Professor John Halket and Dr Anna Caldwell for their support with the GC-MS methodology.

- Dr Richard Southworth and Dr James Clark for kindly providing guidance in the transfer viva in the first year of the programme.
- Cinzia Imberti for acquiring the mass spectrometry data for the *in vitro* blebbistatin/ouabain sequestration experiment and for her kind chemistry advice over the years. I couldn't have asked for a better desky!
- Dr Adam Nabeebaccus for providing initial training in dual phase metabolite extraction.
- David Thakor and Dr Shiney Reji for their kind laboratory support.
- Soba Akinwunmi for his kind IT support (and stimulating discussions on the Premier League!).
- The fantastic friends that I have been lucky enough to meet at the Rayne. They have kept my spirits high and I will miss them all very much.
- Lewis Casey for the many interesting conversations regarding his experience as a paramedic. This has helped to keep the ultimate aim of this research project at the forefront of my mind.
- Tim Pope for kindly providing IT resources which made the thesis write-up a much smoother process than would have been the case without it!
- My family (past and present) for their unwavering love and support over the years and for giving me the confidence to pursue my ambitions.
- Rebecca Pope (my partner, best friend, cook, cleaner, taxi driver and counsellor, to name but a few). Words cannot convey just how grateful I am for everything she has done for me over the years including listening to me waffle on about sodium and metabolism on a daily (sometimes hourly) basis. Becky, thank you so much. I view this thesis as our joint effort!

If

If you can keep your head when all about you
Are losing theirs and blaming it on you,
If you can trust yourself when all men doubt you,
But make allowance for their doubting too;
If you can wait and not be tired by waiting,
Or being lied about, don't deal in lies,
Or being hated, don't give way to hating,
And yet don't look too good, nor talk too wise:

If you can dream—and not make dreams your master;
If you can think—and not make thoughts your aim;
If you can meet with Triumph and Disaster
And treat those two impostors just the same;
If you can bear to hear the truth you've spoken
Twisted by knaves to make a trap for fools,
Or watch the things you gave your life to, broken,
And stoop and build 'em up with worn-out tools:

If you can make one heap of all your winnings
And risk it on one turn of pitch-and-toss,
And lose, and start again at your beginnings
And never breathe a word about your loss;
If you can force your heart and nerve and sinew
To serve your turn long after they are gone,
And so hold on when there is nothing in you
Except the Will which says to them: 'Hold on!'

If you can talk with crowds and keep your virtue,
Or walk with Kings—nor lose the common touch,
If neither foes nor loving friends can hurt you,
If all men count with you, but none too much;
If you can fill the unforgiving minute
With sixty seconds' worth of distance run,
Yours is the Earth and everything that's in it,
And—which is more—you'll be a Man, my son!

By Rudyard Kipling.

In loving memory of Walter Nunn.

TABLE OF CONTENTS

LIST OF FIGURES

LIST OF TABLES

LIST OF ABBREVIATIONS

$[Ca]_i$	Intracellular Ca^{2+} concentration
$[Ca]_m$	Mitochondrial Ca^{2+} concentration
$[Na]_{ex}$	Extramitochondrial Na^+ concentration
$[Na]_i$	Intracellular Na^+ concentration
$[Na]_m$	Mitochondrial Na^+ concentration
[U]-^{13}C-glucose	Universally-labelled $^{13}C_6$ glucose
AAS	Atomic absorption spectroscopy
AD	Alzheimer's disease
ANT	Adenine nucleotide translocator
AP	Action potential
ATP	Adenosine triphosphate
BDM	2,3-butanedione monoxime
Bleb	Blebbistatin
BPM	Beats per minute
CaBI	Calcium binding ATPase inhibitor
CK	Creatine kinase
CK_{mito}	Mitochondrial creatine kinase
CK_{MM}	Intermyofibrillar creatine kinase
CS	Citrate synthase
DCM	Dilated cardiomyopathy
DMSO	Dimethyl sulfoxide

DQF	Double quantum filtered
EC	Excitation-contraction
ECG	Electrocardiogram
ERK	Extracellular signal-regulated kinase
ETC	Electron transport chain
FA	Fatty acid
$FADH_2$	Reduced flavin adenine dinucleotide
FFA	Free fatty acid
FID	Free induction decay
FS	Frank-Starling
GLUT	Glucose transporter
HEP	High energy phosphate
HF	Heart failure
HPLC	High performance liquid chromatography
IDH	Isocitrate dehydrogenase
IVB	Intraventricular balloon
KH	Krebs-Heinseleit buffer
LC-MS/MS	Liquid chromatography tandem mass spectrometry
LVDP	Left ventricular developed pressure
LVEDP	Left ventricular end diastolic pressure
LVH	Left ventricular hypertrophy
MCT	Monocarboxylate transporter
MCU	Mitochondrial Ca^{2+} uniporter
MDH	Malate dehydrogenase

MDV	Mass distribution vector
mmHg	Millimetres of mercury
mNHE	Mitochondrial Na^+/H exchanger
MRM	Multiple reaction monitoring
MS	Mass spectrometry
MVD	Mitral valve disease
NADH	Reduced nicotinamide adenine dinucleotide
NCLX	Mitochondrial Na^+/Ca^{2+} exchanger
NCX	Sarcolemmal Na^+/Ca^{2+} exchanger
NHE	Na^+/H^+ exchanger
NKA	Na^+/K^+ ATPase
NMR	Nuclear magnetic resonance
Oua	Ouabain
PCr	Phosphocreatine
PDH	Pyruvate dehydrogenase
PEA	Pulseless electrical activity
P_i	Inorganic phosphate
PKA	Protein kinase A
PKC	Protein kinase C
PLB	Phospholamban
PLM	Phospholemman
PSP	Peak systolic pressure
QT90%	Activation onset to 90% repolarisation recovery (time)
RF	Radiofrequency

RVH	Right ventricular hypertrophy
RyR	Ryanodine receptor type 2
S:N	Signal-to-noise ratio
SBFI	Sodium-binding benzofuran isophthalate
SCS	Succinyl coenzyme A synthetase
SDH	Succinate dehydrogenase
SEM	Standard error of the mean
SERCA	Sarcoendoplasmic reticulum Ca^{2+} ATPase
SR	Sarcoendoplasmic reticulum
TAC	Transverse aortic constriction
TCA	Tricarboxylic acid
TNI	Transient negative inotropy
TPI	Transient positive inotropy
TQF	Triple quantum filtered
TSP	Trimethylsilyl propanoic acid
TTX	Tetrodotoxin
UCP	Uncoupling protein
αKDH	α-ketoglutarate dehydrogenase
αKG	α -ketoglutarate
$\Delta\Psi_m$	Mitochondrial membrane potential

1 INTRODUCTION

1.1 Overview

Approximately 500,000 people are currently living with heart failure (HF) in the UK (Townsend et al., 2015). It is a life-threatening condition and, with an ageing population, incidence rates are likely to increase further. The identification of novel pharmacological approaches for HF remains an area of unmet need. There is convincing evidence that myocardial intracellular Na^+ ($[Na]_i$) overload and metabolic derangement are two important and interconnected pathophysiological features of this disease. Maintenance of both normal $[Na]_i$ and contractile function are energy requiring processes. Perturbations in ATP supply will subsequently lead to $[Na]_i$ elevation and contractile dysfunction, and eventually to loss of ionic homeostasis and cell death. However, the reverse relationship is less well understood. Whether $[Na]_i$ elevation also plays a causative role in ATP supply-demand mismatching in the heart has received increased interest over the past decade or so (Murphy and Eisner, 2009). The work presented here in the Langendorff perfused heart model investigates whether $[Na]_i$ elevation can lead to alterations in metabolism and ATP supply-demand matching independent of increased contractile demand and whether the tricarboxylic acid (TCA) cycle is implicated in this important process.

1.2 Na transport & excitation-contraction coupling in the healthy heart.

Maintaining intracellular Na^+ homeostasis is imperative for normal functioning of the heart, particularly with respect to the cardiac action potential and excitation-contraction coupling.

1.2.1 The cardiac action potential.

Upon stimulation of the ventricles by an action potential, voltage-gated Na^+ channels open and the sarcolemma depolarises from around -90mV to approximately +25mV. An influx of Ca^{2+} from the extracellular space into the cytoplasm occurs via sarcolemmal L-type Ca^{2+} channels which leads to the opening of intracellular Ca^{2+}-gated calcium channels (ryanodine receptors) of the sarcoplasmic reticulum (SR), increasing the intracellular calcium concentration ($[Ca]_i$) further. The forward mode of the sarcolemmal sodium-calcium exchanger (NCX) is subsequently activated and one Ca^{2+} ion is extruded in exchange for three Na^+ ions. K^+ ions are then extruded from the cytocosol via sarcolemmal K^+ channels and the membrane potential falls to approximately -80mV. This membrane potential is set by the K^+ gradient which is maintained via the simultaneous extrusion of three Na^+ ions and influx of two K^+ ions by the Na^+/K^+ ATPase (NKA) until the arrival of the next action potential.

1.2.2 Structure and regulation of NKA

Under physiological conditions, NKA is the most important efflux pathway for $[Na]_i$ in the heart. NKA has quaternary structure encompassing an α-subunit (consisting of four isoforms: α1, α2, α3 and α4), a β-subunit (consisting of three isoforms: β1, β2 and β3) and a FXYD protein (phospholemman, PLM) (Kaplan, 2002, Sweadner, 1989, Sweadner and Rael, 2000). The α subunit spans the sarcolemma and houses binding sites for Na^+, K^+ and ATP as well as cardiotonic steroids which regulate NKA function (discussed in Section 1.2.5). The β subunit is required for trafficking of the protein to the sarcolemma following its synthesis (Geering, 1991). The isoform profiles of these subunits are species dependent. For example, α1 and α2 predominate in the rat (Hensley et al., 1992) whereas only α1 and α3 are present in canine (Sweadner et al., 1994). It is estimated that the human isoform stoichiometry is α1 (62%), α2 (15%) and α3 (23%) (Zahler et al., 1992). In recent years, there has been increased interest in the PLM subunit of NKA owing to its ability to regulate NKA catalytic activity (Figure 1.1). In the unphosphorylated form, PLM decreases NKA activity and this inhibition is negated following phosphorylation of PLM by protein kinase A (PKA) at Ser68 and by PKC at Ser63, Ser68 and Ser/Thr69. For an extensive review of cardiac NKA regulation (including the role of PLM) see Fuller et al. (2013).

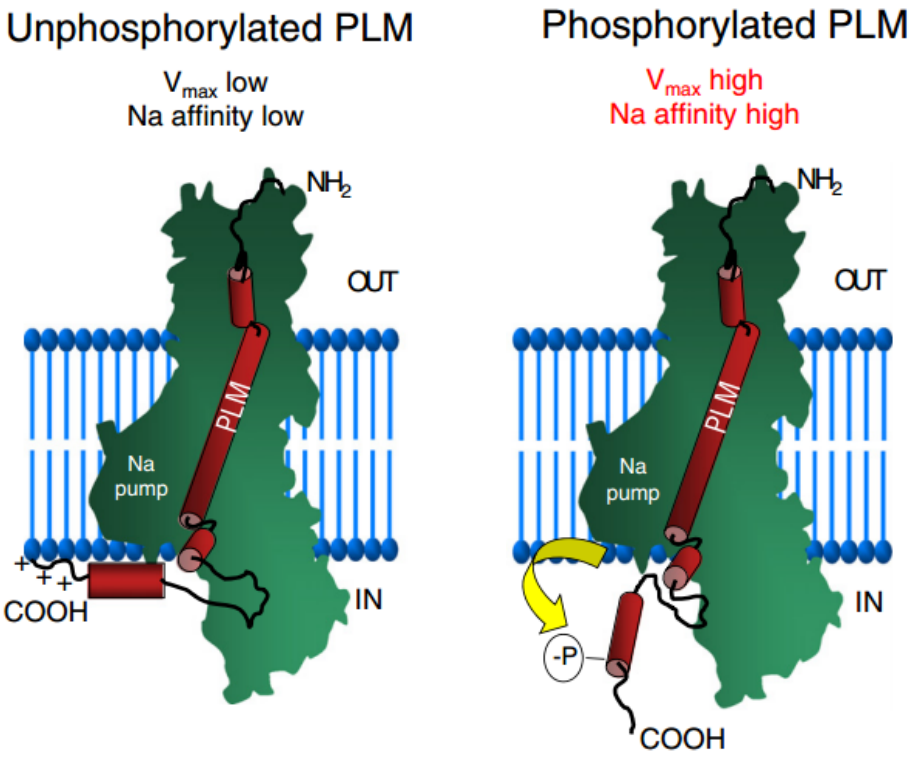

Figure 1.1 Schematic linking the regulation of Na^+/K^+ ATPase (NKA) by phospholemman (PLM) to their structures.

The NKA α subunit (green) has a lower capacity for $[Na]_i$ extrusion when PLM is in the unphosphorylated active form (left panel) compared with the inactive phosphorylated form (right panel). Image taken from Pavlovic et al. (2013a)

1.2.3 Excitation-contraction coupling in the healthy heart.

The functional consequence of the action potential is the triggering of myocardial contraction referred to as 'excitation-contraction (EC) coupling' (summarised in Figure 1.2). Calcium-induced calcium release by the SR during the action potential elevates $[Ca]_i$ from approximately 0.1µM to 0.5-1µM globally and approximately 100µM in the

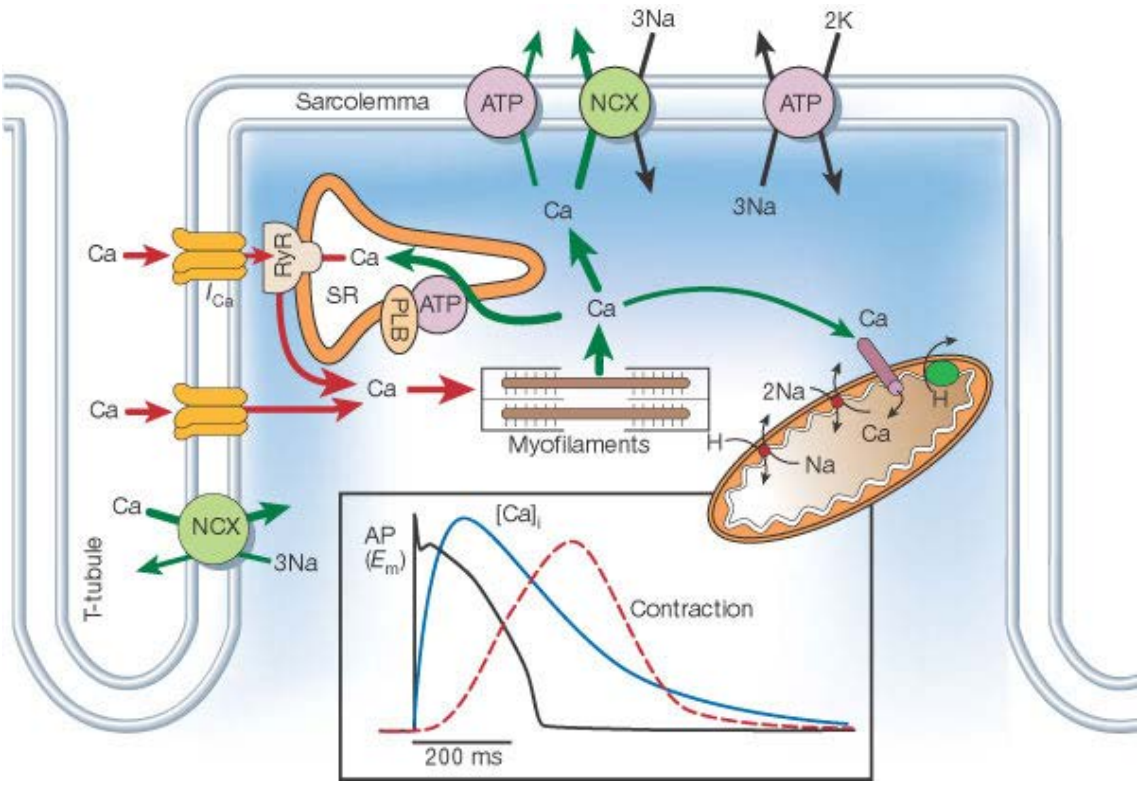

Figure 1.2 Schematic summary of cardiac excitation-contraction coupling. The action potential involves numerous ion movements across the sarcolemma which lead to calcium-induced calcium release by the sarcoplasmic reticulum and increased myofilament contraction. During diastole, this excess systolic calcium is removed from the cytosol via SERCA (which is regulated by PLB), as well as by NCX and the mitochondrial uniporter (pink cylinder). Abbreviations: AP (action potential); sarcoendoplasmic reticulum Ca^{2+} ATPase (SERCA); sarcolemmal Na^+/Ca^{2+} exchanger (NCX); sarcolemmal Na^+/K^+ ATPase (NKA); phospholamban (PLB); ryanodine receptor type 2 (RyR). Image taken from Bers (2002).

dyadic cleft. This leads to elevated $[Ca]_i$ at the myofilaments, as well as in mitochondria (discussed in Section 1.6). Myofilament contraction (inotropy) during systole is dependent upon both Ca^{2+} binding to troponin C in order that cross-bridge cycling can occur (Hajjar et al., 2000) and on the release of free energy from adenosine triphosphate (ATP) (Lymn and Taylor, 1971). In order for the ventricle to relax (lusitropy) during

diastole, Ca^{2+} is mainly removed from the cytosol via the SR Ca^{2+}-ATPase (SERCA), NCX and the mitochondrial Ca^{2+} uniporter.

1.2.4 Other modes of Na^+ transport in the healthy heart.

Under physiological conditions, NKA is the only quantitatively significant efflux pathway of Na^+ in the myocyte (NCX and $Na^+/HCO_3^-/Cl^-$ symporter can, in principle, reverse and efflux Na^+). However, there are numerous Na^+ influx pathways. These include the Na^+/H^+ exchanger (NHE) and the $Na^+/K^+/2Cl^-$ symporter which are both electroneutral whereas the Na^+/PO_3^- symporter, the Na^+/glucose symporter, the $Na^+/HCO_3^-/Cl^-$ symporter and the Na^+/Mg^{2+} exchanger are all electrogenic. These proteins influx much smaller amounts of Na^+ than NCX and Na^+ channels (Despa and Bers, 2013, Gray et al., 2001, Yao et al., 1998, Cook et al., 1997) and are therefore generally deemed less important in EC coupling. A schematic summary of cardiac Na^+ transport is shown in Figure 1.3 with reference to EC coupling (Section 1.2.3), mitochondrial function (Section 1.3.2) and Na^+ overload (Section 1.4).

1.2.5 Regulation of cardiac contractility and $[Na]_i$

The heart has several mechanisms by which it can modulate its contractility in response to changes in the demand for blood supply, for instance, during exercise.

The Frank-Starling effect is the primary mechanism for increasing contraction. There are at least four possible mechanisms underlying this effect: facilitated myofilament

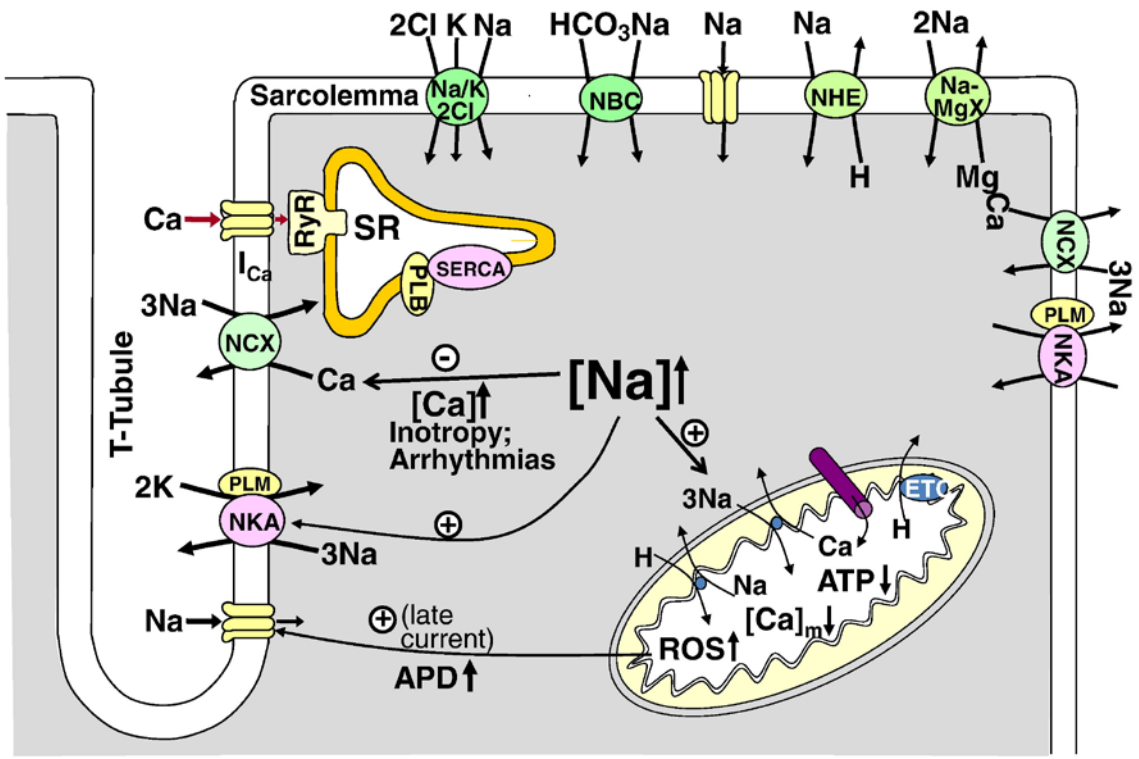

Figure 1.3 Schematic summary of the main cardiac Na^+ transporters. Na^+ transport is tightly linked to Ca^{2+} and excitation-contraction coupling. Abbreviations: action potential duration (APD); Na^+/bicarbonate symporter (NBC); sarcolemmal Na^+/Ca^{2+} exchanger (NCX); Na^+/H^+ exchanger (NHE); $Na^+/K^+/2Cl^-$ symporter (Na/K/$2Cl^-$); sarcolemmal Na^+/K^+ ATPase (NKA); Na^+/Mg^{2+} exchanger (Na-MgX); phospholamban (PLB); phospholemman (PLM); ryanodine receptor type 2 (RyR); sarcoendoplasmic reticulum Ca^{2+} ATPase (SERCA); sarcoendoplasmic reticulum (SR). Image taken from Despa and Bers (2013).

overlap and increased cross bridge-cycling availability (Huxley and Niedergerke, 1954, Huxley and Hanson, 1954), changes in troponin C Ca^{2+} affinity (Kobirumaki-Shimozawa et al., 2014), β-arrestin modulation (Abraham et al., 2016) and PKG-mediated phosphorylation of phosholamban (PLB) (Scotcher et al., 2016).

Sympathetic and parasympathetic activation are also important modulators of contractility, for example, via (de)phosphorylation of phospholamban (unphosphorylated form inhibits Ca^{2+} uptake by SERCA) (Mattiazzi et al., 2005), sensitisation of troponin-C to Ca^{2+} on the myofilaments (Haikala et al., 1995), (de)phosphorylation of L-type Ca^{2+} channels (phosphorylated form has increased Ca^{2+} permeability) (Trautwein and Hescheler, 1990) and the Anrep effect (increase in afterload increases inotropy). Interestingly, it has been suggested that the latter mechanism involves $[Na]_i$ elevation mediated by paracrine changes (reviewed by Cingolani et al., 2013).

Increases in heart rate (chronotropy) lead to elevated inotropy via the Bowditch effect (Zhang et al., 2015). This is due to increased action potential frequency leading to an enhanced time-averaged Ca^{2+} in the cytosol and SR as NCX has less time to extrude the surplus $[Ca]_i$ (Figure 1.2). There is a second postulated mechanism for the Bowditch effect that is $[Na]_i$-dependent and thought to be specific to the electrically-paced isolated heart preparation. That is, an increased action potential frequency leads to an elevated time-averaged $[Na]_i$ as NKA has less time to efflux the additional $[Na]_i$. This decreases NCX forward mode thereby increasing the time-averaged $[Ca]_i$ and contractility.

As the majority of isolated heart experiments are free of catecholamines in the perfusate this effect may only occur in the absence of β-receptor stimulation, thus it is unlikely that this mechanism occurs *in vivo* in which positive chronotropy only occurs during β-receptor stimulation. This is supported by the work of Despa et al. (2008) using isolated myocytes which showed that elevations in $[Na]_i$ due to increased pacing were reduced by isoprenaline.

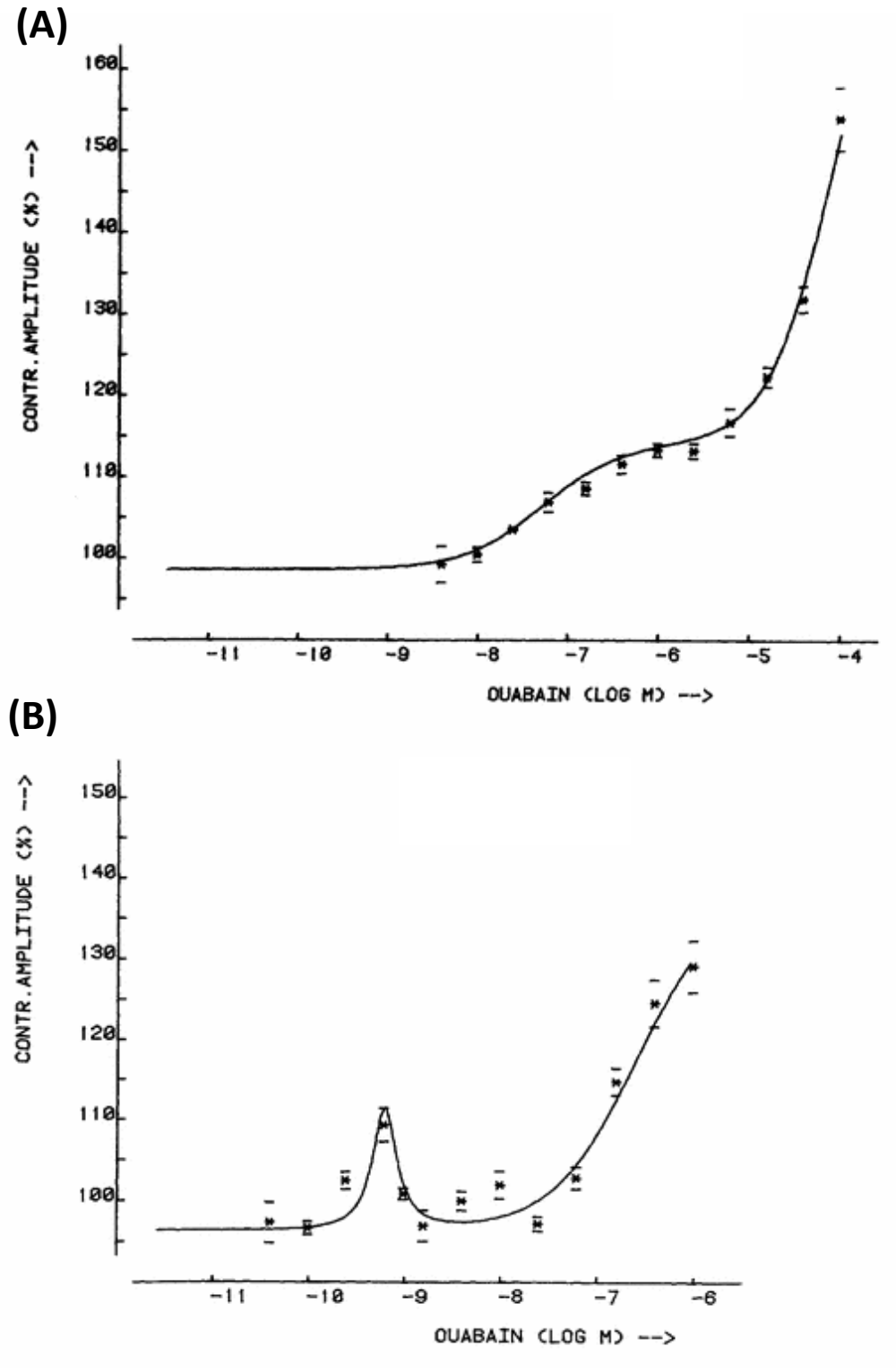

Figure 1.4 Ouabain dose-response curves in isolated heart.

(A) Rat. **(B)** Guinea pig. Experimental data is mean ± SEM (solid line is computational fitting). Image taken from Koomen et al. (1984)

A more established *in vivo* example of the use of $[Na]_i$ elevation to increase contractility is the administration of cardiac glycosides to HF patients. These are steroidal-like compounds found endogenously under normal conditions and are elevated in patients with renal failure (Kolmakova et al., 2011) and HF (Kennedy et al., 2015). Examples include ouabain, digoxin and bufalin (Schoner, 2001). Their clinical use for HF is limited due to their proarrhythmic properties (Gonano et al., 2011, Ferrier, 1977) but are useful for elevating $[Na]_i$ in experimental models. Cardiac glycosides elevate $[Na]_i$ via direct NKA inhibition and their positive inotropic response can vary considerably between species, for example, in the rat versus the guinea pig (Figure 1.4).

Cardiac $[Na]_i$ can also be elevated by several other factors. For example, by increased pH via enhanced NHE activity as seen, for example, following ischaemia-reperfusion injury (Murphy and Allen, 2009). Furthermore, Shattock (1984) showed that myocardial $[Na]_i$ is elevated during hypothermia. This is due to decreased NKA enzyme activity (and thereby reduced $[Na]_i$ efflux) at lower temperatures (Isenberg and Trautwein, 1975, Eisner and Lederer, 1980).

In terms of increasing $[Na]_i$ efflux, sympathetic stimulation has been demonstrated to stimulate NKA α1 and α2 isoforms (Glitsch, 2001, Bossuyt et al., 2009) which increases the Na outward current thereby keeping $[Na]_i$ at baseline. Over the last decade, there has been an increased interest in the regulation of NKA activity by the protein, phospholemman (PLM) (reviewed by Fuller et al., 2013 and Pavlovic et al., 2013). Following β-adrenergic stimulation, protein kinase A (PKA) phosphorylates PLM which reduces its inhibition of NKA thereby increasing $[Na]_i$ efflux. PLM can also be phosphorylated by PKC (Palmer et al., 1991) and work performed in our laboratory has

demonstrated that this phosphorylation is increased by nitric oxide (Pavlovic et al., 2013b).

For a summary of measured cardiac $[Na]_i$ values in different species under physiological and pathophysiological conditions see Section 1.4 (Table 1.1).

Throughout this thesis, inhibition of NKA is carried out using ouabain in order to elevate $[Na]_i$. As discussed later, a key issue with this approach is that the associated positive inotropic effect leads to increased ATP demand (discussed in Section 1.3.1) which in turn may induce metabolic changes that are independent of a reduction in ATP supply due to $[Na]_i$ overload. This is an important example of the close relationship between $[Na]_i$ and metabolism in the heart and is a central concept in this thesis.

1.3 ATP supply-demand matching in the healthy heart.

1.3.1 ATP demand in the healthy heart.

The heart has an immense requirement for ATP in order to sustain cardiac output and ion homeostasis. According to Gibbs (2003), 70-75% of ATP is used for force generation and work output with the remaining 25-30% being used for basal metabolism. With respect to force generation, it is estimated that the actomyosin ATPase accounts for 76% of ATP utilisation with SERCA accounting for 15% and NKA accounting for 9% (Schramm et al., 1994). Experiments in non-beating hearts permit the estimation of cardiac basal metabolism, which is significantly higher than that of other organs such as skeletal muscle (Gibbs, 2003). Under these conditions, it is estimated that 10% of oxygen utilisation is for non-mitochondrial processes, 20% is for

the maintenance of the mitochondrial membrane potential and the remaining 70% is for mitochondrial ATP synthesis to fuel, for example, protein synthesis (20-25%), transmembrane Na^+ homeostasis (20%) and Ca^{2+} homeostasis (5%) (Gibbs and Loiselle, 2001).

1.3.2 ATP supply in the healthy heart.

In order to maintain ATP levels, the heart must constantly and dynamically produce and recycle vast quantities of this molecule (approximately 6 kg / day in the human heart and this is achieved by the regulation of a complex network of metabolic reactions (reviewed in Kolwicz et al., 2013). A summary of these metabolic pathways is shown in Figure 1.5.

The heart has a high degree of substrate flexibility. Under normal conditions, the heart uses free fatty acids (FFAs), glucose and lactate as the main fuel substrates for cataplerosis (ATP generation) and typically in the ranges of 60-90%, 5-20% and 5-20%, respectively (Gertz et al., 1988, Stanley et al., 1997, Wisneski et al., 1985a, Wisneski et al., 1985b, Wisneski et al., 1990). These ranges are a reflection of the greater molar ATP yield per carbon atom of FAs compared with carbohydrates (Darvey, 1999).

During increased exercise, however, glucose and lactate predominate over FAs as fuel substrates (Taegtmeyer et al., 1980) because they produce more moles of ATP per mole of oxygen uptake relative to FAs. On a theoretical basis, the ATP-to-oxygen ratios for glucose, lactate and palmitate are 3.17, 3.00 and 2.80 respectively (Stanley et al., 2005).

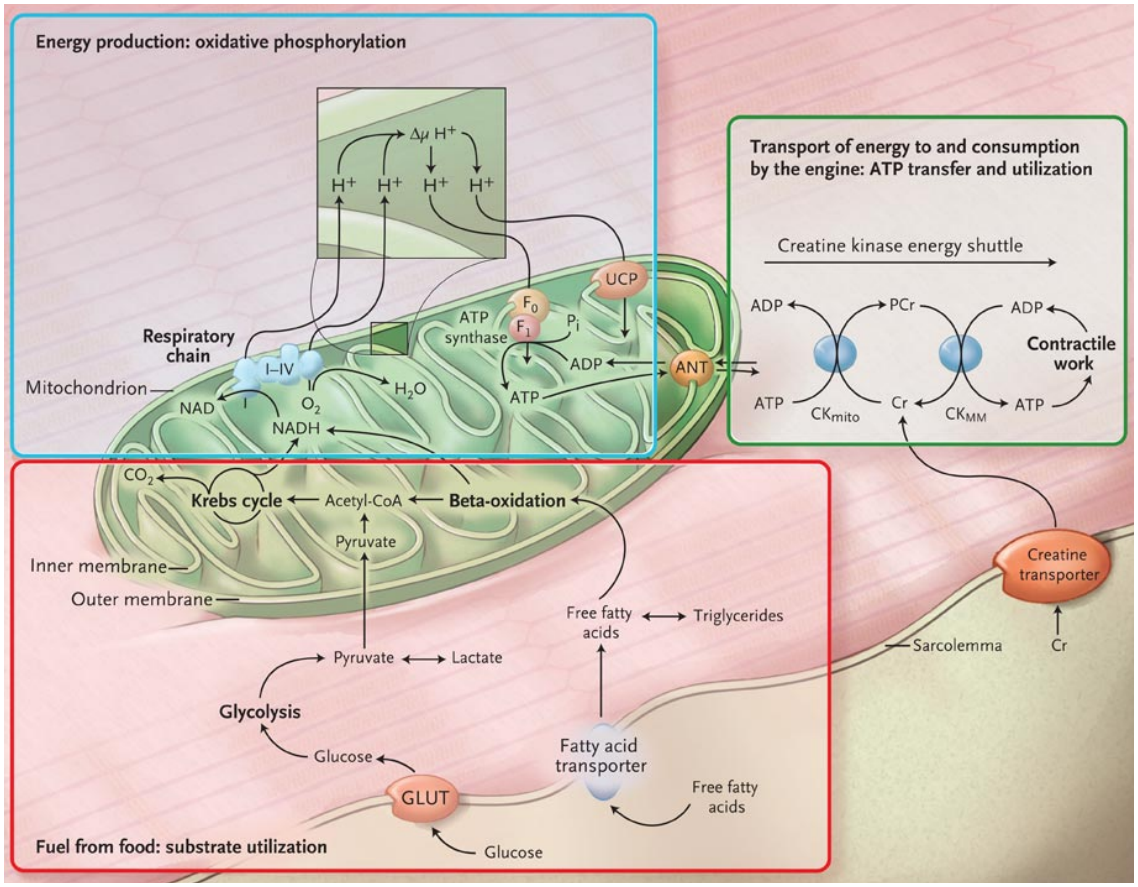

Figure 1.5 Schematic summary of cardiac metabolism.

Cardiac metabolism can be divided into three stages: 1) substrate utilisation: fuel substrates such as glucose and free fatty acids are transported into the cytosol and subsequently converted into acetyl-CoA in the mitochondrion thereby driving the tricarboxylic acid (TCA) cycle which produces the reducing equivalents, nicotinamide adenine dinucleotide (NADH) and flavine adenine dinucleotide (FADH2). 2) oxidative phosphorylation: NADH and FADH2 from the TCA cycle feed electrons into the respiratory chain (containing electron transport chain complex I-V) thereby generating a proton gradient across the inner mitochondrial membrane which drives the production of ATP by ATP synthase. 3.) creatine kinase (CK) energy shuttling: ATP leaves the mitochondrion via the adenine nucleotide transporter (ANT) or by mitochondrial CK (CK_{mito}) thereby producing phosphocreatine (PCr). Intermyofibrillar CK (CK_{MM}) converts this PCr into ATP which is hydrolysed to produce free energy for contraction. Abbreviations: GLUT (glucose transporter); UCP (uncoupling protein). Image taken from Neubauer (2007).

This aligns with the work of Mjos (1971) showing that administration of triglycerides increases FA uptake in dog leading to increased myocardial oxygen consumption but no change in ATP or left ventricular pressure. The apparent opposing relationship between glucose and FAs in the heart is, in part, due to the Randle cycle. This involves the competition between FFA and glucose for intermediary substrates, whereby FFA-derived cytosolic citrate and mitochondrial acetyl CoA inhibits glycolysis and pyruvate dehydrogenase (PDH), respectively (reviewed by Hue and Taegtmeyer, 2009). FFAs and carbohydrates are not the only fuel substrates available to the cardiomyocyte. Ketone bodies can also be absorbed from the bloodstream and converted into acetyl CoA when carbohydrate availability is very low (Forsey et al., 1987).

The TCA cycle is a central component of intermediary metabolism in the heart and is vital to the generation of ATP (via the production of reducing equivalents). The heart uses other molecules in addition to acetyl CoA as a carbon source for the TCA cycle (for example, amino acids such as glutamate and aspartate) via the process of anaplerosis (Figure 1.6). The TCA cycle also plays a role in cataplerosis (biosynthesis) of amino acids and fats. Each turn of the TCA cycle produces three molecules of NADH and one molecule of $FADH_2$ which feed electrons into the respiratory chain (the electron transport chain). Two molecules of CO_2 are also produced which are converted to bicarbonate and removed as a by-product via the bloodstream. The respiratory chain consists of five protein complexes. Complexes I (NADH dehydrogenase) and II (succinate dehydrogenase) are reduced by NADH and $FADH_2$, respectively. Protons are translocated into the intermembrane space to generate a proton gradient across the membrane and electons are passed onto complexes III (cytochrome bc_1 complex) and

IV (cytochrome c oxidase). Complex IV transfers electrons to molecular oxygen supplied from the bloodstream to form H_2O as a by-product of the respiratory chain. Complex V (F_1F_0 ATPase; ATP synthase) uses the proton gradient to produce ATP via the condensation of ADP, inorganic phosphate (P_i) and a proton.

Mitochondrial respiration accounts for greater than 95% of ATP supply in the heart (Kolwicz et al., 2013). The remainder is synthesised during glycolysis in which there is a net gain of 2 molecules of ATP. The end products of glycolysis are pyruvate and lactate which exist in equilibrium, although this equilibrium can shift towards lactate production during increased workload (Goodwin et al., 1998).

As the key sites of ATP utilisation are extramitochondrial (discussed in Section 1.3.1), the ATP is transported out of the mitochondrion in exchange for ADP by the adenine nucleotide translocator (ANT). Mitochondrial creatine kinase (CK) (which resides on the outside of the inner mitochondrial membrane and in close proximity to ANT) uses this ATP as a substrate in order to produce phosphocreatine (PCr) and ADP and cytosolic CK converts PCr back to ATP at the myofilaments (Guzun et al., 2015, Lipskaya, 2001). PCr is known to diffuse significantly faster through the cytosol than ATP (Wyss et al., 1992) and thus the CK shuttle accelerates the transfer of energy from the mitochondria to the sites of utilisation. Another phosphotransfer enzyme involved in ATP supply is adenylate kinase (interconversion of ATP + AMP $\rightleftharpoons$ 2ADP). The importance of this enzyme in the maintenance of ATP supply is highlighted by the work of Pucar et al (2000) in which knockout of adenylate kinase in mice compromises cardiac energetics.

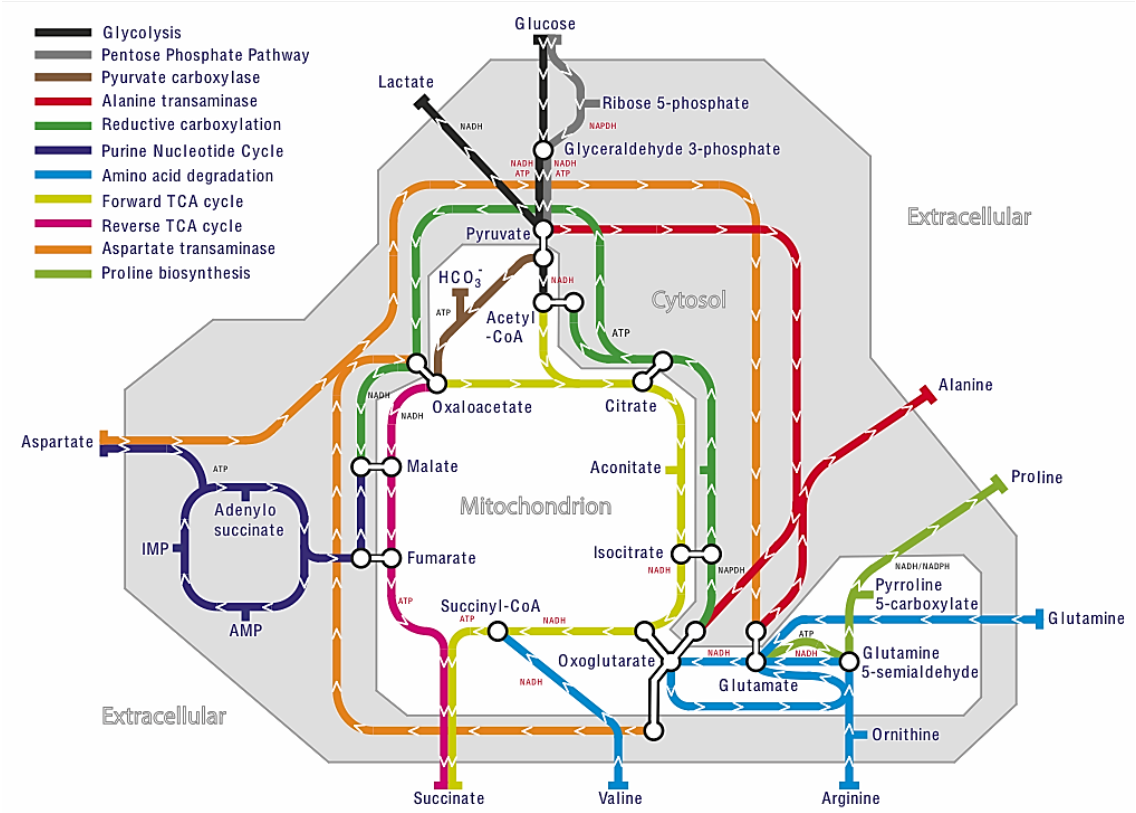

Figure 1.6 Schematic of the TCA cycle and converging metabolic pathways.

Note that the diagram is not an exhaustive summary of intermediary metabolism. For example, fatty acid metabolism is not included. Image taken from Robinson (2015).

1.3.3 Regulation of ATP supply-demand matching in the healthy heart.

The regulation of cardiac metabolism has been extensively studied since the 1950s yet is still an area of active research. Indeed, it is widely accepted that the heart comprises several mechanisms by which it orchestrates metabolism in order to match ATP supply to demand. One of the early mechanisms to be suggested was positive feedback by ADP and several *in vitro* studies have supported this. ADP has been shown to allosterically

activate isocitrate dehydrogenase (IDH) (Vaughan and Newsholm, 1969, Nichols et al., 1994). However, Balaban (2009) argues that the only mitochondrial enzyme regulated by ADP *in vivo* is ATP synthase which is via a direct interaction and only occurs in the presence of $P_{i.}$

When P_i is added alone to cardiac mitochondria, there are increases in the concentration of NADH, the mitochondrial membrane potential and the activity of the electron transport chain (ETC). Bose et al (2003) suggested that this is due to the stimulation of α-ketoglutarate dehydrogenase (αKDH) (Rodriguez-Zavala et al., 2000), IDH (Hansford, 1972) and malate dehydrogenase (MDH) (Blonde et al., 1967) by Pi.

Isolated enzyme experiments have revealed that PDH (Denton et al., 1972, Siess, 1972) and αKDH (McCormack and Denton, 1979) are activated by increased levels of Ca^{2+} in the physiological range (10-1000 nM). Ca^{2+} also reduced the K_m of IDH in this study although there was no influence on the V_{max}. Nonetheless, this may be a key Ca^{2+}-dependent point of regulation given that IDH is the rate limiting enzyme of the TCA cycle. In isolated mitochondria, an increase from sub-physiological to physiological Ca^{2+} caused marked increases in state 3 respiration (Moreno-Sanchez, 1985). Other postulated points of Ca^{2+} activation include ANT (Moreno-Sanchez, 1983), ATP synthase (Harris and Das, 1991), ETC (Murphy et al., 1990), ATP-Mg^{2+}/P_i carrier (del Arco and Satrustegui, 2004, Nosek et al., 1990) and aspartate/glutamate exchangers (citrin and aralar) (Palmieri et al., 2001, Contreras et al., 2007, Marmol et al., 2009). The dependence of oxidative phosphorylation on Ca^{2+} has also been demonstrated *ex vivo* by Wu et al (1992) using Langendorff perfused rat hearts, oxygen probes and fluorescent probes for Ca^{2+}. Furthermore, Bose et al. (2003) showed that Ca^{2+} and P_i

have an additive effect on oxidative phosphorylation. At present, the best evidence that Ca^{2+} partially regulates cardiac energetics is that perfusion of the rat heart with ruthenium red (which reduces Ca^{2+} entry into the mitochondrial matrix via inhibition of the mitochondrial Ca^{2+} uniporter) results in compromised concentrations of high energy phosphates (HEPs) measured by ^{31}P NMR and are unable to maintain contractile function (Unitt et al., 1989). This study also demonstrated the short term (responsive) temporal regulation of cardiac energy metabolism. Following isoprenaline perfusion, [ADP] and [P_i] were significantly elevated and reached a maximum after 10-30 seconds, subsequently returning to baseline within 120 seconds and [ATP] was not significantly altered. However, this recovery period was significantly longer in hearts with perturbed $[Ca]_m$ uptake.

The regulation of cardiac metabolism by Ca^{2+} is summarised in Figure 1.7. Longer-term regulation of cardiac metabolism is also regulated by signalling pathways (for example, insulin and CD36 for glucose and FA uptake, respectively) and transcriptional pathways such as those regulated by peroxisomal proliferator activated receptor (PPAR) leading to changes in mitochondrial function and biogenesis. These areas have been reviewed comprehensively by Lopaschuk et al (2008) and Ventura-Clapier et al (2008) but are out of the scope of this thesis.

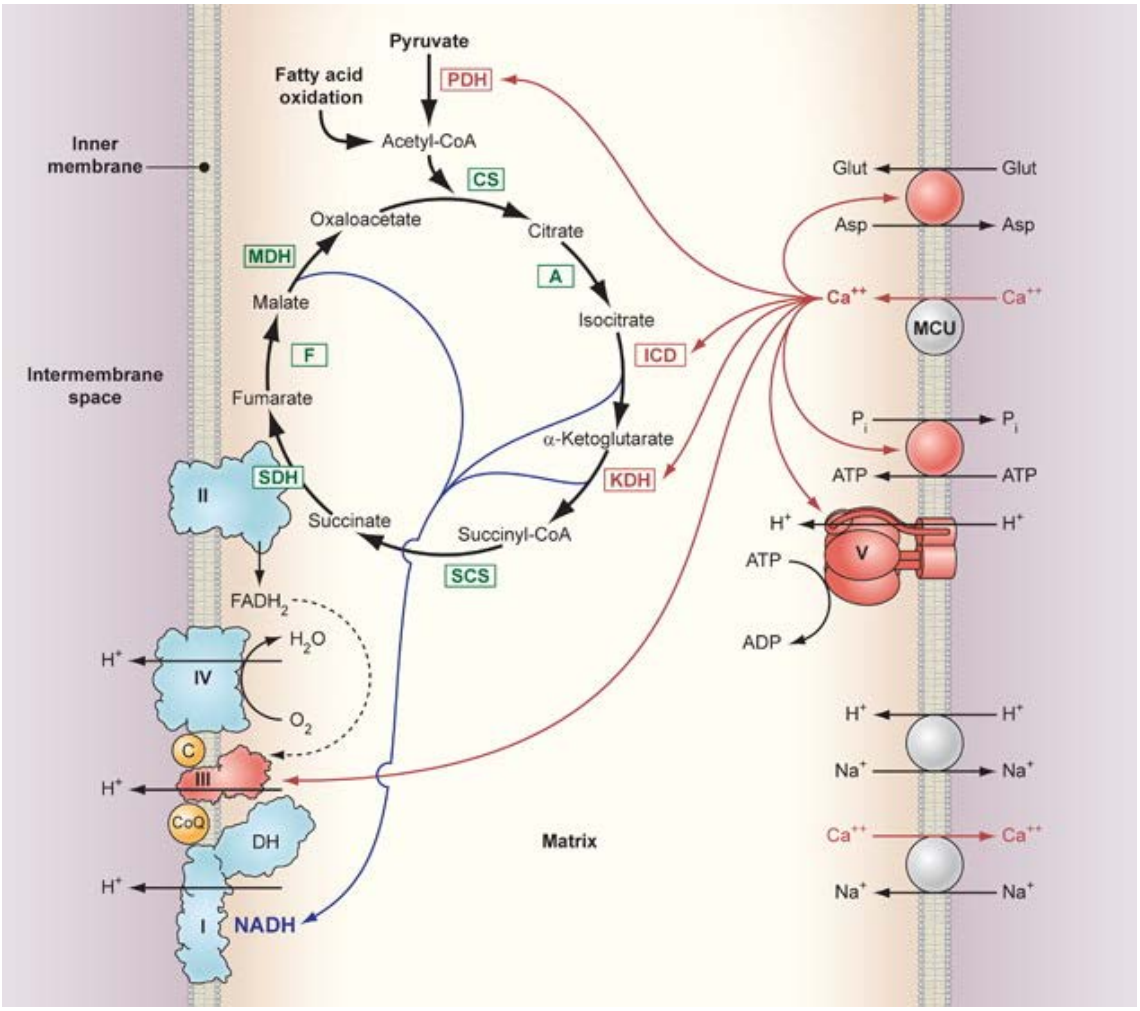

Figure 1.7 Mitochondrial transport of Ca^{2+} and its regulation of cardiac metabolism.

Ca^{2+} enters the mitochondrial matrix via the mitochondrial calcium uniporter (MCU) and is extruded by the mitochondrial Na^+/Ca^{2+} exchanger, which is linked to the Na^+/H exchanger via Na^+. Ca^{2+} positively regulates the glutamate (glut)/aspartate (asp) exchanger, the ATP/Pi exchanger, ATP synthase (complex V), pyruvate dehydrogenase (PDH), isocitrate dehydrogenase (ICD), α-ketoglutarate dehydrogenase (KDH) and cytochrome bc1 (complex III). Abbreviations: succinyl coenzyme A synthetase (SCS); succinate dehydrogenase/complex II (SDH); malate dehydrogenase (MDH); citrate synthase (CS); aconitase (A); NADH dehydrogenase complex (complex I / DH); CoQ (coenzyme Q); cytochrome c (C); cytochrome c oxidase (complex IV). Image taken from Glancy et al (2012).

1.4 Na^+ handling is deranged in the hypertrophied/failing heart.

A hallmark of cardiac hypertrophy and failure is an elevation of the intracellular Na^+ concentration ($[Na]_i$). There is an abundance of literature on this phenomenon although absolute values of measured $[Na]_i$ are often dissimilar, probably owing to methodological differences. Table 1.1 gives a summary of a selection of these studies and allows an approximation to be made of the $[Na]_i$ in the myocyte under both physiological and pathophysiological conditions across various mammalian species. It is known that the rat heart has a higher resting $[Na]_i$ than other species. Using SBFI-loaded rat and rabbit cardiomyocytes, Despa et al (2002) have attributed this species difference to a higher Na^+ influx due to greater activities of Na^+ channels, NHE and NCX in the rat with consequential higher NKA activity in this species.

1.4.1 Evidence for reduced Na^+ efflux.

There is strong agreement that Na^+ efflux is perturbed in cardiac hypertrophy and HF. Semb et al (1998) and Louch et al (2010) used SBFI-loading to show that both the maximal activity of NKA and its affinity for $[Na]_i$ were reduced in failing cardiomyocytes. Moreover, Schwinger et al (1999) reported a decreased expression of NKA protein in myocardial samples from patients with heart failure. In a similar study, no change in the abundance of NKA RNA transcripts (Allen et al., 1992) was observed which may infer that post-transcriptional events occur to NKA that are specific to HF. In the failing rat heart, the α2 isoform of NKA was found to be significantly decreased whereas the more abundant α1 was unchanged reflecting that of the normal rat heart (Verdonck et al., 2003). Furthermore, Bossuyt et al. (2005) reported that failing rabbit

cardiomyocytes express both of these isoforms to a lesser extent than non-failing counterparts. The Bossuyt et al. (2005) study also demonstrated that PLM, which applies a tonic inhibition of NKA when in its unphosphorylated form (see Pavlovic et al., 2013a), exhibits lower overall expression in HF although the fraction of phosphorylated PLM was higher in HF. However, work by El-Armouche et al (2011) demonstrated a trend toward decreased PLM phosphorylation in failing left ventricular samples compared with non-failing controls. The discrepancy in the PLM phosphorylation data may be due to the use of different models of HF. That is, in the Bossuyt et al. (2005) study an unusual rabbit model of volume overload was utilised whereas El-Armouche et al (2011) used left ventricular myocardium from HF patients. Correll et al. (2014) reported that overexpression of NKA α2 attenuated cardiac hypertrophy, increased Ca^{2+} extrusion by NCX1 and reduced PLM expression and phosphorylation. Moreover, overexpression of PLM reduces NKA activity in failing myocytes (Zhang et al., 2006) while knockout of PLM in mice with myocardial infarction improves Ca^{2+} transients and contractile function (Mirza et al., 2012). The most convincing evidence thus far that reduced Na_i efflux is a causal factor in the development of hypertrophy/HF is the work of Boguslavskyi et al (2014), which showed that NKA inhibition and cardiac hypertrophy were significantly increased in knock-in mice expressing PLM that was unphosphorylatable by protein kinases A and C. The potential of targeting PLM therapeutically for cardiac hypertrophy and HF has been reviewed by Shattock (2009).

Table 1.1A Literature values of (patho)physiological cardiac $[Na]_i$.

Region measured	Species/ Condition	$[Na]_i$ (mM)	Method Used	Reference
Bulk cytosolic	Dog/Normal	8.9	Na^+-selective microelectrodes; Purkinje fibers at rest.	Lee and Dagostino (1982)
Bulk cytosolic	Dog/Normal	10.4	Na^+-selective microelectrodes; Purkinje fibers at 1 Hz.	Lee and Dagostino (1982)
Bulk cytosolic	Ferret/Normal	7.8	Na^+-selective microelectrodes; muscle strips at rest.	Baudet et al. (1991)
Bulk cytosolic	Ferret/RVH[1]	8.0	Na^+-selective microelectrodes; muscle strips at rest[2].	Baudet et al. (1991)
Bulk cytosolic	Guinea-pig/Normal	7.3	Na^+-selective microelectrodes; muscle strips at rest.	Gray et al. (2001)
Bulk cytosolic	Guinea-pig/Normal	6.4	^{23}Na NMR; isolated perfused heart.	Jelicks and Siri (1995)
Bulk cytosolic	Guinea-pig/Normal	5.1	SBFI-loaded myocytes at rest.	Harrison et al. (1992)
Bulk cytosolic	Guinea-pig/Normal	5.2	SBFI-loaded myocytes at rest.	Liu et al. (2008)
Bulk cytosolic	Guinea-pig/Normal	38.3	Flame atomic absorption spectroscopy; isolated perfused hearts,	Radford et al. (1998)
Bulk cytosolic	Guinea-pig/Normal	7.5	Na^+-selective microelectrodes; muscle strips at rest.	Wilde and Kleber (1986)
Bulk cytosolic	Guinea-pig/Normal	~6.3	Na^+-selective microelectrodes; muscle strips at rest.	Schmied et al. (1991)
Bulk cytosolic	Guinea-pig/Normal	4.7	Na^+-selective microelectrodes; muscle strips at rest.	Wang et al. (1993)
Bulk cytosolic	Guinea-pig/Normal	8.0	Na^+-selective microelectrodes; atrial muscle strips at rest.	Wang et al. (1993)
Bulk cytosolic	Guinea-pig/Normal	5.8	Na^+-selective microelectrodes; atrial muscle strips at rest.	Cohen et al. (1982)
Bulk cytosolic	Guinea-pig/Normal	7.9	Na^+-selective microelectrodes; atrial muscle strips at 0.5 Hz.	Cohen et al. (1982)
Bulk cytosolic	Guinea-pig/LVH[1]	12.1	Na^+-selective microelectrodes; muscle strips at rest.	Gray et al. (2001)
Bulk cytosolic	Guinea-pig/LVH[1]	12.8	^{23}Na NMR; isolated perfused heart.	Jelicks and Siri (1995)
Bulk cytosolic	Guinea-pig/Failing	16.8	SBFI-loaded myocytes at rest.	Liu et al. (2008)
Bulk cytosolic	Human/Normal	8.0	SBFI-loaded muscle trips paced at 0.25Hz	Pieske et al. (2002)
Bulk cytosolic	Human/MVD	11.8	Na^+-selective microelectrodes; muscle strips at rest.	Gray et al. (2001)
Bulk cytosolic	Human/LVH	14.2	Na^+-selective microelectrodes; muscle strips at rest.	Gray et al. (2001)
Bulk cytosolic	Human/Failing	12.1	SBFI-loaded muscle trips paced at 0.25Hz	Pieske et al. (2002)

Continued overleaf

Table 1.1B Literature values of (patho)physiological cardiac $[Na]_i$ (continued).

Region measured	Species/ Condition	$[Na]_i$ (mM)	Method Used	Reference
Bulk cytosolic	Mouse/Normal	11.6	^{23}Na NMR; isolated perfused heart.	Eykyn et al. (2015)
Bulk cytosolic	Mouse/Normal	14	SBFI-loaded myocytes at rest.	Boguslavskyi et al. (2014)
Bulk cytosolic	Mouse/LVH[1]	23	SBFI-loaded myocytes at rest.	(Boguslavskyi et al., 2014)
Bulk cytosolic	Rabbit/Normal	7.2	Na^+-selective microelectrodes; muscle strips at 0.5 Hz.	Shattock and Bers (1989)
Bulk cytosolic	Rabbit/Normal	4.5	SBFI-loaded myocytes at rest.	Despa et al. (2002a)
Bulk cytosolic	Rabbit/Normal	3.8	SBFI-loaded myocytes at rest.	Levi et al. (1994)
Bulk cytosolic	Rat/Normal	12.7	Na^+-selective microelectrodes; muscle strips at 0.5 Hz.	Shattock and Bers (1989)
Bulk cytosolic	Rat/Normal	28	Na^+-selective microelectrodes; myocytes at rest.	Szabo and Armstrong (1984)
Bulk cytosolic	Rat/Normal	30	Na^+-selective microelectrodes; myocytes at rest.	Wasserstrom (1983)
Bulk cytosolic	Rat/Normal	8.5	Na^+-selective microelectrodes; myocytes at rest.	Grupp et al. (1985)
Bulk cytosolic	Rat/Normal	11.1	SBFI-loaded myocytes at rest.	Despa et al. (2002a)
Bulk cytosolic	Rat/Normal	10.9	SBFI-loaded myocytes at rest.	Levi et al. (1994)
Bulk cytosolic	Rat/Normal	17.5	^{23}Na NMR; isolated perfused arrested hearts.	Schepkin et al. (1998)
Bulk cytosolic	Rat/Normal	21	SBFI-loaded myocytes at rest.	Donoso et al. (1992)
Bulk cytosolic	Rat/Normal	7.8	SBFI-loaded myocytes at rest.	Harrison et al. (1992)
Mitochondrial	Rat/Normal	5.1	SBFI-loaded myocytes at rest.	Donoso et al. (1992)
Bulk cytosolic	Sheep/Normal	6.4	Na^+-selective microelectrodes; Purkinje fibers at 1 Hz.	Lee et al. (1980)
Bulk cytosolic	Sheep/Normal	~5	Na^+-selective microelectrodes; Purkinje fibers at rest.	Eisner et al. (1984)
Bulk cytosolic	Sheep/Normal	5.8	Na^+-selective microelectrodes; muscle strips at rest.	Cohen et al. (1982)
Bulk cytosolic	Sheep/Normal	7.9	Na^+-selective microelectrodes; muscle strips at rest.	Cohen et al. (1982)

[1]Induced by aortic or pulmomary artery constriction. [2]Right ventricular tissue was used (left ventricular tissue was used if not specified). Abbreviations: RVH (right ventricular hypertrophy); MVD (mitral valve disease); NMR (Nuclear Magnetic Resonance Spectroscopy).

Indeed, there are a number of papers reporting a variety of results on the roles of NKA and PLM in cardiac hypertrophy and HF in different models. However, the consensus appears to support the notion that NKA is either unchanged or down-regulated and that the ratio of PLM to NKA α-subunit increases under these conditions which aligns with the widely reported decrease in NKA activity. This is further exacerbated by the enhanced PLM inhibition of NKA due to a reduction in basal phosphorylation of PLM.

1.4.2 Evidence for elevated Na^+ influx.

In addition to reduced Na^+ efflux, increased influx of Na^+ is also thought to contribute to $[Na]_i$ overload in the hypertrophied/failing heart. In failing myocytes from pressure-overloaded and volume-overloaded rabbit hearts, blocking NKA induces a $[Na]_i$ elevation that is double that of healthy hearts mainly due to increased tetrodotoxin (TTX)-sensitive Na^+ channels (Despa et al., 2002b) as well as NHE (Baartscheer et al., 2003b). Furthermore, $[Na]_i$ elevation is reduced by the Na^+ channel antagonist, ranolazine, leading to an improvement in diastolic function (Sossalla et al., 2008, Gremmler and Kisters, 2013) and cariporide, an antagonist of both the late Na^+ channel and the NHE, delays the onset of HF (Baartscheer et al., 2008). Increased NCX expression and activity have also been associated with heart failure in patients (Reinecke et al., 1996) which may act as a compensatory mechanism for decreased SERCA activity in HF (Murphy and Eisner, 2009). Although NCX is known to operate mainly in the forward mode (Ca_i efflux/Na^+ influx) under physiological conditions, there is a shift towards increased reverse mode (Ca^{2+} influx/Na_i efflux) in failing human

cardiomyocytes due to the $[Na]_i$ elevation, as well as decreased SR $[Ca^{2+}]$ and a prolonging of the action potential (Weber et al., 2003).

1.4.3 Consequences of deranged Na^+ handling in the hypertrophied/failing heart.

There is consensus that significant and sustained $[Na]_i$ overload is detrimental to the heart. The two most severe consequences of pathologic $[Na]_i$ elevation are a reduction in contractile function (both systolic and diastolic) and the increased risk of arrhythmias (Noble and Noble, 2006). These consequences are often attributed to $[Ca]_i$ overload and the toxicity that arises from this, such as an increased generation of reactive oxygen species (Viola and Hool, 2011).

1.5 Metabolism is deranged in the hypertrophied/failing heart.

In addition to $[Na]_i$ overload, derangement in energy metabolism is a common pathophysiological feature of cardiac hypertrophy and HF. The report by Herrmann et al (1939) was one of the first to explore the chemical nature of HF. Myocardial tissue samples from canine hearts following coronary occlusion exhibited reduced levels of glycogen, total creatine and creatinine. More recent studies have confirmed metabolic derangement in human HF. For example, Starling et al. (1998) showed that ATP and NAD(H) were significantly depleted in biopsies from patients with dilated cardiomyopathy compared with healthy control hearts. Advances in analytical technologies and understanding of metabolic mechanisms have added much weight to the hypothesis that alterations in cardiac energy homeostasis are important

pathophysiological features of hypertrophy and HF. These alterations can be categorised into those related to substrate utilisation, intermediary metabolism and cardiac energetics.

1.5.1 Evidence for changes in substrate utilisation during hypertrophy and HF.

Cardiac hypertrophy and dilated cardiomyopathy induce a switch in substrate utilisation from mainly oxidation of FFAs towards mainly glucose oxidation, which is similar to the fetal heart (Schisler et al., 2015, Osorio et al., 2002). The onset of this switch (and thereby the stage at which it could potentially be targeted therapeutically) is currently debated. For example, pressure-overload in the rat heart led to a reduction in palmitate oxidation and an elevation in pyruvate oxidation in the early stages of hypertrophy (Akki et al., 2008). In contrast, Chandler et al (2004) suggest that this switch only occurs following end-stage HF and not during compensated HF. The review by Ritchie et al (2006) discussed the potential role that Ca^{2+} handling plays in the time-course of metabolic alterations during hypertrophy. One suggestion is that SERCA preferentially uses glycolytically-derived ATP over oxidative phosphorylation (supported by the work of Xu et al., 1995) and therefore the heart switches to a more glycolytic phenotype during hypertrophy in order to sustain adequate SERCA function and Ca^{2+} handling. This may also be the case for Na^{+} and/or K^{+} handling given that NKA is also thought to be preferentially fuelled by glycolysis (Sepp et al., 2014). Furthermore, Neubauer et al (2007) have highlighted the difficulty in separating the intrinsic alterations in metabolic pathways leading to substrate utilisation from those caused by the altered availability of substrates that is commonly observed in HF (Stanley et al., 2005). Although the

temporal regulation of the substrate switch in HF is currently unclear, a recent study using transverse aortic constriction in mice showed that this switch can be reversed within one week of debanding (Byrne et al., 2016). This finding infers that it may be possible to reverse early metabolic alterations in HF but further work on the mechanism underlying this reversal is needed. In spite of the substantial *in vitro* and pre-clinical evidence to support the targeting of the substrate switch therapeutically, there has been limited translational success into the clinic. For example, sodium dichloroacetate (inhibits PDH kinase thereby increasing pyruvate oxidation) administration (50 mg/kg) appeared to improve contractile performance in ten HF patients but a vehicle control group was not included in this study (Bersin et al., 1994, Bersin and Stacpoole, 1997). Trimetazadine is currently prescribed for longer term inhibition of FFA oxidation and has been shown to reduce angina and improve cardiac function in patients with dilated cardiomyopathy (Fragasso et al., 2006, Tuunanen et al., 2008) although these improvements were modest. Given the limited clinical success of targeting substrate utilisation to date, it is important to evaluate the potential of targeting other aspects of cardiac metabolism, such as intermediary pathways leading to ATP supply.

1.5.2 Evidence for changes in intermediary metabolism and energetics during hypertrophy and HF.

Several catabolic changes are known to occur downstream of acetyl CoA production in the hypertrophied or failing heart. Nemutlu et al (2015) recently carried out metabolomic profiling of plasma samples from control and HF patients using gas chromatrography tandem mass spectrometry and NMR. A significant reduction in

succinate and elevation in glutamate was found in the plasma of HF patients indicating decreased TCA cycle activity. However, concentrations of plasma metabolites may not truly reflect the myocardial situation. Furthermore, experimental animal models have allowed the controlled induction of hypertrophy and HF thereby giving robust metabolomics datasets in myocardial tissue. For example, the TCA cycle and oxidative phosphorylation were downregulated in a chronic aorto-caval fistula rat model (Melenovsky et al., 2011). This is supported by the findings of Lai et al (2014) in which the concentrations of α-ketoglutarate, fumarate and malate were reduced by transverse aortic constriction (TAC)-induced HF in C57BL/6J mice. However, succinate was increased and citrate was unchanged under these conditions. This was not explained by the authors but may be associated with the direct roles of these metabolites in the respiratory chain and fatty acid synthesis, respectively. Interestingly, this study also showed that succinate is uniquely decreased following physiological hypertrophy in which there is an increased ATP demand without metabolic derangement. The metabolomics investigation by Wang et al (2013) also reported downregulated TCA cycle activity driven mainly by a large reduction in the abundance of malate dehydrogenase. However, hearts in this study were from mini-pigs with chronic ischemic HF and therefore may not represent the metabolic alterations that occur in pressure-overload induced-HF that exhibit a demand ischaemia. Interestingly, a pacing-induced model of HF in the dog demonstrated a 60% increase in α-KDH activity thereby inferring enhanced TCA cycle activity during HF (O'Brien et al., 1990).

Alterations to metabolites involved in anaplerotic pathways have also been reported. Russel et al (1991) have shown that the decline in contractile function in working rat

hearts by 44% over 60 minutes of perfusion with acetoacetate is completely negated by perfusion with pyruvate. Sorokina et al (2007) utilised ^{13}C tracing to show that pyruvate carboxylation, as well as glutamate anaplerosis producing α-ketoglutarate, are increased in pressure-induced hypertrophic hearts perfused in the Langendorff mode. This redirecting of carbon flux is thought to be less energy efficient than flux through actyl CoA and thus may contribute to ATP supply-demand mismatching. Pound et al (2009), Atherton et al (2011) and Carley et al (2015) demonstrated that partial reversal of pyruvate carboxylation improved contractile performance in the hypertrophic rat heart. Nguyen et al (2015) hypothesised that anaplerosis increases the channelling of TCA cycle into protein biosynthesis pathways thereby contributing to hypertrophy. Furthermore, glutamate oxidation exhibits a rise in the initial stages of HF but then declines concomitantly with contractile performance and ejection fraction (Gong et al., 2003). As glutamate oxidation increases the concentration of αKG in mitochondria, this is possibly suggestive of an adaptive mechanism in which TCA cycle activity is maintained in the early stages of HF followed by a waning of activity with disease progression. Indeed, enhanced glutamate oxidation may infer elevated glutamate uptake in HF thereby contributing to altered substrate selection (discussed in Section 1.5.1).

There have also been numerous studies inferring reduced activities and/or altered expression of the electron transport chain complexes, ATP synthase and adenine nucleotide translocase in both pre-clinical experimental models as well as in the clinic (summarised in Table 1.2). There is evidence for alterations in the Ca^{2+}-dependent components (Complex III, V and ANT). Respirometry studies in permeabilised cardiac fibres from failing hearts from rat (Garnier et al., 2003, Sanbe et al., 1994), dog

Table 1.2 Summary of studies showing reduced activities of the electron transport chain, ATP synthase and adenine nucleotide translocase.

Experimental Condition	Protein						
	I	II	I-III	III	IV	V	ANT
Human IDCM				Jarreta et al (2000)[A]; Buchwald et al (1990)[A]	Buchwald et al (1990) [A]; Quigley et al (2000)[A]; Arbustini et al (1998)[A].		Sylven et al (1993)[T]; Dorner et al (2006) [A,I]; Dorner et al (2000); Schultheiss et al (1985)[E]
Human Miscellaneous	Scheubel et al (2002)[A]					Unverferth et al (1988)[A]	
Canine rapid pacing	Ide et al (1999)[A]		Unpublished	Marin-Garcia et al (2001a)[A]; Marin-Garcia et al (2001b)[A]		Marin-Garcia et al (2001a)[A]; Marin-Garcia et al (2001b)[A]; Moe et al (2004) [A]; McCutcheon et al (1992) [A]	
Rat aortic banding					Garnier et al (2003)[A]		
Rat spontaneous arterial hypertension					Sparagna et al (2007)[A]		
Rabbit aortic banding	Griffiths et al (2010) [A]	Griffiths et al (2010)[A]					

[A] =Decreased activity. [T] =Increased transcription. [I] = Altered isoform expression profile. [E]= Decreased protein expression. Adapted from Rosca et al (2013).

(Sharov et al., 2000) and human (Sharov et al., 2000, Lemieux et al., 2011) perfused with malate, glutamate and/or succinate as substrates have revealed reduced rates of state 3 respiration. However, an important aspect of respirometry studies is the sub-population of mitochondria that is used for the experiment. Rosca et al (2013) have discussed that subsarcolemmal mitochondria are more affected by HF than intermyofibrillar populations (potentially due to differences in ETC chain complexes) and this may explain inconsistencies in findings using this technique.

A highly-cited study by Neubauer et al (1997) using *in vivo* ^{31}P NMR found that the myocardial PCr-to-ATP ratio (PCr:ATP) is a reliable prognostic indicator of dilated cardiomyopathy (DCM). During a 2.5 year investigational period, 44% of DCM patients with a PCr:ATP of <1.6 died of cardiovascular causes whereas only 5% of DCM patients with a PCr:ATP of >1.6 died of cardiovascular causes. The decrease in this ratio with increasing severity of DCM was driven by reduced myocardial PCr levels although ATP was also reduced in end-stage HF (Figure 1.8). ATP levels are sustained during the early-stages of HF and decrease only during advanced stages of the disease by 30-40% (Starling et al., 1998, Beer et al., 2000, Shen et al., 1972). The heart therefore has the capacity to buffer its ATP pool given the integral importance of this molecule to cardiac function and survival. The CK shuttle (discussed in Section 1.3.2) is a key mechanism by which ATP levels are sustained and this has long been known to be deranged in the earlier stages of HF Herrmann et al (1939). Nascimben et al (1996) observed reduced CK activity in hearts from HF patients as well as an altered CK isoenzyme profile compared with non-failing control hearts (failing hearts exhibited lower cytosolic CK_{MM} and mitochondrial CK but lower cytosolic CK_B). Creatine levels

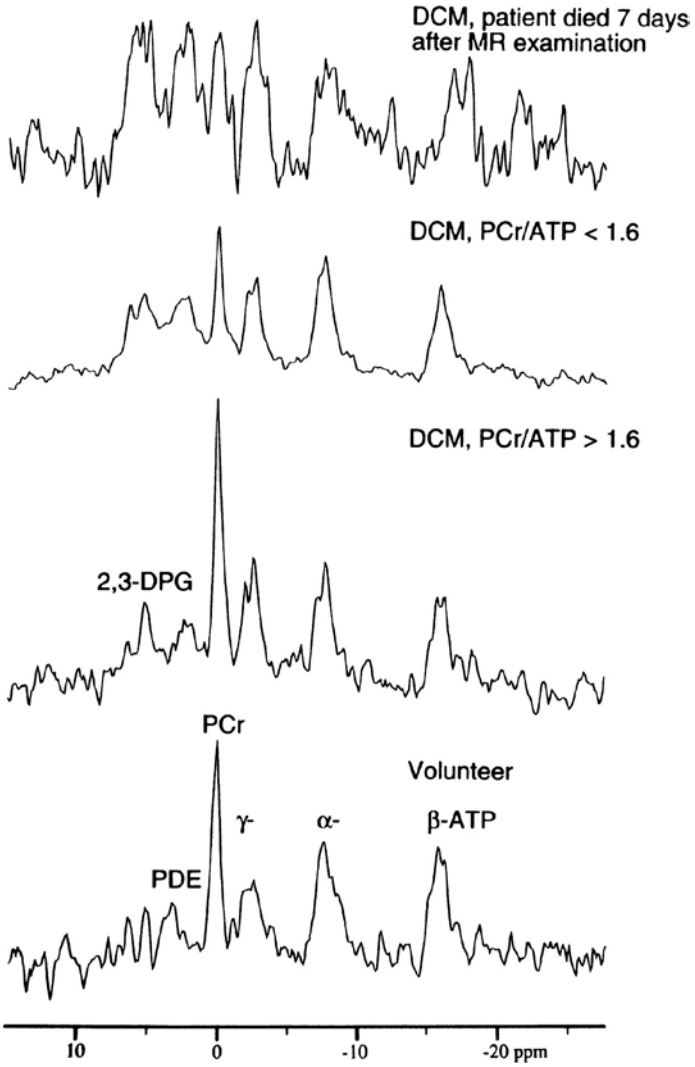

Figure 1.8 ^{31}P nuclear magnetic resonance spectra of a healthy volunteer and three dilated cardiomyopathy (DCM) patients.

PCr:ATP ratio appears to be inversely related to the severity of DCM and prognosis thereof. Abbreviations: magnetic resonance (MR); 2,3-diphosphoglycerate (2,3-DPG); phosphocreatine (PCr); adenosine triphosphate (ATP, 3 peaks representing γ, α and β phosphates); phosphodiester (PDE). Taken from Neubauer et al (1997).

were also significantly lower in failing hearts in this study. This is consistent with the findings of Beer et al (2002) that PCr is 51% lower in patients with DCM-induced HF

compared with normal counterparts. It is speculated that this PCr reduction is, in part, due to reduced creatine transport (Neubauer et al., 1999, Ten Hove et al., 2005). The combined loss of PCr and ATP represent a significant reduction in energy reserve associated with HF which may precede contractile dysfunction (Liao et al., 1996).

1.6 Is there a causal link between $[Na]_i$ overload and bioenergetic remodelling in the hypertrophied/failing heart?

In spite of significant evidence to support the occurrence of both $[Na]_i$ overload and bioenergetic remodelling during cardiac hypertrophy and HF, there have been very few studies investigating the interaction between these pathophysiological events.

Using isolated mitochondria from healthy rat heart, Iwai et al (2002) demonstrated that increasing extramitochondrial Na^+ from physiological (12.5mM) to supraphysiological (≥25mM) concentrations significantly reduced state 3 respiration, inferring reduced mitochondrial ATP supply under these conditions (Table 1.3). The authors also measured mitochondrial membrane potential and found that this was also reduced by supraphysiological levels of extramitochondrial Na^+. The authors did not investigate the mechanism underlying this effect of Na^+ overload on metabolism.

However, this has been elucidated in a series of studies focused on the mitochondrial transport of Na and Ca^{2+} and its relationship with mitochondrial ATP production. At the time of the Iwai et al (2002) study, there was much data to support the stimulation of mitochondrial ATP production by Ca^{2+} (discussed in Section 1.3.3) but Ca_m transport kinetics and its regulation by $[Na]_i$ was incompletely understood. It was known that

Table 1.3 Effect of increasing extramitochondrial Na^+ concentration on state 3 respiration.

	Concentration (mM)	State 3 respiration (n atom O/min/mg protein)	
		Before washing	After washing
Control		248±20	254±22
Sodium chloride	12.5	245±11	239±20
	25	207±19*	211±16*
	50	171±11*	168±17*
Sodium lactate	12.5	226±26	215±29
	25	178±15*	173±15*
	50	109±11*	105±9*

Values denote mean ± SEM (n=4/condition).*P<0.05 vs control group. Taken from Iwai et al (2002).

Ca^{2+} uptake was driven mainly by the mitochondrial Ca^{2+} uniporter (MCU) and that the mitochondrial Na^+/Ca^{2+} exchanger (NCLX) was the predominant mechanism for Ca^{2+} extrusion (Huser et al., 2000). However, it was equivocal whether Ca_m was altered on a beat-to-beat basis with large transients or over a slower time-period where beat-to-beat changes are small.

With respect to the regulation of $[Ca]_m$ by $[Na]_i$, Cox et al (1993) used the fluorophore, fura-2, to measure $[Ca]_m$ in isolated cardiac mitochondria from healthy rabbits. Mitochondria were incubated at increasing concentrations of extramitochondrial Na^+ ($[Na]_{ex}$) using NaCl and measurements of NADH production and state 3 respiration were carried out in the absence or presence of various inhibitors of NCLX (from highest to lowest potency: CGP-37157 > clonazepam > d-cis-diltizam) and the MCU inhibitor,

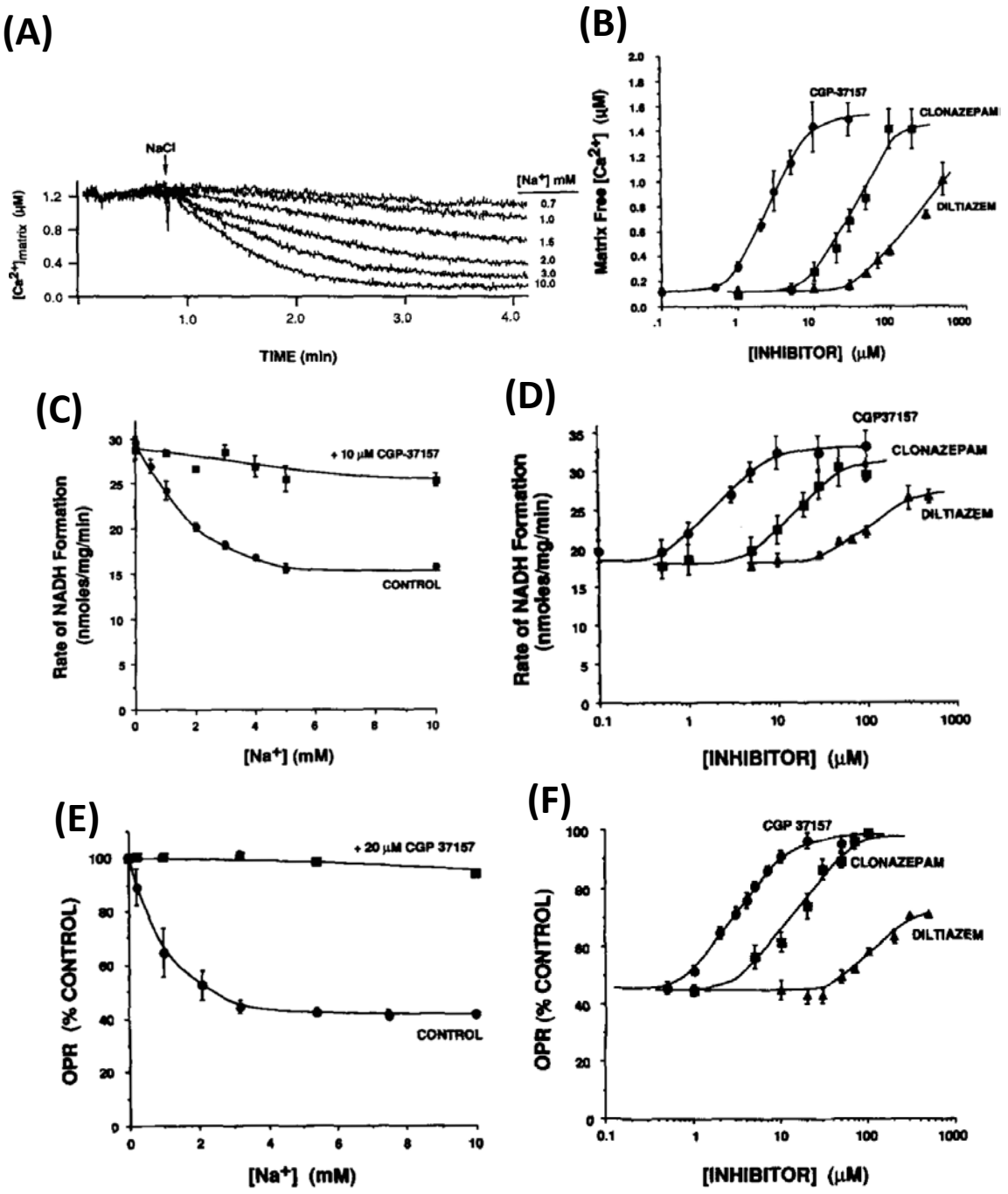

Figure 1.9 Effect of extramitochondrial [Na^+] ($[Na]_{ex}$) elevation and NCLX inhibition on $[Ca]_m$, NADH formation and oxidative phosphorylation rate (OPR) in isolated mitochondria.

(A) Time-course of mitochondrial calcium concentration ($[Ca^{2+}]m$) with increasing $[Na]_{ex}$. **(B)** NADH formation **(D)** and OXPHOS (F) with 10mM [Na]ex and increasing concentrations of various mitochondrial Na^+/Ca^{2+} exchange (NCLX) inhibitors. NADH formation **(C)** and OPR **(E)** with fixed NCLX inhibitor (CGP-37157) concentration (10 and 20 μM respectively) and increasing $[Na]_{ex}$. All experiments used 1 μM ruthenium red (mitochondrial calcium uniporter inhibitor). Adapted from Cox et al (1993).

ruthenium red. Increasing $[Na]_{ex}$ in the physiological range reduced $[Ca]_m$ (Figure 1.9A), NADH production (Figure 1.9C) and oxidative phosphorylation (Figure 1.9E) in a dose-dependent manner (Figure 1.9A). Inhibition of NCLX substantially increased $[Ca]_m$ (Figure 1.9B), NADH production (Figure 1.9D) and oxidative phosphorylation (Figure 1.9F) in a dose-dependent manner using all three inhibitors (in accordance with their relative potencies).

This study supported the findings of Iwai et al (2002) and thus provided weight to the hypothesis that $[Na]_i$ overload deranges ATP supply-demand matching. However, this study did not provide information on the beat-to-beat kinetics of $[Ca]_m$ transport and its relation to mitochondrial energy production. Moreover, isolated mitochondria experiments should be treated with caution given the measurements are performed in the absence of important ATP sinks (myosin ATPase, NKA and SERCA) and substrate utilisation pathways (glycolysis and β-oxidation).

More recently, Maack et al (2006) reported findings in isolated cardiomyocytes from healthy guinea pig heart. A novel method was developed to measure both $[Ca]_i$ and $[Ca]_m$ during systole and diastole in the same cell, thereby providing information on the beat-to-beat regulation of $[Ca]_m$ handling during conditions of increased workload and increased $[Na]_i$ in intact cells. NADH was also measured in these experiments using autofluorescence to give an indication of bioenergetic status under these conditions. As anticipated, isoproterenol increased systolic $[Ca]_i$ (Figure 1.10A) which decreased following washout and was slightly higher in the high $[Na]_i$ group throughout the protocols although was not statistically significant. Diastolic $[Ca]_i$ was unaffected by isoproterenol and high $[Na]_i$. Interestingly, systolic $[Ca]_m$ (Figure 1.10B) slowly tracked

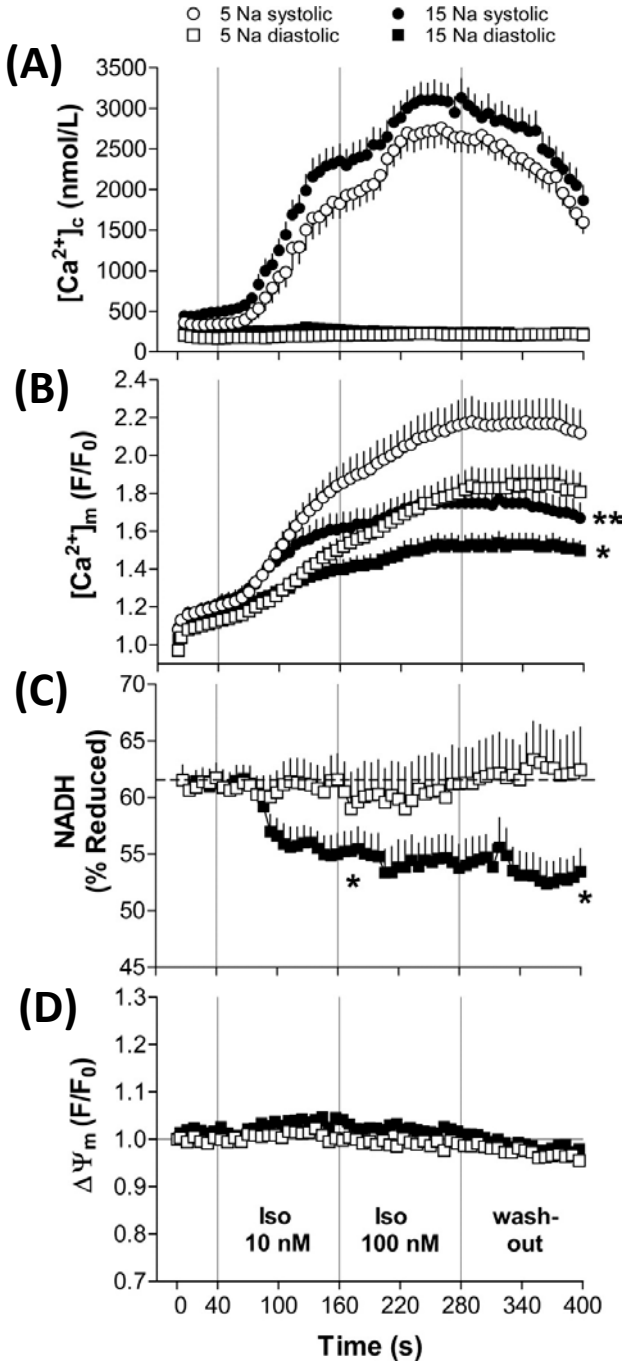

Figure 1.10 Effect of $[Na]_i$ elevation on systolic and diastolic Ca^{2+}, NADH and mitochondrial membrane potential in isolated cardiomyocytes.

Isolated guinea pig cardiomyocytes were patch-clamped, paced at 3 Hz and **(A)** $[Ca^{2+}]_c$, **(B)** $[Ca2+]_m$, **(C)** mitochondrial membrane potential ($\Delta\Psi_m$) and **(D)** NADH were monitored using indo-1, rhod2-acetoxymethyl ester, tetramethyl rhodamine and autofluorescence (λem=450nm), respectively. Symbols and error bars denote mean ± SEM (n=8-38 cells per measurement). White and black symbols represent 5 mM and 15 mM $[Na]_i$ in the pipette solution, respectively. *P<0.05, **P<0.01 vs 5mM $[Na]_i$. Taken from Maack et al (2006). Abbreviations: isoproterenol (Iso).

systolic $[Ca]_i$ and appeared to be reduced at a much slower rate during the washout period than $[Ca]_i$. Diastolic $[Ca]_m$ was also elevated during isoproterenol incubation with similarly slow kinetics. Both systolic and diastolic $[Ca]_m$ were significantly reduced by $[Na]_i$ elevation and this difference was sustained even by the end of the washout period.

Correspondingly, the percentage of NAD(H) in the reduced form was maintained at around 62% in the control group (Figure 1.10C) but started to decline shortly after the addition of isoproterenol in the high $[Na]_i$ group. NADH was significantly lower in the high $[Na]_i$ group versus control and continued to decline even during the washout period. In spite of these changes in $[Ca^{2+}]$ and [NADH], $[Na]_i$ elevation did not affect the mitochondrial membrane potential ($\Delta\Psi_m$) (Figure 1.10D). Furthermore, NCLX inhibition by CGP-37157 was shown to significantly elevate diastolic $[Ca]_m$. Using time-resolved fluorescence measurements, it was also demonstrated that high Na^+ significantly reduced the amplitude and decay of $[Ca]_m$ and also increased the time to peak value. As these effects were not altered by ruthenium red inhibition of the MCU, it is likely a consequence of increased Ca_m extrusion via NCLX on a beat-to-beat basis.

This series of experiments by Maack et al (2006) gave yet more strength to the argument that $[Na]_i$ is an important regulator of cardiac bioenergetics. However, it remains unclear whether this is truly reflective of a regulatory mechanism in the beating heart and, if so, which metabolic pathways are most affected by $[Na]_i$ overload.

1.6.1 The need for a $[Na]_i$-overloaded beating heart preparation.

In order to elucidate the importance of the link between $[Na]_i$ and ATP supply-demand matching in the beating heart, a preparation is required in which a heart can be perfused under physiologically-relevant conditions and in which $[Na]_i$ elevation can be induced and reliably measured. It is also necessary to be able to quantify a wide-range of metabolites involved in energy homeostasis in these hearts. The model of choice in this thesis was the isolated rat heart in the Langendorff mode perfused with ouabain to induce $[Na]_i$ overload. Given the established importance of ATP demand to energy mismatching, this model can also be used in conjunction with electrical pacing or electromechanical uncouplers in order to assess the effects of altered workload. It can also be used in conjunction with NMR thereby permitting the real-time measurement of $[Na]_i$ by ^{23}Na NMR, cardiac energetics by ^{31}P NMR, as well as end-point measurements of metabolites in myocardial tissue and coronary effluent using, for example, NMR and mass spectrometry. Indeed, many studies (particularly those of Denton and Maack) point toward an integral role of the TCA cycle in the sodium-dependent derangement of energy balancing in the heart. However, there have been no reports of specific measurements of its intermediates (nor any other intermediary pathway contributing to ATP supply) in any experimental model of elevated $[Na]_i$.

Therefore, this project combines powerful analytical and biochemical tools in order to determine whether $[Na]_i$ overload alters ATP supply-demand matching in the beating heart.

1.7 Hypothesis

Elevation of $[Na]_i$ causes alterations in the TCA cycle and cardiac energetics in the isolated perfused rat heart. This will lead to a mismatch of ATP supply and demand independent of altered contractility.

1.8 Aims

In order to test this hypothesis, this thesis aims to:

- Investigate the dose-response relationship between ouabain concentration and $[Na]_i$ in both the beating and electromechanically-uncoupled perfused rat heart using ^{23}Na NMR.

- Ascertain the metabolomic profiles of beating and electromechanically-uncoupled perfused rat hearts exhibiting $[Na]_i$ elevation using high-resolution NMR and mass spectrometry.

- Monitor cardiac energetics in real-time during $[Na]_i$ elevation in the perfused rat heart using ^{31}P NMR.

- Measure the activity of the TCA cycle in $[Na]_i$ overloaded perfused rat hearts using ^{13}C isotopologue profiling.

2 METHODS

2.1 Langendorff Heart Perfusions

2.1.1 General Principles

The concept of using beating hearts *ex vivo* for studying cardiac physiology dates back to the 19th century, pioneered by Loebel, Ludwig and Cyon using the frog and later by Oscar Langendorff using retrograde perfusion of the mammalian heart (Zimmer, 1998). The Langendorff heart perfusion technique has become an integral method for the study of contractile and electrophysiological function, arrhythmias, coronary vasculature, metabolism and pathophysiological mechanisms, to name but a few.

The technique involves arresting the heart in a cold cardioplegic solution followed by cannulation of the aorta and then perfusion with a crystalloid buffer closely resembling the ionic composition and pH of the blood, typically containing glucose as a fuel substrate and dissolved oxygen at 37 °C. It is crucial that the heart is ischaemic for as little time as practically possible during this process to avoid either preconditioning (Awan et al., 1999) or irreversible damage that may have bearing upon the experimental data subsequently obtained. Perfusing the heart retrogradely with a crystalloid buffer causes the aortic valve to close due to the exerted perfusion pressure. Perfusate is thereby directed through the coronary ostia of the aortic root into the coronary vasculature. Perfusate then flows into the coronary sinus via the coronary veins and out of the heart from the right atrium. The ventricles are therefore essentially fluid-free in this preparation. In a healthy preparation, the arrested heart will begin to contract almost

immediately upon reperfusion as the cells return to normothermia and the supply of essential ions is resumed.

The key advantages of the Langendorff perfused heart preparation include its relatively simple technical setup and perfusion buffer preparation, high reproducibility, intact autoregulatory mechanisms, isolation from neurohumoral effects that can confound several cardiac properties and the ease of carrying out pharmacological interventions dynamically with real-time functional measurements. A further advantage more specific to this thesis is that it can be used in conjunction with real-time nuclear magnetic resonance spectroscopy (NMR) measurements (discussed in Section 2.2). However, the isolated perfused heart is clearly far less physiological than the *in vivo* situation and therefore can exhibit effects that are specific to the *ex vivo* preparation. For example, coronary flows are substantially higher *ex vivo* in order to compensate for the reduced ability to carry oxygen (due to lack of haemoglobin) and changes in the viscosity of the perfusion medium. Moreover, the Langendorff preparation does not carry out "work" and thus ATP demand is lower than that in the isolated working heart preparation or *in vivo* (Wengrowski et al., 2014). Notwithstanding the limitations of the Langendorff heart, it provides a reliable means by which to compare cardiac function, ion homeostasis and metabolism between control and treatment groups under tightly controlled and near-physiologic conditions.

2.1.2 Setup

A diagram of a basic Langendorff perfused heart setup is displayed in Figure 2.1. The

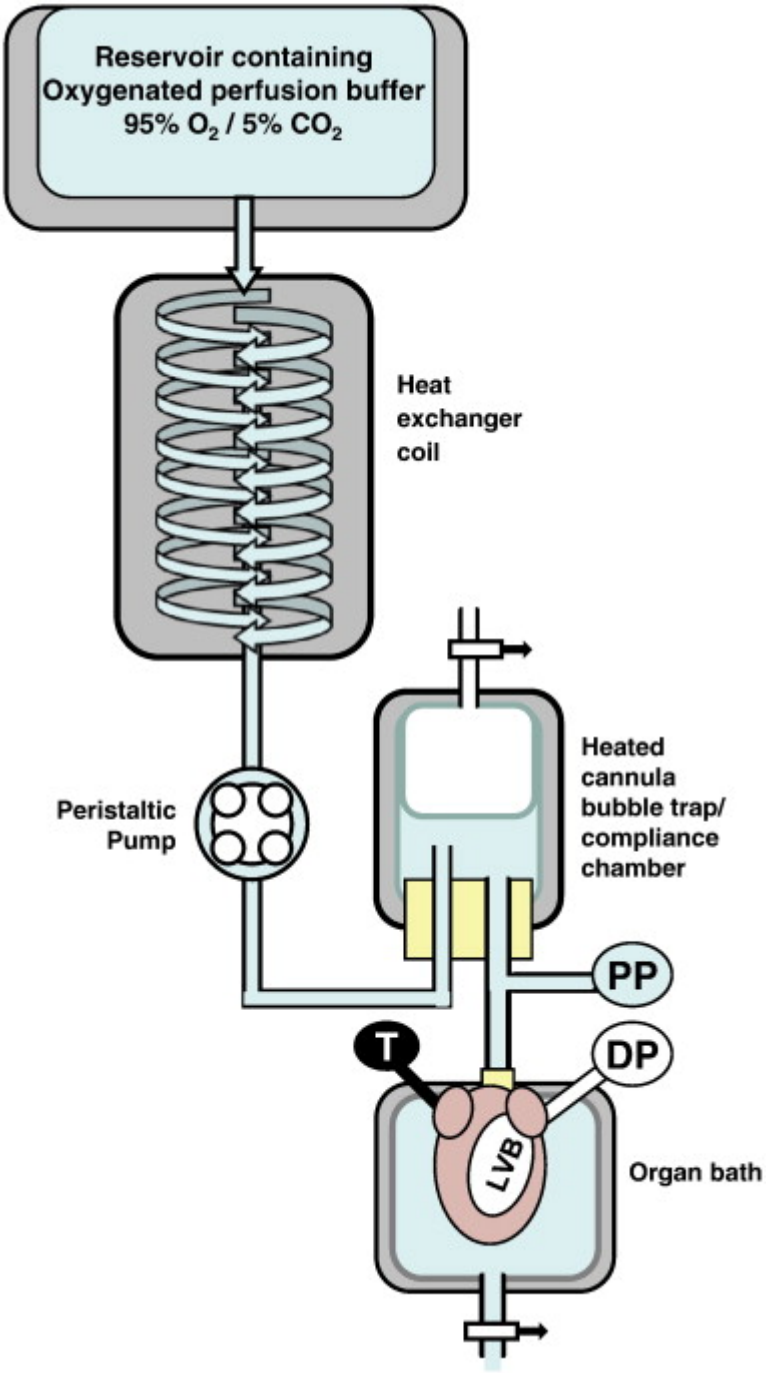

Figure 2.1 Schematic of a generic Langendorff heart perfusion setup.

See text for full details. Abbreviations: thermocouple (T); perfusion pressure transducer (PP); developed pressure transducer (DP); left ventricular balloon (LVB). Image taken from Bell et al (2011).

perfusion rig used for the hearts that were not subjected to NMR measurements consisted of the following: steel cannula (~3mm diameter; made in house), pressure transducer (Cat # 682021, BD Bioscience) to monitor perfusion pressure, left-ventricular water-filled balloon (consisting of a plastic 16 G x 2" intravenous Argyle Medicut™ cannula (Covidien, USA), approximately $2cm^2$ piece of cling film wrap and approximately 300µL distilled water at maximal inflation) attached to a pressure transducer (Cat # 682021, BD Bioscience), water-jacketed delivery tube, Minipuls 3 peristaltic pump (Gilson Inc, USA) with STH Pump Controller (ADInstruments, Australia) to permit switching between constant flow and constant pressure (Shattock et al., 1997), three water-jacketed glass reservoirs (~500mL) for perfusion fluid with sintered base and sintered glass gassing sticks. Perfusion fluid was gassed continuously with carbogen (95% O_2 and 5% CO_2) and plastic tubing clips were located close to the aortic cannula to either direct the KH into the heart or re-circulate when not in use negating undesired switching effects on the heart. All water-jacketed apparatus were connected to a C-85A water circulator (Techne, UK) set to 38°C giving a perfusate temperature of 37°C. Both pressure transducers were calibrated at the beginning of each day using a sphygmomanometer, as was coronary flow rate by the collection of perfusate into a measuring cylinder for one minute. The pressure transducers were fixed at an identical height to the heart to ensure accurate pressure recordings. These transducers (ADInstruments, Australia) were connected via Bridge Amps (4 kHz sampling rate) to a PowerLab 8/30 (ADInstruments, Australia) interface (ADInstruments, Austalia) and the peristaltic pump was connected to this interface directly.

2.1.3 Perfusion buffers

All water used was ultrapure (>18MΩ) using an Elga Purelab Option-Q system. Unless otherwise stated in the chapter-specific methods section, all perfusates were based upon Krebs-Heinseleit buffer (KH) and consisted of the following: 118.5 mM NaCl, 1.4 mM $CaCl_2.2H_2O$, 25.0 mM $NaHCO_3$, 1.19 mM MgSO4.$7H_2O$, 1.75 mM KCl and 11 mM glucose (all from ThermoFisher, UK) dissolved in ultrapure distilled water which had been pre-gassed with carbogen for 20 minutes (hereafter referred to as 'KH'). This was filtered using a Buchnor flask with a 5.0μm Whatman pre-filter (cat# 7195-004) and 0.2μm Whatman filter (cat# 1820-047). KH was phosphate-free to allow comparisons to be made between data from ^{31}P NMR experiments (in which phosphate must be absent from KH to avoid interference with the measurement of endogenous inorganic phosphate) and other experiments.

2.1.4 Animals

Male Wistar rats weighing ~300 g (Envigo, UK) were used for all heart perfusion experiments. Animals were able to access drinking water and a standard diet *ab libitum*. All experiments were performed in accordance with the Home Office guidance in the Operation of the Animals (Scientific Procedures) Act 1986. Animals were anaesthetised by intraperitoneal injection of approximately 170 mg/kg Pentoject pentobarbitone sodium (Animalcare Limited, UK) per kg body weight and approximately 160U heparin (Wockhardt UK ltd). Unconsciousness was confirmed by the absence of a pedal-withdrawal response.

2.1.5 Excision and perfusion setup

Using surgical scissors (Fine Science Tools, Heidelberg), a large incision was made across the abdomen of a rat and then through each side of the rib cage until the clavicles were reached. The diaphragm was incised and the rib cage was inverted, revealing the thoracic cavity. The pericardium was subsequently incised and the beating heart was gently moved away from the thoracic cavity by hand, the lungs were pared away and the heart was released via a single incision of the great vessels and then placed into an arresting solution (KH at 4°C) which was rapidly weighed using a TE162 balance (Sartorious, UK) thus giving the wet weight of the heart. Within one minute of arrest, the heart was revived by cannulation of the aorta and perfusion with carbogenated KH at ~37 °C in the Langendorff mode at 10 mL/min constant flow. The aorta was secured to the cannula using a silk suture and non-myocardial tissue was carefully removed before making a small incision in the pulmonary artery to aid the extrusion of effluent from the preparation. A Traceable™ thermocouple probe (Fisher Scientific, UK) was carefully inserted into the right ventricle via the pulmonary artery to confirm a temperature of 36.5-37.2 °C. A deflated intraventricular balloon (IVB) was carefully inserted through the mitral valve via the left atrium and then into the left ventricle. The IVB was slowly inflated by addition of ~100-150 µL ddH_2O to give a left ventricular end-diastolic pressure (LVEDP) of 3-10 mmHg to reflect the *in vivo* range (Fletcher et al., 1981). The setup was then changed to constant pressure mode (73-74 mmHg) which was maintained throughout the entirety of the perfusion protocol. The heart was then positioned in the centre of an organ bath, covered with a piece of parafilm and a clamp was tightened slightly around the exit tubing of the organ bath. This helped to maintain a constant temperature and humidity in the bath during perfusion. All

perfusion protocols included an initial stabilisation period of at least 20 minutes with standard KH to assess whether the heart was acceptable for use in the final dataset based on pre-determined exclusion criteria.

2.1.6 Exclusion Criteria

Hearts were excluded from the final dataset if they exhibited a mean LVDP of less than 80 mmHg with LVEDP set between 3 and 10 mmHg, a mean coronary flow of less than 7 mL/min or a mean heart rate of less than 250 BPM. Furthermore, hearts were immediately excluded if ventricular fibrillation occurred at any point during the stabilisation period.

2.1.7 Electrical pacing

Electrical pacing was used in experiments that required artificial control of heart rate. Bipolar pacing was via an active fine silver-wire electrode impaled into the apex of the left-ventricular referenced to the stainless steel aortic cannula. The cannular and pacing wire were connected to a Multistim System-D330 (Digitimer, UK), a Powerlab™ interface (ADInstruments, Australia) and Labchart software version 7 (ADInstruments, Australia). Square step pulses of 5 msec duration were applied to the frequencies specified in the individual protocols.

2.1.8 Electrocardiogram (ECG)

In studies where an ECG recording was made, these were recorded using similar electrode placements to those used for pacing. That is an apical silver wire recording electrode was referenced to the stainless steel aortic cannula. The ECG was recorded via a Bioamp and Powerlab™ running LabChart (v.7) (ADInstruments, Australia) and sampled at 4 kHz.

2.1.9 Snap-freezing of perfused hearts

At the end of perfusion, the IVB (and pacing/ECG wires if applicable) were carefully removed from the heart. Exempting the aorta, all non-ventricular tissue was rapidly excised from the beating heart using surgical scissors (Fine Science Tools, Germany) and the ventricles were then snap-frozen *in situ* using Wollenberger clamps pre-cooled in liquid nitrogen for five minutes. The clamps were then carefully pulled away from the perfusion cannula thereby separating the ventricles from the aorta and residual aortic tissue and frozen perfusion buffer were rapidly excised from the ventricles. The ventricles were stored at -80°C until analysis. The process described above was completed within one minute.

2.1.10 Data acquisition and processing

All perfusion data were acquired using LabChart software Version 7 (ADInstruments, Australia) and processed using LabChart 8 (ADInstruments, Australia). Left ventricular

pressure (LVP), perfusion pressure, coronary flow, peak systolic pressure (PSP; derived from LVP), heart rate (derived from LVP), LVEDP (derived from LVP) and left ventricular developed pressure (LVDP, Equation 2.1) were acquired for all hearts. LVDP was used as an indicator of contractile "effort".

$$\mathrm{LVDP} = \mathrm{PSP} - \mathrm{LVEDP} \qquad \textit{Equation 2.1}$$

where, LVDP = left ventricular developed pressure (mmHg)

PSP = peak systolic pressure (mmHg)

LVEDP = left ventricular end-diastolic pressure (mmHg)

All perfusion parameters were averaged into five minute time windows using MS Excel. For ECG recordings, the time from the onset of activation to 90% recovery of repolarization (QT90%) values of the final five complexes in each treatment period were manually determined from the ECG trace and averaged for each heart. Heart rate from ECG recording was calculated automatically using the ECG analysis feature of LabChart and averaged into five minute time windows using MS excel. All averaged data were plotted as mean ± standard error of the mean (SEM) using GraphPad Prism version 5 (Graphpad Software Inc., USA).

2.2 Assessment of cardiac metabolism and $[Na]_i$ by nuclear magnetic resonance spectroscopy (NMR).

NMR is a powerful tool for the real-time assessment of ion homeostasis and cardiac energetics in the Langendorff perfused heart (reviewed in Singhal et al., 2009). In this thesis, ^{23}Na NMR and ^{31}P NMR were used to measure $[Na]_i$ and high energy phosphates respectively under both control and high $[Na]_i$ conditions.

2.2.1 General Principles of NMR

Nuclei comprising an odd number of nucleons (protons and neutrons) exhibit net nuclear spin and thereby possess a magnetic moment. When placed into a magnetic field, these nuclei are quantised either in alignment with or in opposition to the external magnetic field. For a spin I = ½ nucleus such as ^{1}H or ^{31}P the different energy levels are populated according to the Boltzmann distribution (Equation 2.2).

$$\frac{Ni}{Nj} = e^{(-\frac{\Delta E}{kT})} \qquad \textit{Equation 2.2}$$

where,

Ni = Number of nuclei in upper energy state.

Nj = Number of nuclei in lower energy state.

ΔE =Energy difference between nuclear spin states.

k = Boltzmann constant = 1.38×10^{-23} J K^{-1}.

T = Temperature (in K).

The energy difference (ΔE) is small compared to the thermal energy (kT) and therefore lower or higher spin states have approximately equal populations (i.e, Ni/Nj ≈1). However, a small population difference exists which can be detected by NMR. Excitation of the spins with a radio frequency pulse causes them to be excited and then undergo precession which is quantified according to the Larmour Frequency (Equation 2.3).

$$\omega_0 = \gamma \cdot B_0 \qquad \textit{Equation 2.3}$$

where,

ω_0 = Larmor frequency (MHz).

γ = Gyromagnetic ratio (magnetism:spin ratio, nucleus-specific, eg, ^1H = 42.5 MHz T^{-1}).

B_0 = External Magnetic Field (T).

When a radiofrequency (RF) pulse is applied (at the Larmour frequency of the nucleus of interest), resonance occurs exciting spins from the lower to the higher energy state. Upon removal of this radiofrequency pulse, the excited nuclei precess at their respective Larmor frequencies and return to their lower energy state via two relaxation processes: longitudinal recovery (or spin-lattice decay, T_1) or transverse recovery (spin-spin decay, T_2). Importantly, the precessing magnetic moment of the nuclear spin induces a current in the receiver coil of the NMR probe known as the free induction decay (FID), the magnitude of which is directly proportional to the number of nuclei present. Conversion

of the FID to an NMR spectrum using Fourier transformation permits integration of signals (peaks) from the nuclei of interest. For nuclei within molecules, different chemical shifts of the peaks arise due to differences in electron shielding within the molecule. The area (integral) of a peak is proportional to the abundance (concentration) of that nucleus within the sample. In order to maximise signal-to-noise (S:N) of the analytes of interest, multiple 'scans' of the sample are summed, where one scan encompasses one RF pulse sequence in which nuclei are excited and then allowed to relax. For n number of scans, the signal increases according to n and the noise by $n^{1/2}$, thus the S:N increases by $n^{1/2}$ (for example, 100 scans of a sample increases S:N by 10-fold). Comparing the areas of an NMR peak in a control and treatment sample (be it a solution or whole organ) gives a semi-quantitative measure of the relative change in the concentration of that analyte due to the treatment. An internal standard can be added to the sample in order to quantify absolute concentrations of metabolites.

Two modes of NMR were used in this thesis: real-time NMR measurements of isolated perfused hearts (discussed in sections 2.2.2) and high-resolution NMR of aqueous metabolite extracts from snap-frozen myocardial tissue (discussed in Section 2.4.3).

2.2.2 NMR measurements of the isolated perfused heart (setup)

The setup for ^{23}Na NMR and ^{31}P NMR measurements was identical other than different RF coils being used. The Langendorff perfusion rig setup was identical to that used for non-NMR studies but with the following alterations: four glass perfusion reservoirs; a long (~2 m) water-jacketed piece of plastic tubing between the peristaltic pump and cannula; a rigid plastic cannula; circulator for water-jacketing was set to 39 °C giving a

perfusate temperature of 37 °C at the aortic cannula; the heart was placed into an NMR tube rather than an organ bath; an exhaust line was connected to a second peristaltic pump so that there was a constant and steady removal of coronary effluent from the NMR tube throughout perfusion.

After setting up the isolated perfused heart preparation (as detailed in 2.1.5), the heart was carefully placed into a 15 mm NMR tube (OD 15 mm) (Wilmad, UK) and secured with a silicon cap through which the aortic cannula, tubing connecting the IVB to the LVP pressure transducer and exhaust sipper line were fixed. This NMR tube was then centred within an RF coil (either $^{1}H/^{23}Na$ or $^{1}H/^{31}P$ dual-tune coil) (Figure 2.2A) within a microimaging probe (Figure 2.2B). A Bruker Avance III 400 MHz (9.4T) wide-bore spectrometer (Bruker, Germany) (Figure 2.2C) with triple-axis gradients (kept at a constant temperature of ~313K using a second water circulator) was used for all real-time perfused heart NMR measurements. The resonance frequency was then optimised for the particular nuclei being measured by adjusting the tune and match controls on the appropriate channel of the probe. Magnetic homogeneity was optimised by fine tuning the shimming gradients in the *z*, z^2, z^3, *x* and *y* planes thus maximising S:N.

2.2.3 Assessment of $[Na]_i$ by triple quantum-filtered (TQF) ^{23}Na NMR.

The real-time measurement of $[Na]_i$ in the beating heart under near-physiological conditions is challenging. This is mainly because the Larmor frequency of the intracellular $[Na]_i$ and extracellular $[Na]_e$ pools is identical and, also, $[Na]_i$ is approximately 10-fold lower than $[Na]_e$. This results in a small $[Na]_i$ signal being

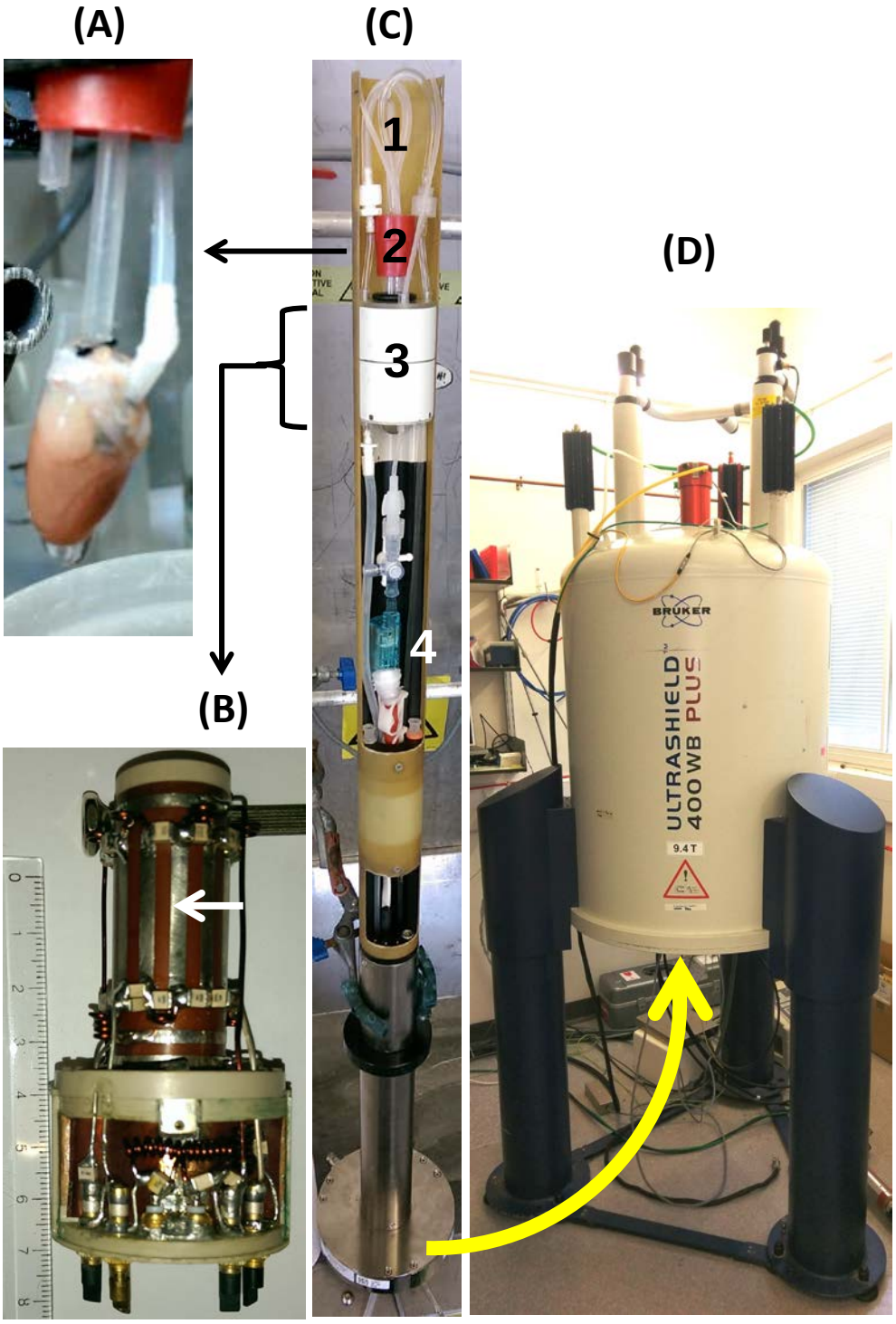

Figure 2.2 Photographs of the NMR perfusion setup.

(A) Isolated perfused rat heart. **(B)** Nuclear Magnetic Resonance (NMR) birdcage radiofrequency coil. Ruler units are centimetres. White arrow indicates the position at which the heart was centred. **(C)** NMR microimaging probe. 1: Inflow and exhaust lines; 2: 15 mm NMR tube centred in RF coil using rubber O-ring; 3: RF coil (Figure 2.2B) with protective casing; 4: left ventricular pressure transducer. **(D)** NMR spectrometer.

overlapped by a large $[Na]_e$ signal in the NMR spectrum and thus neither of these populations can be integrated under these circumstances. At present, there are two key approaches used to distinguish these populations: the use of shift reagents and triple quantum filtering.

NMR shift reagents, such as Tm(DOTP) (Buster et al., 1990), are labile anions that are unable to cross the sarcolemma and therefore bind only to $[Na]_e$ but not $[Na]_i$. The unpaired electron density of the paramagnetic shift reagent interacts with the magnetic dipole of Na^+ (known as the dipolar hyperfine mechanism) thereby shifting the Larmor frequency of $[Na]_e$ but not $[Na]_i$. This separates the spectral signals of $[Na]_e$ and $[Na]_i$ thereby permitting their quantification. The key issue with shift reagents is that, as anions, they are efficient chelators of Ca^{2+} and thereby alter contractile and electrophysiological properties of the heart (often inducing toxicity) and reduce the physiological relevance of the preparation.

Multiple quantum filtered ^{23}Na NMR permits less invasive and more physiological measurements of $[Na]_i$ in the absence of shift reagents. This approach relies on the differences in physicochemical environment of $[Na]_e$ and $[Na]_i$. The majority of $[Na]_i$ is bound to macromolecular structures (such as those in the sarcolemma or cytoskeleton) whereas the majority of $[Na]_e$ is in isotropic solution. As ^{23}Na is a spin 3/2 system, multiple quantum coherences can be induced and detected (Figure 2.3). Triple quantum filtered (TQF) and double quantum filtered (DQF) NMR pulse sequences both filter out the bulk isotropic signal leaving only anisotropic Na^+ signals; TQF giving rise mainly to intracellular Na^+ bound to macromolecules while DQF is selective for Na^+ bound to ordered structures in the extracellular space, for example, membranes and tissue fibres.

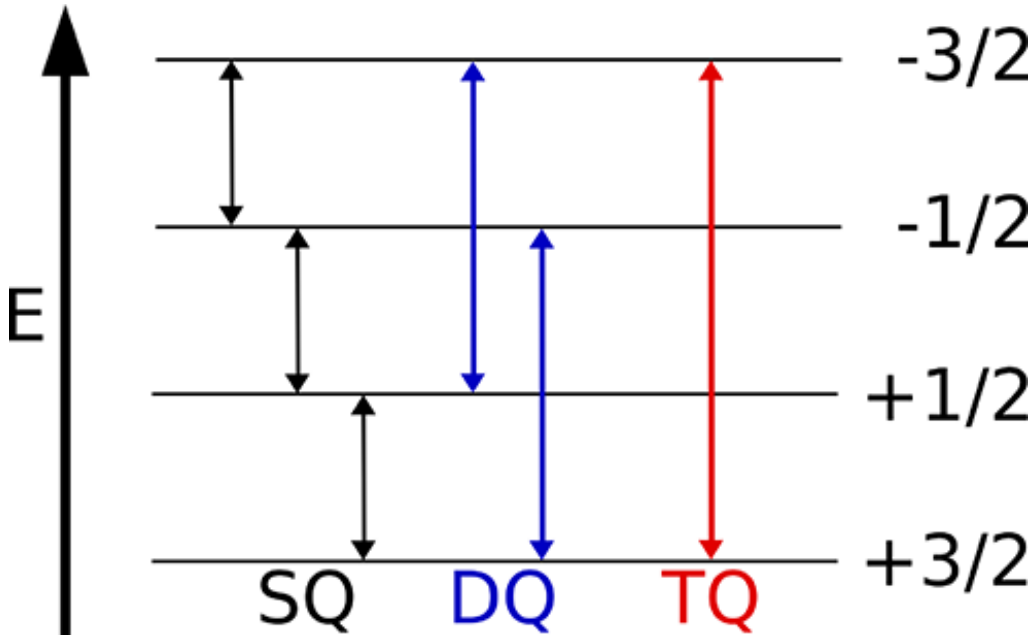

Figure 2.3 Multiple quantum coherences in ^{23}Na.

Spin 3/2 nuclei can exist in one of four energy states. Single quantum (SQ) transitions (black arrows) occur between neighbouring energy levels whereas double quantum (DF; blue arrows) and triple quantum (TQ; red arrow) transitions occur when nuclei skip one and two energy levels respectively. Image taken from Gottwald et al. (2016).

There have been numerous reports of this technique being utilised in conjunction with the isolated perfused rat heart (Payne et al., 1990, Dizon et al., 1996, Tauskela et al., 1997, Schepkin et al., 1998). The technique has previously been developed in our lab in the perfused mouse heart (Eykyn et al., 2015) showing that $[Na]_i$ contributes approximately 68% of the TQF signal and does not contribute to the smaller DQF signal. Therefore, assuming that $[Na]_e$ is constant then the TQF signal will be proportional to $[Na]_i$.

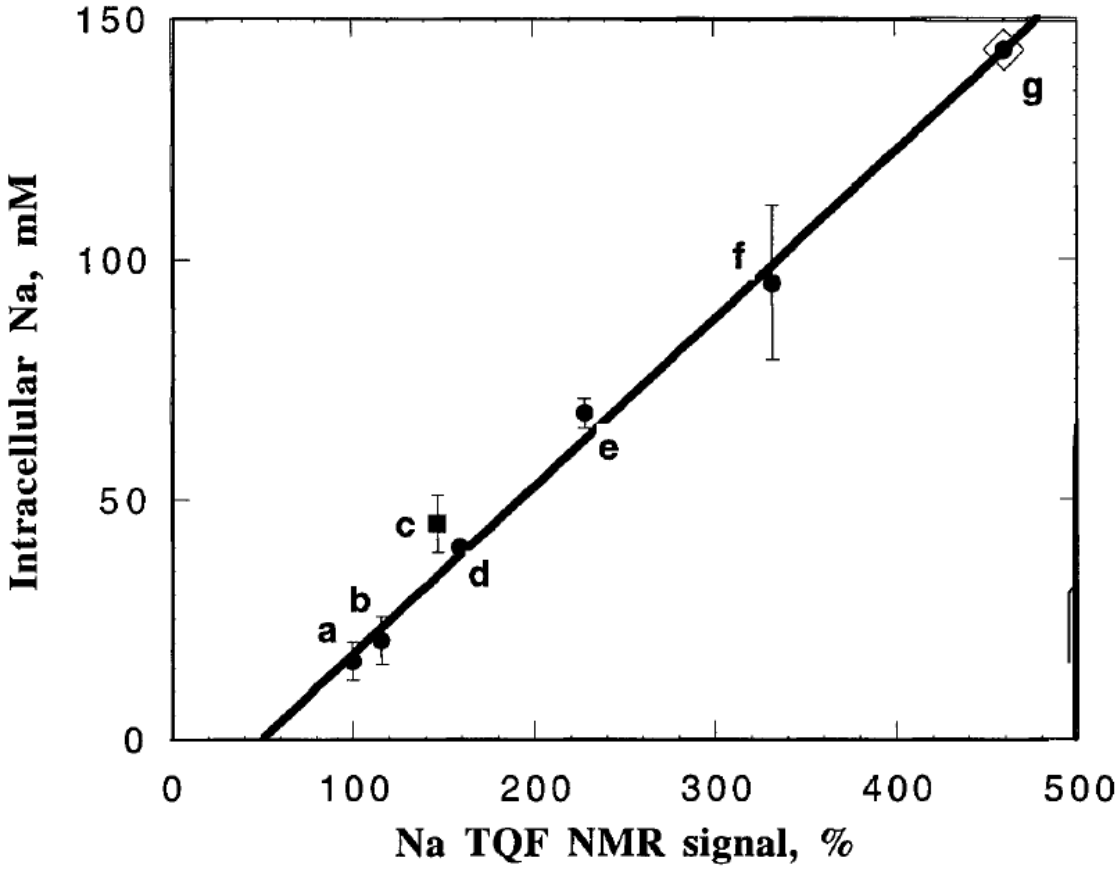

Figure 2.4 Correlation plot of $[Na]_i$ measured by ^{23}Na NMR with shift reagent vs TQF NMR signal in isolated perfused rat heart.

Baseline $[Na]_i$ is 17.5 mM according to the shift reagent experiments. a = normal; b = 200 µM ouabain with washout; c = stop-flow ischemia; d = 200 µM ouabain; e = K^+-free; f = Ca^{2+}-free ; g = K^+/Ca^{2+}-free. Image taken from Schepkin et al (1998).

In a similar study by Schepkin et al (1998), $[Na]_i$ was elevated to different extents (using stop-flow ischaemia, K^+-free KH, ouabain, Ca^{2+}-free KH and K^+/Ca^{2+}-free KH) in the Langendorff rat heart preparation and was measured using atomic absorption spectroscopy (AAS) as well as TQF. It was found that there was a very strong positive correlation ($r = 0.995$) between $[Na]_i$ measured by AAS and the TQF signal with a slope of 0.35 ± 0.015 mM/% and an intercept of 50 ± 5% (Figure 2.4). $[Na]_i$ was 17.5 mM in the normal heart under baseline conditions. These observations, combined with the technique previously implemented in our lab, formed the basis of the TQF measurements in this thesis. Therefore, the absolute $[Na]_i$ values reported in this thesis are derived using the Schepkin et al (1998) study.

In terms of ^{23}Na NMR data acquisition, alternating TQF and DQF measurements were performed in an interleaved fashion in order to assess $[Na]_i$ and $[Na]_e$ in real-time, respectively. The acquisition duration of each TQF and DQF spectrum was approximately 1.3 minutes and acquisition parameters were identical to those described in Section 2.3 of Eykyn et al (2015). Representative spectra from isolated perfused rat hearts under baseline conditions and perfused with increasing concentrations of ouabain are displayed in Figures 2.5A and 2.5B, respectively. Each TQF and DQF spectrum was magnitude-corrected and then baseline-corrected. Peak integration was performed automatically using TopSpin software (Bruker, Germany) and all peaks were integrated on the same scale to permit relative comparisons. Baseline integrals were averaged and then incorporated into Equation 2.4 to give an estimation of $[Na]_i$ at each time point. Correcting for differences in baseline measurements between hearts is important as the TQF and DQF signals are dependent upon the heart size/weight and the position of the

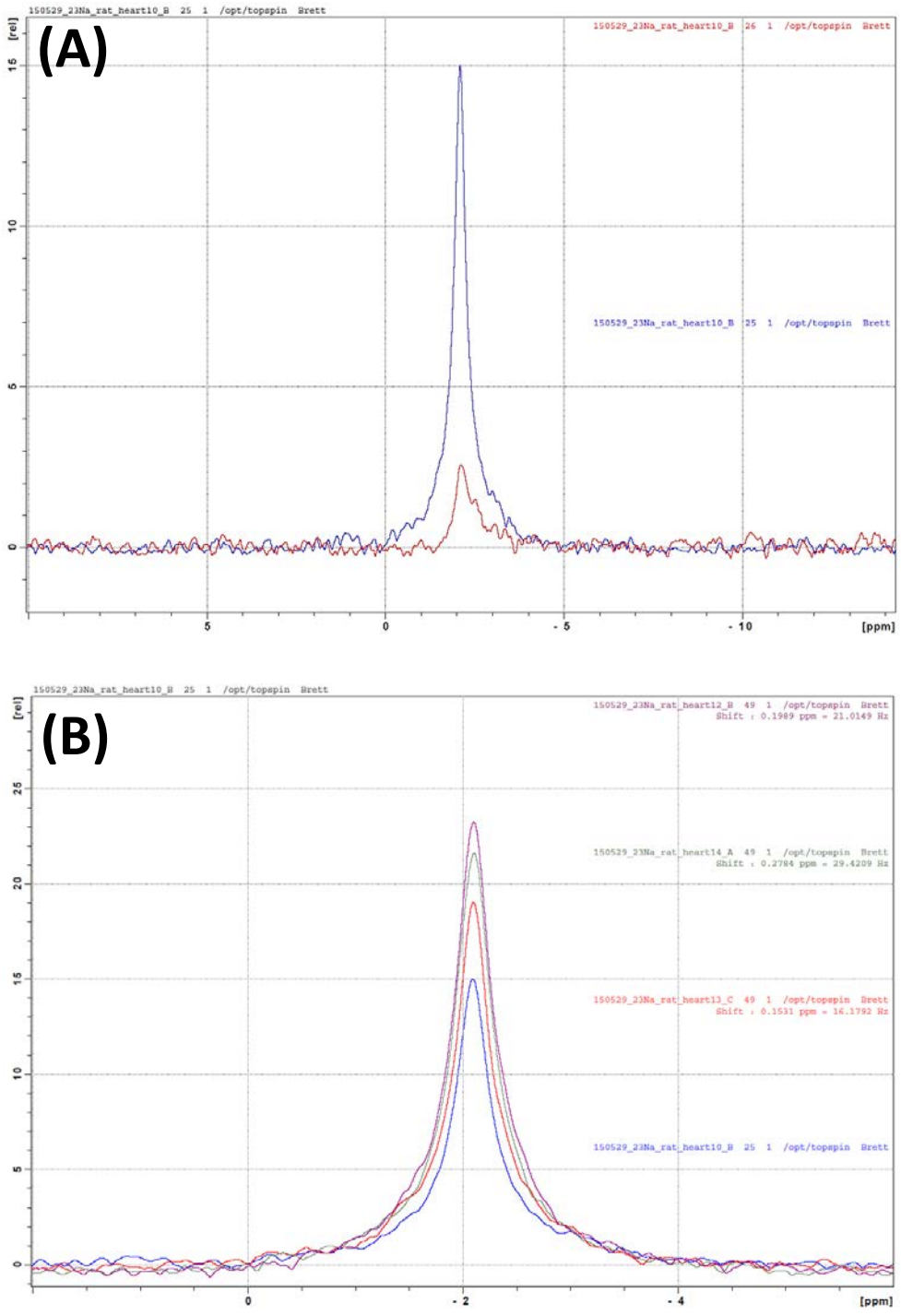

Figure 2.5 Representative ^{23}Na TQF and DQF NMR spectra of isolated rat hearts at baseline and perfused with ouabain.

(A) TQF (large blue peak) and DQF (small red peak) at baseline perfusion. **(B)** TQF signals increasing in height and area due to increasing ouabain concentration in the perfusate. From smallest to largest: baseline/0 µM ouabain (blue peak); 50 µM ouabain (red peak); 75 µM ouabain (green peak); 100µM ouabain (pink peak).

heart within the active region of the RF coil, which can both differ between experiments. ‘Normalised TQF’ and ‘normalised DQF’ herein refer to the measured signal normalised to its respective baseline value.

$[Na]_e$ was assumed to be linearly related to DQF and thus the reliability of Equation 2.3 was confirmed by an absence of change in the DQF signal over the time course of the experiment, as Schepkin et al (1998) showed that 50% of the TQF is attributable to $[Na]_e$.

$$[Na]_i = \left(\left(\frac{TQF}{TQF_{\bar{x}}} \text{ x } 100\right) - 50\%\right) \text{x } 0.35 \qquad \textit{Equation 2.3}$$

where,

$[Na]_i$ = Derived intracellular Na^+ (mM).

TQF = Integral of triple quantum filtered (TQF) ^{23}Na NMR signal at a particular time-point.

$TQF_{\bar{x}}$ = Mean integral of TQF ^{23}Na NMR signal during stabilisation period.

50% = Contribution of extracellular Na^+ to TQF ^{23}Na NMR signal.

0.35 = Slope of relationship between $[Na]_i$ and TQF ^{23}Na NMR signal in mM/%.

2.2.4 Assessment of cardiac energetics by ^{31}P NMR

The use of real-time ^{31}P NMR for the assessment of energetics in muscle dates back to the 1970s and is now widespread tool in cardiovascular research. Any metabolite containing ^{31}P at a concentration of at least ≈600 μM is detectable using this technique (Taegtmeyer et al., 2016). This includes inorganic phosphate (P_i), phosphocreatine

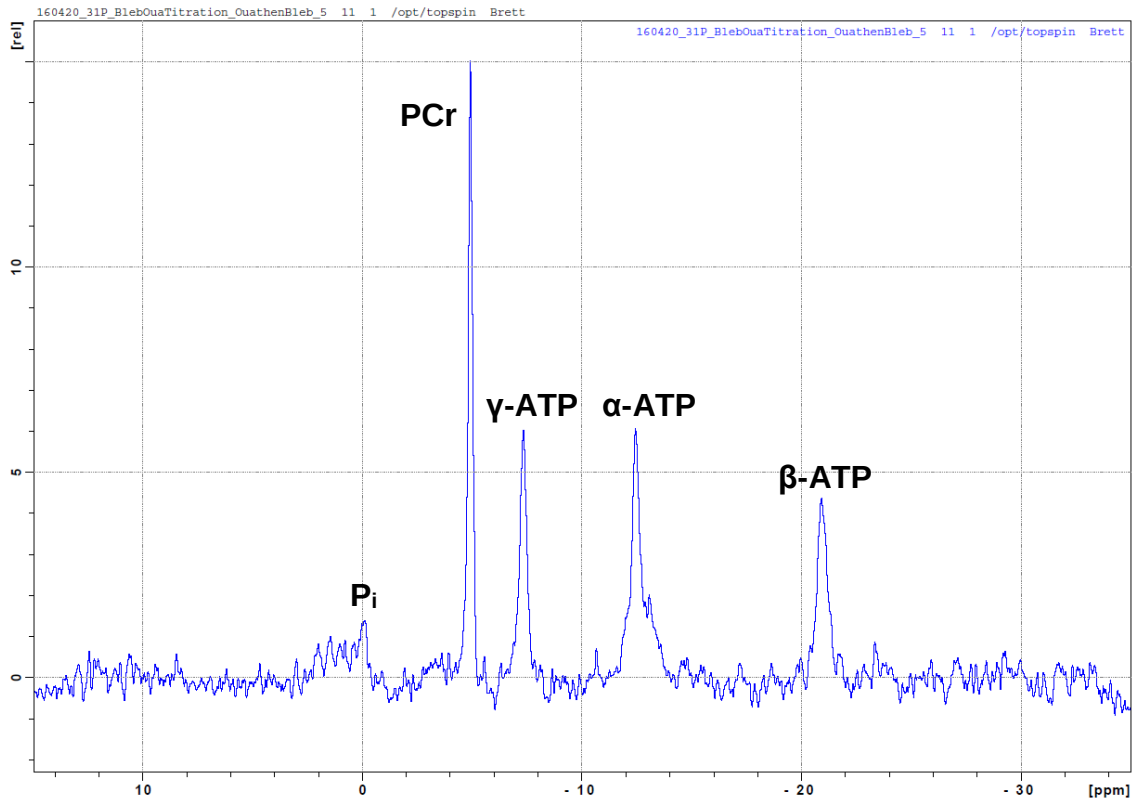

Figure 2.6 Representative ^{31}P NMR spectrum of an isolated perfused rat heart under normal baseline conditions.

As ADP and NAD contribute to the γ-ATP and α-ATP signals, respectively, only the β-ATP signal was used as a determinant of ATP concentration in the heart. The chemical shift difference of Pi and PCr in this example is 4.8ppm equating to an intracellular pH of 7.1. Abbreviations: intracellular inorganic phosphate (Pi); phosphocreatine (PCr).

(PCr) and ATP which are imperative to cardiac function and survival. Under certain conditions, monophosphate esters can be observed as well as glycolytic intermediates such as glucose-6-phosphate during hypoxia. This approach also permits the determination of intracellular pH which is linearly proportional to the difference in chemical shift between the P_i and PCr signals. In contrast to the measurement of $[Na]_i$ by ^{23}Na NMR, using ^{31}P NMR to assess P_i, phosphocreatine (PCr) and ATP does not require the perfusion of shift reagents or multiple quantum filtering as the Lamor

frequencies of these metabolites are different. However, given that ^{31}P is less NMR sensitive than ^{23}Na due to lower concentrations of these metabolites, longer acquisition times are required when measuring the former thereby reducing temporal resolution in order to give an acceptable S:N.

^{31}P NMR acquisition parameters were as per Wilder et al (2016) with the only difference being that each spectrum was obtained using 73 scans over a five minute period. Each spectrum (Figure 2.6) was phased and baseline-corrected and each peak was then integrated manually using the same scaling. To correct for differences in heart size/mass and position within the RF coil active region, each integral for all measured metabolites was divided by the mean PCr integral during the stabilisation (baseline) period. This also permitted direct comparison between the relative concentrations of PCr, ATP and P_i. Intracellular pH was calculated using Equation 2.4.

$$pH_i = 6.72 + \log \frac{\delta_{Pi} - 3.17}{5.72 - \delta_{Pi}} \qquad \textbf{\textit{Equation 2.4}}$$

where, (Sidell et al., 2002)

pH = Intracellular pH.

δP_i = Chemical shift difference between intracellular inorganic phosphate peak and phosphocreatine peak (ppm).

2.3 Lactate analysis of coronary effluent

Elevated extrusion of lactate from the myocardium is indicative of increased glycolytic activity and is a classic marker of metabolic stress (Becker et al., 2013, Mansor et al., 2016, Trueblood et al., 2000). Quantification of the lactate efflux rate in the isolated perfused heart is therefore a convenient way in which to gain an insight into the metabolic status of the beating myocardium under control and high $[Na]_i$ conditions without the need for challenging NMR protocols.

The 2300 STAT Plus (YSI, USA) is an enzyme-based electrode technique capable of quantifying lactate down to 1 µM in biological matrices. At the beginning of each day of analysis, the instrument was flushed thoroughly with YSI cleaning buffer (cat# 2357) and the current was allowed to stabilise. The instrument was then calibrated using 5 mM lactate calibration solution (cat# 2747). Coronary effluent samples were collected on ice and analysed immediately using 25 µL sample volume. Absolute lactate concentrations (mM) were incorporated into Equation 2.5 to give lactate efflux rate from each heart.

$$\text{Lactate efflux} = \frac{[\text{Lac}] \times 1000 \times \left(\frac{\text{CF}}{\text{Time}}\right)}{\text{Wet wt}} \qquad \textit{Equation 2.5}$$

where,

Lactate efflux = Efflux of lactate from the heart (nmol/min/g wet weight)

[Lac] = Lactate (mM) in coronary effluent according to 2300 STAT Plus.

CF = Coronary flow (mL/min) during collection of coronary effluent.

Time = Duration of coronary effluent collection (mins).

Wet wt = Weight of heart immediately before perfusion (g).

2.4 Metabolomic Profiling

2.4.1 General principles

Metabolomics (also known as metabonomics, metabolic profiling and metabolic fingerprinting) is becoming an increasingly important tool in several areas of research such as cardiovascular (Marcinkiewicz-Siemion et al., 2016), drug discovery (Cuperlovic-Culf and Culf, 2016, Wishart, 2016) and cancer (Mikkonen et al., 2016). Developments in the field of analytical chemistry have provided powerful tools (particularly NMR and mass spectrometry) for the simultaneous quantification of multiple metabolites in a single biological sample. Historically, mainly enzymatic/ spectrophotometric assays were used for this purpose but these are slowly being replaced by metabolomics approaches as its advantages are realised. There are two key modes of metabolomic analysis. 'Untargeted metabolomics' involves semi-quantitatively assessing hundreds or thousands of metabolites in order to identify potential biomarkers of, for example, a particular disease state. This is often used in the early stages of research and is useful for hypothesis generation. A more focused approach is known as 'targeted metabolomics' whereby a smaller number of known metabolites are measured with respect to a specific hypothesis on the role of a pre-selected metabolic pathway under a particular condition.

In this thesis, semi-targeted metabolomic evaluation of energy metabolism was achieved using NMR. In addition, mass spectrometry was utilised for targeted assessment of the TCA cycle and pyruvate.

2.4.2 Dual-phase extraction of metabolites.

The three key techniques used for the isolation of polar metabolites in biological matrices are dual-phase extraction, acetonitrile extraction and perchloric acid extraction (full methodological details can be found for each of these in Beckonert et al., 2007). The dual-phase extraction technique has also more recently been described by Chung et al. (2016). All three methods were trialled using snap-frozen tissue from perfused control rat hearts. Following reconstitution of lyophilised extracts, it was found that extracts from the acetonitrile and perchloric acid procedures were not translucent indicative of the presence of undesired lipid species. However, extracts derived from the dual-phase technique were translucent and NMR analysis did not detect the presence of lipid species in these solutions but was positive for several polar metabolites relevant to energy metabolism. The dual-phase extraction technique was therefore utilised for all metabolomic investigations in this thesis.

In brief, snap frozen rat heart was ground under liquid nitrogen, an aliquot (500-800 mg) was electromechanically homogenised in ice-cold methanol (2 mL/g tissue) followed by addition of water (total = 2.85 mL/g tissue) and chloroform (total = 2 mL/g tissue) with vortexing. Suspensions were centrifuged at 3600 RPM for one hour at 4°C. Three layers were formed: an upper aqueous layer containing small, polar entities; a middle solid layer containing protein and cell debris; and a lower lipophilic layer containing lipid species. For NMR analysis, the upper aqueous phase was subsequently added to a fresh Falcon tube containing 20-30 mg chelex-100 which was vortexed and centrifuged at 3600 RPM for 1 minute at 4°C. The supernatant was then added to a fresh Falcon tube containing 10-20 µL universal indicator followed by vortexing and

lyophilisation. For mass spectrometry analysis, the chelex-100 and universal indicator steps were omitted. Lyophilised extracts were stored at -80°C until analysis.

2.4.3 High resolution ^{1}H NMR of metabolite extracts

High resolution ^{1}H NMR provides a means by which to simultaneously quantify several organic entities within a single sample with high degree of precision and accuracy. Any molecule containing proton is detectable by this technique but NMR has relatively low sensitivity and often overlapping signals thus its applicability is limited to the more abundant metabolites in the heart. A key advantage, however, is that a single proton-containing internal standard can be used for the reliable quantification of all metabolites with an appropriate S:N.

^{1}H NMR was used to obtain a semi-targeted metabolomic profile. That is, some of the metabolites measured by this technique were directly relevant to the pre-defined hypothesis (perturbation of the TCA cycle and ATP production) whereas others were indirectly relevant (such as amino acid anaplerosis). Furthermore, ^{1}H NMR was only able to measure two TCA cycle intermediates (succinate and fumarate) with a generally poor S:N.

Lyophilised, dual-phase-extracted metabolites were reconstituted in 600 µL deuterium oxide (containing 8 g/L NaCl, 0.2 g/L KCl, 1.15 g/L Na_2HPO_4, 0.2 g/L KH_2PO_4 and 0.0075% w/v trimethylsilyl propanoic acid (TSP)) and adjusted to pH ≈6.5 using 1 M hydrochloric acid and/or 1M sodium hydroxide (<5 µL of each) prior to vortexing. The solution was transferred to a 5 mm NMR tube (Norel Inc., USA) and then analysed

using a Bruker Avance III 400 MHz (9.4 T) wide-bore spectrometer (Bruker, Germany) with a high-resolution broadband spectroscopy probe at 298 K. A NOESY 1D pulse sequence was used with 152 scans and an acquisition duration of 20 minutes. Using TopSpin software version 2.1 (Bruker, Germany), each FID was Fourier-transformed to give a ^{1}H NMR spectrum (Figure 2.7) which was then phased, baseline-corrected and chemical shifts were normalised by setting the TSP signal to 0 ppm. Peaks of interest (Table 2.1) were initially integrated automatically using a pre-written integral text file and integration regions were manually adjusted where required (this was particularly important for the taurine signal as its chemical shift is highly pH-dependent). All metabolite integrals were scaled to the TSP integral. Peak assignments were confirmed using Chenomx NMR Profiler Version 8.1 (Chenomx, Canada). The concentration of each metabolite of interest in each sample was determined by incorporating the integrals of the metabolite and TSP into Equation 2.6.

$$[\text{Metabolite}] = \frac{[\text{TSP}] \times \frac{(I_{\text{Met}}/n_{\text{Met}})}{(I_{\text{TSP}}/n_{\text{TSP}})}}{\text{Wet wt}} \qquad \textit{Equation 2.6}$$

where,

[Metabolite] = Concentration of metabolite in sample (nmol/g wet weight of heart).

[TSP] = Concentration of TSP internal standard in sample (nmol).

I_{Met} = Integral of metabolite peak relative to TSP peak integral.

n_{Met} = Number of protons giving rise to the metabolite peak.

I_{TSP} = Integral of TSP peak.

n_{TSP} = Number of protons giving rise to the TSP peak.

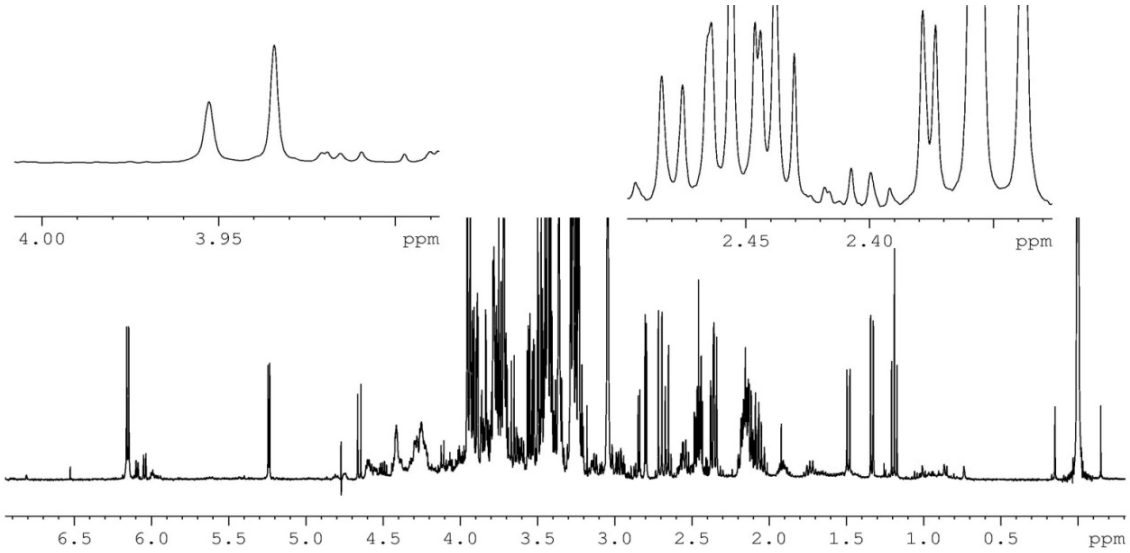

Figure 2.7 Representative ^{1}H NMR spectrum of an isolated perfused rat heart under normal baseline conditions.

When multiple peaks arose from a single metabolite, only the peak with the highest signal-to-noise ratio and least interference from neighbouring peaks was used for integration of that metabolite. See Table 2.1 for peak assignments.

Table 2.1 ^{1}H NMR chemical shift values of peaks used for metabolite integrations.

Metabolite	δ (ppm)
Formate	8.460
NAD(H)	8.433
ATP+ADP	8.274
Fumarate	6.521
Glucose	5.239
Phosphocreatine	3.955
Creatine	3.935
Glycine	3.566
Taurine	3.433
Carnitine	3.235
Phosphocholine	3.224
Choline	3.212
Acetylcarnitine	3.198
Phosphocreatine+Creatine	3.051
Aspartate	2.815
Glutamine	2.475
Succinate	2.408
Glutamate	2.355
Acetate	1.922
Alanine	1.486
Lactate	1.332
Valine	1.095
Isoleucine	0.997
TSP	0.147

The ^{13}C satellite peak downfield of TSP at 0.147 ppm was used as the TSP integral.

2.4.4 High performance liquid chromatography tandem mass spectrometry (LC-MS/MS) of metabolite extracts.

Given the central importance of the TCA cycle to the thesis hypothesis, it was important to use a method that permitted robust measurements of as many of the TCA cycle intermediates as possible. Quantification of multiple TCA cycle intermediates in a single analysis is challenging due to their relatively low concentrations in muscle and similar chemical structures and properties (particularly citrate and isocitrate). As the TCA cycle intermediates are all weak acids they can be separated using ion exchange chromatography as demonstrated by Lu et al (2003). However, this method was only able to quantify malate and citrate due to issues with S:N of (and interference with) the other intermediates and encompassed lengthy acquisition times using gradient elution. An alternative method developed by Bylund et al (2007) involved high performance liquid chromatography tandem mass spectrometry (LC-MS/MS) in ion exclusion mode. Owing to its high selectivity and sensitivity, LC-MS/MS is an ideal method for targeted metabolomics. LC-MS/MS combines the separation powers of HPLC with the high sensitivity of multiple reaction monitoring (MRM) using triple quadrupole mass spectrometry instrumentation. MRM involves the measurement of multiple pre-defined MS transitions during different and specific time-points of a chromatographic separation. During each MS transition, quadrupole 1 (Q_1) is used to filter-out all non-parent ions, Q_2 acts as a collision cell in which the parent ion is fragmented into a daughter ion and Q_3 detects and quantifies the abundance of this daughter ion.

An adaptation of the Bylund et al (2007) LC-MS/MS method was used for the quantification of the majority of the TCA cycle intermediates, as well as pyruvate and

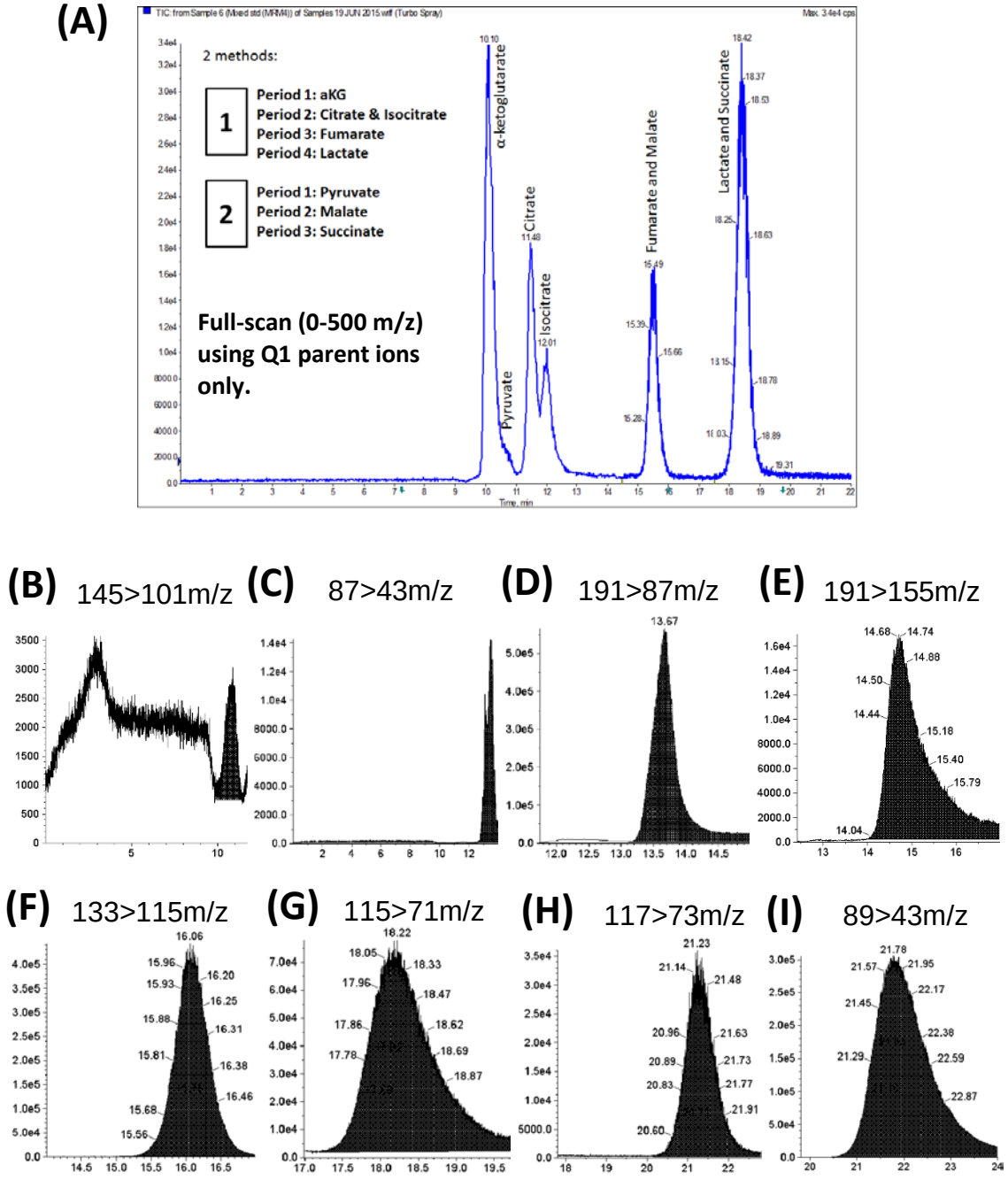

Figure 2.8 Representative LC-MS/MS chromatograms of metabolite extracts from isolated perfused rat heart.

(A) A single full scan experiment of mixed standard solution (in this example a guard column was not used hence peaks generally eluted earlier than those in 'B-I' for which a guard column was used). For studies, two separate chromatographic runs were performed in order to maximise resolution and signal-to-noise (this full scan image is for presentation purposes only and was not used for studies). MRM was carried out for each metabolite during their particular retention times: **(B)** α-ketoglutarate; **(C)** pyruvic acid; **(D)** citric acid; **(E)** isocitric acid; **(F)** malic acid; **(G)** fumaric acid; **(H)** succinic acid; **(I)** lactic acid. Y-axis = Raw counts; X-axis = minutes. Signal at 0-9.5 mins is due to background.

lactate, in myocardial samples from perfusion studies.

Lyophilised aqueous metabolite extracts were reconstituted in 350µL ultrapure water. A series of mixed external standards were prepared in ultrapure water containing 0.0025-50 µM of each metabolite. Representative chromatograms are shown in Figure 2.8.

An Agilent 1100 HPLC system (Agilent Technologies, USA) consisting of an autosampler, a binary pump, a degasser unit and a column oven coupled to an Applied Biosystems Sciex API 3000 mass spectrometer with Turbo Ionspray interface (MDS Sciex, Canada) were used for LC-MS/MS analysis. Chromatograpic separation was achieved using a Supelcogel C610-H column (300 mm x 7.7 mm) with a Supelcogel H guard column (50 mm x 4.6 mm) (Supelco, USA) with an isocratic flow (0.4 mL/min) of mobile phase consisting of 0.01% v/v formic acid and methanol (90:10) and an injection volume of 100µL. The HPLC eluate was split (4:1) just before the Turbo Ionspray interface resulting in a flow of 0.1 mL/min into the mass spectrometer. The mass spectrometer acquisition parameters were exactly as described in Bylund et al (2007). In order to eliminate peak to peak interference, two separate acquisitions were performed for each sample and standard. Acquisition 1 included α-ketoglutarate (145>101 m/z), citrate (191>87 m/z), isocitrate (191>155 m/z), fumarate (115>71 m/z) and lactate (89>43 m/z) while Acquisition 2 included pyruvate (87>43 m/z), malate (133>115 m/z) and succinate (117>73 m/z). Data were acquired using Analyst software (version 1.4.2) and metabolite concentrations in the samples were interpolated using calibration curves of each metabolite as per Bylund et al (2007). These concentrations were incorporated into Equation 2.7 to calculate the molar content of each metabolite in each heart.

$$\text{Met} = \frac{[\text{Met}] \text{ x } 0.00035 \text{ x } 1000}{\text{Wet wt}} \qquad \textit{Equation 2.7}$$

where,

Met = Metabolite content of heart (nmol/ g wet wt)

[Met] = Metabolite concentration in reconstituted extract according to LC-MS/MS (µM).

0.00035 = Dilution factor (350µL used for reconstitution)

1000 = Conversion factor (µmol→nmol)

Wet wt = Wet weight of tissue used for LC-MS/MS (g).

2.4.5 Gas chromatography tandem mass spectrometry (GC-MS) of metabolite extracts

An alternative means by which to quantify the TCA cycle intermediates in myocardial tissue is GC-MS (Guo et al., 2016, Shibayama et al., 2015, Atherton et al., 2006). In summary, the metabolite extract is dissolved in a volatile diluent and is injected into a heated source thereby vapourising the extract. The sample is carried by an inert gas through a column lined with a suitable stationary phase within a heated oven. Analogous to LC-MS/MS, the time of elution into the detector (retention time) of a given metabolite depends upon its partitioning between the stationary phase which is governed by its physicochemical properties (particularly boiling point). The majority of GC-MS method use electron impact ionisation which involves electron bombardment of the sample leading to a loss of an electron and generation of an M^+ parent ion of the analyte. A limitation of using GC-MS for the measurement of small polar molecules

(such as the TCA cycle intermediates) is the necessity for increasing their volatility using derivatisation with, for example, N-tert-Butyldimethylsilyl-N-methyltrifluoro-acetamide (MTBSTFA). The addition of the derivitisation agent to the analyte increases its molecular mass which is taken into account when interpreting the mass spectra. An adaptation of the method used by Mamer et al. (2013) was used in Chapter 6 for the measurement of TCA cycle intermediates as well as metabolites involved in anaplerosis (alanine, aspartate and glutamate) and glycolysis (dihydroxyacetone phosphate (DHAP), pyruvate and lactate).

Metabolites were isolated from 20-40 mg of myocardial tissue by the addition of 1.5 mL ice-cold methanol and 10 μL D_3-methylmalonic acid internal standard (1 mg/mL) followed by homogenisation using a TissueLyser II (Qiagen, Germany) at 30 Hz for five minutes. Homogenates were then centrifuged for 10 minutes at 3500 RPM. The supernatant was evaporated to dryness under nitrogen. The extracts were heated at 80 °C for 15 minutes in 30 μL methyldroxyalmine hydrochloride (20 mg/mL in pyridine) to methoxymate the α-ketoacids thereby improving their stability. Upon cooling, MTBSTFA (30 μL) and hexane (70 μL) were added followed by brief vortexing and heating at 80 °C for 30 minutes. The solution was then transferred into an injection vial with a crimped septum cap to minimise sample loss due to evaporation.

GC-MS was performed using a 6890 gas chromatograph (Agilent Technologies, USA) with 7683 autosampler (Agilent Technologies, USA) and 122-5532UI DB-5ms 30 m x 0.25 mm internal diameter capillary column with 0.25 μm film thickness (Agilent Technologies, USA). The injector was kept at 280 °C and the flow rate of helium gas

was kept at 1.0 mL/min. The column oven was held at an initial temperature of 50 °C for one minute which was increased at a rate of 10 °C/ minute and held at a final temperature of 320 °C for 10 minutes. The injection volume was 1.00 μL. Each sample was analysed twice. The first injection was split 1:10 for the measurement of metabolites with a relatively high signal:noise ratio (pyruvate, lactate, alanine, succinate, malate, aspartate and glutamate) whereas the second splitless injection permitted the measurement of metabolites with lower signal-noise (fumarate, oxaloacetate, αKG, DHAP, citric and isocitric). The effluent was carried into a 5973 mass selective detector (single quadrupole) mass spectrometer (Agilent Technologies, USA) via an MSD transfer line maintained at 280 °C and fragmented using an electron beam of 70eV. Detection of analytes in selected ion monitoring mode was started after a solvent delay of 8.60 minutes. MSD ChemStation D.02.00 software was used for GC-MS data analysis. Peaks of interest were integrated automatically or manually where appropriate. Peak assignments were confirmed using a derivatised mixed standard solution containing all metabolites of interest. Addition of MTBSTFA to samples resulted in tert-butyldimethylsilylation of hydroxyl groups which was reflected in the mass ions observed. Representative GC-MS chromatograms are displayed in Figure 2.9. The integral for each isotopologue of these metabolites were used to calculate mean ^{13}C enrichment and mass distribution vector (MDV) in Chapter 6. Representative GC-MS spectra of ^{13}C-labelled and unlabelled myocardial extracts are displayed in Figure 2.10 (malate has been used as an example).

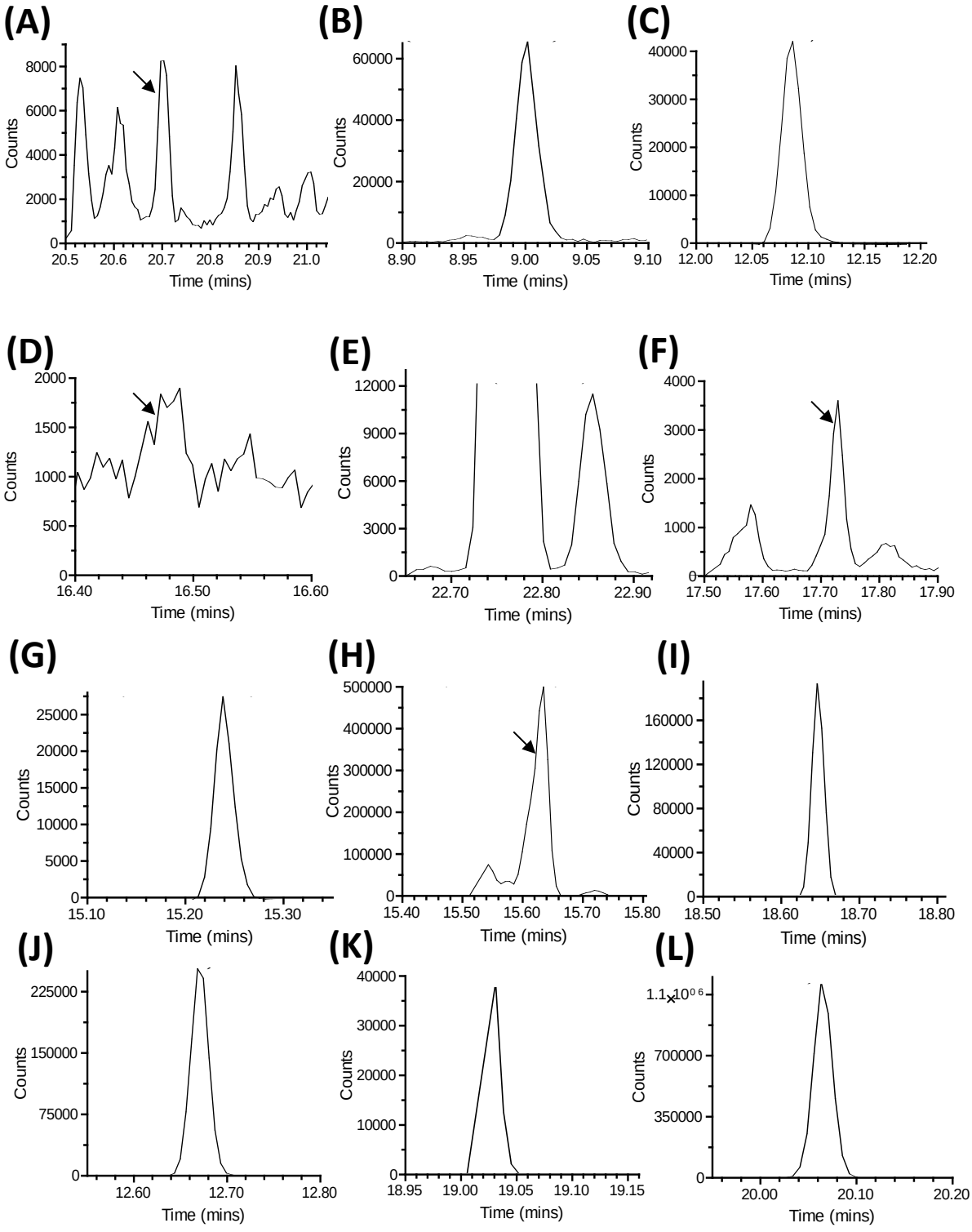

Figure 2.9 Representative GC-MS chromatograms of metabolite extracts from isolated perfused rat heart.

(A) Dihydroxyacetone phosphate. **(B)** Pyruvate. **(C)** Lactate. **(D)** Oxaloacetate. **(E)** Citrate (larger peak at 22.75 minutes) & isocitrate (smaller peak at 22.85 minutes). **(F)** α-ketoglutarate. **(G)** Succinate. **(H)** Fumarate **(I)** Malate. **(J)** Alanine. **(K)** Aspartate. **(L)** Glutamate. Arrow indicates metabolite of interest where multiple peaks are present.

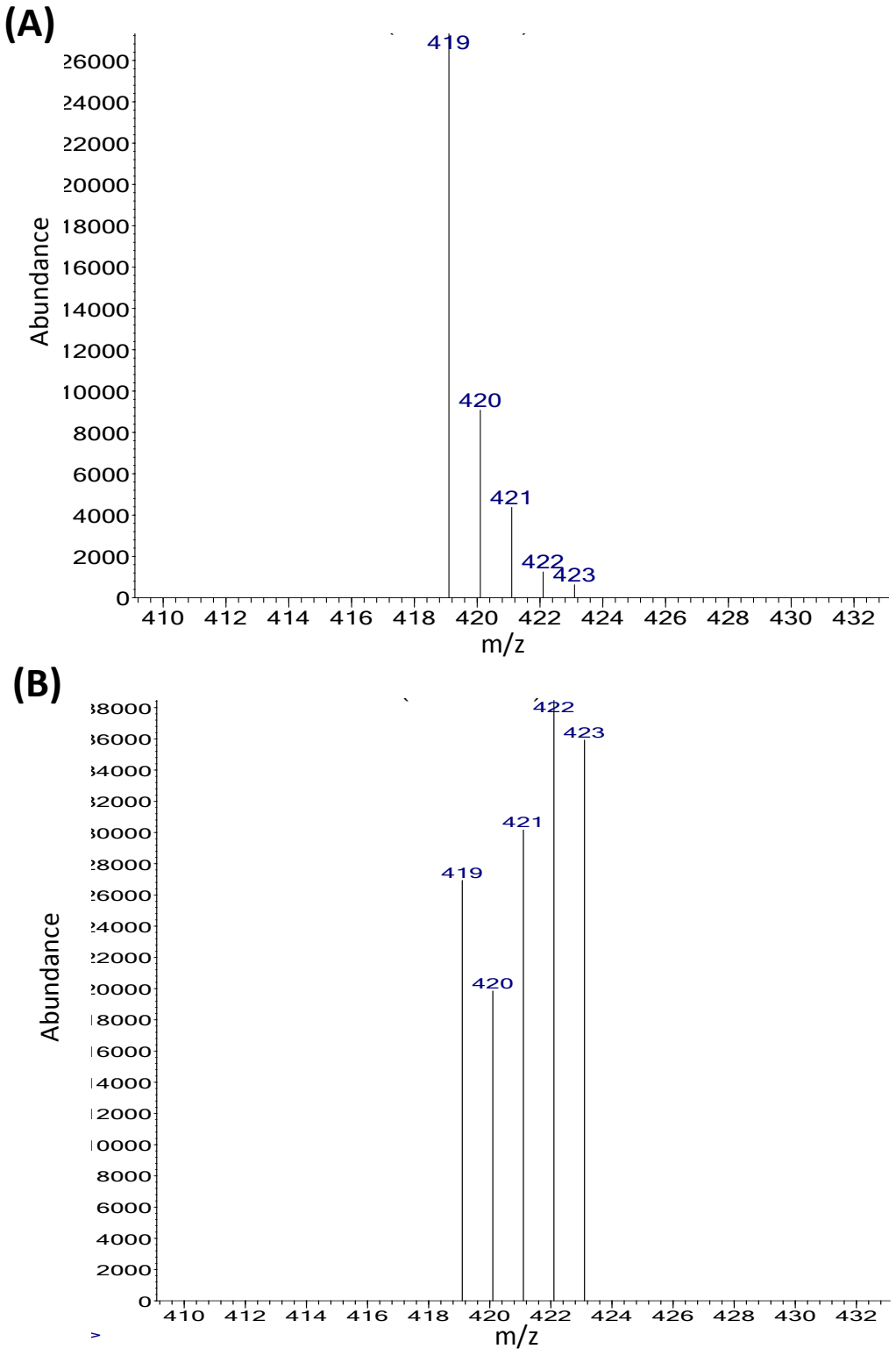

Figure 2.10 Representative GC-MS spectra of malate isotopologues from isolated perfused rat heart.

(A) Perfused with [U]-^{12}C-glucose. **(B)** Perfused with [U]-^{13}C-glucose. Hearts had elevated $[Na]_i$ due to ouabain.

2.5 Statistics

All calculations were performed using Microsoft Excel. GraphPad Prism Version 5 (Graphpad Software Inc., USA) was used for all statistical analyses and graphs. Data were expressed as mean ± SEM unless otherwise stated. Two-tailed, unpaired Student's t-test was used unless otherwise stated ($P<0.05$ was considered statistically significant). All metabolomics datasets were subjected to outlier detection and removal using the median absolute deviation method (± 2.5 threshold) (Leys et al., 2013).

3 INVESTIGATING THE EFFECTS OF OUABAIN ON $[Na]_i$ AND METABOLISM IN THE ISOLATED PERFUSED RAT HEART.

3.1 Introduction

In order to investigate the relationship between $[Na]_i$ elevation and altered metabolism in the beating heart, it is necessary to develop and optimise a Langendorff preparation in which $[Na]_i$ can be elevated to a significant level and measured in real-time. Previous studies have used modified ion compositions in KH to increase $[Na]_i$ such as those free of K^+, Ca^{2+} or Mg^{2+} (Eykyn et al., 2015, Schepkin et al., 1998). However, these buffers alter electrophysiology and lead to functional impairment in isolated perfused hearts. Other methods known to elevate $[Na]_i$ include electrical pacing. For example, 3 Hz (or 180 'BPM') has been shown to increase $[Na]_i$ by up to ~30% in isolated ventricular myocytes and muscle strips versus unpaced controls (Cohen et al., 1982, Despa et al., 2002b). However, this does not appear to reflect the response of the intact heart. Simor et al. (1997) showed that increasing pacing rate from 4.2 Hz (250 BPM) to 8.3 Hz (500 BPM) elevated $[Na]_i$ by only 9%. Furthermore, increasing heart rate by pacing reduces developed pressure due to the negative force frequency relationship in the rat (Schouten and ter Keurs., 1991) and therefore any metabolic changes driven by $[Na]_i$ may also be subject to changes in contractile function. A more suitable approach is to use a pharmacological agent in order to either inhibit $[Na]_i$ efflux or enhance $[Na]_e$ influx. As discussed in Section 1.2.3, NKA is the only quantitatively important efflux pathway for

$[Na]_i$ under physiological conditions whereas there are numerous influx pathways for this ion. Therefore, the most widely used approach is inhibition of NKA with real-time ^{23}Na NMR measurements to assess the rise in [Na] (detailed in Section 2.3.3).

The use of ouabain to elevate $[Na]_i$ and measurements employing ^{23}Na NMR have previously been implemented in our laboratory in the mouse heart (Eykyn et al., 2015) and elsewhere in the rat heart (Schepkin et al., 1998). Ouabain was therefore used to elevate $[Na]_i$ while simultaneously measuring $[Na]_i$ using ^{23}Na NMR in the Langendorff rat heart preparation. Schepkin et al (1998) used 1 mM ouabain, resulting in cardiac arrest and $[Na]_i$ of approximately 40 mM (Figure 2.4), whereas previous measurements in the perfused mouse heart using 50 µM ouabain increased $[Na]_i$ from 16 mM to 26 mM (Eykyn et al., 2015). In addition, Koomen et al (1984) and Maixent (1998) showed that hearts perfused with 100µM ouabain do not exhibit arrest and Peng et al (1996) demonstrated that ouabain does not affect myocyte viability at or below 100 µM but does above this concentration. Initial studies in this chapter investigated the dose response relationship for 50-100 µM ouabain to establish the most suitable concentration to elevate $[Na]_i$ in the perfused rat heart.

Following these initial dose-response experiments, a single concentration was chosen to investigate possible metabolomics changes associated with ouabain treatment in both an unpaced group of hearts with baseline heart rate and a group with an elevated heart rate using electrical pacing where ATP demand is elevated. End-point metabolomics measurements were performed using a semi-targeted ^{1}H NMR approach. Lactate efflux was measured throughout the perfusion protocols to assess whether glycolytic flux was altered in response to ouabain.

3.2 Aims

The aims of the studies described in this chapter were:

1. To determine a dose-response relationship between ouabain concentration and $[Na]_i$ in the perfused rat heart.

2. To determine whether a semi-targeted metabolomics approach using ^{1}H NMR probes alterations in metabolism in response to ouabain in unpaced or paced hearts.

3.3 Establishing dose-response between [ouabain] and $[Na]_i$

This study investigated the dose-response of 50-100 µM ouabain and $[Na]_i$ in the perfused rat heart.

3.3.1 Experimental methods

Hearts were blinded and randomised into either control group (n=6) or treated groups with three different concentrations of ouabain (50, 75 & 100µM; n=6/group) and were perfused in Langendorff mode within the NMR magnet as described in Sections 2.2 and 2.1.2. Ouabain octahydrate was obtained from Sigma (UK).

Hearts were stabilised for 30 minutes with standard KH (Section 2.1.3) and then perfused with treatment KH (control or ouabain) for 25 minutes. Derived $[Na]_i$ was monitored throughout the protocols using TQF ^{23}Na NMR interleaved with DQF ^{23}Na

NMR (Section 2.2.3). Left ventricular developed pressure (LVDP), heart rate and coronary flow were monitored throughout all experiments.

3.3.2 Results - Ouabain induces a dose dependent elevation of $[Na]_i$

All perfusion parameters remained constant during the stabilisation period, according to previously defined exclusion criteria (detailed in Section 2.1.6) and were not significantly different between any of the groups. Mean baseline LVDP (Figure 3.1A) was 97±10 mmHg in the control group. In the 50 µM, 75 µM and 100 µM ouabain groups, LVDP was elevated by a maximum of 15, 28 and 38 mmHg at 40 minutes respectively versus their baseline values. However, LVDP returned to baseline values in all groups by the end of perfusion. There were no significant differences in LVDP between any of the four groups at any point of the perfusion protocol. Heart rate in the control group (Figure 3.1B) did not deviate from baseline values (302±6 BPM) at any point of perfusion. 50, 75 and 100 µM ouabain decreased heart rate by a maximum of 52, 56 and 59 BPM versus baseline values, respectively. The time at which maximum bradycardia was reached differed between these ouabain groups (45, 55 and 50 minutes, respectively). End-point heart rate at 55 minutes was not significantly different to control (312±8 BPM) in the 50µM and 75µM ouabain groups however was significantly lower (211±23 BPM, $P<0.01$) in the 100µM ouabain group at this time. Coronary flow (Figure 3.1C) averaged 10±1 mL/min for all hearts in this study with no significant differences ($P>0.05$) between any of the groups.

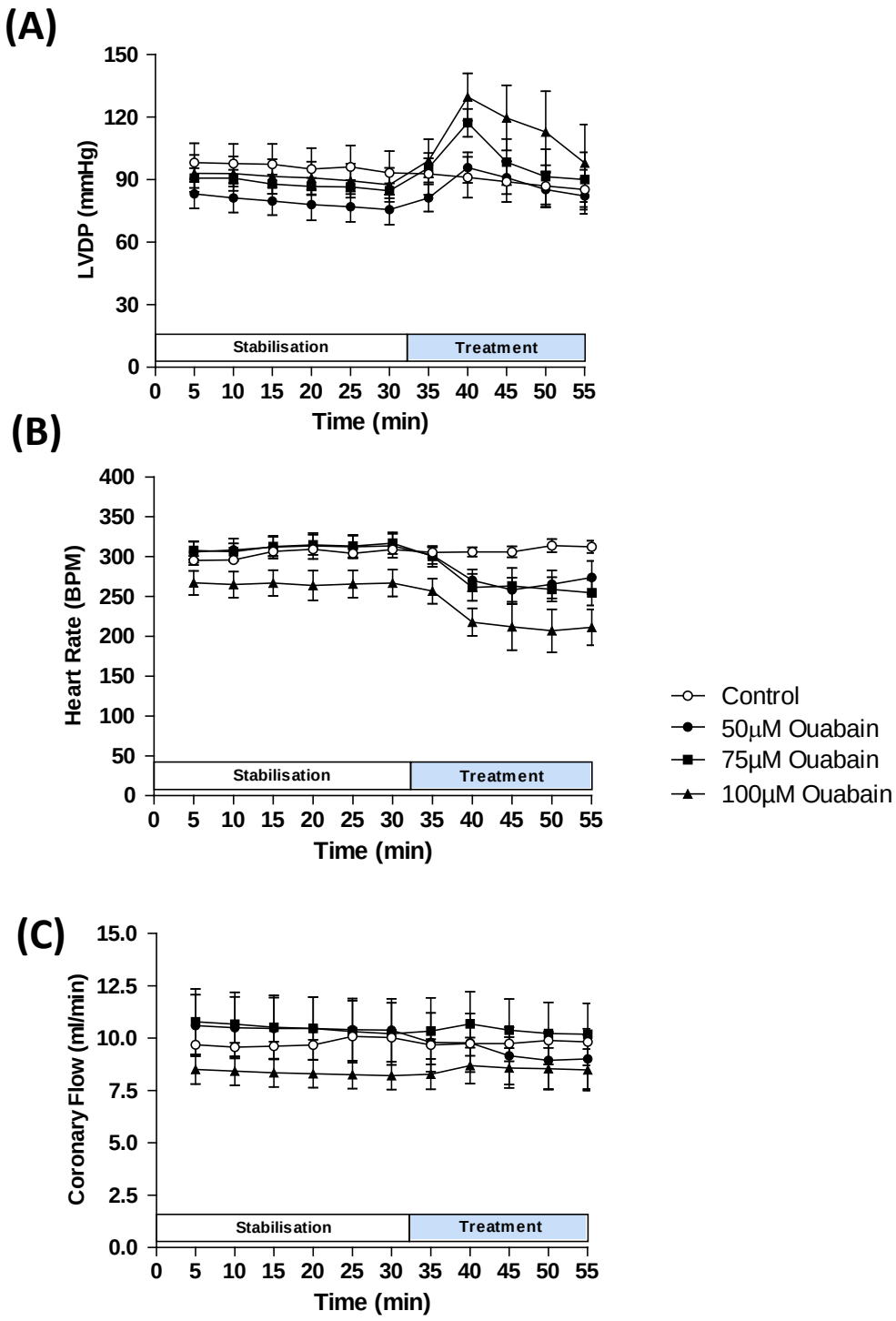

Figure 3.1 Dose response studies, ex vivo functional parameters recorded during stabilisation and control, 50uM, 75uM and 100uM ouabain treatment periods.

(A) Left ventricular developed pressure (LVDP). **(B)** Heart rate. **(C)** Coronary Flow. Symbols and error bars represent mean±SEM of five minute time windows (n=6/group).

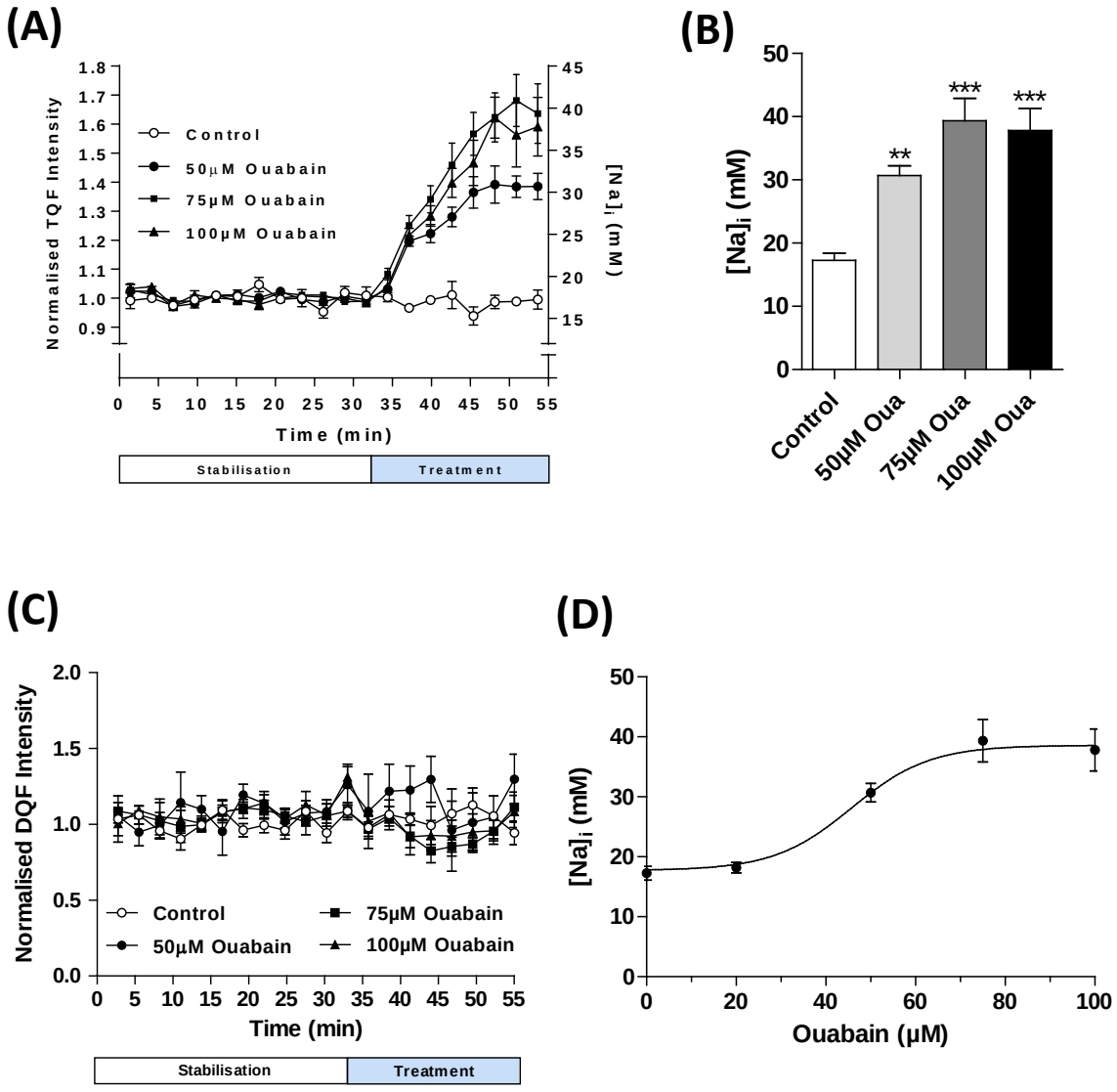

Figure 3.2 Dose-response studies using real-time ^{23}Na NMR during stabilisation and control, 50uM, 75uM and 100uM ouabain treatment periods.

(A) Normalised TQF signal as a function of time (left axis) and corresponding derived [Na]i (right hand axis). **(B)** End-point derived [Na]i for control and treatment groups. **(C)** Normalised DQF signal as a function of time. **(D)** Dose-response curve of end-point derived [Na]i values as a function of ouabain concentration. Curve fitting constraints were applied: bottom=17.71 mM; top=38.59mM; slope=0.05. EC_{50}=45.8μM (NB. 20μM ouabain datapoint was acquired in another study using the same protocol (see Appendix 8.3). Data are displayed as mean±SEM (n=6/group).

The ^{23}Na TQF (Figure 3.2A) remained constant throughout the stabilisation period (0-30 minutes) in all groups and also remained constant throughout the entire protocol in the control group (30-55 minutes) with a calculated $[Na]_i$ of 17±0.8 mM (using the calibration curve of Schepkin et al., 1998). During the treatment period, the initial slope of derived $[Na]_i$ elevation was the same in all ouabain groups between 30 and 37 minutes reaching 25±0.9 mM. Following this, the TQF elevation of the 50 µM ouabain group plateaued earlier than the other ouabain groups, while the 75 µM and 100 µM ouabain groups showed almost identical ^{23}Na TQF profiles throughout the entirety of the protocol. At the end of perfusion (55 minutes), all treatment groups exhibited significantly elevated $[Na]_i$ (Figure 3.2B) than control (control = 17±1.1 mM; 50 µM = 31±1.5 mM, $P<0.01$ vs control; 75 µM = 39±3.5 mM; $P<0.001$ vs control; 100 µM = 38±3.5 mM, $P<0.001$ vs control). The ^{23}Na DQF signal (Figure 3.2C) did not markedly deviate from baseline (1.0±0.1 arbitrary units) at any point of perfusion in any of the groups, although this had a lower signal-to-noise ratio than the ^{23}Na TQF measurements. The dose-response relationship (Figure 3.2D) between [ouabain] and $[Na]_i$ was sigmoidal with a calculated EC_{50} of 45.8 µM ouabain.

3.4 A semi-targeted metabolomics study of ouabain response in the perfused rat heart

To assess whether ouabain induces metabolic alterations in the perfused rat heart, a single concentration of 50µM ouabain was used for further investigation as it was shown in the previous study to induce significant and sustained $[Na]_i$ elevation without observable toxicity. Two bench protocols were performed, either an unpaced group

allowed to free-run at the intrinsic heart rate or a paced group where heart rate and therefore ATP demand were elevated. These protocols were not conducted in the NMR magnet but on a separate isolated heart perfusion rig. End-point metabolomics was assessed in a semi-targeted fashion using ^{1}H NMR. Lactate efflux was monitored throughout the protocols.

3.4.1 Experimental methods

Hearts were perfused with either control or 50 μM ouabain KH in a randomised and blinded fashion (n=6/group). Unpaced hearts were stabilised for 30 minutes with standard KH (Section 2.1.3) and then perfused with either control KH or ouabain for a further 20 minutes followed by snap-freezing (Section 2.1.9). In the paced study, hearts were stabilised for 20 minutes with standard KH perfusion (Section 2.1.3) during which they were paced (Section 2.1.7) at 3.35 Hz (320 BPM). Between 20 and 80 minutes, hearts were perfused with either control KH or 50 μM ouabain and subsequently paced at higher rate (9.16 Hz; 550 BPM) followed by snap-freezing (Section 2.1.9) at 80 minutes. In both groups aqueous metabolites were extracted (Section 2.4.2) and quantified by high-resolution ^{1}H NMR (Section 2.4.3). Coronary effluent was taken at five minute intervals throughout the perfusion and analysed using the 2300 STAT Plus giving lactate efflux rate (Section 2.3). Left ventricular developed pressure (LVDP), heart rate, left ventricular end diastolic pressure (LVEDP) and coronary flow were monitored throughout all experiments.

3.4.2 Results – 50 µM ouabain induces metabolomic changes in the unpaced heart.

All perfusion parameters remained constant during the stabilisation period according to predefined exclusion criteria (detailed in Section 2.1.6). Baseline LVDP (Figure 3.3A) was 151±4 mmHg (average) in the control group and did not significantly deviate from this between 30 and 50 minutes (average=143±5 mmHg). In the ouabain group, LVDP was elevated to a maximum of 184±5 mmHg at 40 minutes (after 10 minutes of perfusion with 50µM ouabain) and remained significantly elevated at 55 minutes (177±2 mmHg, $P<0.001$) versus control (140±3 mmHg). Mean control heart rate during stabilisation was 289±14 BPM (Figure 3.3B). Coronary flow and LVEDP averaged 15±1 mL/min and 5.6±0.7 mmHg respectively for all hearts in this study with no significant differences ($P>0.05$) between any of the groups.

Lactate efflux rate during the stabilisation period (Figure 3.4) averaged 348±45 nmol/min/g for all hearts with no significant differences between the two groups ($P>0.05$) and reached steady-state within 30 minutes. Lactate efflux increased to a maximum of 673±61 nmol/min/g after 5 minutes of 50 µM ouabain perfusion and remained significantly elevated at the end of perfusion (504±37 nmol/min/g) versus control (229±49 nmol/min/g, $P<0.01$).

High resolution ^{1}H NMR permitted the quantification of numerous metabolites in a semi-targeted metabolomics approach (Figure 3.5). Metabolites were categorised into pathways related to ATP supply (including glycolysis, the TCA cycle, acetyl carnitine shuttling, anaplerosis and energetics) and those that were less important to ATP supply

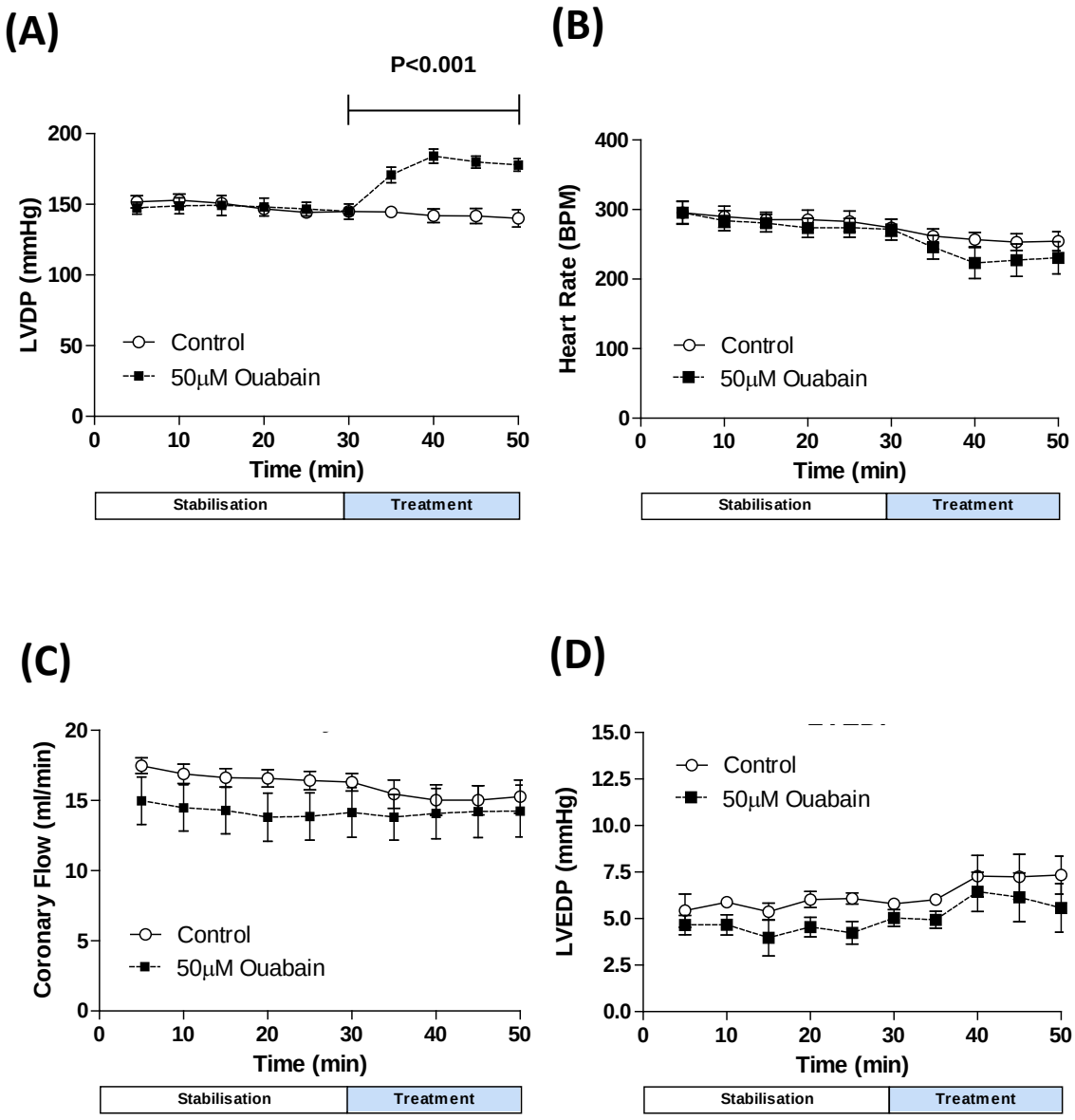

Figure 3.3 Perfusion measurements (unpaced ouabain bench study).

(A) Left ventricular developed pressure (LVDP). **(B)** Heart rate. **(C)** Coronary flow. **(D)** Left ventricular end diastolic pressure (LVEDP). Symbols and error bars represent mean±SEM of five minute time windows (n=6/group). Hearts were snap-frozen at 50 minutes. P-values represent unpaired student's t-test of area under the curve between 30 and 50 minutes.

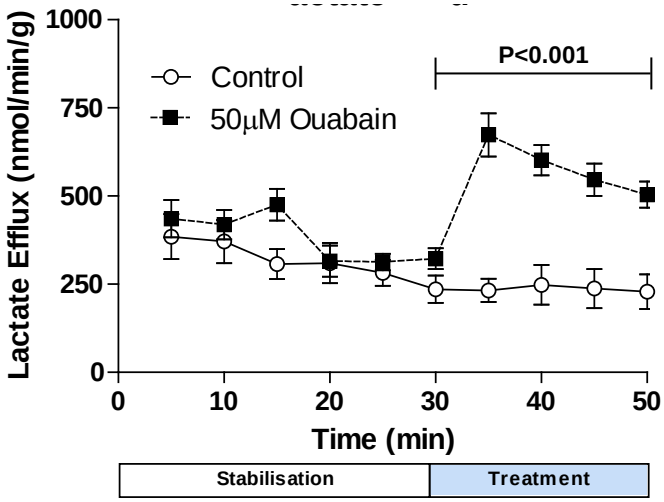

Figure 3.4 Lactate efflux (unpaced ouabain bench study).

Symbols and error bars represent mean±SEM of five minute time windows (n=6/group). Significant p-values are shown (unpaired student's t-test of area under the curve between 30 and 50 minutes).

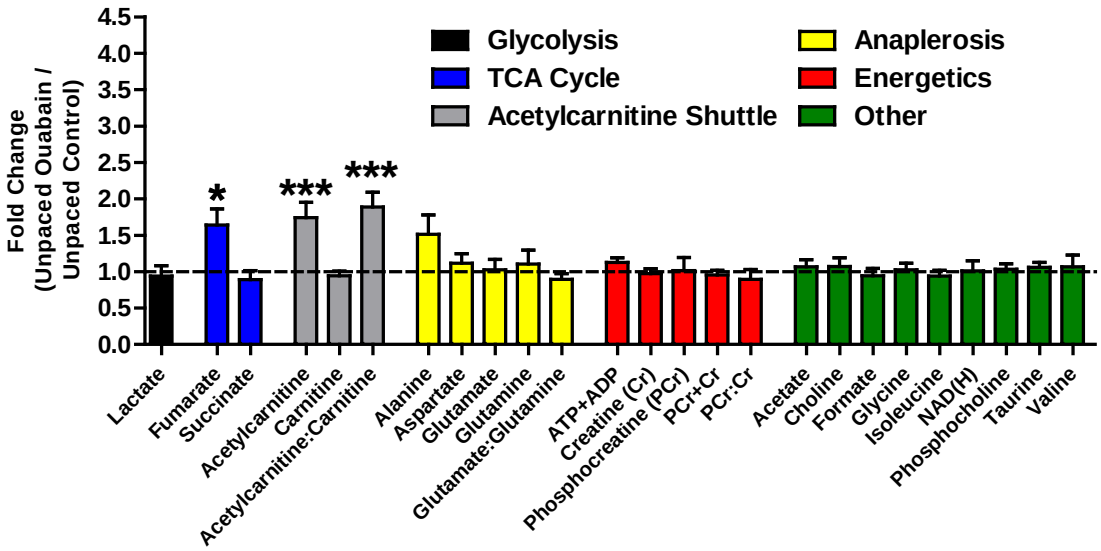

Figure 3.5 ^{1}H nuclear magnetic resonance spectroscopy metabolomic profile of myocardium (unpaced ouabain bench study).

Hearts were snap-frozen at 50 minutes. Bars and error bars represent mean fold change ± propagated SEM (n=4-6/metabolite/group). A fold change of '1.0' represents zero change vs control. The y-axis scale has been matched to that of the paced ouabain metabolomics plot (Figure 3.8) for comparison purposes. *p<0.05; **p<0.01; ***p<0.001; $^{\#}$p<0.0001.

('other'). Figure 3.5 shows fold change of metabolite concentrations in treated versus control.

50 μM ouabain lead to increased fumarate by 64% ($P<0.05$), acetyl carnitine by 74% ($P<0.001$) and an 88% elevation in the acetyl carnitine-carnitine ratio ($P<0.001$). The trend towards an increase in alanine by 51% did not reach statistical significance ($P>0.05$). All other metabolites were unaltered following 50μM ouabain treatment. Full details of the unpaced metabolomics dataset are shown in Appendix 8.1.

3.4.3 Results – 50 μM ouabain induces metabolomic changes in the paced heart.

Perfusion parameters were stable according to predefined exclusion criteria (detailed in Section 2.1.6) except LVDP (Figure 3.6A) which was elevated at the start of the perfusion (control = 169±10 mmHg; ouabain = 178±6 mmHg) and took 40 minutes to reach steady-state (116±4 mmHg) in the control group. There was no difference ($P>0.05$) in LVDP between the control and ouabain group in the first 20 minutes during which all hearts were paced at 320 BPM in the absence of ouabain. LVDP was higher in the ouabain group versus control throughout the treatment period (20-80 minutes) and was significantly higher at the end of perfusion (control = 72±1 mmHg; ouabain = 91±2 mmHg; $P<0.0001$). Following increased pacing rate from 320 BPM to 550BPM (Figure 3.6B), LVDP significantly decreased in both groups (control = 113±5 to 81±2 mmHg, $P<0.0001$; ouabain = 136±7 to 89±9 mmHg, $P<0.001$). Coronary flow (Figure 3.6C) was not significantly altered ($P>0.05$) by ouabain or pacing. There was a trend towards increased LVEDP (Figure 3.6D) with high pacing rate (control = 6±1 to 14±4 mmHg;

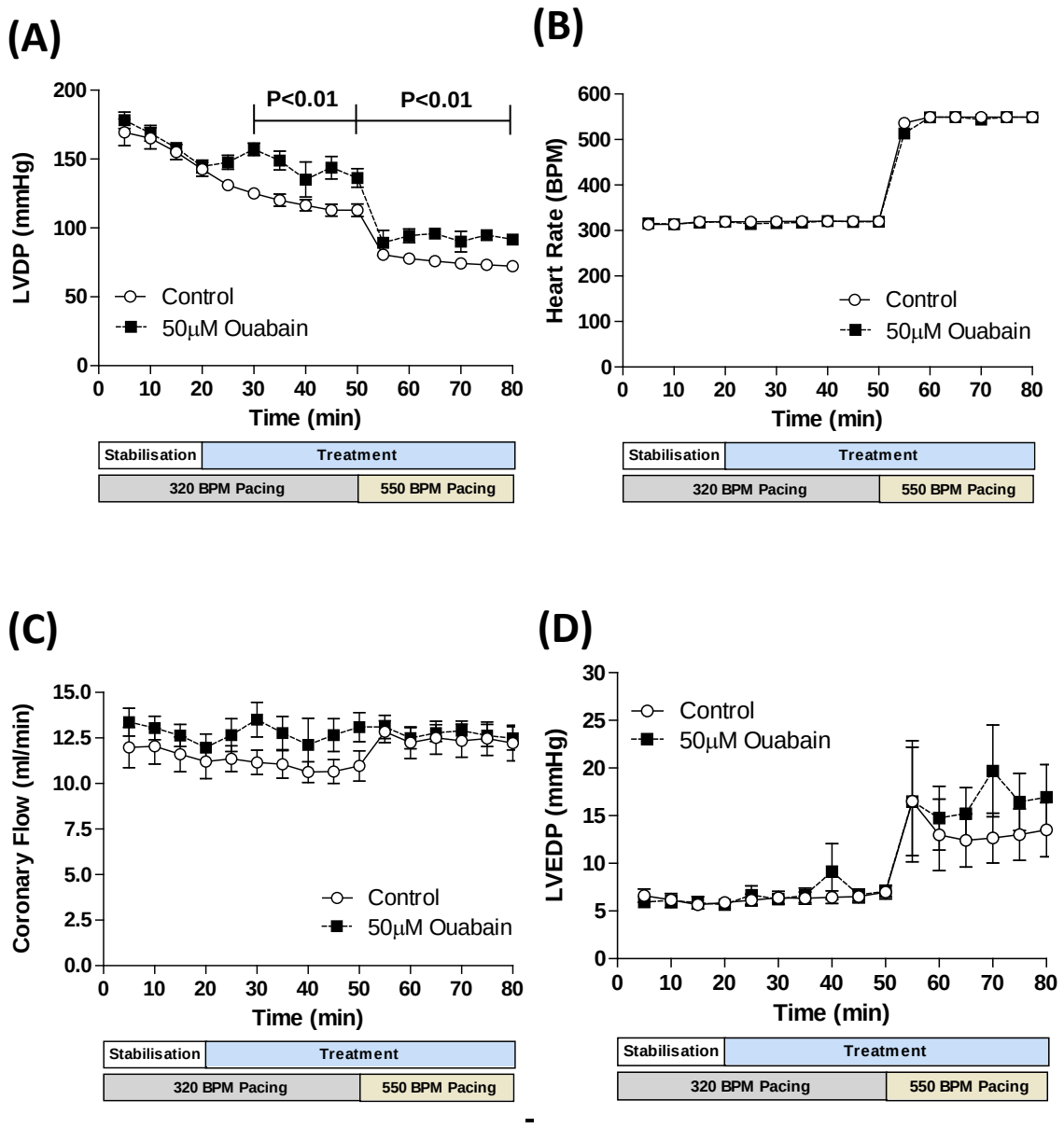

Figure 3.6 Perfusion measurements (paced ouabain bench study).

(A) Left ventricular developed pressure (LVDP). **(B)** Heart rate. **(C)** Coronary flow. **(D)** Left ventricular end diastolic pressure (LVEDP). Symbols and error bars represent mean±SEM of five minute time windows (n=6/group). Hearts were snap-frozen at 80 minutes. Significant p-values are shown (unpaired student's t-test of area under the curve between either 20 and 50 minutes or 50 and 80 minutes as specified).

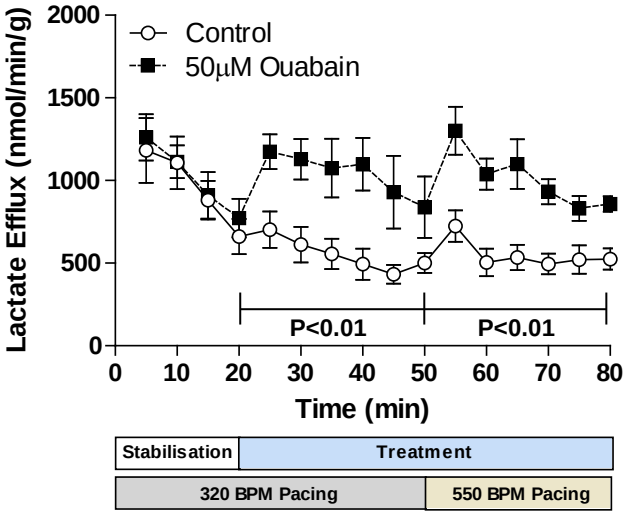

Figure 3.7 Lactate efflux (paced ouabain bench study).

Symbols and error bars represent mean±SEM of five minute time windows (n=6/group). Significant p-values are shown (unpaired student's t-test of area under the curve between either 20 and 50 minutes or 50 and 80 minutes).

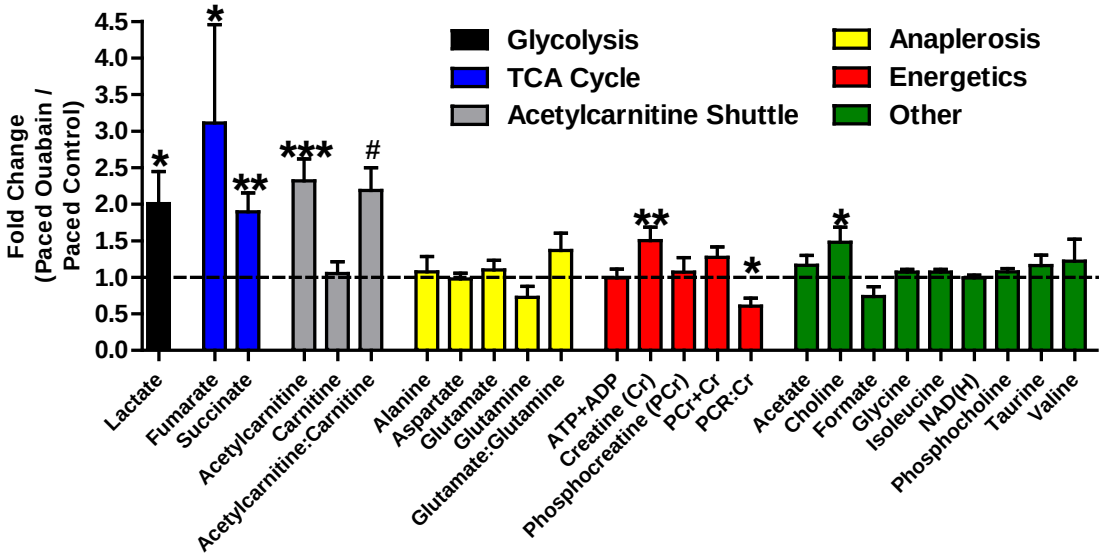

Figure 3.8 ^{1}H nuclear magnetic resonance spectroscopy metabolomic profile of myocardium (paced ouabain bench study).

Hearts were snap-frozen at 80 minutes. Bars and error bars represent mean fold change ± propagated SEM (n=4-6/metabolite/group). A fold change of '1.0' represents zero change vs control. The y-axis scale has been matched to that of the unpaced ouabain metabolomics (Figure 3.5) plot for comparison purposes. *p<0.05; **p<0.01; ***p<0.001; $^{\#}$p<0.0001.

ouabain = 7±1 to 17±4 mmHg) although this was only significant in the ouabain group ($P<0.05$).

Rates of lactate efflux during the stabilisation period (Figure 3.7) were the same in the control (1014±124 nmol/min/g) and ouabain groups (958±145 nmol/min/g). There was a decline in the lactate efflux rate during this period (control = -24 nmol/min/g; ouabain = -26 nmol/min/g). In the control group, steady-state was reached at 40 minutes from the start of perfusion. Lactate efflux was not significantly increased by elevating pacing rate from 320 BPM to 550 BPM ($P<0.05$) in either group. Lactate efflux was 200-500 nmol/min/g higher in the ouabain group versus control throughout the treatment period and was significantly elevated at the end of perfusion, 857±47 nmol/min/g and 524±64 nmol/min/g ($P<0.01$), respectively.

In the end-point metabolomics (Figure 3.8) from the two paced groups of hearts, treatment with 50µM ouabain resulted in increased lactate (101%; $P<0.05$), fumarate (211%; $P<0.05$), succinate (88%; $p<0.01$), acetyl carnitine (132%; $P<0.001$), acetyl carnitine-carnitine ratio (119%; $P<0.0001$), creatine (Cr) (50%; $P<0.01$) and choline (48%; $P<0.05$). The increased Cr resulted in a reduction in the phosphocreatine PCr:Cr ratio (-39%; $P<0.05$). All other metabolites were unaltered following 50 µM ouabain treatment. Full details of the paced metabolomics dataset are shown in Appendix 8.2.

3.5 Discussion

3.5.1 Dose response between derived $[Na]_i$ and ouabain.

Ouabain caused a dose-dependent elevation in TQF signal in the absence of any change in DQF, giving confidence in the ^{23}Na NMR methodology used to assess intracellular and extracellular pools of Na^+ in the perfused rat heart.

The peak elevation in derived $[Na]_i$ induced by 50 μM ouabain (31±1 mM) was two-fold higher than the baseline value (17±1 mM), which is in agreement with the relative changes seen by Lotan et al. (1992) using a similar protocol. The derived $[Na]_i$ value using this concentration of ouabain was similar to that previously measured in the mouse (26±5 mM, Eykyn et al., 2015). Perfusion with 50-100 μM ouabain gave rise to a dose response that was similar to that observed by Koomen et al. (1984) (Figure 1.4). In further agreement with the literature (Koomen et al., 1984, Maixent et al., 1998, Peng et al., 1996), perfusion with ouabain up to 100 μM gave rise to a positive inotropic effect in the absence of functional impairement. The ouabain dose-response measurements carried out in this chapter will act as a guide for increasing $[Na]_i$ to desired levels in the perfused rat heart in subsequent chapters of this thesis.

3.5.2 Lactate efflux

Lactate efflux was significantly increased in both paced (Figure 3.7) and unpaced (Figure 3.4) hearts during perfusion with 50μM ouabain. Lactate is extruded by the sarcolemmal monocarboxylate transporter (MCT) (Zhu et al., 2013) and therefore likely

suggests an elevation in anaerobic glycolysis, possibly due to increased inotropy. The isolated rat heart is known to release a relatively small amount of lactate under basal conditions (approximately 0.5 μmol/min/g, Allen et al., 1986) which aligns with the values shown in Figure 3.4. Lactate efflux is known to be elevated during increased contractile demand (Allen et al., 1986) and following ischaemia (Wilder et al., 2016) but the effect of $[Na]_i$ elevation on lactate efflux has not been previously reported.

3.5.3 Metabolomics

Figure 3.5 revealed that perfusion of unpaced rat hearts with 50 μM ouabain was associated with significant elevations in fumarate but not succinate, while paced rat hearts revealed an elevation in both these metabolites in response to ouabain suggesting a possible change in the TCA cycle. The acetyl carnitine-carnitine ratio is an indicator of the extent of shuttling of acetyl groups into the mitochondria for the production of acetyl CoA and was also significantly elevated by ouabain perfusion in both paced and unpaced hearts. Elevated acetyl carnitine levels have been reported previously in urine (Matsui et al., 1994) and plasma (Turer et al., 2009) from patients with contractile dysfunction although the role of $[Na]_i$ was not investigated in these studies. Despite the elevation in lactate efflux due to ouabain, the end-point myocardial levels of lactate were unaltered in unpaced hearts following ouabain perfusion. This is indicative of increased anaerobic glycolysis and increased extrusion of lactate.

Figure 3.8 demonstrated that increased contractile demand via elevated pacing augmented the metabolic alterations induced by ouabain identified in unpaced hearts.

Fumarate and acetyl carnitine-carnitine ratio were elevated to a greater extent than in unpaced hearts. Furthermore, some metabolites that were not significantly altered by 50 μM ouabain in unpaced hearts were significantly increased by ouabain during elevated pacing. Increased succinate was observed in the paced group which, taken together with the elevation in fumarate, adds weight to the hypothesis that the TCA cycle is altered in these experiments, either due to increased $[Na]_i$ or increased inotropy. The rates of lactate efflux were similar at the end of perfusion in both unpaced and paced ouabain metabolomics studies, but myocardial lactate was elevated in the paced hearts suggesting that lactate efflux may become saturated at higher pacing rates leading to a build-up of intracellular lactate. Creatine also became elevated by ouabain in the paced group. As discussed in Section 1.3.2, creatine is essential for the creatine kinase reaction in order to maintain ATP supply instantaneously with increased contractile demand. However, PCr and total ATP+ADP were unaltered by ouabain suggesting unaltered energetic reserve. Taken together with the other metabolite elevations due to ouabain, this may reflect a shift of metabolism in order to sustain cardiac energetics during $[Na]_i$ elevation. Choline was also increased by ouabain in paced hearts. *In vivo* choline supplementation has been shown to sustain both systolic and diastolic contractile performance as well as reduce the release of brain natriuretic peptide (a biomarker of myocardial infarction) (Strilakou et al., 2013). Furthermore, increased choline release occurs following global ischaemia-reperfusion insult in the perfused rat heart (Bruhl et al., 2004) due to enhanced hydrolytic cleavage of membrane phosphocholine.

The metabolomic changes induced by 50 μM ouabain in both unpaced and paced (550 BPM) rat hearts are summarised in Table 3.1.

Table 3.1 Summary of alterations due to 50 µM ouabain in unpaced and paced hearts.

Analyte	Unpaced		Paced	
	% change	P-value	% change	P-value
Acetylcarnitine	↑ 74	0.0009	↑ 132	<0.0001
Fumarate	↑ 64	0.022	↑ 211	0.015
Succinate	N/A	N/A	↑ 88	0.002
Lactate	N/A	N/A	↑ 101	0.032
Creatine	N/A	N/A	↑ 50	0.003
Choline	N/A	N/A	↑ 48	0.013

% changes are for unpaced control group vs unpaced 50µM ouabain group or high-rate paced control group vs high-rate paced 50µM ouabain ouabain group at the end of perfusion where '0%' change represents no change from baseline. N = 6 per group. 'N/A': These metabolites were unaltered by 50µM ouabain perfusion in unpaced hearts.

3.5.4 The problem with ouabain: undesired inotropic effects.

The studies described in this chapter have given an initial insight into the relationship between ouabain concentration, $[Na]_i$ and metabolism during 'normal' and 'high' ATP demand. Although several metabolites were observed to be altered by ouabain including two TCA cycle intermediates, the impact of the associated positive inotropic effect on these metabolites is unknown. Hence, the sensitivity of these metabolites to $[Na]_i$ *per se* remains obscure. Whereas there have been very limited studies on the effect of $[Na]_i$ elevation on metabolism, more is known about the effects of increased contractile work

on metabolism. For example, acetyl carnitine concentration has been shown to increase in skeletal muscle upon prolonged exercise in humans (Sahlin et al., 1990) and elevating peak systolic pressure from 60 mmHg to 120 mmHg in the working rat heart increases creatine by 26% (Kobayashi and Neely, 1983). Also, an increase in myocardial lactate concentration was observed in a similar model reported by Goodwin et al (1998). The importance of choline to *in vivo* contractile performance in the rat heart has been demonstrated (Strilakou et al., 2013). It is therefore likely that many of the metabolic changes observed in these studies may simply reflect an increase in inotropy and hence energetic demand induced by elevated $[Na]_i$.

3.6 Summary

In this chapter, studies were carried out in order to determine the effects of ouabain on $[Na]_i$ (derived using TQF ^{23}Na NMR) and metabolism (using high resolution ^{1}H NMR metabolomics of snap-frozen myocardium) in the Langendorff rat heart preparation at both intrinsic heart rate and elevated heart rate (using electrical pacing). The degrees of $[Na]_i$ elevation induced by 50, 75 and 100 µM ouabain were substantial and sustained. Acetyl carnitine and fumarate were significantly elevated by 50 µM ouabain in unpaced hearts and this was augmented by high pacing rate. Increasing contractile demand by pacing appeared to enhance the sensitivities of other metabolite concentrations to 50 µM ouabain, which were significantly elevated in paced hearts but not in unpaced hearts including lactate, succinate, creatine and choline. However, it is unclear whether these metabolic alterations were in response to the $[Na]_i$ elevation induced by ouabain or its

associated positive inotropic effect. It is therefore important to develop a method which allows this to be elucidated. Proceeding Chapters will therefore aim to establish methods to uncouple the effects of enhanced inotropy during $[Na]_i$ elevation and thereby unravel any metabolic changes that are due to $[Na]_i$ overload alone.

4 ELECTROMECHANICAL UNCOUPLING TO NORMALISE OUABAIN-INDUCED INOTROPY.

4.1 Introduction

In Chapter 3, a number of metabolomic alterations were observed in response to 50 μM ouabain perfusion in both unpaced and paced perfused hearts. These potentially arose from those that are $[Na]_i$-dependent as well as those that are inotropy-dependent. To compare control and treated groups where $[Na]_i$ is elevated, a technique is required to normalise differences in inotropy between hearts. Two techniques were evaluated.

The first method involved the induction of a positive inotropy in the control group by increasing intraventricular balloon volume and stretch via the Frank-Starling effect thereby elevating left ventricular developed pressure (LVDP) to that of the corresponding ouabain group. However, the corresponding ouabain group did not exhibit a sustained elevation in $[Na]_i$ and thus this approach was not developed further. Full details of this protocol are given in Appendix 8.3.

An alternative approach is the removal of inotropy using electromechanical uncoupling. Metabolomic alterations could then be assessed in a non-contracting control versus a non-contracting ouabain group in which $[Na]_i$ remained elevated but the positive inotropic response of ouabain was negated. Metabolic differences between these two groups would be considered $[Na]_i$-dependent in the absence of inotropic differences.

Electromechanical uncoupling is commonly used to remove motion artefacts in optical mapping studies of isolated perfused hearts (Lang et al., 2011). This usually involves the cessation of contraction using inhibitors of the myofilament myosin ATPase, for example, 2,3-butanedione monoxime (BDM, Figure 4.1A) and blebbistatin (Figure 4.1B). BDM and blebbistatin are both reported to inhibit myosin ATPase by the same uncompetitive mechanism, Herrmann et al. (1992) and Kovács et al. (2004), respectively. In brief, BDM and blebbistatin bind allosterically to the myosin head with ADP and phosphate (P_i) bound to the substrate binding site. A conformational change induced by blebbistatin reduces the release of P_i from the active site thereby decreasing myosin-actin interaction (cross-bridge formation). IC_{50} values of force inhibition by BDM have been reported as 7.22 mM (Brixius et al., 2000) and 22±8 mM (Hebisch et al., 1993). BDM concentrations in the range 10-30 mM are often used for elimination of contractility in the Langendorff model (Kettlewell et al., 2004, Daly et al., 1987, Sill et al., 2009, Doumen et al., 1995, Hebisch et al., 1993, Yaku et al., 1993). Blebbistatin is enantiomeric and Shu et al. (2005) reported that racemic blebbistatin contains 59 % (-) and 41 % (+) and that a 100 % solution of (-)-blebbistatin inhibits myosin II ATPase with an IC_{50} of ~3-4 µM. This is similar to the IC_{50} value (1.2 µM) reported by Limouze et al. (2004).

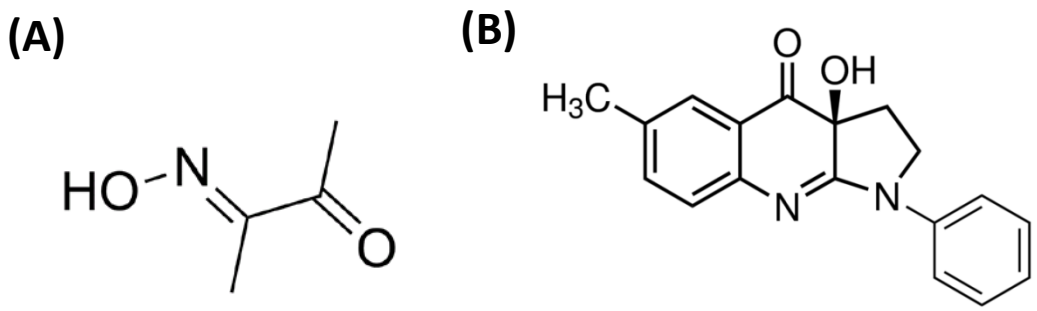

Figure 4.1 Chemical structures of 2,3-butanedione monoxime (BDM) and blebbistatin.

(A) BDM (PubChem= 6409633). **(B)** (-)-blebbistatin (**PubChem CID:3476986)**.

In this chapter, experiments were performed in isolated rat hearts perfused with BDM (10-30 mM) or 5 μM (±)-blebbistatin (≈2.95 μM (-)-blebbistatin) to uncouple contraction in the absence or presence of ouabain. The protocols were carried out in conjunction with TQF ^{23}Na NMR measurements to assess the dose-response relationship of $[Na]_i$ to ouabain in uncoupled preparations.

In a separate bench perfusion study, ouabain was administered to blebbistatin treated non-contracting hearts to assess possible metabolomic changes using semi-targeted metabolomics (^{1}H NMR) and lactate efflux measurements.

4.2 Aims

The aims of the studies described in this chapter are:

1. To assess the $[Na]_i$ dose-response and contractile response to ouabain in the electromechanically uncoupled perfused rat heart treated with BDM (10-30 mM).

2. To assess the $[Na]_i$ dose-response and contractile response to ouabain in the electromechanically uncoupled perfused rat heart treated with 5 µM blebbistatin.

3. To determine whether a semi-targeted metabolomics approach using ^1H NMR probes alterations in metabolism in response to ouabain in the non-contracting perfused rat heart.

4.3 Uncoupling contraction with 2,3-butanedione monoxime

4.3.1 Experimental methods

BDM was dissolved in standard KH (unless otherwise stated) to the required concentration (10, 20 and 30 mM) using sonication and vigorous mixing. Daly et al. (1987) showed that 30 mM BDM sequesters 1.3 mM Ca^{2+} and compensated for this by adding an extra 1.3 mM Ca^{2+} to their KH to a final concentration of 2.6 mM (giving a free Ca^{2+} concentration of 1.3 mM). Extra Ca^{2+} was added to the BDM solutions in this chapter based on the assumption that 30 mM BDM sequesters 1.3 mM Ca^{2+} and that this is a linear relationship across all BDM concentrations. Solutions of 10, 20 and 30 mM BDM were prepared with Ca^{2+} concentrations of 1.83, 2.27 and 2.70 mM, respectively, to give an estimated final free Ca^{2+} concentration of 1.4 mM.

Rat hearts were perfused in Langendorff mode as described in Section 2.2. Hearts were stabilised for 20 minutes with standard KH (Section 2.1.3) followed by 12 minutes of BDM perfusion. Hearts were subsequently perfused for a further 20 minutes with the same concentration of BDM in the absence or presence of 100µM ouabain. Interleaved

TQF and DQF ^{23}Na NMR measurements (Section 2.2.3) were performed throughout all perfusions. LVDP, heart rate and coronary flow were monitored throughout all perfusions.

A Vetscan® i-STAT®1 analyser with CG8+ cartridge (Abaxis UK) was used to determine the concentrations of Na^+, K^+ and Ca^{2+} in 20 mM BDM KH containing 2.27 mM $CaCl_2$ (as used in the BDM perfusion study) or 3.0 mM $CaCl_2$ to assess whether increasing Ca^{2+} concentration affects any of the iSTAT measurements.

To assess whether BDM alters the interaction of Na^+ with protein (which gives rise to the TQF signal), solutions containing 145 mM NaCl, 10 mg/mL bovine serum albumin (BSA, obtained from Sigma, UK) in the absence or presence of BDM (5, 10, 15 or 20 mM) were analysed by TQF ^{23}Na NMR (Section 2.2.3).

4.3.2 Results – Impact of BDM on functional parameters and $[Na]_i$

Isolated perfused hearts were initially perfused in a pilot study with 10, 20 and 30 mM BDM (n=1/group). 20 mM BDM was chosen for the main study (n=6/group) as it reduced contractility to a greater extent than 10 mM BDM and to the same extent as 30 mM BDM (Figure 4.2A). All perfusion parameters (Figure 4.2) reached steady-state by the end of the stabilisation period (0-20 minutes), according to previously defined exclusion criteria (detailed in Section 2.1.6) and were not significantly different ($P>0.05$) between any of the groups. BDM induced an immediate and significant ($P<0.0001$) negative inotropy with LVDP values of 3.3±0.6 mmHg and 2.9±0.4 mmHg in the 20 mM BDM group and the 20 mM BDM+Oua group, respectively. A small but

significant positive inotropic response occurred in the 20 mM BDM+Oua group during the ouabain treatment period that was sustained until the end of perfusion ($P<0.05$ vs 20 mM BDM group at 50 minutes). BDM reduced heart rate in a dose-dependent manner (Figure 4.2B). The reductions from baseline heart rate at the end of perfusion were 17 BPM (10 mM BDM), 69±13 BPM (20 mM BDM, $P<0.05$ vs baseline) and 187 BPM (30 mM BDM). Ouabain decreased heart rate further in the presence of 20 mM BDM (reduced by 115 BPM in the 20 mM BDM+oua group versus baseline; $P<0.001$). BDM reduced coronary flow (Figure 4.2C) by 4.8 mL/min (10 mM), 3.6±0.4 mL/min (20 mM; $P<0.0001$) and 5.2 mL/min (30 mM) at the end of perfusion versus baseline. There was no difference ($P>0.05$) in end-point coronary flow between the 20 mM BDM group (6.0±0.3 mL/min) and 20 mM BDM+oua group (6.0±0.6 mL/min).

Baseline derived apparent $[Na]_i$ (Figure 4.3A) was 18.0±0.4 mM in the 20 mM BDM group and was not different to that in the 20 mM BDM+Oua group (17.4±0.5 mM). BDM perfusion at 20 minutes resulted in an immediate decline in the normalised TQF signal and therefore derived $[Na]_i$ in both groups. After 10 minutes of perfusion with BDM, derived $[Na]_i$ was 11.8±0.4 mM in the 20 mM BDM group ($P<0.001$ vs baseline; paired t-test) and 12.6±0.4 mM in the 20 mM BDM+Oua group ($P<0.01$ vs baseline; paired t-test). This affect appeared to be dose dependent as the derived $[Na]_i$ in the 10 mM and 30 mM were 14.0 mM and 7.55 mM respectively. The dose-dependent separation persisted until the end of perfusion with derived end-point $[Na]_i$ values for the 10mM, 20 mM and 30 mM BDM of 14.2, 12.3±0.6 and 8.4 mM, respectively. In the 20 mM BDM+Oua group, there was an elevation in $[Na]_i$ after five minutes of ouabain

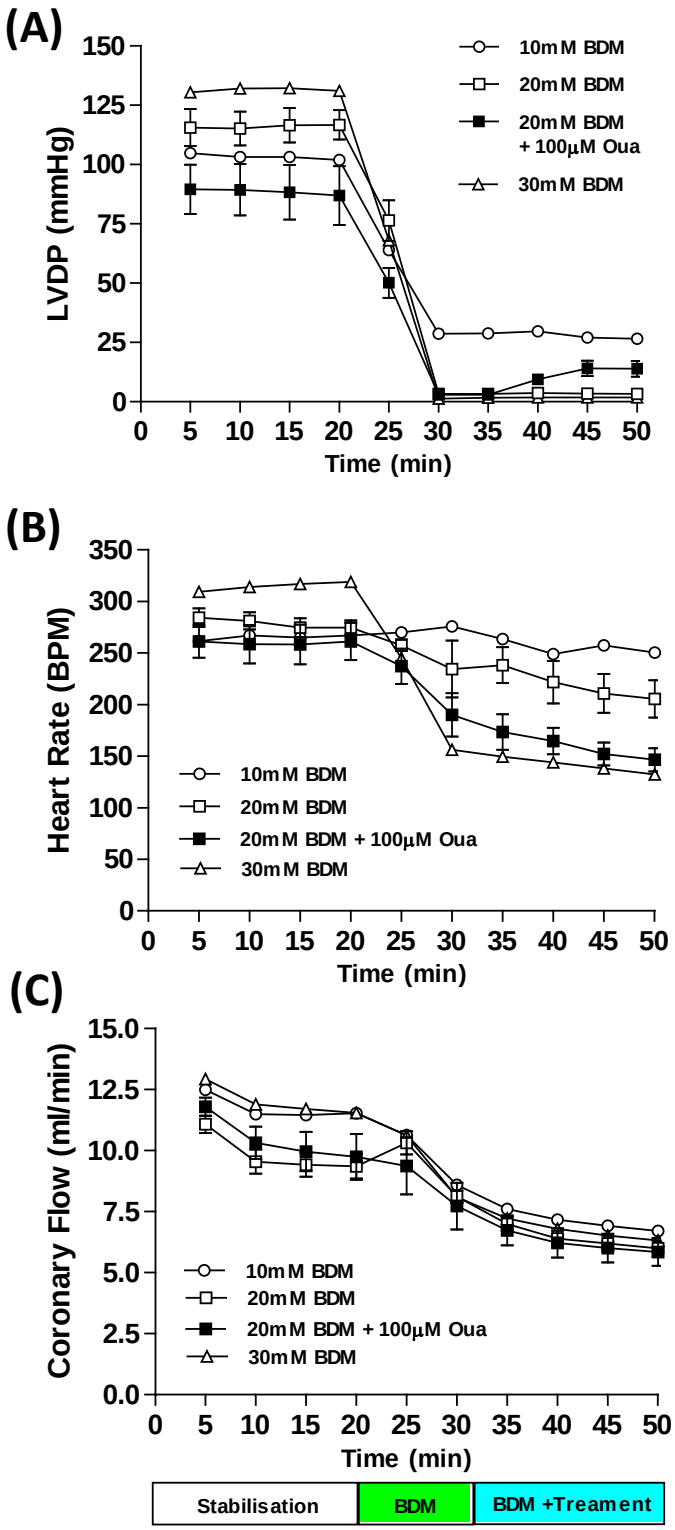

Figure 4.2 Ex vivo functional parameters recorded during stabilisation, BDM and BDM+Ouabain (Oua).

(A) Left ventricular developed pressure (LVDP). **(B)** Heart rate. **(C)** Coronary Flow. Symbols and error bars represent mean±SEM of five minute time windows (n=6/group).

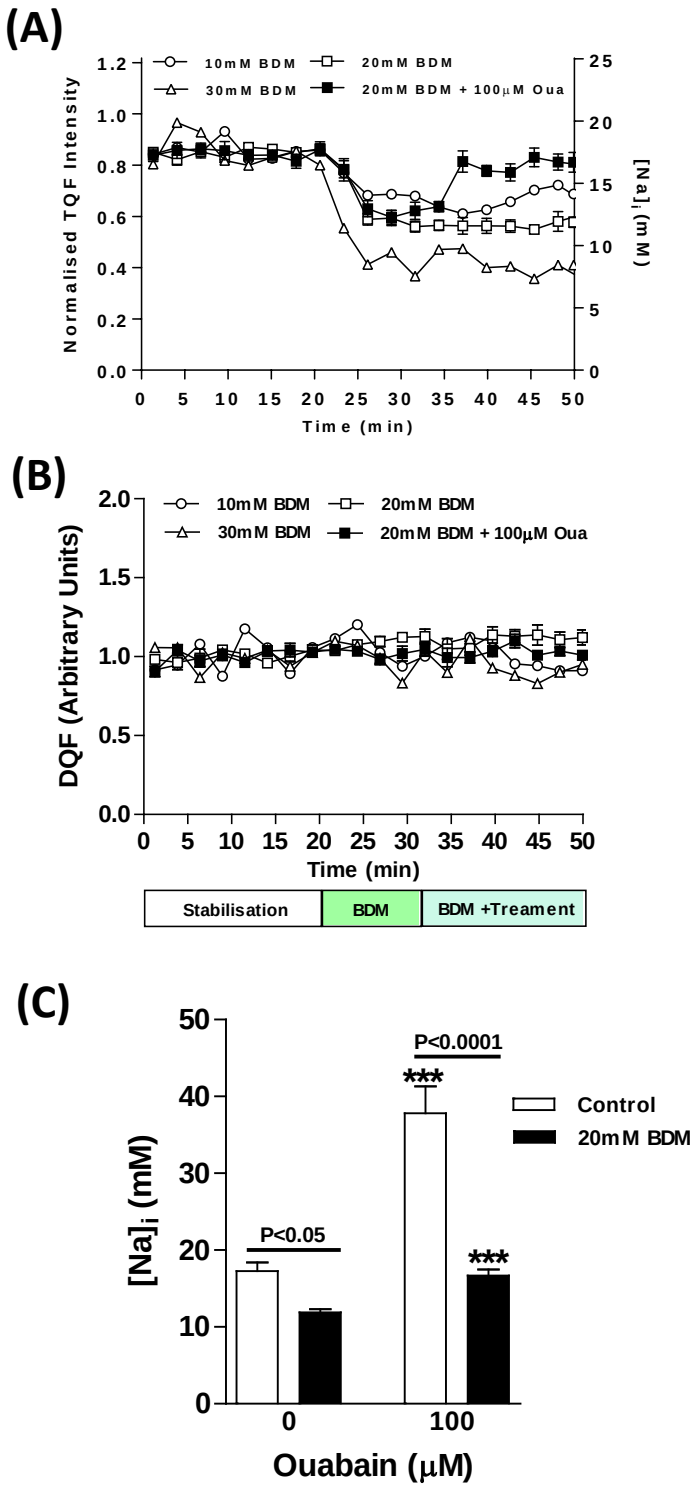

Figure 4.3 Effect of 2,3-butanedione monoxime (BDM) on TQF/DQF ^{23}Na NMR measurements.

(A) Normalised TQF signal as a function of time (left axis) and corresponding derived $[Na]_i$ (right hand axis). **(B)** Normalised DQF signal as a function of time. **(C)** End-point derived $[Na]_i$ for control and BDM group (***p<0.001 vs corresponding ouabain-free group). Data are displayed as mean±SEM (n=6/group). BDM-free data was from Section 3.3.2 (see Figure 3.1A for full $[Na]_i$ time profile of BDM-free control group).

treatment which reached a steady-state at 16 mM. This was sustained until the end of perfusion and was significantly higher than the 20 mM BDM group ($P<0.01$ at 50 minutes).

The normalised DQF signal (Figure 4.3B) did not markedly deviate from baseline (1.0±0.2) at any point of perfusion in any of the groups. Figure 4.3C displays the derived end-point $[Na]_i$ values from the 20 mM BDM study and the control study in Chapter 3. This data demonstrates that 20 mM BDM significantly decreased end-point apparent $[Na]_i$ versus control hearts by 31% ($P<0.05$) and 56% ($P<0.0001$) in the absence and presence of ouabain, respectively.

4.3.3 Results – Impact of BDM on free Na^+ and TQF ^{23}Na NMR signal *in vitro*.

The mechanism underlying the apparent drop in ^{23}Na TQF signal and therefore derived Na^+ in the presence of BDM is worth further investigation and may reflect a change in the visibility of Na^+ by TQF NMR rather than a real drop in $[Na]_i$. *In vitro* experiments were carried out in order to investigate a possible mechanism by which BDM reduces apparent observed $[Na]_i$. Table 4.1 shows the measured values of Na^+, K^+ and ionised Ca^{2+} (iCa) for a 20 mM BDM solution. The apparent concentration of free Na^+ was decreased by 30.3 % while the apparent concentration of free K^+ increased by only 2.2 % versus standard BDM-free KH. The measurement of free Na^+ and K^+ was not altered by different concentrations of added Ca^{2+}. However, iCa could not be measured in these BDM solutions due to “chemical interference” (according to the iSTAT instrument).

Nonetheless, the reduction in free Na^+ indicate that BDM directly chelates Na^+ with a stoichiometry of $2xNa^+$ per BDM molecule.

Table 4.1 Concentrations of free Na^+, K^+ and Ca^{2+} with BDM.

Sample	Na^+ (mM)	K^+ (mM)	iCa^{2+} (mM)
20 mM BDM KH with 2.27 mM $CaCl_2$	101	4.6	*Could not measure
20 mM BDM KH with 3.0 mM $CaCl_2$	101	4.6	*Could not measure

*Due to chemical interference (according to the iSTAT instrument). Blebbistatin (bleb); 2,3-butandione monoxime (BDM); ionised Ca^{2+} (iCa); KH (standard Krebs-Heinseleit buffer; see Section 2.1.3).

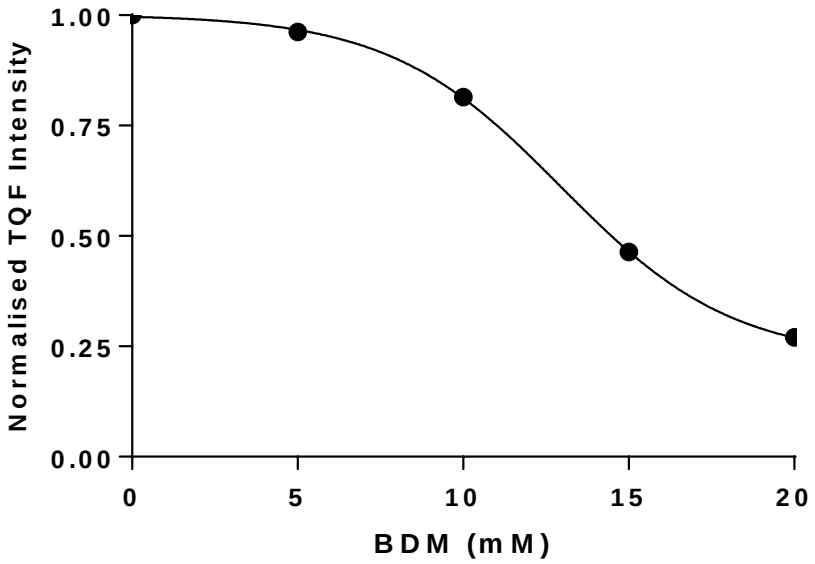

Figure 4.4 Normalised triple quantum filtered (TQF) ^{23}Na NMR intensity of NaCl solution with bovine serum albumin (BSA) and increasing concentrations of 2,3-butanedione monoxime (BDM).

Concentrations of NaCl and BSA were 145 mM and 10 mg/mL respectively in all solutions (n = 1 solution / BDM concentration).

Since BDM appeared to bind Na^+ based on the iSTAT measurements it was also investigated whether BDM would sequester Na^+ bound to protein and therefore change the visibility of Na^+ measured using ^{23}Na TQF NMR. The relationship between BDM concentration (0-20 mM) and normalised TQF intensity in solutions containing 145 mM Na^+ and 10 mg/mL BSA (Figure 4.4) was investigated and showed an inverse sigmoid with an IC_{50} value of 13 mM and a plateau of 0.25 at 20 mM BDM. This suggests that binding of Na^+ to BDM is able to sequester protein bound Na^+ and reduce the observability of Na^+ by TQF NMR.

4.4 Uncoupling contraction with Blebbistatin.

4.4.1 Experimental methods

Blebbistatin was dissolved according to the guidelines set out by Swift et al. (2012) to prevent the formation of precipitates within the microvasculature which can lead to ischaemia. (±)-blebbistatin (obtained from Bertin Pharma, France) was reconstituted in DMSO to a concentration of 17.11 mM followed by sonication and vortex mixing to ensure homogeneity. This stock solution was sub-aliquoted and stored at -80 °C until required for perfusion. Swift et al (2012) demonstrated that perfusion with 5 µM blebbistatin reduces contraction to negligible levels after 10 minutes in the isolated perfused rat heart. A 5 µM blebbistatin KH solution was prepared as follows: an aliquot of blebbistatin stock solution (17.11 mM) was allowed to thaw at room temperature and

then added directly into the final volume of standard KH (Section 2.1.3). This KH had been pre-heated to 43-45 °C with vigorous carbogen gassing and magnetic stirring for five minutes to ensure complete dissolution, followed by continued gassing until the solution was <30°C. Blebbistatin was protected from light at all times during preparation and perfusion using amber glassware and aluminium foil.

An initial bench study was performed with blebbistatin to assess function in the presence or absence of ouabain. Hearts were stabilised in standard KH for 20 minutes followed by 10 minutes of 5 µM blebbistatin KH perfusion. Hearts were then perfused with either 5 µM blebbistatin (bleb control group) or 5 µM blebbistatin containing 50µM ouabain (bleb+oua group) for 20 minutes. ECG was recorded continuously throughout perfusion and the time from the onset of activation to 90% recovery of repolarization (QT90%) was used as an indicator of electrophysiological status. Coronary effluent was collected every five minutes for lactate efflux assessment (Section 2.3). LVDP, heart rate, left ventricular end diastolic pressure (LVEDP) and coronary flow were monitored throughout all heart perfusions. Due to loss of the ventricular pressure during blebbistatin perfusion, heart rate was determined using ECG rather than ventricular pressure. At the end of the protocol hearts were snap-frozen (Section 2.1.9), followed by dual-phase extraction of metabolites (Section 2.4.2) and high resolution ^{1}H NMR metabolomics (Section 2.4.3).

Following the bench study a dose-response study of 50-155µM ouabain was then performed in the presence of blebbistatin using the ^{23}Na NMR perfusion setup (Section 2.2.2). All hearts were stabilised for 20 minutes with perfusion of standard KH (Section 2.1.3) followed by 12 minutes of perfusion with 5µM blebbistatin KH. Hearts were

subsequently perfused for 25 minutes with KH containing 5µM blebbistatin alone or 5µM blebbistatin containing 50, 75, 100 or 155 µM ouabain. TQF and DQF ^{23}Na measurements were performed throughout perfusion in an interleaved fashion (Section 2.2.3). LVDP, heart rate and coronary flow were monitored throughout all heart perfusions. Ventricular pressure was used for heart rate determination as ECG wires could not be used in conjunction with the NMR setup due to the introduction of external radiofrequencies that destroy the NMR signal.

The influence of DMSO as an additional vehicle was assessed in the absence of blebbistatin. The protocol was identical to that used for the Bleb+50µM group other than that blebbistatin was not added to the perfusate. Hence, the perfusate was 0.029% v/v DMSO KH between 20 and 32 minutes and 0.029% v/v DMSO KH + 50 µM ouabain between 32 and 55 minutes.

To assess any direct interaction between ouabain and blebbistatin, an Agilent 1200 LC and Agilent 6510 Q-TOF mass spectrometer with electrospray ionisation source (positive mode) was used to assess whether mixing blebbistatin (DMSO) and ouabain together in aqueous solution leads to the production of any new chemical entities or binding between the two drugs. The mobile phase was 0.1% formic acid (aq) : methanol (1:1). Three solutions were analysed via direct infusion: 5 µM blebbistatin (0.029% v/v DMSO) in water, 50 µM ouabain in water and 5 µM blebbistatin (0.029% v/v DMSO) + 50 µM ouabain in water. Data acquisition was kindly performed by Cinzia Imberti (Imaging Chemistry & Biology department, The Rayne Institute, KCL).

4.4.2 Results – Impact of blebbistatin on functional parameters, electrophysiology and metabolism in the isolated perfused rat heart.

Functional parameters were constant during the stabilisation period, according to predefined exclusion criteria (detailed in Section 2.1.6) and were not different ($P>0.05$) between the bleb control and bleb+oua group at any point of the perfusion protocol (0-50 minutes). Mean baseline values in the bleb control group of LVDP (Figure 4.5A), heart rate (Figure 4.5B), coronary flow (Figure 4.5C) and LVEDP (Figure 4.5D) were 133±4 mmHg, 283±9 BPM, 12±2 mL/min and 6±1 mmHg, respectively. LVDP (Figure 4.5A) decreased immediately and significantly ($p<0.0001$) following 5 µM blebbistatin perfusion at 20 minutes and was 9±1 mmHg in the bleb control group at 30 minutes (rate of decline during this '5µM bleb' period = 12±2 mmHg/min). The rate of decline during the 5µM 'bleb + treatment' period (0.4± 0.1 mmHg/min) was considerably lower ($p<0.0001$; paired t-test) than that during the '5µM bleb' period. At the end of the perfusion, LVDP was 1±0.8 mmHg in the bleb control group. Blebbistatin perfusion appeared to have no effect on heart rate (Figure 4.5B) as measured by ECG. However, coronary flow (Figure 4.5C) was similar to the LVDP profile, declining rapidly during the '5µM bleb' period and then appeared to reach a new steady-state value (4.7±0.9 mL/min in the bleb control group) at 35 minutes that was significantly different ($p<0.05$; paired t-test) to baseline. LVEDP (Figure 4.5D) was significantly elevated by blebbistatin at the end of perfusion (19±2 mmHg in the bleb control group; $p<0.001$; paired t-test) versus baseline. There were no differences in functional parameters between bleb control and bleb+oua. The lactate efflux profile (Figure 4.5E) was similar to the LVDP and coronary flow profiles. There was a sharp and significant reduction

($p<0.01$; paired t-test) from a baseline of 310±55 nmol/min/g at 20 minutes to 162±33 after five minutes of perfusion with blebbistatin, followed by a slower decrease during the '5μM bleb + treatment' period with a value of 111±26 nmol/min/g at the end of perfusion in the bleb control group ($p<0.01$ vs baseline; paired t-test). There were no differences ($P>0.05$) in lactate efflux between bleb control and bleb+oua at any point of perfusion.

Perfusion of 5 μM blebbistatin had no notable effects on the shape of the ECG trace (Figure 4.6A) despite cessation of contractility. QT90% (Figure 4.6B) was not significantly different ($P>0.05$) between baseline and 5μM blebbistatin measurements.

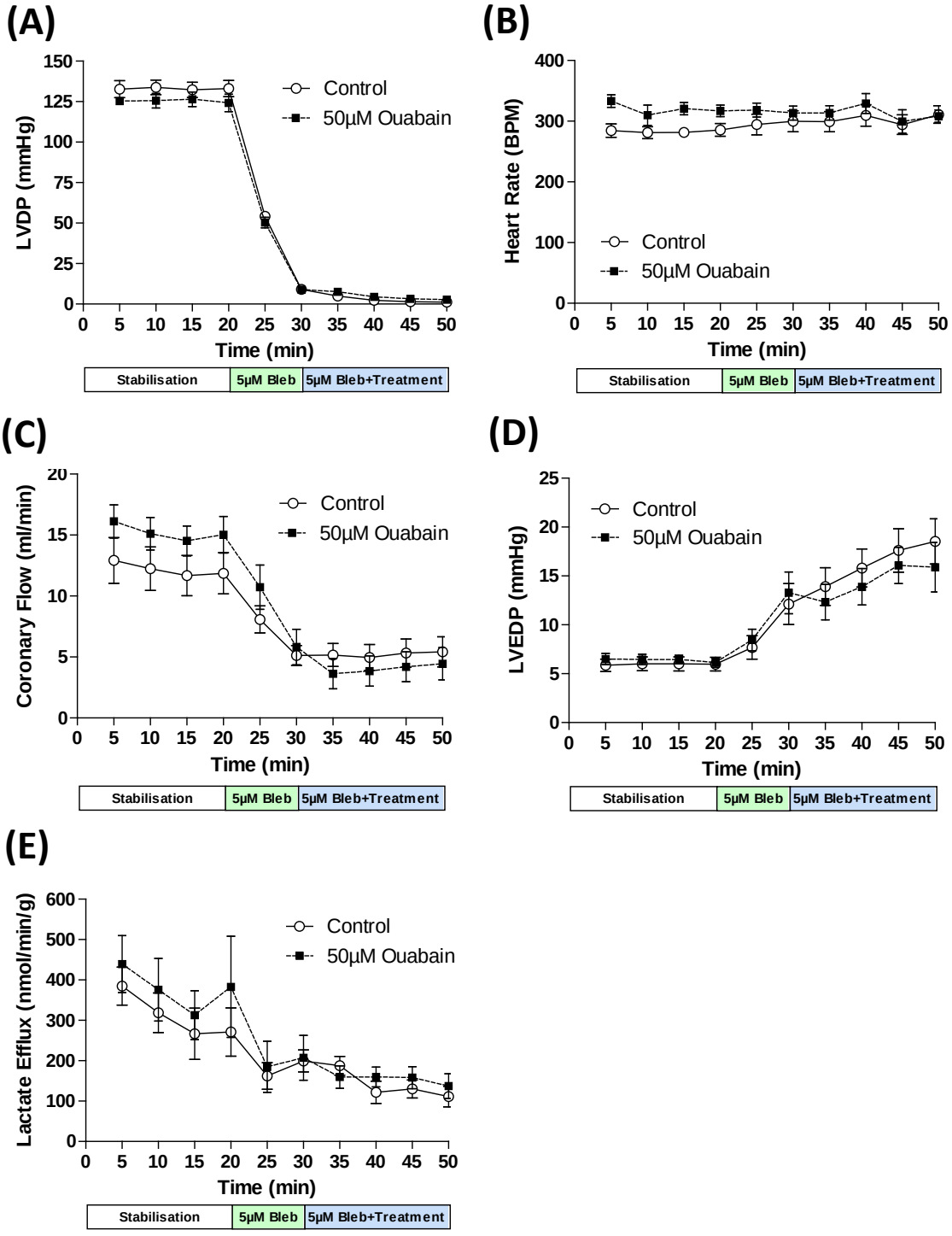

Figure 4.5 Effect of 5 µM blebbistatin and 50 µM ouabain on functional measurements and lactate efflux.

(A) Left ventricular developed pressure (LVDP). **(B)** Heart rate. **(C)** Coronary flow. **(D)** Left ventricular end diastolic pressure (LVEDP). **(E)** Lactate efflux. Symbols and error bars represent mean±SEM of five minute time windows (n=6/group). Hearts were snap-frozen at 50 minutes.

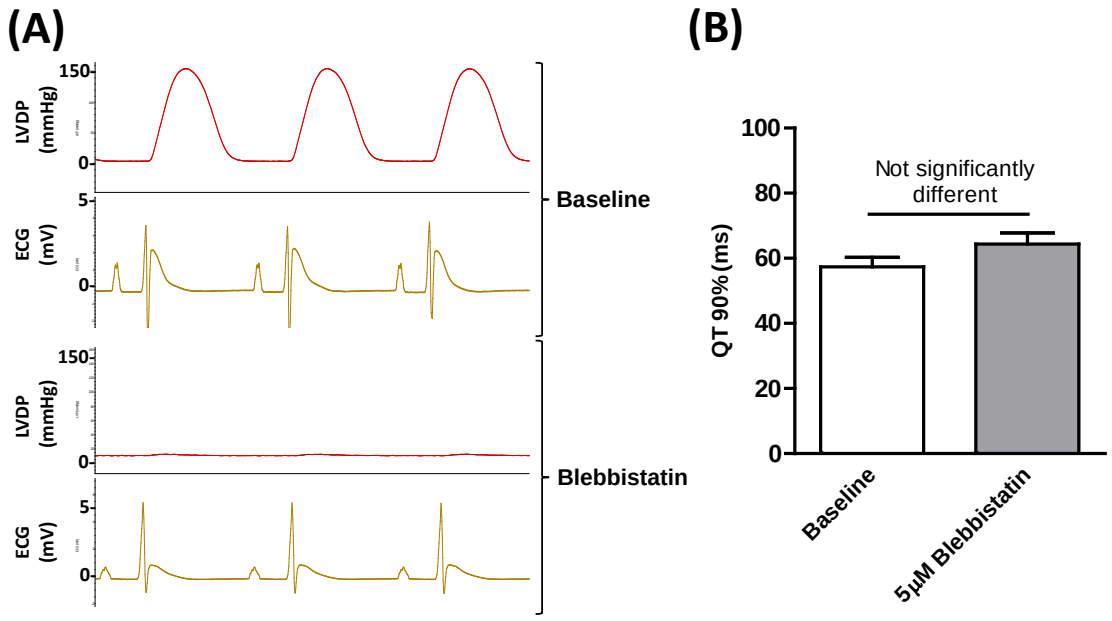

Figure 4.6 Blebbistatin does not significantly affect electrophysiology.

(A) Representative left ventricular developed pressure (LVDP) traces and corresponding ECG traces before blebbistatin (baseline) and following 30 minutes of 5 μM blebbistatin in the same heart. **(B)** QT90% at baseline ('stabilisation' period) and following 30 minutes of perfusion with 5 μM blebbistatin ('bleb + treatment' period). Data correspond to mean±SEM of five ECG complexes at the end of the perfusion period with n=6 hearts/group, i.e, 30 complexes/group. Statistical significance was assessed using paired t-test.

Hearts were snap frozen at the end of the protocol in Figure 4.5 and metabolites were extracted for high resolution ^{1}H NMR metabolomics (Figure 4.7). In the two non-contracting groups of hearts, treatment with 50 μM ouabain resulted in decreases in fumarate (-36%; $P<0.05$), glutamate (-22%; $P<0.001$) and glutamine (-14%; $P<0.05$) whereas acetate was increased (6%; $P<0.001$) under these conditions. Full details of the non-contracting metabolomics dataset is shown in Appendix 8.4.

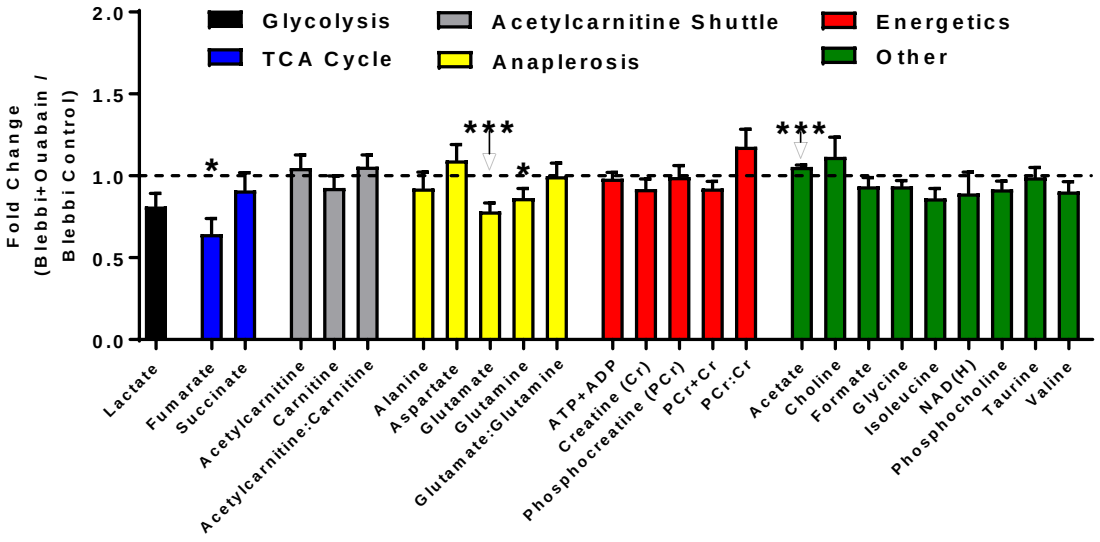

Figure 4.7 ^{1}H NMR metabolomic profile for 5 μM Blebbistatin alone vs 5 μM blebbistatin + 50 μM ouabain.

Data represent mean fold change ± propagated SEM (n=4-6/metabolite/group). A fold change of '1.0' represents zero change vs control. *p<0.05; **p<0.01; ***p<0.001; #p<0.0001.

4.4.3 Results - Ouabain induces a dose dependent elevation of $[Na]_i$ but is attenuated in the presence of blebbistatin.

The dose-response relationship between ouabain concentration and $[Na]_i$ in the presence of 5 μM blebbistatin was investigated using TQF ^{23}Na NMR. Functional parameters (Figure 4.8) were constant throughout the stabilisation period according to predefined acceptance criteria (Section 2.1.6). Mean LVDP values (Figure 4.8A) of greater than 70 mmHg were considered acceptable during this period to account for trace levels of blebbistatin present in the perfusion rig from preceding experiments. There were no differences in LVDP (P>0.05) between the bleb control, bleb+50 μM ouabain, bleb+75 μM ouabain and bleb+100 μM ouabain groups during stabilisation. Baseline LVDP was significantly higher in the bleb+155μM oua group compared with the bleb control and

bleb+75µM oua groups. However, as baseline levels of derived $[Na]_i$ (Figure 4.9), heart rate (Figure 4.8B) and coronary flow (Figure 4.8C) in the bleb+155µM oua group were not different to the other groups and because $[Na]_i$ was the main focus of the study, the bleb+155µM oua was included. Blebbistatin significantly reduced LVDP (Figure 4.8A) in all groups to <30 mmHg after 10 minutes perfusion ($P<0.01$ versus baseline; paired t-test). In the bleb control and bleb+50µM oua groups, LVDP continued to fall slowly during the bleb+treatment period with end-point values of 1.6±0.2 mmHg and 2.3±0.2 mmHg respectively. These were not significantly different ($P>0.05$; one-way ANOVA) to end-point LVDP values for bleb+75µM oua (5.0±0.9 mmHg) and bleb+100µM oua (4.6±0.5 mmHg). However, a small, transient positive inotropy occurred in the bleb+75µM oua and bleb+100µM oua groups which peaked at 40 minutes with values of 12±2 mmHg and 10±2 mmHg ($p<0.05$ vs bleb control group at 40 minutes). A large positive inotropic effect occurred in Bleb+155µM oua with a maximum value of 67±3 mmHg at 40 minutes that was significantly higher than all other groups ($P<0.0001$; one-way ANOVA) at this time point. End-point LVDP in Bleb+155µM oua was also significantly higher ($P<0.0001$; one-way ANOVA) in this group (22±2 mmHg) compared with all other groups. There were no significant deviations ($P>0.05$; paired t-test) from baseline heart rate in any of the groups at any stage of the perfusion protocol (Figure 4.8B). Coronary flow (Figure 4.8C) mimicked the general LVDP profile with significantly reduced flow due to blebbistatin at 35 minutes ($p<0.05$ vs baseline, paired t-test). End-point coronary flow was significantly higher ($P<0.05$) in the bleb+155µM oua group versus the bleb+50µM oua group. There were no other differences in end-point coronary flow between the groups ($P>0.05$; one-way ANOVA).

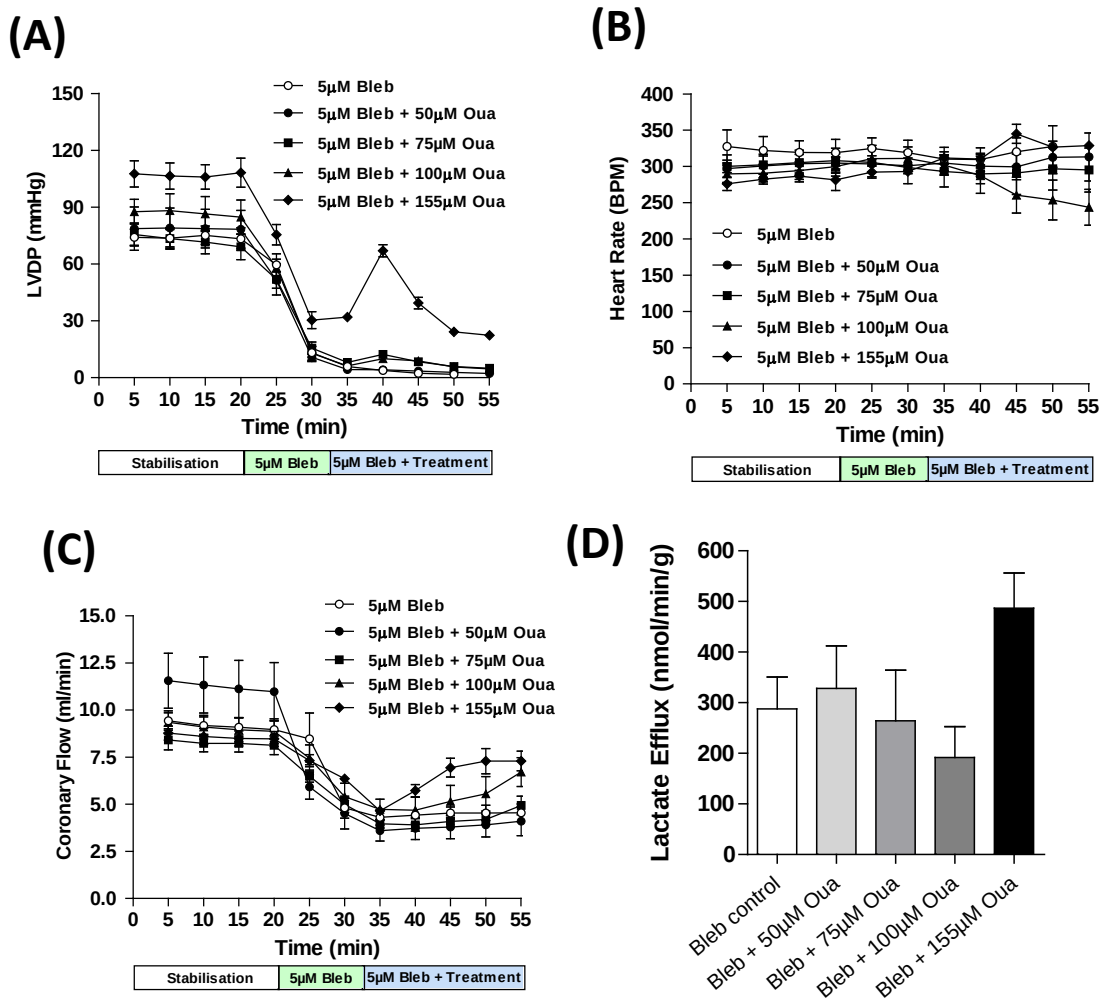

Figure 4.8 Effect of 5 µM blebbistatin (bleb) and 50, 75, 100 and 155 µM ouabain on functional measurements and lactate efflux.

(A) Left ventricular developed pressure (LVDP). **(B)** Heart rate. **(C)** Coronary flow. **(D)** Lactate efflux (during '5 µM Bleb + Treatment' period). Symbols and error bars represent mean±SEM (n=6/group).

Pooled coronary effluent was collected throughout the 'bleb+oua period' (32-55 minutes) and lactate efflux was determined (Figure 4.8D). Values were 288±63 nmol/min/g (bleb control), 328±84 nmol/min/g (bleb+50µM oua), 264±100 nmol/min/g (bleb+75µM oua), 191±60 nmol/min/g (bleb+100µM oua) and 487±70 nmol/min/g

(bleb+155µM oua). There were no significant differences between any of the groups ($P>0.05$; one-way ANOVA).

$[Na]_i$ measured by TQF ^{23}Na NMR (Figure 4.9A) was constant throughout the stabilisation period (0-20 minutes) in all groups and there were no differences between the groups ($P>0.05$; one-way ANOVA). Normalised DQF (Figure 4.9B) did not markedly deviate from baseline (1.0±0.2; $P>0.05$; paired t-test) at any point of perfusion in any of the groups. In the bleb control group, there appeared to be a trend towards decreased $[Na]_i$ after 10 minutes of perfusion with 5µM blebbistatin which seemed to reach a new steady-state at 15±1.6 mM. However, this was not significantly different ($P<0.05$) to the bleb-free/oua-free control value from Chapter 3 (Figure 4.10A). Perfusion with bleb+50µM oua did not induce a significant elevation ($P>0.05$) in end-point derived $[Na]_i$ (20±0.6 mM) versus bleb control and was significantly lower ($P<0.0001$) than the corresponding bleb-free 50 µM ouabain value (31±1.5 mM) ascertained in Chapter 3 (Figure 4.10).

End-point derived $[Na]_i$ values in bleb+75 µM oua (23±1.1 mM) and bleb+100 µM (28±1.0 mM) were significantly elevated compared to the bleb control group. Derived $[Na]_i$ in the bleb+75 µM ouabain and bleb+100 µM ouabain was significantly lower ($P<0.05$) than their bleb-free counterparts (39±3.5 mM and 38±3.5 mM respectively). In the presence of 5 µM blebbistatin, the concentration of ouabain required to induce an equivalent end-point derived $[Na]_i$ to that of bleb-free 75 µM oua and bleb-free 100 µM was 155 µM ($[Na]_i$ = 42±3 mM). A comparison of the dose-response curves (Figure 4.10B) for ouabain in the absence (Chapter 3) and presence (Chapter 4) of blebbistatin

reveals that blebbistatin significantly altered the dose response relationship between [ouabain] and $[Na]_i$.

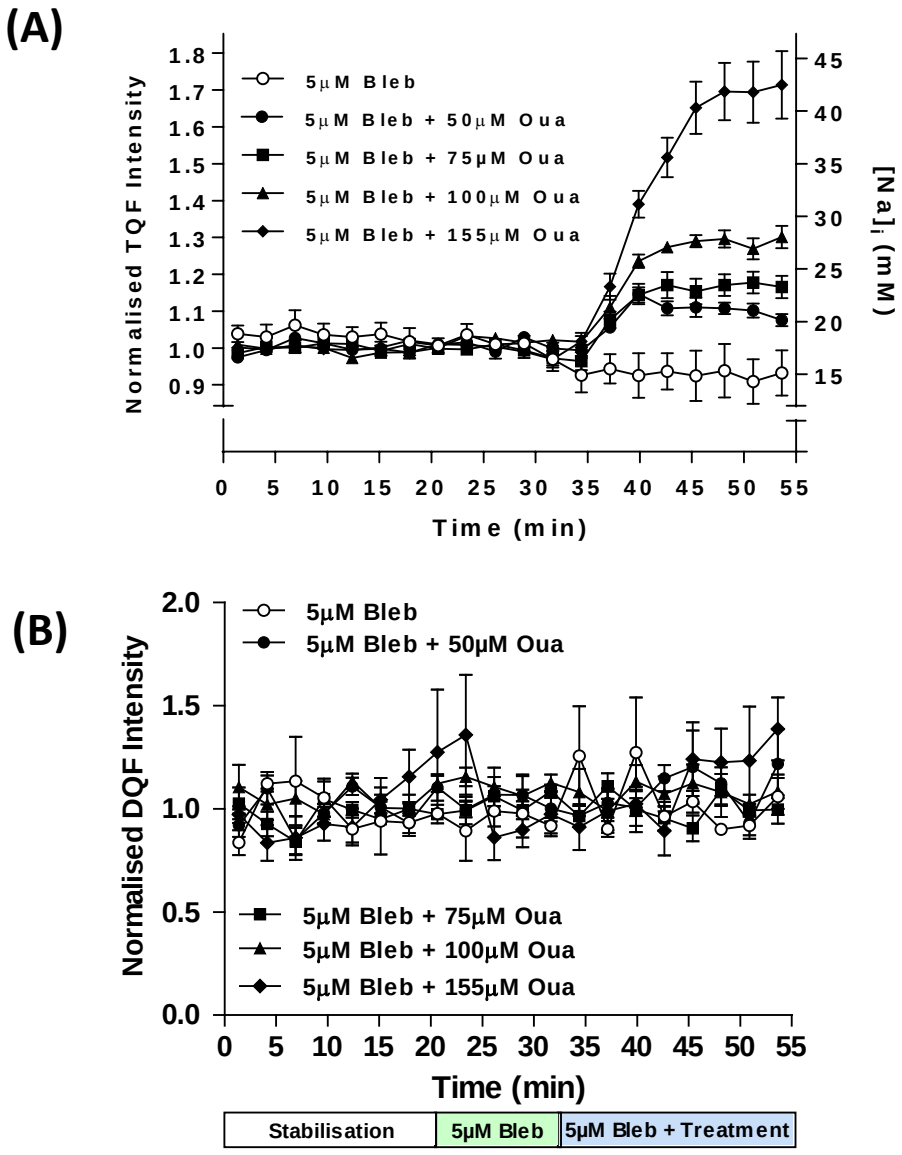

Figure 4.9 Dose-response of ouabain and derived $[Na]_i$ in the presence of blebbistatin.

(A) Normalised TQF signal as a function of time (left axis) and corresponding derived $[Na]_i$ (right hand axis). **(B)** Normalised DQF signal as a function of time. Data are displayed as mean±SEM (n=6/group).

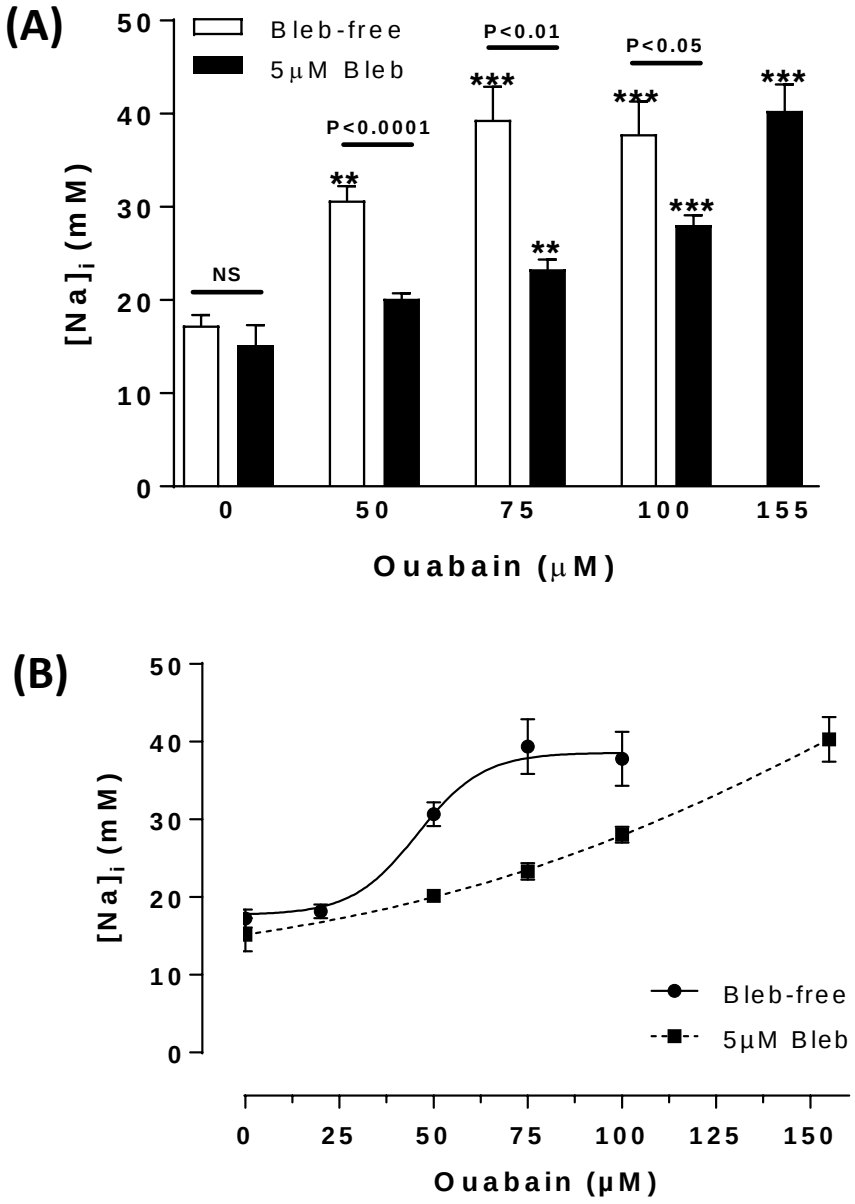

Figure 4.10 Ouabain concentration versus end-point derived intracellular sodium concentration ($[Na]_i$) in the absence and presence of 5μM blebbistatin (bleb).

(A) Dose-response histogram. P-values above columns represent comparisons between bleb-free and 5μM bleb values at the same ouabain concentration. Stars above columns represent comparisons between ouabain concentration and corresponding ouabain-free control at the same bleb concentration (*P<0.05, **P<0.01, ***P<0.001; one-way ANOVA with Dunnet's post-hoc test). **(B)** Dose-response curves. Bleb-free was constrained (bottom=17.71; top=38.59; slope=0.05). Data plotted as mean±SEM at the end of perfusion (55 minutes). Bleb-free data was from Section 3.3.2. See Figures 3.1A (bleb-free) and 4.9A (with 5μM bleb) for full $[Na]_i$ time profiles.

Perfusion with 0.029% v/v DMSO KH (n=1) in the absence of blebbistatin had no effect on baseline derived $[Na]_i$ (17.4 mM) and subsequent perfusion for 25 minutes with 0.029% v/v DMSO KH + 50 µM ouabain increased derived $[Na]_i$ to an end-point value of 36.4 mM. DMSO had no effect on normalised DQF signal which was stable throughout perfusion. LVDP, HR and coronary flow were within normal ranges during stabilisation (according to pre-defined exclusion criteria described in Section 2.1.6) and were not altered by perfusion with DMSO. A small, transient positive inotropic effect occurred following subsequent perfusion with 50 µM ouabain.

4.4.4 Does blebbistatin attenuate ouabain inhibition of NKA in ventricular cardiac myocytes?

In vitro experiments were carried out in order to investigate possible mechanisms by which blebbistatin attenuates ouabain action. A whole-cell voltage-clamp study was kindly performed by Dr Sergiy Tokar (Cardiovascular Division, KCL) to assess whether blebbistatin attenuates ouabain inhibition of NKA. The objective was to determine whether blebbistatin (5mM) interferes with the ability of ouabain (50µM) to inhibit the Na^+/K^+ pump.

The activity of electrogenic sarcolemmal ion transporters in isolated cardiomyocytes can be ascertained using the whole-cell voltage-clamp technique (reviewed by Bebarova, 2012). In brief, a micropipette is used to form a tight seal between the electrode glass and the cell surface. The membrane under the tip of the pipette is ruptured allowing the electrode electrical access to the cell interior. Current flow across the entire cell membrane can then be measured with respect to an extracellular

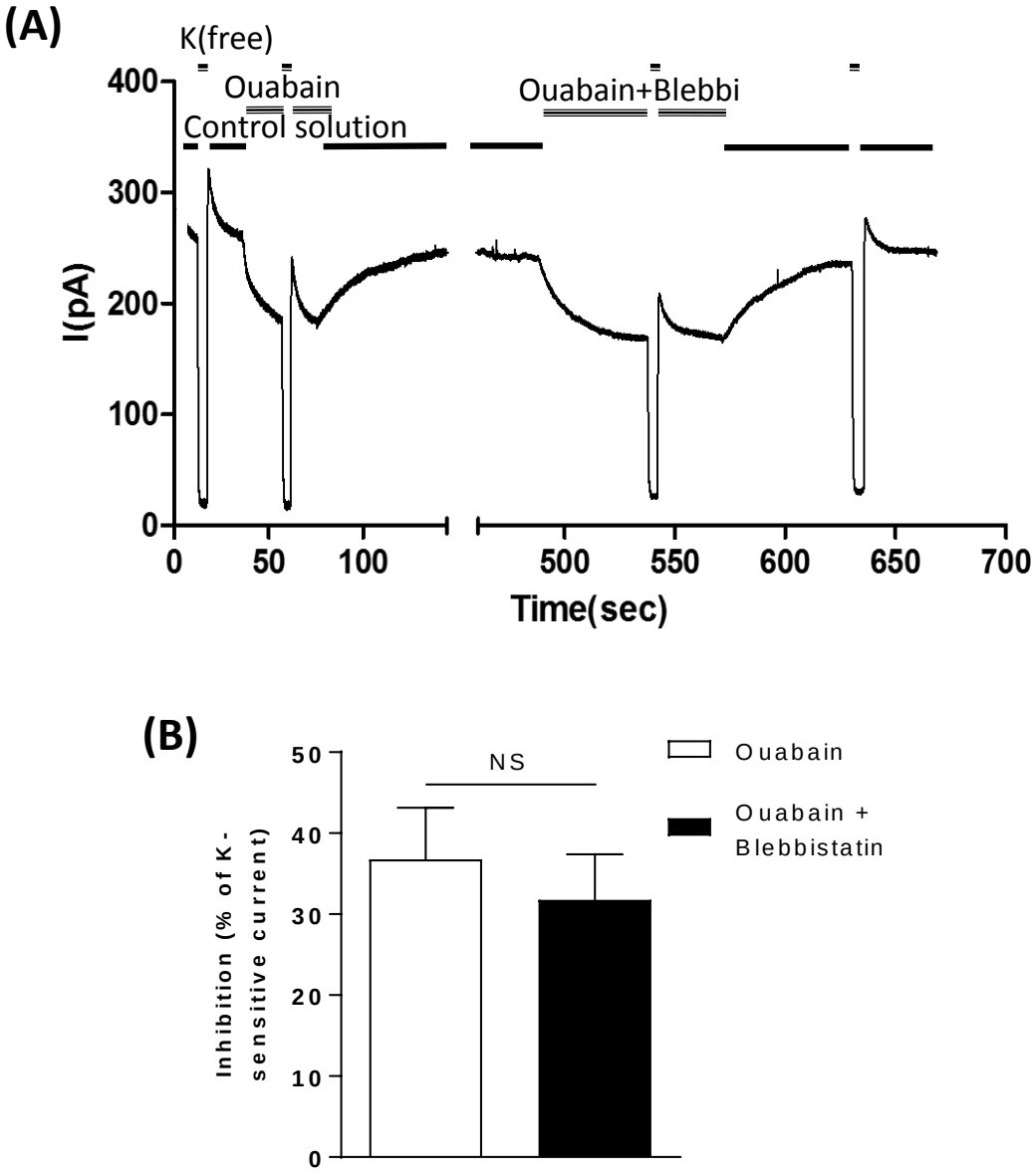

Figure 4.11 Whole-cell patch-clamp measurements with 5 μM blebbistatin and 50 μM ouabain.

These experiments were kindly performed by Dr Sergiy Tokar (Cardiovascular Division, The Rayne Institute, KCL) using the method described in Pavlovic et al (2007) with solutions slightly modified as follows: pipette solution contained (in mM): CsCH3O3S (95), NaCH3O3S (25), CsCl (20), Hepes (10), EGTA (5), MgATP (5), sodium creatine triphosphate (5), CaCl2 (1), MgCl2 (1). External solution contained (in mM): NaCl (140), KCL (5), Hepes (10), NiCl2 (2), MgCl2 (1), BaCl2 (1) (in K^+ free solution 5 mM of KCl were replaced with same amount of NaCl). **(A)** Representative raw current trace of a rat left ventricular cardiomyocyte. **(B)** Mean inhibition of Na^+/K^+ ATPase by ouabain with and without blebbistatin plotted as % of current during K^+-free period. Values were taken during steady-state (n = 7-9 cells/group; 5 hearts used in total).

reference. The pipette and extracellular solutions are formulated to isolate the electrogenic current of interest (in this case the Na^+/K^+ pump current) and the cell membrane is clamped to 0mV to inactivate Na^+ channels. Under these conditions, the Na^+/K^+ pump current is defined as that sensitive to removal of extracellular K^+. Cells were exposed to ouabain (50µM) and ouabain (50µM) + blebbistatin (5mM).

4.4.5 Results - Patch clamp

The control membrane current values (Figure 4.11A) were similar to those obtained previously (Shattock and Matsuura, 1993, Silverman et al., 2005). The extent of NKA inhibition by 50 µM ouabain (37±2 % of the maximally available pump current as defined by the K^+ sensitive current) was not significantly altered by the presence of 5 µM blebbistatin (32±2 %, $P>0.05$) (Figure 4.11B).

4.4.6 Results – Blebbistatin does not sequester ouabain or Na^+.

Mass spectrometry data acquired of a mixed solution of blebbistatin and ouabain revealed that the molecular ions of blebbistatin (292 g/mol) at 293 m/z and DMSO (78 g/mol) at 79 m/z and its corresponding Na^+ adduct at 101 m/z were present as well as the molecular ion of ouabain (585 m/z) and the corresponding Na^+ adduct at 607 m/z. However there were no new peaks of any notable abundance. No new chemical entities were formed after mixing 5 µM blebbistatin with 50 µM ouabain according to mass spectrometry analysis and it can therefore be concluded that blebbistatin does not sequester ouabain. Mass spectra for these analyses are shown in Appendix 8.5.

A Vetscan® i-STAT®1 analyser with CG8+ cartridge (Abaxis UK) was used to determine the concentrations of Na^+, K^+ and iCa in 5 µM blebbistatin KH and were unchanged with respect to standard KH composition (145, 4.5 and 1.3 mM respectively).

4.4.7 Results - Does contractile motion affect the observability of $[Na]_i$ by TQF ^{23}Na NMR?

Changes in contractility and cardiac motion have the potential to change the observability of ^{23}Na by NMR due to changes in magnetic field homogeneity. Peak line-width is a reflection of field homogeneity and therefore the detectability of an analyte using NMR.

Removal of contractility using either 5 µM blebbistatin or 20 mM BDM did not change the shape (Figures 4.12A & 4.12B) or line-width (Figures 4.12C & 4.12D) of the TQF/DQF ^{23}Na peak compared with time-matched contracting control hearts.

4.5 Discussion

4.5.1 BDM inhibits contraction and significantly attenuates the dose response of ouabain observed by TQF NMR.

In agreement with previous reports, BDM significantly reduced inotropy (Figure 4.2A) (Kettlewell et al., 2004, Daly et al., 1987, Sill et al., 2009, Doumen et al., 1995, Hebisch et al., 1993, Yaku et al., 1993) but was associated with significant bradycardia (Figure 4.2B). BDM also resulted in a significant reduction in derived end-point baseline

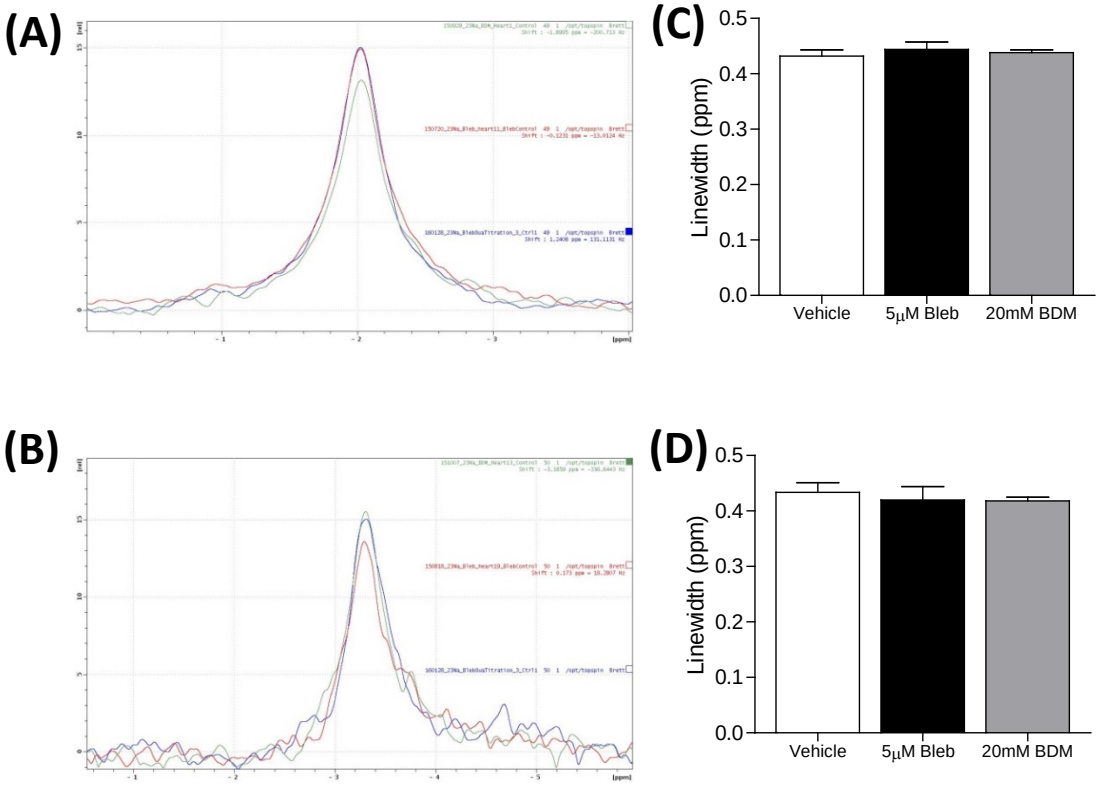

Figure 4.12 Contractile motion does not alter ^{23}Na NMR measurements in isolated perfused rat hearts.

(A) Triple quantum filtered (TQF) signal and (B) double quantum filtered (DQF) signal. Peaks are time-matched representative spectra at end of perfusion in contracting vehicle (DMSO, blue), non-contracting blebbistatin ('bleb', red) and non-contracting 2,3-butanedione monoxime (BDM, green). Linewidths (width at half peak height) of TQF signal (C) and DQF signal (D) were plotted for each group (n=5-6). *P<0.05 (one-way ANOVA).

(Control) $[Na]_i$ by 31% (Figure 4.3C) as measured by TQF NMR and also attenuated the apparent $[Na]_i$ elevation due to 100 μM ouabain by 56% (Figure 4.3C). Despite this attenuation, $[Na]_i$ was significantly higher in the BDM+100 μM oua group versus the BDM control group. Addition of 100 μM ouabain to 20 mM BDM led to a significant positive inotropy hence a higher concentration of BDM would be required to negate this

effect in future studies. However, 30 mM BDM was associated with even greater reductions in heart rate and baseline $[Na]_i$ which may further confound metabolic measurements compared with 20 mM BDM.

4.5.2 BDM sequesters Na^+ *in vitro*.

The reduction in baseline apparent $[Na]_i$ in the perfused heart could be a result of BDM sequestering $[Na]_i$. *In vitro* investigations demonstrated that BDM reduced free-Na^+ by approximately one-third and prevented the measurement of Ca^{2+} using the iSTAT instrument (Table 4.1) presumably due to interference with the Ca^{2+}-sensitive electrochemical detector. Increasing the concentration of Ca^{2+} in this BDM solution did not overcome this issue and so it was not possible to confirm the work of Daly et al. (1987) showing that BDM is a chelator of Ca^{2+}. Nonetheless, this study demonstrated that BDM sequesters Na^+ with an apparent stoichiometry of 2xNa per BDM molecule and may explain the reduction in baseline TQF observability of $[Na]_i$ following perfusion of rat hearts with 20 mM BDM (Figure 4.3C).

Furthermore, the reduction in the normalised TQF signal in the presence of protein *in vitro* (Figure 4.4) indicates that BDM binds competitively to Na^+ (given that the TQF signal is dependent upon Na^+-protein interactions). This is in agreement with the BDM-Na^+ sequestration data as well as the BDM-induced reduction in baseline $[Na]_i$ in perfused hearts. Although the BDM-induced reduction in TQF signal *in vitro* was very large (75% decrease), it should be noted that a relatively high [Na] (145 mM) was used with a relatively low concentration of protein (10 mg/mL) in order to amplify any

effects of BDM. *In vivo*, the concentrations of $[Na]_i$ and protein are closer to 10 mM and 100 mg/mL respectively, which may explain why the BDM-induced reduction in normalised TQF intensity in the perfused heart experiments (by ~33%) was more modest than that in the *in vitro* experiment.

4.5.3 Blebbistatin inhibits contraction in the absence of altered electrophysiology.

Perfusion of hearts with 5 μM blebbistatin rapidly decreased contractile function to negligible levels (Figures 4.5A and 4.8A). This is in agreement with Swift et al. (2012) and Brack et al. (2013). The concomitant decreases in coronary flow (Figures 4.5C and 4.8C) and lactate efflux (Figures 4.5E and 4.8D) are most probably due to reduced oxygen consumption. The reason for LVEDP elevation following blebbistatin perfusion (Figure 4.5E) could be due to increased ventricular stiffness as a consequence of conformational changes in the myofilament proteins. Elevated LVEDP due to blebbistatin perfusion was also reported by Brack et al. (2013).

Despite elimination of LVDP, blebbistatin had no effect on QT90% (Figure 4.6B). The strong agreement between values of QT90% for control rat hearts obtained in this chapter (~60 ms) with those obtained elsewhere (Clements-Jewery et al., 2002, Dhanjal et al., 2013, Rees and Curtis, 1993). Furthermore, Fedorov et al. (2007) demonstrated that blebbistatin does not significantly alter pacemaker activity, conduction, repolarization or $[Ca]_i$ cycling in both the rat and rabbit heart.

The ouabain-dose response study using TQF ^{23}Na NMR described in Chapter 3 was repeated in this chapter except with the addition of blebbistatin. Perfusion with

blebbistatin alone did not have any significant impact upon baseline derived $[Na]_i$ (Figure 4.10A) which aligns with its lack of electrophysiological effects. Interestingly, blebbistatin appeared to both attenuate, and change the shape of, the dose-response curve from a sigmoidal relationship to a more linear relationship between [ouabain] and derived $[Na]_i$ (Figure 4.10B). The mechanism by which blebbistatin attenuates ouabain action has not been previously reported. Mass spectrometry data acquired of a mixture of ouabain and blebbistatin revealed no binding between the two drugs suggesting that blebbistatin does not sequester ouabain. Furthermore, iSTAT analysis revealed that blebbistatin does not sequester Na^+ and patch clamp experiments (Figure 4.11B) using isolated cardiomyocytes suggested that blebbistatin does not attenuate the ability of ouabain to inhibit NKA. In the blebbistatin protocols there is potential for interference of the DMSO vehicle on the derived $[Na]_i$, particularly as there is evidence to suggest that DMSO is a Na^+-channel antagonist (Jacob and de la Torre, 2009). DMSO had no effect on baseline derived $[Na]_i$ or ouabain-induced $[Na]_i$ elevation in the perfused rat heart, and therefore the probability of this having any impact on the blebbistatin-induced attenuation of ouabain in this model seems low. Also, a Na^+ channel agonism by either blebbi or DMSO would alter the QRS duration of the ECG and also QT90 (Suzuki et al., 1991).

4.5.4 Contractile motion does not affect the measurement of $[Na]_i$ by TQF ^{23}Na NMR.

Figure 4.12 demonstrates that removal of contraction using either blebbistatin or BDM did not alter the linewidth of the TQF ^{23}Na NMR peak thereby inferring that Na^+

visibility due to changes in magnetic field homogeneity is not affected by changes in contractile motion in the perfused rat heart.

4.5.5 Blebbistatin is more sensitive and has less impact on $[Na]_i$ than BDM.

The perfusate concentration of BDM required for the cessation of contraction was 10,000-fold higher than that for blebbistatin. This is in agreement with the differences in IC_{50} values for force inhibition by these compounds reported by Brixius et al. (2000), Shu et al. (2005) and Limouze et al. (2004). Perfusion with 100 µM ouabain in the presence of BDM led to a significant elevation in derived end-point $[Na]_i$ (16 mM). If this value is normalised for the initial BDM-induced reduction in derived $[Na]_i$ (from 18 to 12 mM) then a corrected value of 28 mM is obtained. This value was also obtained for the bleb+100µM ouabain group and represents an attenuation compared with the BDM-free/bleb-free 100µM ouabain group in Chapter 3 (Figure 4.10A). Despite a significantly higher concentration of BDM used in these experiments compared with blebbistatin, the extent of ouabain attenuation (accounting for the differences in pre-ouabain $[Na]_i$) appears to be very similar between these electromechnical uncouplers. In contrast, there was no significant reduction in $[Na]_i$ following perfusion with ouabain-free blebbistatin but a large reduction in $[Na]_i$ with ouabain-free BDM. Taken together, this may infer that the effects of these compounds on $[Na]_i$ have two components: one that is dependent on the concentration of the electromechanical uncoupler in the absence of ouabain and another that is independent of the concentration of the electromechanical uncoupler in the presence of ouabain. These findings are suggestive of a mechanism that could be common to electromechanical uncouplers leading to ouabain attenuation

although further work is necessary to elucidate this mechanism. Comparison of the chemical structures of blebbistatin and BDM (Figures 4.1A and 4.1B) reveals little similarity although they inhibit myosin II ATPase in the same uncompetitive manner (Kovács et al., 2004, Herrmann et al., 1992) which may be relevant to the mechanism by which they attenuate ouabain action.

Blebbistatin shows substantially higher efficacy as an electromechanical uncoupler than BDM and has no marked effect on baseline $[Na]_i$. Furthermore, there are several reports of BDM exhibiting off-target effects at concentrations required for the cessation of contractility including metabolic effects (Doumen et al., 1995, Hebisch et al., 1993, Scaduto and Grotyohann, 2000) and altered concentrations of intracellular ions (Kettlewell et al., 2004, Liu et al., 1993, Baker et al., 2004, Watanabe et al., 2001). BDM has also been shown to have reversible inhibitory effects on metabolism (Doumen et al., 1995, Hebisch et al., 1993, Scaduto and Grotyohann, 2000) and electrophysiology (Kettlewell et al., 2004). Other studies have suggested that BDM decreases Ca^{2+} and K^+ currents (Liu et al., 1993), $[Ca]_i$ (Baker et al., 2004) and EC coupling including sarcolemmal NCX exchange (Watanabe et al., 2001).

4.5.6 Ouabain does not alter metabolomic profile in blebbistatin treated non-contracting hearts.

None of the ouabain concentrations used in this study in the presence of blebbistatin significantly altered lactate efflux in non-contracting hearts (Figure 4.5E & 4.8D), in contrast to their contracting counterparts in Chapter 3 (Figures 3.4 and 3.7). End-point metabolomics in non-contracting hearts perfused with 50 μM ouabain (Figure 4.7)

largely abolished most of the metabolic alterations observed in contracting hearts in Chapter 3 (Figures 3.5 & 3.8). The reduction in fumarate is in contrast to the elevation observed in the contracting models following ouabain perfusion in Chapter 3. The reason for this is unclear but may reflect its concentration being sensitive to both $[Na]_i$ elevation and alterations in inotropy. Furthermore, the elevations in acetylcarnitine, creatine and choline observed in Chapter 3 were not observed in the non-contracting model in this chapter. This suggests that these metabolites are inotropy dependent rather than $[Na]_i$ dependent. The reductions in glutamate and glutamine observed in non-contracting hearts could potentially reflect an increase in anaplerosis following perturbations in ATP supply-demand matching due to $[Na]_i$ elevation. The very modest elevation in acetate by 6% was measured with a high degree of precision using ^1H NMR. Despite the limited magnitude of this change, the very low error associated with the measurement revealed that this change was statistically significant ($P<0.001$). A small reduction in fatty acid substrate utilisation from triglyceride stores following $[Na]_i$ elevation is a possible explanation for this although it seems unlikely that this would have any significant bearing on the overall metabolic status of the heart.

The metabolomic changes observed in the absence of a positive inotropic effect following ouabain perfusion under non-contracting conditions infer a modest sensitivity of the TCA cycle, anaplerosis and possibly substrate utilisation to $[Na]_i$ elevation. However, the relevance of this to contracting hearts is probably limited. The non-contracting isolated heart model used in this chapter has made clearer which metabolites are sensitive to the positive inotropic effect of ouabain but is clearly unphysiological. Pulseless electrical activity (PEA; a type of cardiac arrest) is the only *in vivo* situation in

which the heart sustains normal electrophysiology in the absence of cardiac output and is out of the scope of this thesis. An important difference between contracting and non-contracting hearts is the significant reduction in ATP demand and oxygen consumption thus differences in intermediary metabolism are likely. For example, Peuhkurinen et al. (1982) found that TCA cycle flux is 42% lower in arrested hearts perfused with K^+-free KH compared with beating hearts. It is therefore likely that any metabolic remodelling due to $[Na]_i$ elevation is different between contracting and non-contracting hearts.

4.6 Summary

In this chapter, two electromechanical uncouplers (BDM and blebbistatin) were evaluated in the perfused rat heart, in order to remove inotropy and thereby distinguish $[Na]_i$-dependent from inotropy-dependent metabolic consequences of ouabain. BDM (20 mM) eliminated contractility but was associated with a significant reduction in baseline apparent $[Na]_i$ measured by real-time TQF ^{23}Na NMR. Blebbistatin eliminated contractility with a higher efficacy (5 μM) than BDM and did not alter baseline $[Na]_i$ or electrophysiology (QT90%). Both BDM and blebbistatin appeared to attenuate the ability of ouabain to elevate $[Na]_i$. This was overcome in blebbistatin-perfused hearts by adding additional ouabain to the perfusate (155 μM ouabain + 5 μM blebbistatin elevated $[Na]_i$ to the same degree as 100 μM ouabain alone). *In vitro* investigations revealed that BDM sequesters Na^+ with a stoichiometry of 2xNa per BDM molecule and that BDM competes with protein for Na^+ thereby reducing the TQF ^{23}Na NMR signal. However, blebbistatin does not sequester Na^+ or ouabain. Moreover, patch

clamping experiments in isolated cardiomyocytes suggested that blebbistatin does not alter NKA inhibition by ouabain. In contrast to contracting hearts in Chapter 3, 50 μM ouabain did not alter lactate efflux in non-contracting hearts perfused with blebbistatin. Furthermore, blebbistatin largely abolished the metabolomic changes due to ouabain observed in contracting hearts in Chapter 3. Small reductions in fumarate, glutamate and glutamine and a small increase in acetate occurred due to $[Na]_i$ elevation in this non-contracting preparation. However, the relevance of these alterations to the beating heart is questionable given the marked reduction in ATP demand in the absence of contraction. Due to its substantially higher efficacy and lower impact on $[Na]_i$ compared with BDM, blebbistatin was selected as the most suitable electromechanical uncoupler. This method was developed further in Chapters 5 and 6 in which the positive inotropic effect of ouabain was titrated out using blebbistatin in contracting hearts with $[Na]_i$ overload.

5 DISTINGUISHING $[Na]_i$-DEPENDENT FROM INOTROPY-DEPENDENT ALTERATIONS IN ENERGETICS AND METABOLOMICS.

5.1 Introduction

In Chapter 4, it was concluded that co-infusion of ouabain, to elevate $[Na]_i$, in combination with blebbistatin, to uncouple contraction, did not profoundly alter the metabolite profile in non-contracting hearts as measured using ^1H NMR. However, removing all contractility from the heart leads to a large reduction in ATP demand, potentially masking metabolomic alterations that may have occurred due to $[Na]_i$ elevation. It was also previously highlighted the difficulty in distinguishing between metabolic alterations that may be due to $[Na]_i$ elevation directly from those that were due to the positive inotropy (and increased ATP demand) associated with $[Na]_i$ elevation. It is therefore necessary to assess whether metabolic alterations occur due to ouabain induced $[Na]_i$ elevation in hearts allowed to contract intrinsically with a more physiological ATP demand while removing the confounding influence of positive inotropy using blebbistatin. The idea is that the blebbistatin concentration can be titrated in to prevent a positive inotropy but not abolish contraction. That is, when ouabain is added, contractility should not change despite the elevation in intracellular Na^+. Blebbistatin has slightly slower pharmacokinetics than ouabain (Figures 4.5A and 3.1A) therefore simply co-perfusing these compounds at fixed concentrations throughout the perfusion protocol would induce transient periods of inotropy. Two perfusion protocols were therefore developed in which ouabain and blebbistatin were co-perfused into the

Langendorff rat heart in an opposite order to induce $[Na]_i$ overload while reversing inotropic effects. Perfusion initially with ouabain alone followed by a period of titration with blebbistatin plus ouabain initially elevated contractility which subsequently returned back down to baseline levels, while maintaining a sustained elevation of $[Na]_i$. This is referred to as the transient positive inotropy (TPI) group. On the other hand, perfusing initially with blebbistatin plus ouabain followed by ouabain alone initially depressed contractility followed by a recovery back up to baseline but again with a sustained elevation of $[Na]_i$. This is referred to as the transient negative inotropy (TNI) group. Taken together, the TPI and TNI protocols would assess metabolic alterations that are common to both studies and therefore considered $[Na]_i$-dependent and contractility-independent, while those occurring in only one study would be considered contractility-dependent, i.e, whether the heart has "metabolic memory" for contractility. This may elucidate which metabolic pathways, if any, are remodelled in contracting hearts due to $[Na]_i$ overload. End-point metabolomic analysis by ^{1}H NMR and targeted LC-MS/MS, as well as real-time cardiac energetics were assessed during the perfusion protocols by ^{31}P NMR.

5.2 Aim

The aim of this chapter is to determine whether $[Na]_i$ elevation gives rise to metabolic alterations that are independent of inotropic changes in the contracting perfused rat heart.

5.3 Experimental Methods

In Chapter 3, it was shown that 100 µM ouabain elevated derived $[Na]_i$ to approximately 40 mM (Figure 3.2A & 3.2B) without observable toxic effects, while in Chapter 4, it was demonstrated that the effect of ouabain on $[Na]_i$ was attenuated by blebbistatin and that 155 µM ouabain was required to elevate derived $[Na]_i$ to approximately 40 mM (Figures 4.9A, 4.10A & 4.10B). In order to determine the concentrations of blebbistatin and ouabain required for the TNI and TPI protocols, different concentrations of these compounds were co-perfused in preliminary test hearts to ascertain the appropriate doses. Different concentrations were titrated in the two protocols to give approximately equal but opposite degrees of positive or negative inotropy while yielding an equivalent elevation of end-point $[Na]_i$.

Rat hearts were perfused in the Langendorff mode as described in Section 2.1. The TPI and TNI protocols were carried out in independent studies each with a vehicle counterpart. Hearts were perfused in a randomised-fashion. The perfusion protocols are summarised in Table 5.1. LVDP, heart rate, coronary flow and LVEDP were recorded continuously throughout each experiment. Based on initial experiments, it was estimated that the mean concentration of vehicle (DMSO, used for blebbistatin reconstitution) at 55 minutes in ‘TPI’ and ‘TNI’ hearts was approximately 800 µM and this concentration was therefore used in the ‘Vehicle’ groups. Separate perfusion reservoirs were used for each of the different perfusion solutions. Titrations were carried out by adding a small volume (approximately 5-10 mL every 5 minutes) of the appropriate stock solution into the appropriate reservoir containing the initial perfusion solution (pre-warmed to 39 °C and gassed vigorously with carbogen). This resulted in a

gradual and stable return to baseline LVDP at which time no further titrant was added. Homogeneity of the perfusion solutions was ensured by vigorous gassing and manual mixing by hand using the gas distribution tube in each perfusion reservoir.

Heart perfusions were performed within the NMR spectrometer using the perfusion setup as described in Section 2.2.2. Hearts were split into two sub-groups (n=6/sub-group): one in which interleaved ^{23}Na TQF and ^{23}Na DQF NMR measurements were performed (described in Section 2.2.3) and the other in which ^{31}P energetics were performed (described in Section 2.2.4). Both NMR protocols were acquired in real-time throughout the entirety of the perfusion protocols (0-55 minutes). Hearts were snap-frozen at approximately 55 minutes as described in section 2.1.9.

Aqueous metabolites were isolated as per Section 2.4.2. High resolution ^{1}H NMR (n=5-6/group) was performed to obtain a global insight into metabolism (Section 2.4.3) and TCA cycle intermediates were quantified using LCMSMS (n=10-12/group) as described in Section 2.4.4.

Table 5.1 Perfusion protocols used in the TPI/TNI study

Group	0-20 mins	20-30 mins	30-55 mins	55 mins
Vehicle	Stabilisation	800μM DMSO	800μM DMSO	Snap-freezing
Transient Positive Inotropy (TPI)		100μM ouabain	100μM ouabain (titrated with a single solution of 155μM ouabain + 5 μM blebbistatin)	
Transient Negative Inotropy (TNI)		1.5μM blebbistatin + 50μM ouabain	100μM ouabain (titrated with 200μM ouabain)	

5.4 Results – TPI and TNI protocols remove transient inotropy while sustaining elevated $[Na]_i$.

All perfusion parameters were constant during the stabilisation period, according to predefined exclusion criteria (detailed in Section 2.1.6) and there were no differences during this period between TPI or TNI compared with their corresponding vehicle. Baseline LVDP (Figures 5.1A and 5.1E) was 104±5 mmHg in vehicle and was not altered by subsequent DMSO perfusion (103±6 mmHg; $P>0.05$; paired t-test). In the TPI group, LVDP was elevated significantly ($P<0.0001$; paired t-test) to a maximum of 173±8 mmHg at 30 minutes (after 10 minutes of perfusion with 100µM ouabain) but returned to baseline at 45 minutes (114±9 mmHg) following blebbistatin/ouabain titration and remained stable then until 55 minutes (104±6 mmHg). In the TNI group, LVDP initially increased ($P<0.01$) versus baseline after 5 minutes of perfusion with 1.5µM blebbistatin + 50µM ouabain and then decreased to a minimum of 42±3 mmHg at 35 minutes (following 15 minutes of perfusion with 1.5µM blebbistatin + 50µM ouabain; $P<0.0001$ vs baseline; paired t-test). LVDP then returned to baseline at 50 minutes (99±6 mmHg) following blebbistatin-free ouabain titration for 15 minutes and remained stable until 55 minutes (106±6 mmHg). Heart rate (Figure 5.1B and 5.1F) was 283±10 BPM at baseline and was not altered by DMSO vehicle (284±11 BPM; $P>0.05$; paired t-test). The TPI group exhibited a significant bradychardia at 30 minutes (213±21 BPM; $P<0.01$ vs vehicle) but returned to baseline levels by the end of perfusion (Figure 5.1B).

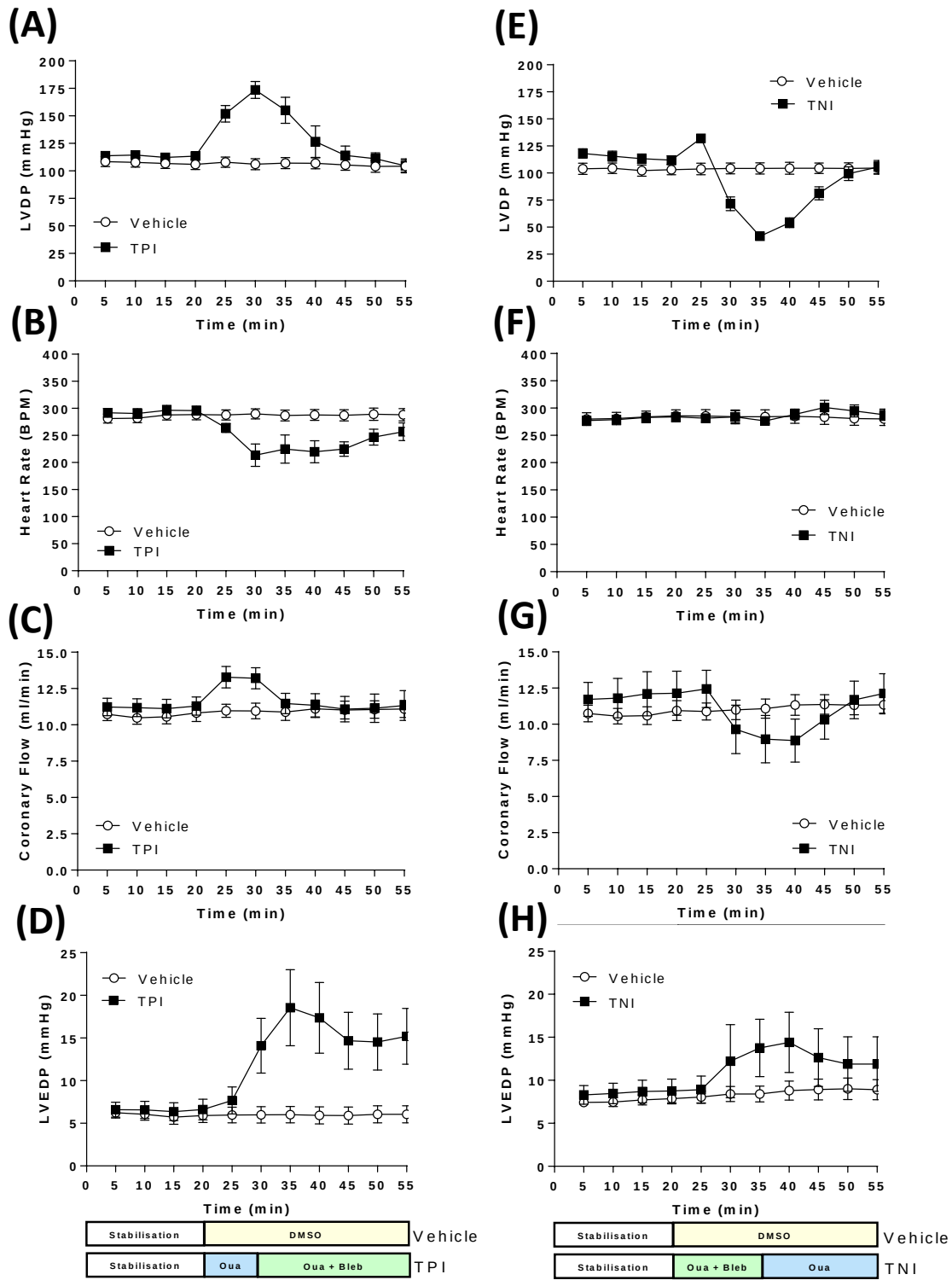

Figure 5.1 Functional measurements in the transient positive inotropy (TPI) and transient negative inotropy (TNI) protocols.

TPI: **(A)** Left ventricular developed pressure (LVDP). **(B)** Heart rate. **(C)** Coronary flow. **(D)** Left ventricular end diastolic pressure (LVEDP). TNI: **(E)** LVDP. **(F)** Heart rate. **(G)** Coronary flow. **(H)** LVEDP. Symbols and error bars represent mean±SEM of five minute time windows (n=11-12/group). Hearts were snap-frozen at 55 minutes. Blebbistatin (Bleb); dimethyl sulfoxide (DMSO); ouabain (Oua). See Table 5.1 for full protocol details.

No significant change in heart rate occurred at any point during the TNI protocol ($P>0.05$ vs vehicle) (Figure 5.1F). DMSO had no effect ($P>0.05$) on coronary flow (Figure 5.1C & 5.1G) which was 11±0.6 mL/min at baseline in vehicle. Ouabain caused a small but significant elevation in coronary flow at 25-30 minutes (13±1mL/min, $P<0.05$ vs vehicle) before returning to baseline levels at 35 minutes which was sustained until the end of perfusion (Figure 5.1C). In the TNI group, coronary flow (Figure 5.1G) was similar to the LVDP profile with a transient reduction ($P>0.05$ vs baseline) following blebbistatin+ouabain perfusion but then returned to baseline following perfusion with blebbistatin-free ouabain. LVEDP (Figures 5.1D and 5.1H) was 7.7±1.3 mmHg at baseline in vehicle and was not altered by DMSO perfusion ($P>0.05$; paired t-test). However, LVEDP was significantly higher ($P<0.0001$) at 30-55 minutes in the TPI group (16±3.6 mmHg) vs vehicle (6.0±1.0 mmHg) and showed a trend towards an elevation during the TNI period (13±3.5 mmHg) although did not reach statistical significance ($P>0.05$).

$[Na]_i$ derived from the TQF signal (Figures 5.2A and 5.2C) was constant throughout the stabilisation period in vehicle (18±0.6 mM), TPI (18±0.4 mM) and TNI (18±0.4 mM). DMSO vehicle had no effect on derived $[Na]_i$ (17±0.9 mM; $P>0.05$; paired t-test). Derived $[Na]_i$ was significantly higher ($P<0.001$) in the TPI group (29.1±1.7 mM) compared with its vehicle group (17.3±1.1 mM) at the end of perfusion (Figure 5.2A). Derived end-point $[Na]_i$ was also significantly higher ($P<0.01$) in the TNI group (30.7±2.9 mM) compared with its vehicle group (16.8±1.2 mM) at the end of perfusion (Figure 5.2C). DQF signal did not markedly deviate from baseline (1.0±0.1 arbitrary units) at any point of perfusion in both groups (Figures 5.2B and 5.2D).

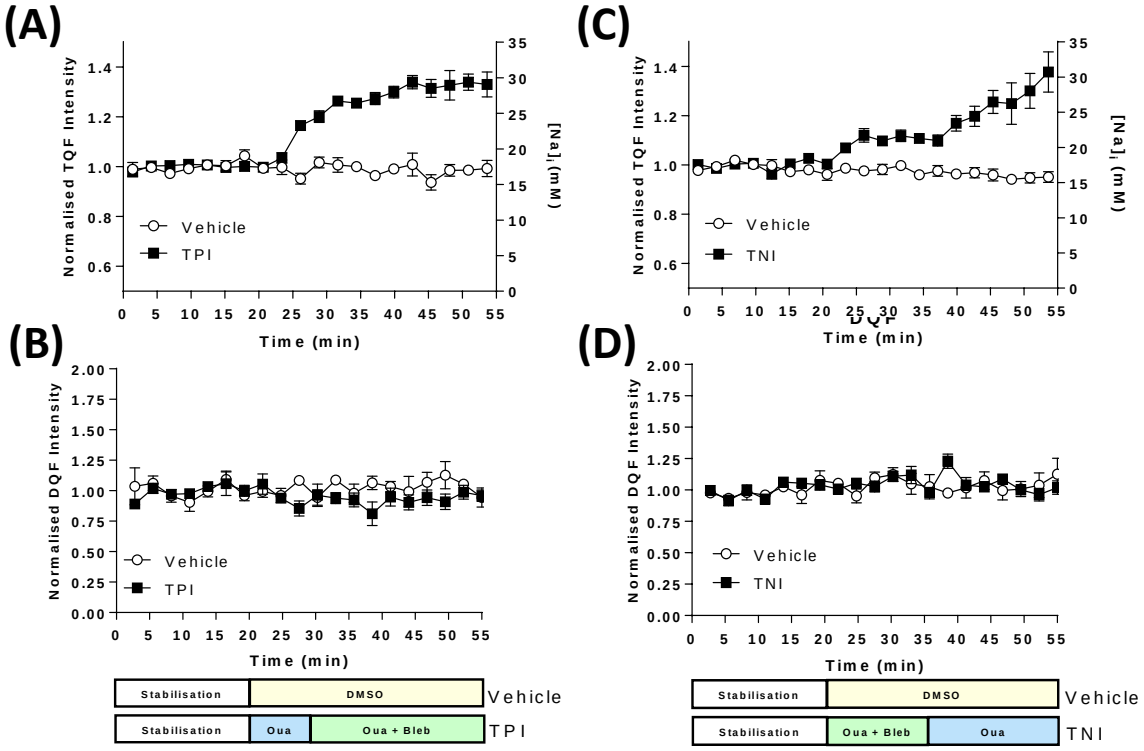

Figure 5.2 TQF/DQF ^{23}Na NMR measurements in transient positive inotropy (TPI) and transient negative inotropy (TNI).

TPI: **(A)** Normalised triple quantum filtered (TQF) ^{23}Na NMR intensity (left axis) with derived intracellular $[Na]_i$ (right axis). **(B)** Normalised double quantum filtered (DQF) ^{23}Na NMR intensity. TNI: **(C)** Normalised TQF ^{23}Na NMR intensity (left axis) with derived intracellular $[Na]_i$ (right axis). **(D)** Normalised double quantum filtered (DQF) ^{23}Na NMR intensity. Symbols and error bars represent mean±SEM of 1.5 minute time windows (n=6/group). Hearts were snap-frozen at 55 minutes. Blebbistatin (Bleb); dimethyl sulfoxide (DMSO); ouabain (Oua). See Table 5.1 for full protocol details.

5.5 Results - Cardiac energetics measured by ^{31}P NMR.

Representative ^{31}P NMR spectra of the P_i, PCr and β-ATP peaks are shown as a function of time in Figure 5.3. All cardiac energetics parameters had reached a steady-state by the end of the stabilisation period with no significant differences between TPI

(Figure 5.4) and TNI (Figure 5.5) groups versus their respective vehicles during this period. In the vehicle groups, DMSO caused no significant deviations from baseline levels of any of the measured parameters ($P>0.05$). However, ATP slowly declined in the TPI group (Figure 5.4A) immediately upon ouabain perfusion and plateaued at 35% below baseline levels at 35 minutes. Similarly, ATP slowly declined in the TNI group immediately upon perfusion with 1.5µM blebbistatin + 50µM ouabain (Figure 5.5A). At 55 minutes, ATP was significantly lower in both TPI (Figure 5.6A) and TNI (by 27%, Figure 5.7A) compared with their vehicle groups ($P<0.01$). There was a strong, negative correlation ($r = -0.9$; $P<0.0001$) between ATP and derived $[Na]_i$ in both TPI and TNI (Figure 5.8).

In TPI, PCr fell by 50% during the transient period of positive inotropy compared with baseline after five minutes of ouabain perfusion (Figure 5.4B) but returned to baseline levels by the end of perfusion following blebbistatin perfusion (Figure 5.6B). In the TNI group, PCr fell by approximately 20% from baseline after five minutes of blebbistatin + ouabain perfusion (Figure 5.5B) but then returned to baseline for 15 minutes before decreasing to a plateau at 50 minutes. Nonetheless, there was no difference in PCr between TNI and vehicle at 55 minutes ($P>0.05$) (Figure 5.7B). In conjunction with these ATP and PCr profiles, the end-point PCr:ATP ratio was almost two-fold higher ($P<0.01$) in TPI (Figure 5.6D) and almost a third higher in the TNI group (Figure 5.7D) versus their vehicle groups at 55 minutes. There were no significant differences ($P>0.05$) in P_i between the vehicle and TPI group (Figure 5.4C) although P_i showed a trend towards elevation in the TPI group vs baseline levels at the end of perfusion (Figure 5.6C).

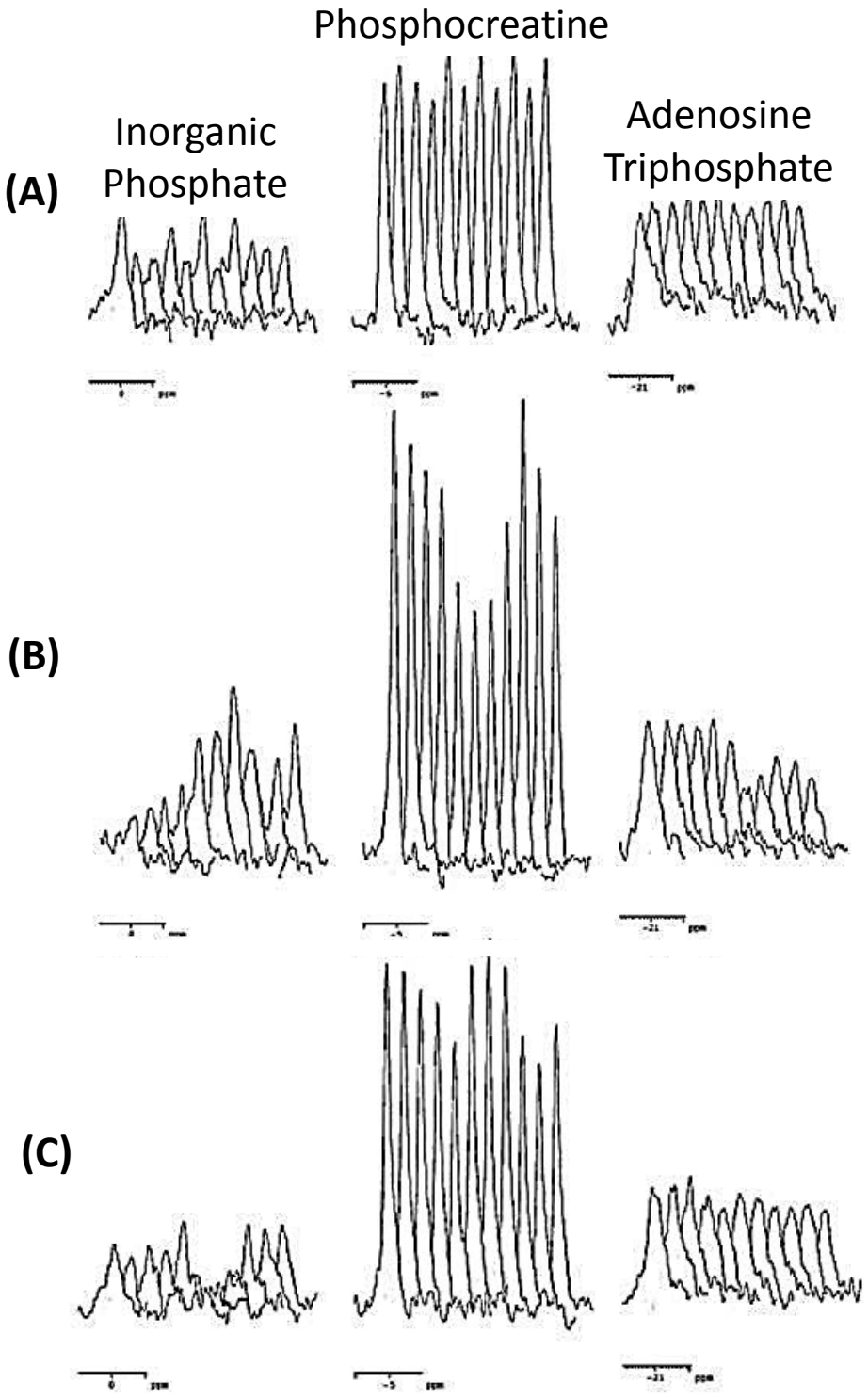

Figure 5.3 Representative ^{31}P Nuclear Magnetic Resonance Spectra.

(A) Vehicle. **(B)** Transient positive inotropy (TPI). **(C)** Transient negative inotropy (TNI). Each peak represents a five minute acquisition window. See Table 6.1 for full protocol details.

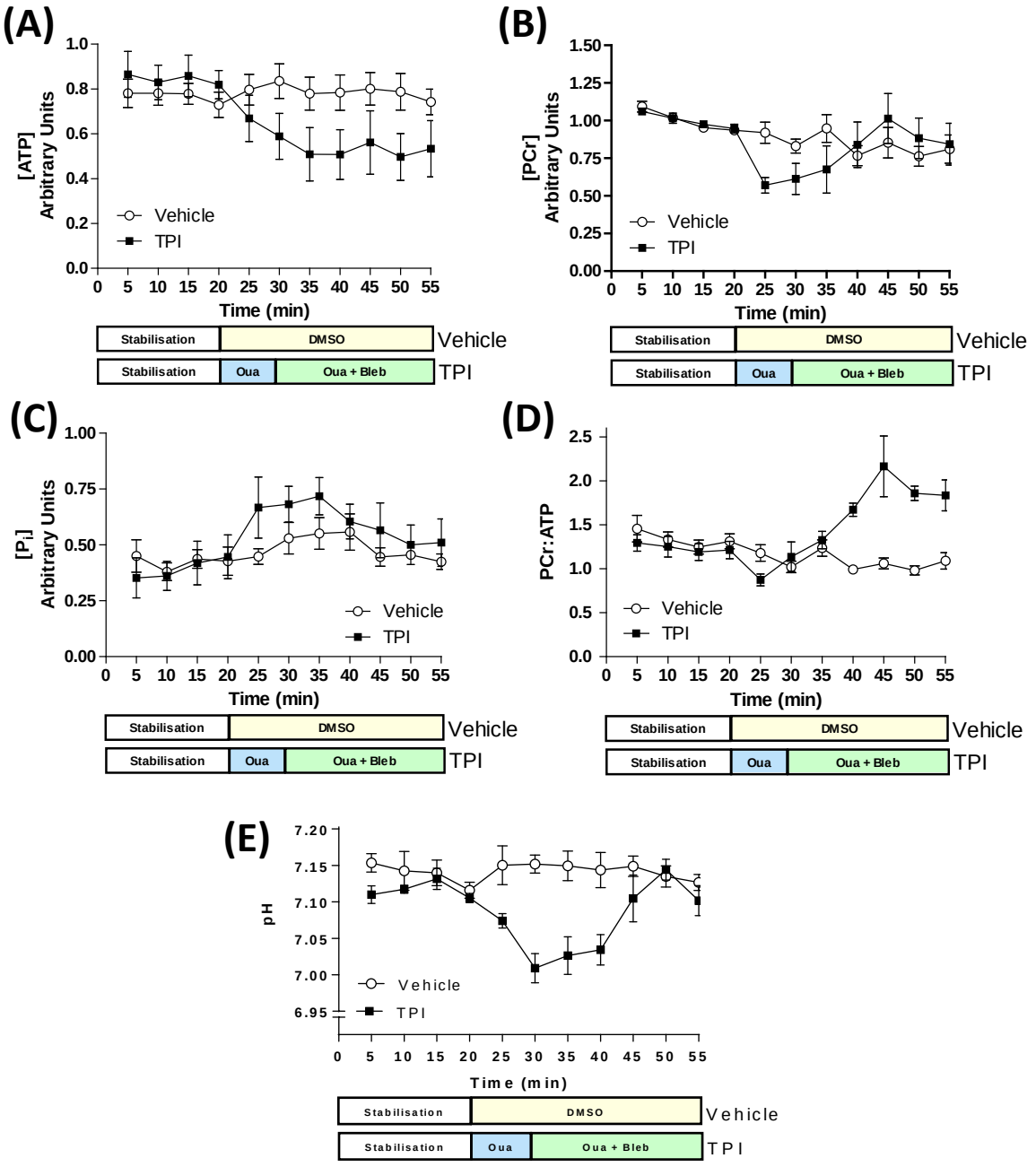

Figure 5.4 Real-time ^{31}P nuclear magnetic resonance measurements for transient positive inotropy (TPI).

(A) ATP. **(B)** Phosphocreatine (PCr). **(C)** Inorganic phosphate (P_i). **(D)** PCr-ATP ratio. **(E)** pH. Symbols and error bars represent mean ± SEM of five minute time windows (n=6/group). Hearts were snap-frozen at 55 minutes. Abbreviations: blebbistatin (Bleb); dimethyl sulfoxide (DMSO); ouabain (Oua).

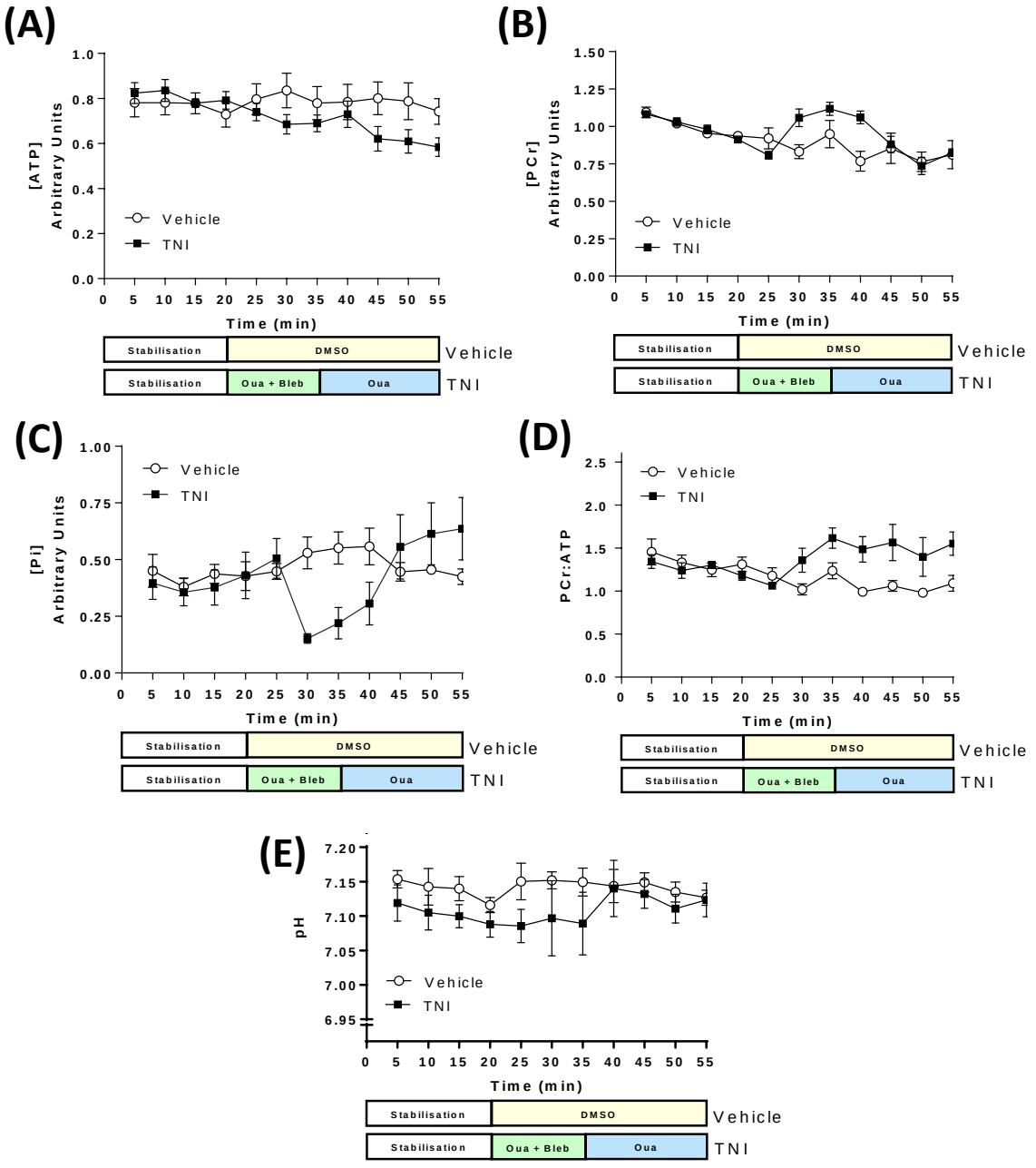

Figure 5.5 Real-time ^{31}P nuclear magnetic resonance measurements for transient negative inotropy (TPI).

(A) ATP. **(B)** Phosphocreatine (PCr). **(C)** Inorganic phosphate (P_i). **(D)** PCr-ATP ratio. **(E)** pH. Symbols and error bars represent mean ± SEM of five minute time windows (n=6/group). Hearts were snap-frozen at 55 minutes. Abbreviations: blebbistatin (Bleb); dimethyl sulfoxide (DMSO); ouabain (Oua).

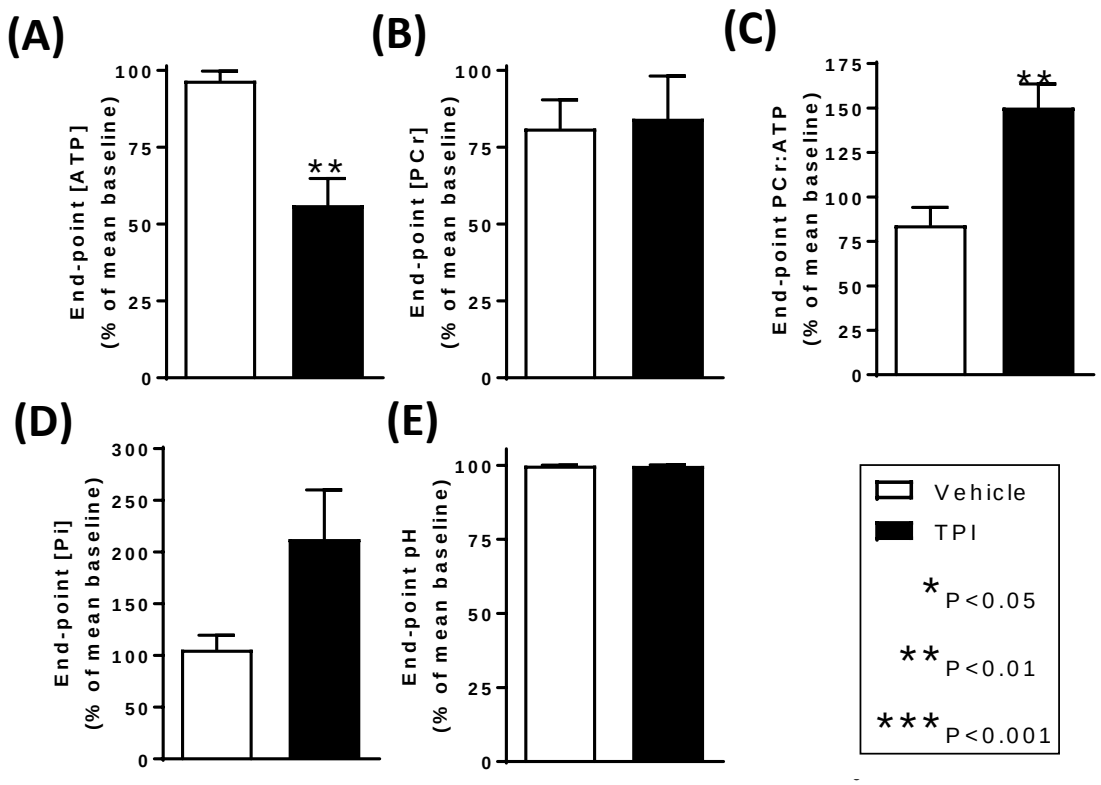

Figure 5.6 End-point ^{31}P nuclear magnetic resonance measurements for transient positive inotropy (TPI).

(A) ATP. **(B)** Phosphocreatine (PCr). **(C)** Inorganic phosphate (P_i). **(D)** PCr-ATP ratio. **(E)** pH. Bars and error bars represent mean ± SEM of five minute time windows (n=6/group). Hearts were snap-frozen at 55 minutes. Abbreviations: blebbistatin (Bleb); dimethyl sulfoxide (DMSO); ouabain (Oua).

In the TNI group (Figure 5.5C), P_i did not deviate from baseline levels following five minutes of blebbistatin + ouabain perfusion but then began to follow the TNI LVDP profile, decreasing to 71% below the corresponding vehicle value at 30 minutes ($P<0.01$). P_i then gradually increased in the TNI group and was significantly higher than vehicle levels by the end of perfusion ($P<0.05$) (Figure 5.7D).

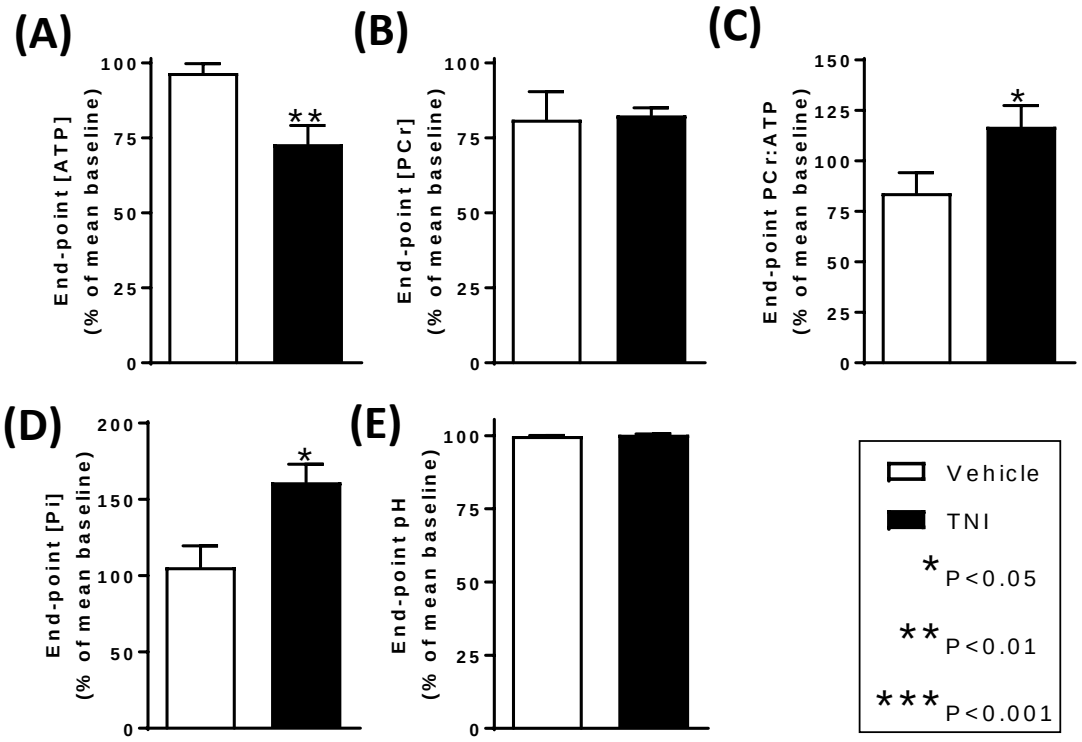

Figure 5.7 End-point ^{31}P nuclear magnetic resonance measurements for transient negative inotropy (TNI).

(A) ATP. **(B)** Phosphocreatine (PCr). **(C)** Inorganic phosphate (P_i). **(D)** PCr-ATP ratio. **(E)** pH. Bars and error bars represent mean ± SEM of five minute time windows (n=6/group). Hearts were snap-frozen at 55 minutes. Abbreviations: blebbistatin (Bleb); dimethyl sulfoxide (DMSO); ouabain (Oua).

In regard to pH, ouabain perfusion resulted in a substantial reduction from 7.11 at 20 minutes to a minimum of 7.01 at 30 minutes ($P<0.0001$; paired t-test) although, similar to PCr, slowly returned to baseline as the positive inotropy was titrated out in TPI (Figure 5.4E) and was not significantly different to vehicle pH levels at 55 minutes ($P>0.05$) (Figure 5.6E). There were no differences in pH between vehicle and TNI at any point of the perfusion protocol ($P>0.05$) (Figures 5.5E and 5.7E).

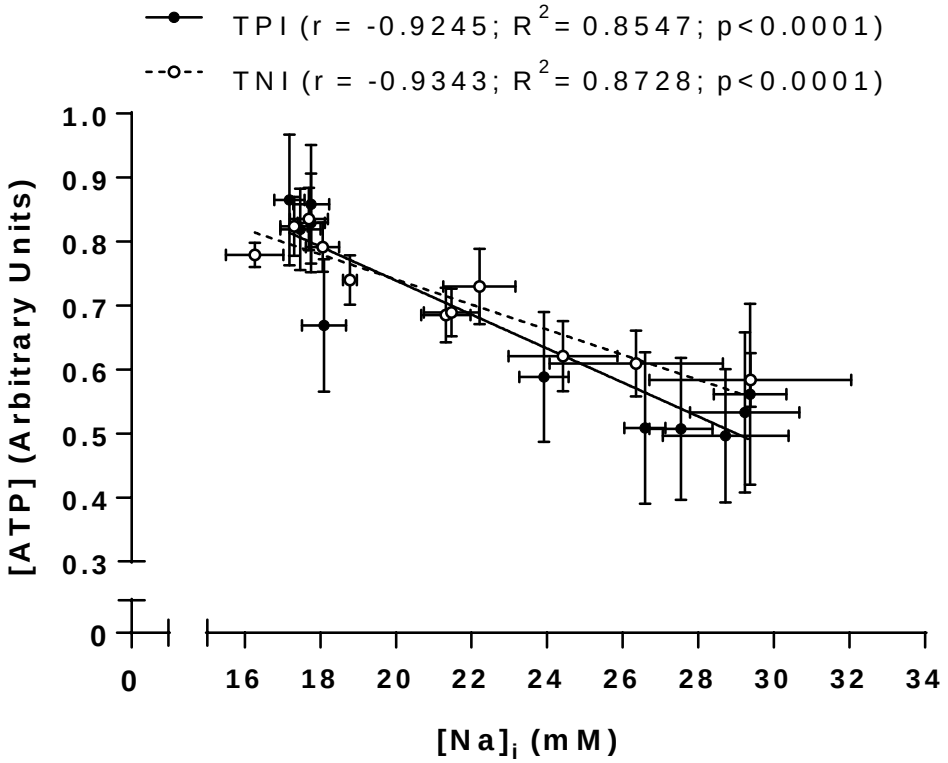

Figure 5.8 Real-time derived $[Na]_i$ versus [ATP] in transient positive inotropy (TPI) and transient negative inotropy (TNI).

Symbols and error bars represent mean ± SEM. $[Na]_i$ values were derived from normalised TQF signal measured every 1.5 min (Figure 5.2) and were averaged to correspond with the five minute ATP windows (Figure 5.4 and 5.5).

5.6 Results - Global metabolomics in TPI and TNI by ^{1}H NMR and LC-MS/MS

Figures 5.9A and 5.9B show the metabolomic profiles obtained using ^{1}H NMR for TPI and TNI respectively. The significant increase in acetylcarnitine ($P<0.05$) and decrease in carnitine ($P<0.05$) resulted in a highly significant increase in the acetylcarnitine-carnitine ratio ($P<0.001$) in the TPI group versus vehicle. The TPI group was also associated with higher concentrations of alanine ($P<0.05$) and there was a trend towards

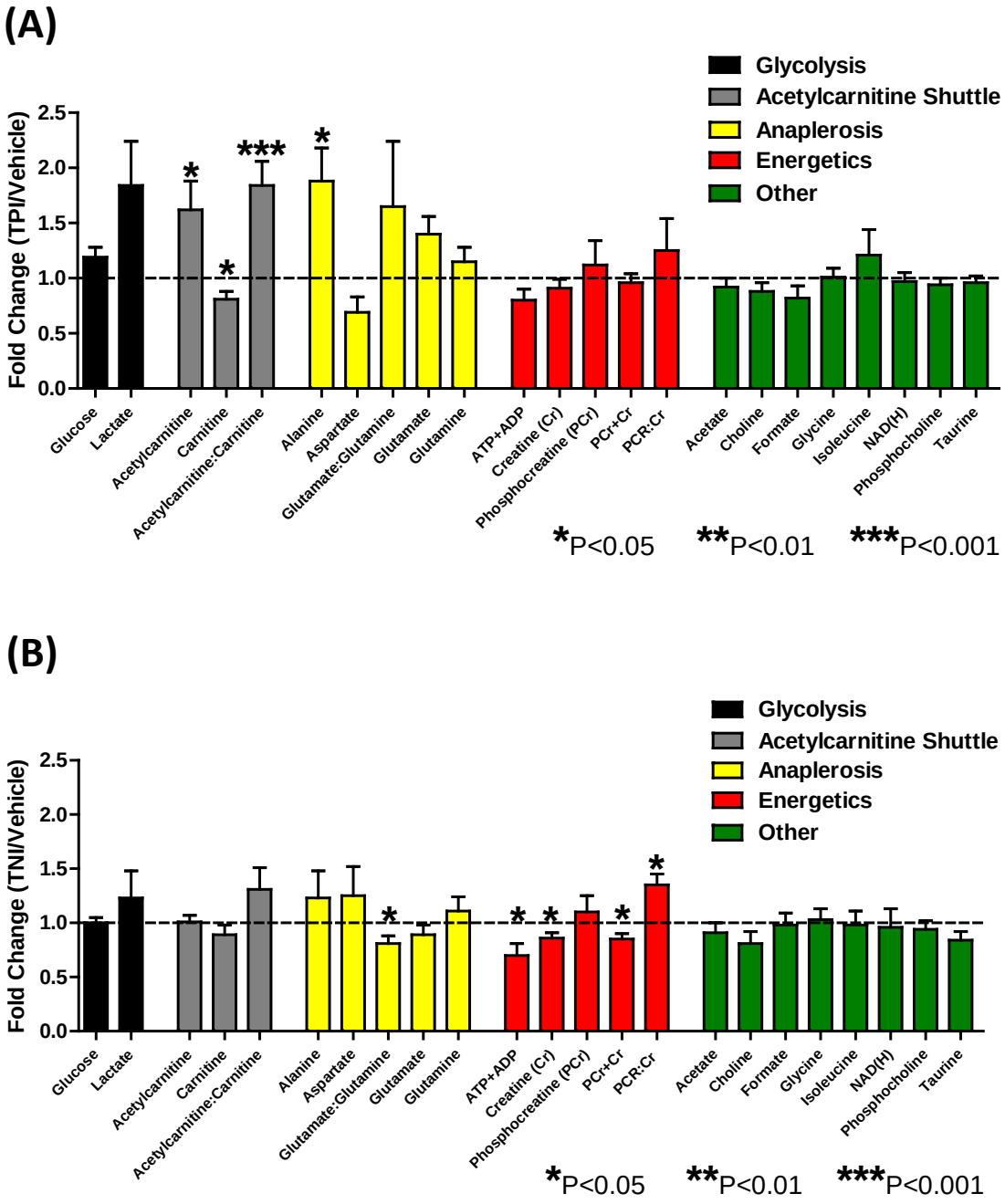

Figure 5.9 ^{1}H NMR metabolomic profiles of transient positive inotropy (TPI) and transient negative inotropy (TNI).

(A) TPI. **(B)** TNI. Bars and error bars represent mean ± propagated SEM (n=4-6/metabolite/group). A fold change of '1.0' represents zero change vs vehicle.

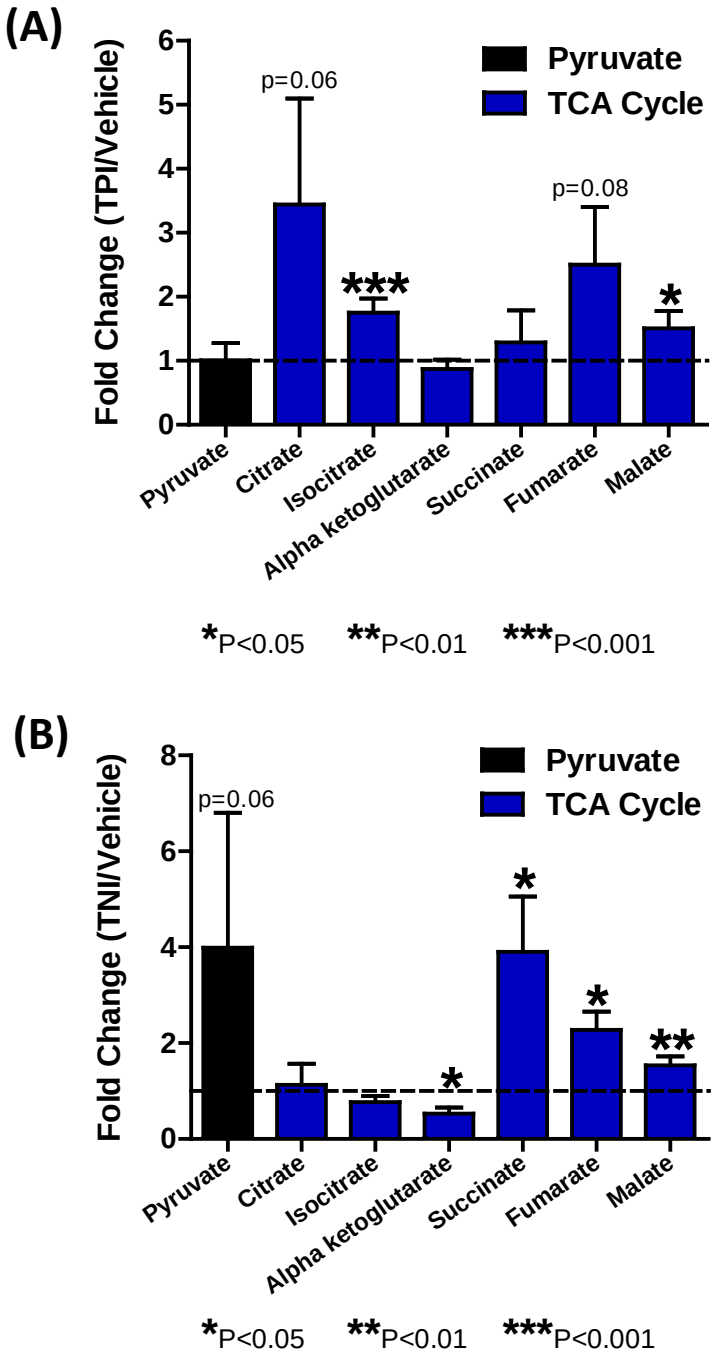

Figure 5.10 Tricarboxylic acid profiles of transient positive inotropy (TPI) and transient negative inotropy (TNI) measured by LC-MS/MS.

(A) TPI. **(B)** TNI. Bars and error bars represent mean ± propagated SEM (n=8-12/metabolite/group). A fold change of '1.0' represents zero change vs vehicle.

an increase in lactate (P=0.09) although the latter metabolite did not reach statistical significance. There were no marked changes in metabolites associated with cardiac energetics in TPI. In the TNI group, the small increase in glutamine and decrease in glutamate resulted in a significant decrease in the glutamate-glutamine ratio (P<0.05) versus vehicle. The TNI group was also associated with a smaller pool of total ATP+ADP (P<0.05) and lower concentration of creatine (Cr) (P<0.05) which resulted in a significantly higher PCr:Cr ratio (P<0.05). There were no marked changes in metabolites associated with glycolysis or the acetylcarnitine shuttle.

Quantification of pyruvate and the TCA cycle metabolites by LC-MS/MS revealed significant elevations in isocitrate (P<0.001) and malate (P<0.05) in the TPI group versus vehicle (Figure 5.10A). There was also a trend towards elevations in citrate (P=0.06) and fumarate (P=0.08) although these did not reach statistical significance. There were significant elevations in succinate (P<0.05), fumarate (P<0.05) and malate (P<0.01) and a significant decrease in α-ketoglutarate (P<0.05) in the TNI group versus vehicle (Figure 5.10B), as well as a trend towards elevation in pyruvate although this was not statistically significant (P=0.06). Full details of TPI and TNI metabolomics datasets are shown in Appendices 8.7-8.10.

5.7 Discussion – TPI and TNI perfusion measurements.

In this chapter, two studies were carried out in order to determine whether $[Na]_i$ elevation alters cardiac energetics and/or the intermediary metabolism irrespective of inotropic changes. It is important to stress that metabolic comparisons were made at a

time when contractility had returned to 100% and Na^+ was substantially elevated – however, while the Na^+ contractility were identical at the time of metabolic assessment, the immediate history of the hearts differed between TNI and TPI groups. The TPI group had previously experienced a transient positive inotropy whilst hearts in the TNI group had a recent history of a transient negative inotropy.

Significant bradycardia was observed following 100 µM ouabain in the TPI group and was also observed in the 100 µM ouabain group in Chapter 3 (Figure 3.1B). Interestingly, subsequent titration with 155 µM ouabain + 5 µM blebbistatin increased heart rate back to baseline. Heart rate elevation due to 5 µM blebbistatin has been reported previously (Brack et al., 2013) although this was not statistically significant.

As anticipated, the coronary flow profiles were similar to the corresponding LVDP profiles of the TPI and TNI groups. As coronary flow is the most reliable indicator of oxygen demand in the isolated crystalloid perfused heart preparation (Aksentijevic et al., 2016), the lack of difference in coronary flow between TPI, TNI and vehicle at 55 minutes suggests that oxygen demand, as well as oxygen delivery, were the same for all groups at the end of perfusion.

LVEDP was elevated in both TPI and TNI groups upon $[Na]_i$ elevation. There are three possible explanations for this. Firstly, $[Na]_i$ elevation is thought to decrease NCX forward mode activity (Baartscheer et al., 2003a) and increase reverse mode activity (Barry et al., 1985) thereby increasing diastolic $[Ca]_i$ and, at the relatively high heart rates in the isolated rat heart, this leads to incomplete relaxation between beats. Secondly, the reduction in ATP (measured by ^{31}P NMR) during both the TPI and TNI

periods may have lowered lusitropy given that removal of Ca^{2+} from the cytosol during diastole requires approximately 15% of the total energy cost of the cardiac cycle (Langer and Brady, 1974). Thirdly, it was shown in Chapter 4 that blebbistatin alone elevates LVEDP, thus there may have been a contribution of blebbistatin to the negative lusitropy observed. However, this effect occurred profoundly with ouabain in the absence of blebbistatin during the TPI period thus $[Na]_i$ is likely to be the key driver of this phenomenon.

5.8 Discussion- $[Na]_i$ measurements

As observed previously in Chapters 3 and 4, the TQF ^{23}Na NMR methodology permitted derivation of $[Na]_i$ in real-time. There were no changes in baseline measurements of derived $[Na]_i$ in any group during the stabilisation periods but substantial elevations in $[Na]_i$ occurred following ouabain perfusion. However, the maximum derived $[Na]_i$ achieved in these studies (30 mM) was lower than previous chapters which demonstrated that perfusion of hearts with 100 µM ouabain alone (Chapter 3) or 155µM ouabain+5µM blebbistatin (Chapter 4) lead to derived $[Na]_i$ values of 35-45mM. There were no notable differences in DQF signal during any of the studies giving confidence that concentrations of extracellular Na^+ were stable throughout all perfusion protocols. Importantly, despite this unexplained discrepancy, derived $[Na]_i$ was identical (30 mM) at the end of perfusion in both the TPI and TNI groups. However, this value of $[Na]_i$ was reached approximately 10 minutes earlier in the TPI group than in the TNI group. TPI hearts were therefore exposed to a longer duration of $[Na]_i$ elevation during the treatment period. In addition, TPI hearts were at

steady state at the end of perfusion whereas $[Na]_i$ was still on an upwards slope at this time in the TNI group. It was concluded from preliminary investigations that 1.5µM blebbistatin+50µM ouabain were the most suitable concentrations to achieve a significant negative inotropy concomitantly with a significant elevation in $[Na]_i$. In order for the $[Na]_i$ profile of the TNI group to be identical to that of the TPI group, a higher concentration of ouabain would be required at the start of the TNI period. To overcome the inevitable positive inotropy that would arise, a higher concentration of blebbistatin would then also be necessary at this time. Owing to its irreversible binding, it is probable that the subsequent $[Na]_i$ required to elevate contractility back to baseline would far exceed ~30mM. Further work is required to identify whether it is practically feasible to obtain identical $[Na]_i$ profiles in the TPI and TNI groups.

5.9 Discussion - ^{31}P NMR energetics measurements

^{31}P NMR permitted the real-time monitoring of ATP, PCr, P_i and pH. During the TPI period, PCr was transiently decreased and P_i was transiently increased. A close relationship between LVDP and HEPs has been demonstrated previously in the isolated rat heart (Honda et al., 2002). That is, a transient rise in LVDP was associated with transient decreases in PCr and ATP and a transient increase in P_i. However, ATP did not return to baseline levels in either TPI or TNI in this chapter. Taken together with the Honda et al (2002) study, this supports the hypothesis that $[Na]_i$ elevation deranges ATP supply-demand matching in the isolated heart. Furthermore, the reduction in ATP upon $[Na]_i$ elevation is in agreement with the work of Iwai et al (2002) showing that elevating extra-mitochondrial sodium from 12.5 mM to 25 mM significantly reduces state 3

respiration (oxidative phosphorylation). Strikingly, end-point PCr was not lower in the TPI and TNI groups versus vehicle and PCr:ATP was elevated with increasing $[Na]_i$ reflecting the drop in ATP. There is widespread literature reporting a reduced PCr:ATP under pathophysiological conditions associated with elevated $[Na]_i$, for example, dilated cardiomyopathy (Neubauer et al., 1997), cardiac hypertrophy (Perings et al., 2000) and myocardial infarction (Naumova et al., 2006). There are, however, substantially fewer reports of elevated PCr:ATP under pathophysiological conditions. For instance, Consolini et al (2004) reported an increased PCr:ATP following an ischaemia/reperfusion protocol in the Langendorff rat heart, although PCr and ATP both declined under these conditions whereas ATP declined but PCr was unaltered at the end-point in the TPI/TNI studies in this chapter. Weiss et al (2002) demonstrated an increased PCr:ATP in GLUT4 null mice but this was driven by elevations in creatine and PCr in the absence of changes in ATP. Indeed, caution should be taken when comparing the findings of these pathophysiological studies with those of the TPI/TNI studies, as $[Na]_i$ elevation is just one of several maladaptations within the former studies that could potentially alter cardiac energetics. However, these comparisons may shed light upon the unexpected observation that PCr:ATP appears to be dependent upon $[Na]_i$ irrespective of inotropic alterations.

A crucial aspect of the TPI/TNI studies was that contractility (the primary ATP sink in the heart) was identical for all groups at end-point. Thus, the reduction in ATP in both TPI and TNI groups upon $[Na]_i$ elevation cannot be attributed to increased ATP demand but instead to decreased ATP synthesis. This supports the hypothesis that $[Na]_i$ elevation perturbs ATP supply-demand matching in the heart. However, as cardiac ATP

levels are known to be very tightly buffered by creatine kinase (CK), these findings suggest that $[Na]_i$ elevation may reduce creatine kinase activity (specifically myofilament CK rather than mitochondrial CK as the latter resides in the inter-membrane and cristae spaces (Wegmann et al., 1991) and therefore is not in contact with $[Na]_m$). Szasz et al (1976) showed that elevating Na^+ in blood serum decreases CK activity although the relevance of this to the perfused heart is equivocal. It has been shown previously that incubation of rat heart mitochondria in high Na^+ media (83mM Na^+ phosphate or 100 mM Na^+ acetate) causes the mitochondria to swell and release CK from their membranes in the soluble form (Jacobus and Lehninge.Al, 1973).

It is improbable that blebbistatin is responsible for the elevated PCr:ATP as ATP declines rapidly with blebbistatin-free ouabain (during the intial stages of the TPI period) despite PCr levels falling concomitantly. In the healthy heart, CK sustains normal ATP over a wide range of contractile demand (Wu and Beard, 2009) suggesting a reduced capacity of CK to maintain normal ATP during the TPI period in which $[Na]_i$ was high. There is no evidence in the literature to suggest that blebbistatin inhibits CK whereas it has been shown to stimulate CK activity in fully relaxed permeabilised skinned fibres in which the ATP demand was low (Perry et al., 2012).

Alternatively, rather than CK activity being directly affected by $[Na]_i$, it may be an associated elevation in $[Ca]_i$ that is responsible for the increased PCr:ATP. Cerebellum is known to contain CK-MM (Hemmer et al., 1994) which is the predominant cytosolic isoform in the mammalian heart (Eppenberger et al., 1967) and high Ca^{2+} (20 mM) has been shown to inhibit CK activity in the cerebellum (Khan, 1976). Although 20mM is substantially higher than myocardial $[Ca]_i$ (typically in the nanomolar range) (Jansen et

al., 2000), "$[Ca]_i$ sparks" significantly elevate this value (Cheng et al., 1996) and occur in close proximity to sarcolemmal- (Saks et al., 1977) and SR- (Rossi et al., 1989) localised CK.

As anticipated, there was an increase and decrease in P_i upon LVDP elevation in the TPI group and upon LVDP reduction in the TNI group, respectively. The P_i profiles were the inverse of their respective PCr profiles which corresponds with the strong positive correlation between cardiac workload and CK activity (PCr→ATP then hydrolysis by ATPases to give P_i) (Dawson et al., 1980). In contrast to end-point PCr, there were substantial elevations in end-point P_i in both TPI and TNI groups compared with vehicle. In the absence of changes in PCr, this adds weight to the possibility that CK activity is altered by $[Na]_i$ elevation. However, the elevated P_i in the TPI group versus vehicle did not reach statistical significance (perhaps owing to the low signal:noise and higher associated error compared with PCr and ATP) hence greater *n* numbers are required to substantiate this.

The transient reduction in pH observed in the TPI period reflects a greater release of protons from the hydrolysis of ATP. However, end-point pH was not altered by increased $[Na]_i$. Taken together with the P_i data, this is in favour of the TPI and TNI hearts being in a state of reduced ATP synthesis rather than increased ATP hydrolysis at the end of perfusion.

5.10 Discussion - Metabolomics measurements.

Several of the identified alterations in energetics and intermediary metabolism were common to both the TPI study and the TNI study. These are summarised in Table 5.2.

As discussed in previous chapters in this thesis, ^{1}H NMR and LC-MS/MS permitted the quantification of several aqueous metabolites involved in energy homeostasis in heart extracts.

Table 5.2 Summary of alterations common to both TPI and TNI groups.

Analyte	TPI		TNI	
	% change	P-value	% change	P-value
Fumarate	↑ 150	0.076	↑ 128	0.013
Malate	↑ 51	0.038	↑ 54	0.002
ATP	↓ 41	0.001	↓ 25	0.007
PCr:ATP	↑ 44	0.003	↑ 28	0.048

% changes are for Transient Positive Inotropy group (TPI) or Transient Negative Inotropy group (TNI) vs vehicle at 55 minutes where '0%' change represents zero fold-change. Fumarate and malate were acquired using LC-MS/MS of dual-phase extracts. ATP and PCr:ATP were acquired using real-time ^{31}P NMR of perfused hearts.

Elevated acetylcarnitine:carnitine was observed in the TPI profile but not the TNI profile and was also elevated in both paced and unpaced contracting hearts perfused

with blebbistatin-free ouabain (discussed in Chapter 3). This suggests that the acetylcarnitine shuttle is altered due to positive inotropy but also that it remains altered once the positive inotropy has waned. Acetylcarnitine has been shown to increase in skeletal muscle upon prolongued exercise in humans (Sahlin et al., 1990).

Alanine also appeared to be elevated by TPI but not TNI. As high levels of lactate (which was also markedly higher than vehicle in TPI) inhibit glycolysis (Rovetto et al., 1975), alanine transaminase activity is stimulated following elevated contractile work (Felig and Wahren, 1971) thereby converting more pyruvate into alanine and less into lactate. Alanine elevation was not observed previously in the blebbistatin-free ouabain-perfused hearts (Chapter 3).

TPI also elevated isocitrate (and possibly citrate). This is supported by the work of Stuewe et al (2000) which highlighted increased citrate synthase (but not malate dehydrogenase or α-ketoglutarate dehydrogenase) activity and expression in the left ventricle of dogs with exercise-induced increases in contractile work. This infers increased TCA cycle activity with elevated contractile demand. However, this disagrees with the findings of Sharma et al (2005) that 4-carbon intermediates (succinate, fumarate and malate), but not 6-carbon intermediates, are elevated by high cardiac work. The authors used the β-agonist, dobutamine, to elevate contractile work thus non-contractile effects of this drug may have contributed to their metabolomic profile.

The significant reductions in glutamate:glutamine and α-ketoglutarate in the TNI profile are consistent with reduced anaplerosis into the TCA cycle via glutamate dehydrogenase. However, this is opposed by the ^{13}C flux assessment of KCl-arrested

perfused hearts (Lewandowski, 1992) which, when compared with normally contracting controls, exhibited no change in the total size of the glutamate pool and an elevation in contribution of carbons into the TCA cycle via anaplerosis relative to citrate synthase. However fully-arrested hearts have a vastly different ATP demand to those contracting but with a history of TNI.

There were also changes in energetics that were exclusive to the TNI study including reductions in the total ATP+ADP pool and creatine. Combined with the ^{31}P NMR measurements, it is likely that the reduced adenylate pool size reflects reduced ATP upon $[Na]_i$ elevation. Interestingly, the ATP+ADP pool was also decreased in the TPI group (versus vehicle) but was more subtle than the TNI profile and did not reach statistical significance. The reason for the lowered creatine level is less clear given that end-point PCr in the TNI group was not different to vehicle.

The increased succinate in the TNI group may be due to its accumulation following the transient reduction in ATP demand and subsequent downregulation of complex II and oxidative phosphorylation. Further work would be required to substantiate this.

Perfused hearts exhibiting 60mmHg systolic pressure were shown to contain 38% more pyruvate than those exhibiting 120mmHg systolic pressure (Kobayashi and Neely, 1983). The authors suggested that this was due to increased pyruvate dehydrogenase activity upon elevated contractile demand. This aligns with the observation that pyruvate is significantly higher than vehicle in the TNI study but not in the TPI study.

The identification of metabolomic changes that were exclusive to either the TPI study or the TNI study supports the hypothesis that the heart has “metabolic memory” for

contractility. That is, it is possible for certain metabolomic alterations induced by brief changes in inotropy were sustained for some time after the waning of that inotropy.

The concentrations of malate and fumarate were elevated in an almost identical fashion in both the TPI and TNI studies (although fumarate did not reach statistical significance in the TPI study, it was elevated by 150% and was approaching significance). Similar to ATP, these TCA cycle intermediates may therefore potentially be considered to be $[Na]_i$-dependent irrespective of alterations in inotropy. Accumulations in malate and fumarate are indicative of reduced malate dehydrogenase activity. The apparent K_m and V_{max} of this enzyme have been shown to decrease and increase *in vitro* with increasing $[Na^+]$, respectively (Kelavkar and Chhatpar, 1993). Malate dehydrogenase is a key producer of NADH in the myocyte and Maack et al (2006) have shown that NAD^+:NADH rises upon $[Na]_i$ elevation.

The interpretation of the metabolic aspects of the TPI/TNI studies is very complex given the strong association between contractile state, ATP demand and intermediary metabolism. Metabolites were categorised as 'TPI-dependent', 'TNI-dependent' or '$[Na]_i$-dependent' but this is probably an oversimplification. It is likely that all metabolic enzymes are regulated by contractile demand (either directly or indirectly and to different extents) and the linearity of this relationship for each metabolite concentration is not known. Large changes in metabolite concentrations due to TPI or TNI may mask smaller metabolite changes due to regulation by $[Ca^{2+}]$ or $[Na^+]$. It may also be the case that regulation of metabolism by $[Ca^{2+}]$ and/or $[Na^+]$ becomes increasingly important with increasing contractile demand. The TPI and TNI protocols

could be repeated under conditions of high workload, for example, by using high rates of electrical pacing or increased extracellular [Ca].

5.11 Summary

In this chapter, it has been shown using a combination of NMR and LC-MS/MS approaches that, in normally-contracting perfused hearts, a transient increase or decrease in inotropy with a sustained elevation of $[Na]_i$ resulted in an elevated PCr:ATP ratio due to a decrease in ATP. This showed a strong inverse correlation with $[Na]_i$ elevation (despite no change in PCr), indicating a possible role for $[Na]_i$ in the regulation ATP synthesis, TCA cycle activity or creatine kinase.

In the TPI group, increases were observed in acetylcarnitine as well as the concentrations of alanine (potentially due to increased alanine transaminase activity), citrate and isocitrate (suggesting increased TCA cycle activity). On the other hand, a transient reduction in inotropy was associated with decreases in glutamate:glutamine and α-ketoglutarate (potentially due to reduced glutamate anaplerosis) as well as decreases in the total ATP+ADP pool and creatine. These changes support the existence of “metabolic memory” for contractility in the heart. Malate and (more tentatively) fumarate increased due to $[Na]_i$ elevation, suggesting a possible link between $[Na]_i$ and TCA cycle activity or malate dehydrogenase activity in the perfused heart.

6 ASSESSMENT OF TRICARBOXYLIC ACID CYCLE ACTIVITY IN HEARTS WITH ELEVATED $[Na]_i$ IN THE ABSENCE OF CHANGES IN CONTRACTILITY.

6.1 Introduction

In Chapter 5, it was concluded that $[Na]_i$ elevation perturbs ATP supply in the perfused rat heart which may have been associated with the observed increase in the TCA cycle intermediate, malate, as well as a trend towards elevation in fumarate. According to the main thesis hypothesis, $[Na]_i$ elevation would reduce the $[Ca]_m$-driven stimulation of the TCA cycle potentially leading to decreased TCA cycle activity during $[Na]_i$ elevation, which could explain the observed increase in malate or fumarate. It is also possible that particular enzymes of this pathway may be more sensitive to $[Na]_i$ elevation than other TCA cycle enzymes in the isolated heart.

Isotopic labelling is a powerful means by which to assess TCA cycle activity as well as other metabolic pathways in the Langendorff preparation. This entails perfusing a fuel-substrate (commonly glucose, palmitate or acetate) containing an isotopic label (or labels). The label(s) can be located at any atomic position(s) of the molecule and is usually ^{13}C, although ^{2}H and ^{15}N have also been utilised (Carvalho et al., 2001, Li et al., 2015, Pisarenko et al., 1980). Mass spectrometry has been used in previous chapters in this thesis to quantify total concentrations of metabolites. Its ability to distinguish between chemical entities with a resolution as low as one Dalton makes this technique applicable for the detection of isotopologues (molecules that differ only in the number of isotopic labels) and isotopomers (molecules that that differ only in the atomic

position of the isotopic label(s)) (McNaught and Wilkinson, 2000). As the labelled fuel-substrate is metabolised by the cell, the label is incorporated into the resultant enzymatic products which can be quantified by mass spectrometry. Changes in the concentrations of these labelled metabolites due to an intervention, for example, perfusion of a pharmacological agent or elevation of $[Na]_i$ could infer altered activity of the pathway or pathways in which that metabolite is involved.

There are several important factors to consider when designing isotopologue mass distribution studies. Firstly, the fuel-substrate must be optimal for the particular metabolic pathway under question, in this case, the TCA cycle. Universally labelled ^{13}C glucose ([U]-$^{13}C_6$-glucose) was chosen as the fuel-substrate for the study described in this chapter as its isotopic labels will be incorporated into glycolytic intermediates and end products as well as the TCA cycle. Secondly, the heart must be at metabolic steady-state, that is, the pool sizes of all metabolites and also cardiac function should be constant and at equilibrium during the infusion. As contractile demand is known to be a key driver of metabolic change (discussed in previous chapters) it is crucial that the [U]-$^{13}C_6$-glucose is perfused during a period of stable LVDP and coronary flow. Analogously, the label must be perfused during a period of stable $[Na]_i$ given the main thesis hypothesis that elevated $[Na]_i$ alters metabolism. Thirdly, the heart must be at an isotopic steady-state at the point of snap-freezing. This has been defined by Buescher et al (2015) as the point at which "^{13}C enrichment into a given metabolite is stable over time relative to experimental error and/or the desired measurement accuracy [and is governed] by both the fluxes and the pool sizes [of all metabolites involved in this enrichment]". Comte et al (1997) showed that glycolytic (glucose to

pyruvate/lactate/acetyl CoA) and TCA cycle (pyruvate to TCA cycle intermediates) pools reach isotopic steady-state in approximately 15 minutes and 10-15 minutes, respectively. Furthermore, Jeffrey et al. (1995) showed that [U]-^{13}C-glucose achieves isotopic steady-state with respect to TCA cycle pools after ~20 minutes perfusion in the perfused rat heart. As the TCA cycle is tightly coupled to glycolysis and anaplerosis (Figure 1.6) the presence of ^{13}C label was assessed in all three pathways in this chapter.

The analysis and interpretation of ^{13}C isotopomer datasets is challenging for two key reasons. Firstly, numerous labelling patterns are possible for each metabolite. This is because metabolites can participate in unidirectional and/or reversible enzymatic reactions as a substrate and/or a product and those reactions can be linear or cyclic. The incorporation of ^{13}C into the TCA cycle from [U]-$^{13}C_6$-glucose is displayed in Figure 6.1. Secondly, the process of "deisotoping" must be performed prior to drawing any reliable conclusions from isotopomer datasets. This entails correcting for the contribution of naturally occurring isotopes (for example, ^{13}C, ^{15}N, ^{17}O and ^{18}O) to the acquired isotopomer signals. At present, there are several means by which to do this including numerous algorithms (Moseley, 2010, Lee et al., 1991) and software, for instance, LS-MIDA (Ahmed et al., 2013) and IsoCor (Millard et al., 2012). IsoCor was used in this chapter as it is capable of rapidly processing large quantities of data encompassing different metabolites. It also has a feature which corrects for isotopic purity of the tracer.

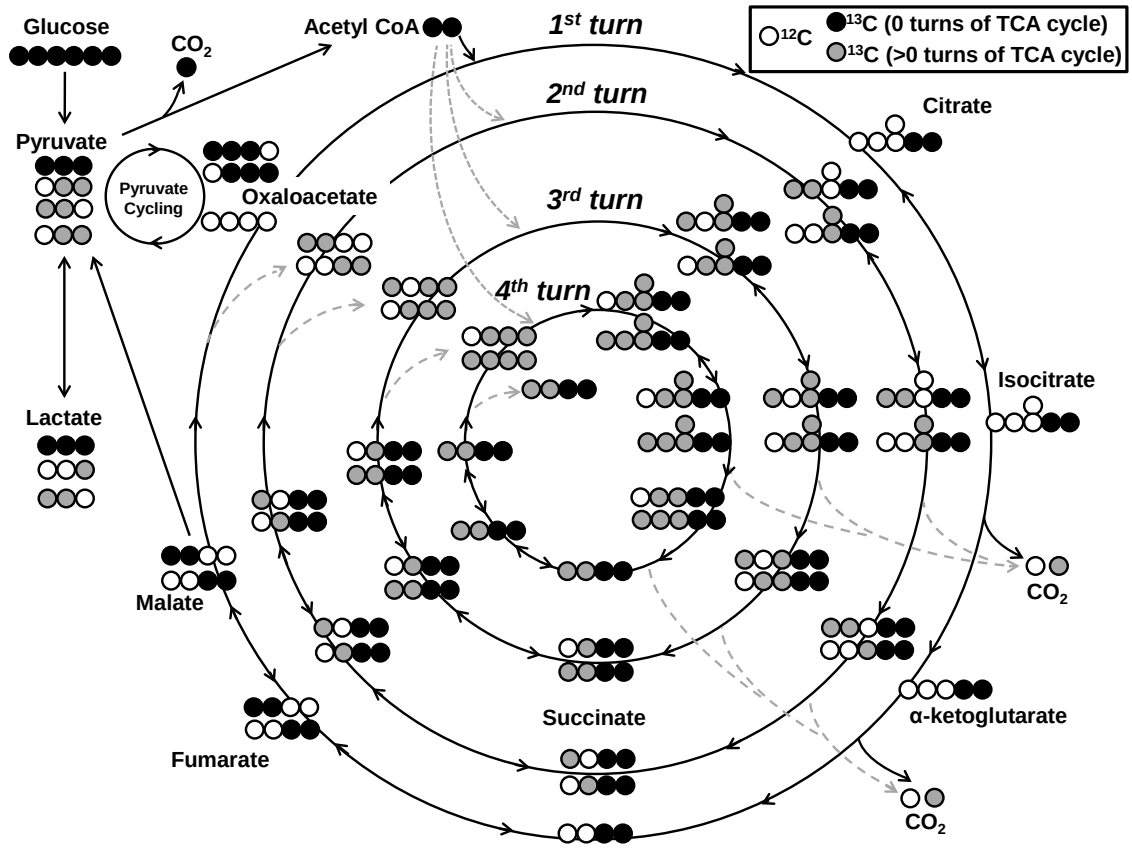

Figure 6.1 Pathway map of ^{13}C incorporation into the TCA cycle.

$^{13}C_6$-(universally-labelled) glucose is converted into $^{13}C_3$-pyruvate following glycolysis. This pyruvate is then decarboxylated to form $^{13}C_2$-acetyl CoA which undergoes condensation with unlabelled (white-filled circles)-oxaloacetate forming 13C2-citrate thereby feeding two ^{13}C labels (black-filled circles) into the first turn of the TCA cycle. These labels are passed around the cycle following numerous oxidative reactions to form $^{13}C_2$-oxaloacetate which can then be condensed with a second molecule of $^{13}C_2$-acetyl CoA. This therefore initiates a second turn of the TCA cycle which increases the abundance of ^{13}C label in the TCA cycle intermediates. After four turns of the TCA cycle, ^{13}C universally-labelled forms of all TCA cycle intermediates are present in the heart. The abundance of ^{13}C-labelled TCA metabolites is therefore directly proportional to TCA cycle activity. Furthermore, the presence of $^{13}C_1$ and $^{13}C_2$ isotopologues of pyruvate and lactate is suggestive of malate-pyruvate cycling (note that not all isotopomers are shown). Dihydroxyacetone phosphate (DHAP, not shown) is a branch point of glycolysis and is interconverted to glyceraldehyde-3-phosphate via triosephosphate isomerase. Alanine (not shown) is interconverted to pyruvate via alanine transaminase, aspartate (not shown) is interconverted to oxaloacetate via aspartate transaminase and glutamate (not shown) is interconverted to α-ketoglutarate via glutamate dehydrogenase (see Figure 1.6).

6.2 Aims

The aims of this chapter are:

1. To determine whether $[Na]_i$ elevation, in the absence of altered contractility, alters the activity of the TCA cycle using isotopic incorporation of [U]-$^{13}C_6$-glucose.

2. To determine whether any observed alterations in fluxes can infer whether the TCA cycle activity is increased or decreased in response to elevated $[Na]_i$.

6.3 Experimental Methods.

6.3.1 Perfusion protocols and measurements.

Rat hearts were perfused in the Langendorff mode as described in Section 2.1. The study included a vehicle group and a high $[Na]_i$ group (n=6/group). These groups were identical to the vehicle and TPI groups in Chapter 5, respectively, other than the presence of [U]-^{13}C-glucose (Cambridge Isotope Laboratories, USA) and an extension of each treatment period by 25 minutes to ensure that metabolic and isotopic steady-states had been achieved at that point of snap-freezing. Hearts were perfused in a randomised-fashion and the perfusion protocols are summarised in Table 6.1. Separate perfusion reservoirs were used for the different perfusion solutions. $[Na]_i$ elevation was induced by carefully pouring a small volume (approximately 5-10mL every 5 minutes) of 5μM blebbistatin+155μM ouabain KH into the titration reservoir initially containing

Table 6.1 Perfusion protocols used in the ^{13}C isotopologue study.

Group	0-20 mins	20-30 mins	30-55 mins	55-80 mins	80 mins
Vehicle	Stabilisation [U]-$^{12}C_6$-glucose	800µM DMSO [U]-$^{12}C_6$-glucose	800µM DMSO [U]-$^{12}C_6$-glucose	800µM DMSO [U]-$^{13}C_6$-glucose	Snap-freezing
High $[Na]_i$		100µM ouabain [U]-$^{12}C_6$-glucose	100µM ouabain (titrated with a single solution of 155µM ouabain + 5µM blebbistatin) [U]-$^{12}C_6$-glucose	100µM ouabain (titrated with a single solution of 155µM ouabain + 5µM blebbistatin) [U]-$^{13}C_6$-glucose	

250 mL 100 µM ouabain KH (pre-warmed to 39°C and gassed vigorously with carbogen). This resulted in a gradual and stable return to baseline LVDP at which time no further titrant was added. Homogeneity of the perfusion solutions was ensured by vigorous gassing and manual mixing by hand using the gas distribution tube in each perfusion reservoir. It was important to minimise changes in cardiac function upon switching from [U]-^{12}C-glucose blebbistatin+ouabain KH to [U]-^{13}C-glucose blebbistatin+ouabain KH at 55 minutes in the high $[Na]_i$ group. This was accomplished by having the same initial volume (250 mL) of 100µM ouabain in each of these perfusion reservoirs from the start of the perfusion protocol and by adding the same volume of 155µM ouabain + 5µM titrant to both reservoirs during the titration period (the volume required varied slightly between experiments). LVDP, heart rate, coronary

flow and LVEDP were recorded continuously throughout each experiment. Hearts were removed from the NMR spectrometer at 80 minutes and snap-frozen as described in section 2.1.9.

6.3.2 ^{23}Na NMR protocols.

Heart perfusions were performed within the NMR spectrometer using the in-house NMR perfusion setup as described in Section 2.2.2. ^{23}Na TQF NMR measurements were performed from 0 to 80 minutes and ^{23}Na DQF NMR measurements were performed from 0 to 55 minutes.

6.3.3 ^{13}C isotopologue measurements of myocardial tissue by GC-MS.

Aqueous metabolites were isolated using methanol extraction (Section 2.4.5) and isotopologue patterns of the TCA cycle (oxaloacetate, citrate, isocitrate, αKG, succinate, fumarate and malate), anaplerosis (alanine, aspartate and glutamate) and glycolysis (DHAP, pyruvate and lactate) were measured using GC-MS in single ion monitoring mode (described in Section 2.4.5).

6.3.4 ^{13}C isotopologue measurements of myocardial tissue by LC-MS/MS.

Aqueous metabolites were isolated using dual-phase extraction (Section 2.4.2) and ^{13}C isotopomer analysis was subsequently carried out using LC-MS/MS. The setup and acquisition parameters were as described in Section 2.4.4 other than that different

chemical transitions were programmed into the Analyst software in order to detect ^{13}C isotopomers of metabolites in addition to ^{12}C (unlabelled) metabolites. Individual isotopomer intensities were pooled into their appropriate isotopologue groups to permit correction of natural abundance by IsoCor. For instance, the raw intensities of the two m+1 isotopomers of fumarate were added together to give the total intensity of the m+1 isotopologue of fumarate.

6.3.5 Correction of ^{13}C isotopologue measurements for natural isotopic abundance using IsoCor software.

^{13}C isotopologue intensities were compiled in a text-delimited input file and processed using IsoCor software (Version 1.0). This corrected for the natural abundance of the isotopic tracer (^{13}C) as well as the isotopic purity (99%) of the [U]-^{13}C-glucose used in the experiments. The elemental formulas for isocitrate, lactate, pyruvate, DHAP, alanine and glutamate were not present in the original 'Metabolites.dat' file and thus were added manually. As chemical derivatisation of extracted metabolites was not used in the LC-MS/MS study, the 'Derivatives.dat' file was not used and this column was left empty in the input file. The output (result) file included mass distribution vector values for each isotopologue as well as mean enrichment of each metabolite.

6.4 Results - Perfusion measurements.

All perfusion parameters were stable, within acceptable ranges according to previously defined exclusion criteria (detailed in Section 2.1.6) and were not different between the

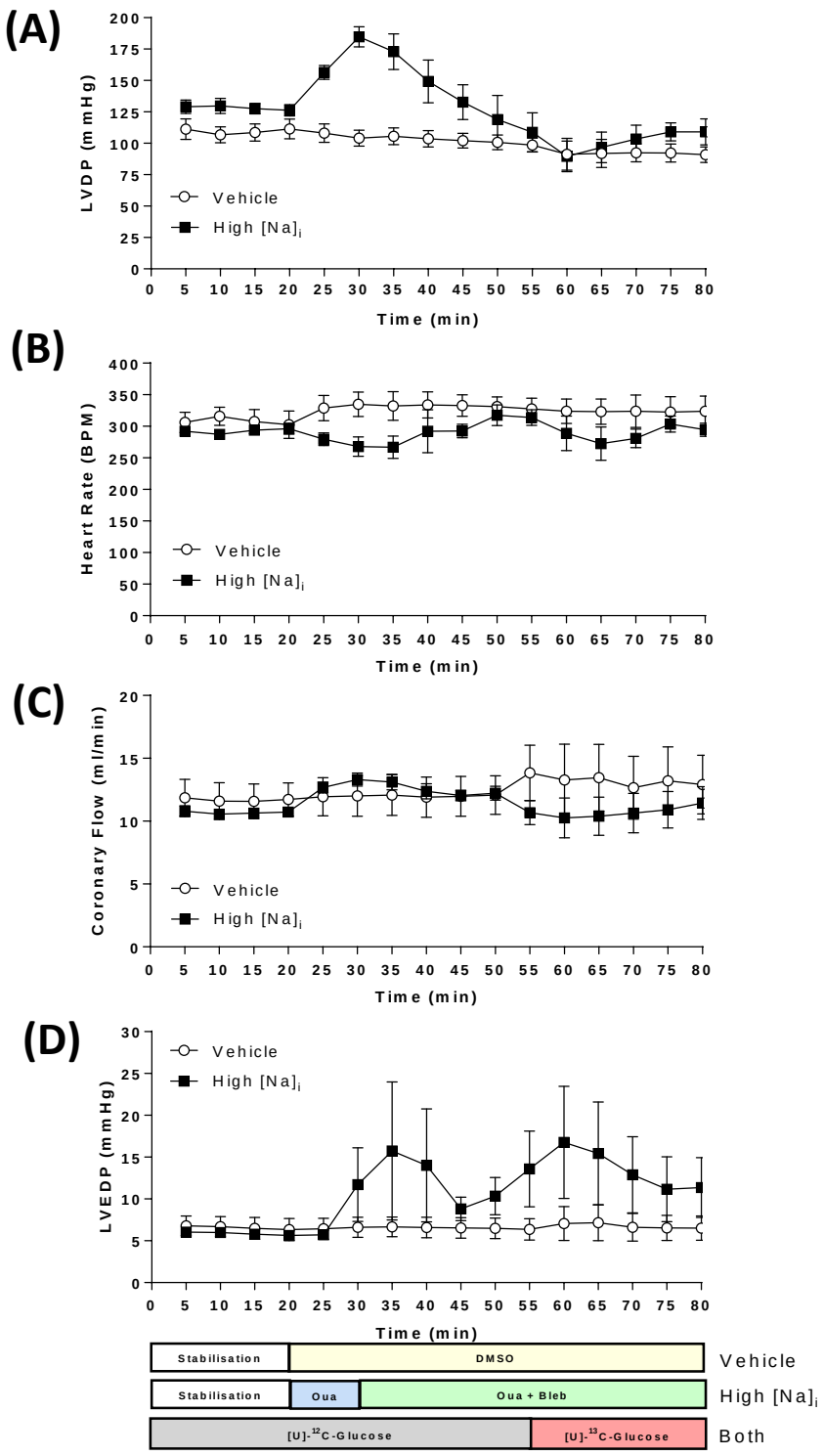

Figure 6.2 Functional measurements in the vehicle and high $[Na]_i$ groups (^{13}C study).

(A) Left ventricular developed pressure (LVDP). **(B)** Heart rate. **(C)** Coronary flow. **(D)** Left ventricular end diastolic pressure (LVEDP). Symbols and error bars represent mean±SEM of five minute time windows (n=5-6/group). Hearts were snap-frozen at 80 minutes. Blebbistatin (Bleb); dimethyl sulfoxide (DMSO); ouabain (Oua).

vehicle and high $[Na]_i$ group during the stabilisation period. Baseline LVDP (Figure 6.2A) was 110±7 mmHg in the vehicle group and was not altered ($P>0.05$) by subsequent DMSO perfusion (98±7 mmHg; $P>0.05$; paired t-test). In the high $[Na]_i$ group, LVDP was elevated to a maximum of 185±8mmHg at 30 minutes (after 10 minutes of perfusion with 100µM ouabain; $P<0.0001$ vs vehicle) but returned to baseline at 50 minutes (118±19 mmHg) following blebbistatin/ouabain titration and remained stable then until 80 minutes (109±10 mmHg). Heart rate (Figure 6.2B) was 308±18 BPM at baseline and was not altered by DMSO (328±21 BPM; $P>0.05$; paired t-test) in the vehicle group. The high $[Na]_i$ group exhibited a significant bradychardia at 30 minutes (268±15 BPM; $P<0.05$ vs vehicle) but returned to baseline levels by the end of perfusion.

Coronary flow (Figure 6.2C) was 12±1 mL/min at baseline in the vehicle groups and DMSO perfusion had no effect (13±2 mL/min). There was no difference in coronary flow between vehicle or high $[Na]_i$ throughout the entirety of the experiment ($P>0.05$). LVEDP (Figure 6.2D) was 6.6±1.3 mmHg in the vehicle group at baseline and did not change upon vehicle DMSO perfusion (6.6±1.3 mmHg; $P>0.05$; paired t-test). Furthermore, there was no difference in LVEDP between vehicle and high $[Na]_i$ at any point in the protocol ($P>0.05$), despite a larger error associated with the latter group.

6.5 Results- $[Na]_i$ and DQF measurements.

$[Na]_i$ (Figure 6.3A) remained constant throughout the stabilisation period in both vehicle (17±0.6 mM) and TPI (18±0.5 mM). The vehicle DMSO had no effect on

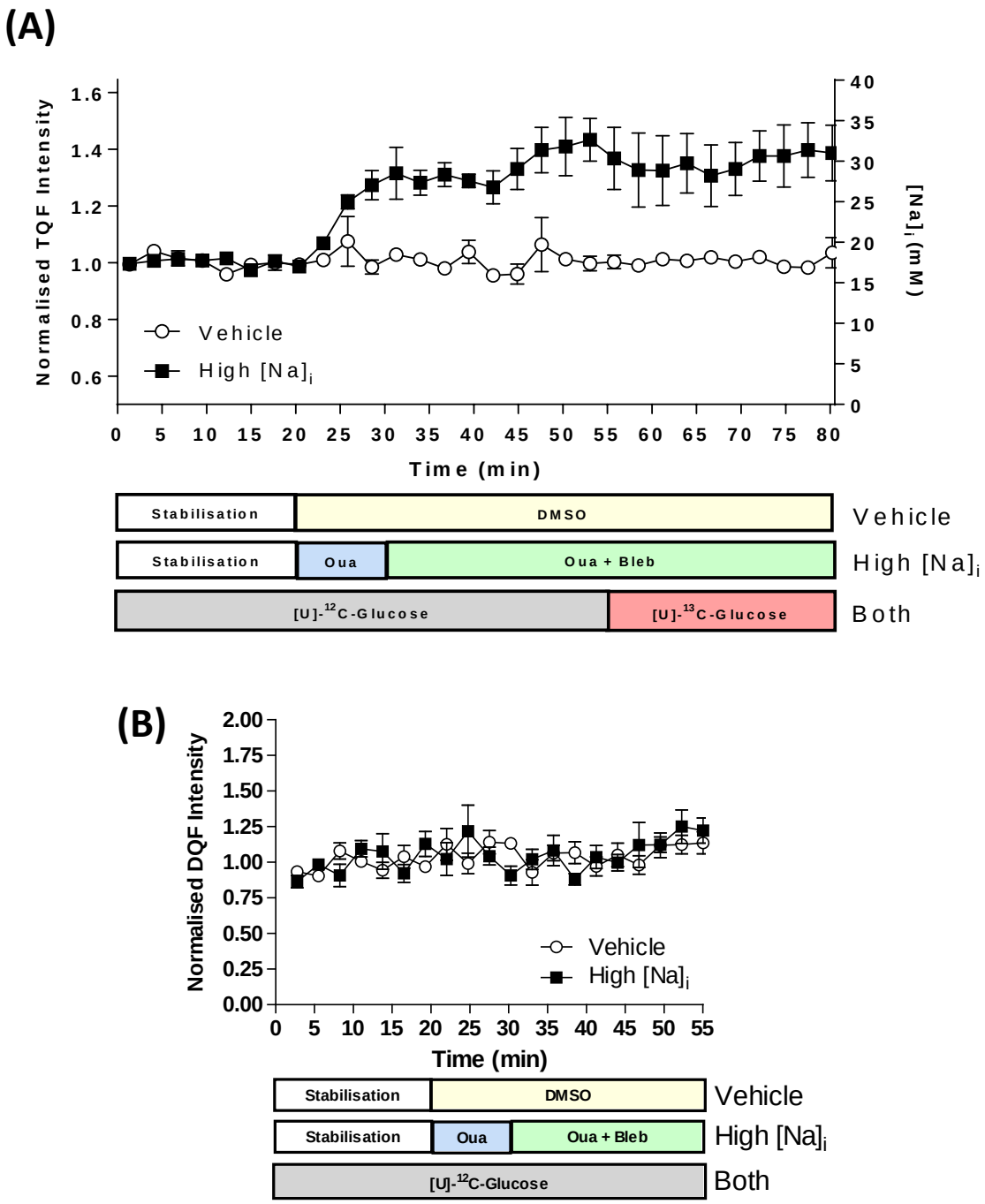

Figure 6.3 TQF/DQF ^{23}Na NMR measurements (^{13}C study).

(A) Normalised triple quantum filtered (TQF) ^{23}Na NMR intensity (left axis) with derived intracellular $[Na]_i$ (right axis). **(B)** Normalised double quantum filtered (DQF) ^{23}Na NMR intensity. Symbols and error bars represent mean±SEM of 1.5 minute time windows (n=5-6/group). Hearts were snap-frozen at 80 minutes. See Table 6.1 for details of protocol. Blebbistatin (Bleb); dimethyl sulfoxide (DMSO); ouabain (Oua).

derived $[Na]_i$ during the treatment period (18±1.0 mM). $[Na]_i$ was significantly higher ($P<0.05$) in the high $[Na]_i$ group (31.0±.3.4 mM) compared with the vehicle group (18.7±1.9 mM) at the end of perfusion and was stable during the period of [U]-^{13}C-glucose infusion. DQF signal did not markedly deviate from baseline (1.0±0.1 arbitrary units) at any point between 0 and 55 minutes (Figure 6.3B).

6.6 Results - ^{13}C isotopologue measurements of myocardial tissue by GC-MS.

The GC-MS method permitted the measurement of seven TCA cycle intermediates, three anaplerotic metabolites and three glycolytic metabolites.

The total extent of enrichment of these metabolites with ^{13}C label is shown in Figure 6.4. Significant increases in mean enrichment of citrate (25%; $P<0.01$), α-ketoglutarate (6%; $P<0.05$), fumarate (25%; $P<0.01$), malate (21%; $P<0.05$) and alanine (23%; $P<0.01$) were observed in the high $[Na]_i$ group versus vehicle.

With respect to the mass distribution vectors of the glycolytic metabolites, the m+3 isotopologue of DHAP (Figure 6.5A) was elevated in the high $[Na]_i$ group compared with vehicle (53%; $P<0.05$). However no changes were observed in the isotopologues of pyruvate or lactate. The m+0 (-28%; $P<0.01$) and m+1 (-20%; $P<0.05$) isotopologues of alanine were significantly lower in the high $[Na]_i$ group versus vehicle whereas the m+3 form was significantly higher in the high $[Na]_i$ group (25%; $P<0.01$) (Figure 6.5D). In addition, m+1 aspartate (-16%; $P<0.01$), m+1 glutamate (-22%; $P<0.05$) and m+2 glutamate (-25%; $P<0.01$) were significantly lower in the high $[Na]_i$ group (Figure

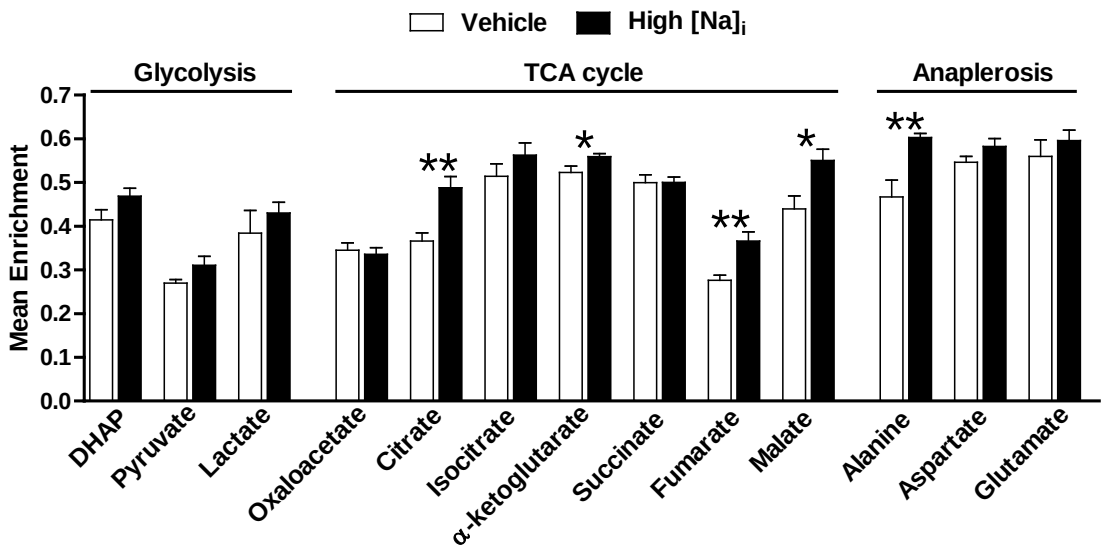

Figure 6.4 ^{13}C mean enrichment of metabolites involved in glycolysis, tricarboxylic acid (TCA) cycle and anaplerosis by GC-MS.

Columns and error bars represent mean±SEM (n=3-6/metabolite/group). '0' and '1' represent 0% and 100% isotopic labelling of the metabolite pool respectively. *P<0.05; **P<0.01.

6.5E&F). There was also a trend towards reduced levels of m+0 and m+2 aspartate (Figure 6.5E) as well as m+0 and m+3 glutamate (Figure 6.5F) in the high $[Na]_i$ group versus vehicle but were not significantly different (P>0.05). Furthermore, the m+5 isotopologue of glutamate was substantially higher in the high $[Na]_i$ group compared with vehicle (42%; P<0.05). In regard to the TCA cycle intermediates, oxaloacetate (Figure 6.6A) displayed no marked differences between the treatment groups. There was a lower abundance of m+0 citrate (-23%; P<0.05) and m+2 citrate (-9%; P<0.05) in the high $[Na]_i$ group compared with vehicle whereas m+5 citrate (28%; P<0.05) was more abundant in the former group (Figure 6.6B). A trend towards an elevation was observed in m+6 citrate (40%; P=0.082) in the high $[Na]_i$ group versus vehicle however was not statistically significant. A substantial reduction occured in m+1 isocitrate in the

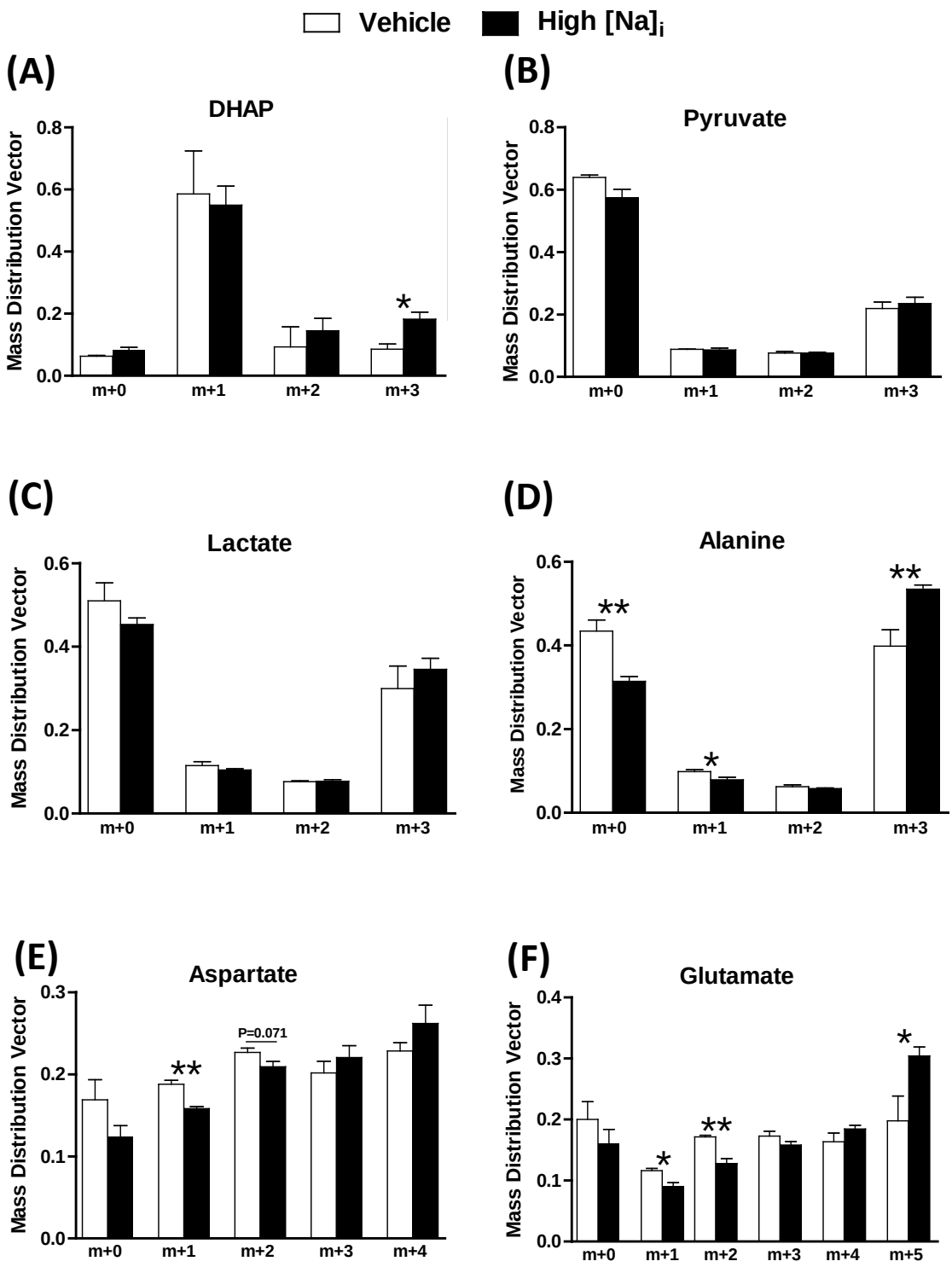

Figure 6.5 ^{13}C isotopologue mass distribution vectors (MDVs) of glycolytic and anaplerotic metabolites by GC-MS.

(A) Dihydroxyacetone phosphate (DHAP). **(B)** Pyruvate. **(C)** Lactate. **(D)** Alanine. **(E)** Aspartate. **(F)** Glutamate. Columns and error bars represent mean±SEM (n=3-6/metabolite/group). *P<0.05; **P<0.01.

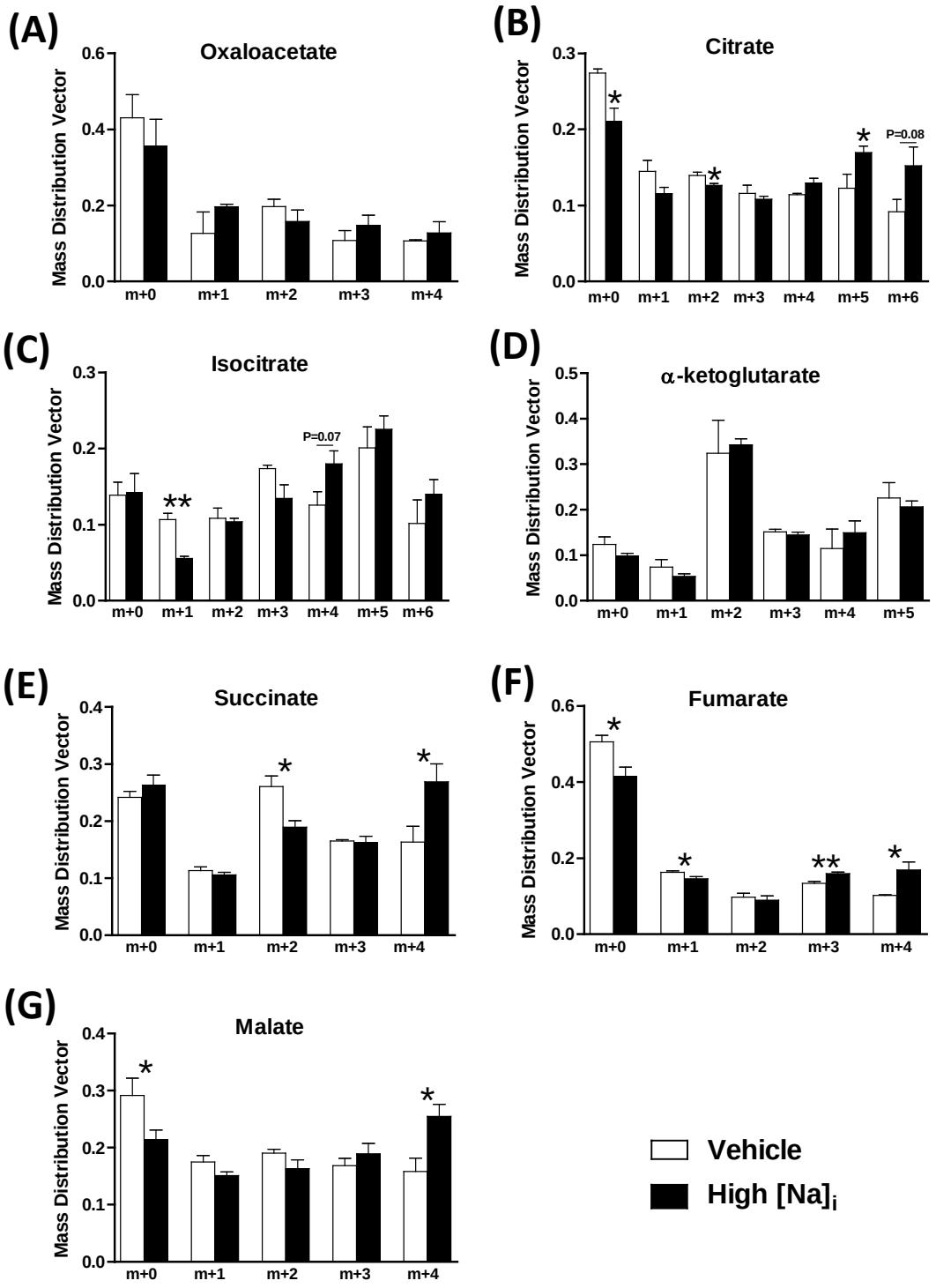

Figure 6.6 ^{13}C isotopologue mass distribution vectors (MDVs) of TCA cycle intermediates by GC-MS.

(A) Oxaloacetate. **(B)** Citrate. **(C)** Isocitrate. **(D)** α-ketoglutarate. **(E)** Succinate. **(F)** Fumarate. **(G)** Malate. Columns and error bars represent mean±SEM (n=3-6/metabolite/group). *P<0.05; **P<0.01.

high $[Na]_i$ group versus vehicle (-48%; P<0.01) and the m+4 isotopologue exhibited a trend towards elevation in the high $[Na]_i$ group but was not statistically significant (30%; P=0.065). There was also a trend toward reductions in the m+0 and m+1 isotopologues of α-KG (Figure 6.6D) in the high $[Na]_i$ group versus vehicle (-21% and -27% respectively) although these values were not statistically significant. M+2 succinate and m+4 succinate were 27% lower and 39% higher respectively in the high $[Na]_i$ group compared with vehicle (P<0.05) (Figure 6.6E). Multiple isotopologue changes were observed in fumarate (Figure 6.6F) with reductions in m+0 (18%; P<0.05) and m+1 (10%; P<0.05) and elevations in m+3 (15%; P<0.01) and m+4 (40%; P<0.05) in the high $[Na]_i$ group compared with vehicle. Malate exhibited a similar pattern of ^{13}C label distribution to fumarate. M+0 malate was 26% higher (P<0.05) in the high $[Na]_i$ group versus vehicle and m+4 malate was 38% lower (P<0.05) in the former versus the latter. There was a trend towards a reduction in m+1 and m+2 malate in the high $[Na]_i$ group compared with vehicle but did not reach statistical significance (P>0.05). Full details of the ^{13}C GC-MS datasets are shown in Appendices 8.11-8.12.

6.7 Results - ^{13}C isotopologue measurements of myocardial tissue by LC-MS/MS.

^{13}C labelling of pyruvate, lactate and TCA cycle intermediates in the myocardial tissue samples was also assessed by LC-MS/MS. Isotopologues were detected for all eight of the metabolites targeted by this technique (pyruvate, lactate, citrate, isocitrate, α-ketoglutarate, succinate, fumarate and malate) in the heart tissue extracts. Figure 6.7 summarise the mean enrichments of three of these metabolites. Due to technical issues with the mass spectrometer, it was not possible to calculate mean enrichment for the

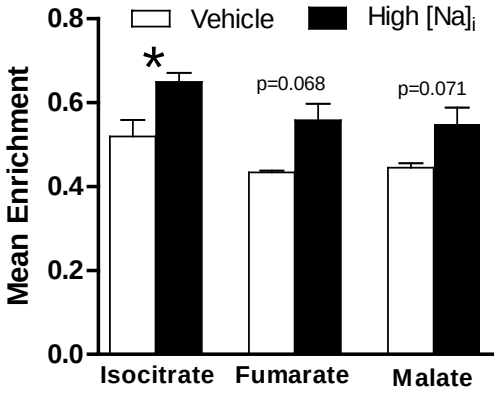

Figure 6.7 ^{13}C mean enrichment of tricarboxylic acid (TCA) cycle intermediates.

Columns and error bars represent mean±SEM (n=5-6/group). '0' and '1' represent 0% and 100% isotopic labelling of the metabolite pool respectively. Mean enrichment of the other TCA cycle intermediates as well as pyruvate and lactate could not be calculated due to a technical issue. *P<0.05; **P<0.01.

other five targeted metabolites as not all of their isotopomers were detected. Isocitrate, fumarate and malate were all enriched by >40% in both groups and isocitrate enrichment was significantly higher in the high $[Na]_i$ group compared with the vehicle group (P<0.05). Enrichment of fumarate and malate also showed a trend towards higher enrichment in the high $[Na]_i$ group although did not reach statistical significance. Figure 6.8 displays the relative abundances of the isotopologues, i.e., 'mass distribution vectors' (MDVs) for isocitrate, fumarate and malate. As the isotopologue sets were incomplete for the other metabolites, it was not possible to plot MDVs for these. Therefore, the mean raw LC-MS/MS intensity of the m+0 isotopologue signals of these metabolites (Figure 6.9) were compared between vehicle and high $[Na]_i$ to give an alternative indication as to whether there was a difference in the concentration of the unlabelled forms of these metabolites at the end of perfusion. There was a consistent trend towards a lower abundance of the m+0 isotopologues of isocitrate (Figure 6.8A),

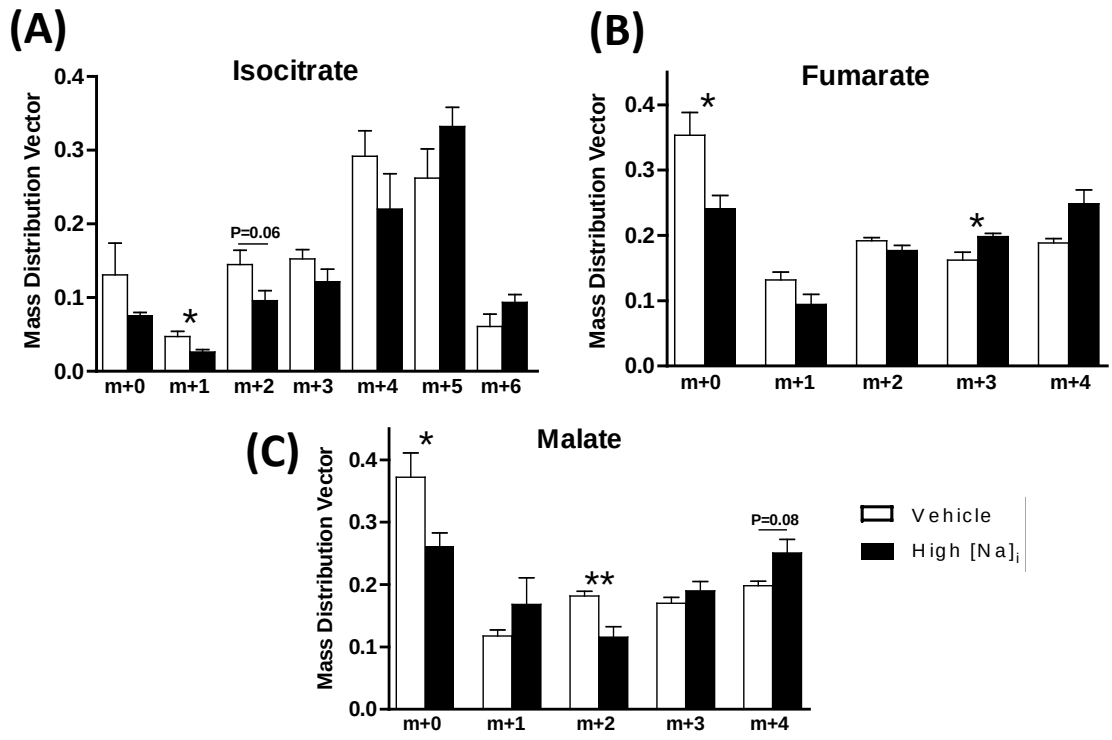

Figure 6.8 ^{13}C Isotopologue Mass Distribution Vectors (MDVs).

(A) Isocitrate. **(B)** Fumarate. **(C)** Malate. Columns and error bars represent mean±SEM (n=5-6/group).

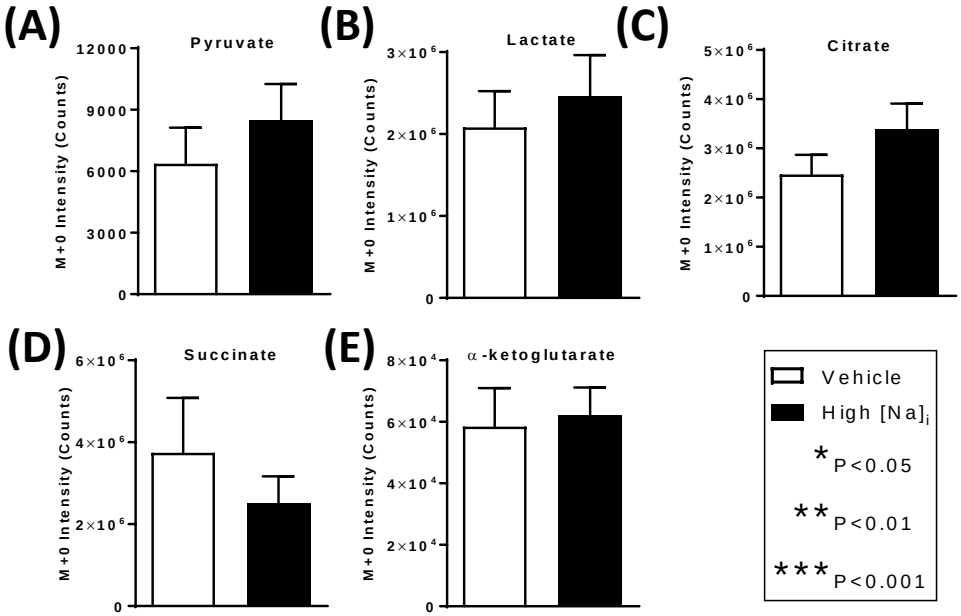

Figure 6.9 M+0 (unlabelled) raw LC-MS/MS counts.

(A) Pyruvate. **(B)** Lactate. **(C)** Citrate. (**D)** Succinate. **(E)** α-ketoglutarate. Columns and error bars represent mean±SEM (n=5-6/group).

fumarate (Figure 6.8B) and malate (Figure 6.8C) and succinate (Figure 6.9D) in the high $[Na]_i$ group versus vehicle. Both malate ($P<0.05$) and fumarate ($P<0.001$) reached statistical significance although isocitrate and succinate did not. The m+1 isotopologues of isocitrate and fumarate, as well as the m+2 isotopologues of isocitrate and malate, also displayed a tendency to lower abundances in the high $[Na]_i$ group compared with vehicle but were not statistically significant ($P>0.05$). There were no clear trends for the m+3 ($P<0.05$) isotopologues of the TCA cycle. However, the m+4 isotopologue profiles of fumarate and malate were inverse to those of the m+0, m+1 and m+2 isotopologues. That is, m+4 exhibited a higher abundance in the high $[Na]_i$ group versus the vehicle counterparts which was statistically significant. There was also a similar trend in the m+5 and m+6 isotopologues of isocitrate although were not statistically significant ($P>0.05$). There was a high degree of similarity between the overall isotopologue profiles of fumarate and malate. There were no differences ($P>0.05$) between the perfusion groups with respect to the raw intensities of the m+0 isotopologues of pyruvate (Figure 6.9A), lactate (Figure 6.9B), citrate (Figure 6.9C), α-ketoglutarate (Figure 6.9D) and succinate (Figure 6.9E). Full details of the ^{13}C LC-MS/MS datasets are shown in Appendices 8.13-8.15.

6.8 Discussion

In this chapter, a vehicle group and a high $[Na]_i$ group were perfused with ^{13}C-labelled glucose to assess whether TCA cycle activity is altered by $[Na]_i$ elevation. As the groups exhibited the same LVDP during the labelling period, increased ^{13}C

incorporation (measured by GC-MS and LC-MS/MS) in the high $[Na]_i$ group were indicative of altered TCA cycle activity that were independent of contractile demand.

6.8.1 Perfusion measurements

As anticipated, 100µM ouabain resulted in a significant TPI that resembled the LVDP profile of the TPI group in Chapter 5 (Figure 5.1). LVDP was at steady-state during the ^{13}C labelling period in both groups. In agreement with Figure 3.1 and Figure 5.1 in previous studies, perfusion with 100 µM ouabain gave rise to a significant bradycardia (Figure 7.2) which had waned prior to the infusion of ^{13}C label at 55 minutes. Increases in coronary flow (Figure 6.2) and LVEDP (Figure 6.2) upon 100 µM ouabain perfusion were characteristic of the profiles discussed in previous chapters (Figures 3.1 & 5.1). However, importantly when the inotropy had been titrated back to baseline there was then no significant difference in coronary flow between control and treated groups.

6.8.2 $[Na]_i$ measurements

There were no changes in baseline measurements of $[Na]_i$ in either group during the stabilisation periods but significant elevations in TQF and therefore in the derived $[Na]_i$ occurred following ouabain perfusion (Figure 6.3). The $[Na]_i$ profiles between 0 and 55 minutes for the vehicle and high $[Na]_i$ groups exhibited a high degree of similarity with those of the vehicle and TPI groups in Chapter 5 (Figure 5.1), respectively. In concurrence with the studies detailed in Chapter 5, neither group described in this chapter exhibited alterations in DQF signal between 0 and 55 minutes. Although DQF

was not measured between 55 and 80 minutes (the ^{13}C labelling period) due to a technical issue, there is no difference between hearts perfused with $^{13}C_6$-glucose to those perfused with ^{12}C-glucose. Importantly, TQF and therefore derived $[Na]_i$ was at steady-state in both groups throughout the entirety of the ^{13}C labelling period (55-80 minutes).

6.8.3 ^{13}C isotopologue measurements

^{13}C incorporation into the TCA cycle was assessed by both GC-MS and LC-MS/MS. There was good agreement between the control (vehicle) values in these datasets compared with those obtained by Chouchani et al. (2014) using the isolated mouse heart. Tables 6.2 and 6.3 summarise the alterations in mean enrichment and mass distribution vectors measured by GC-MS and LC-MS/MS in this thesis. There was strong agreement between these techniques in terms of elevated mean enrichment of fumarate (GC-MS: 25%; LC-MS/MS: 22%) and malate (GC-MS: 21%; LC-MS/MS: 19%) in the high $[Na]_i$ group versus vehicle although the GC-MS values did not reach statistical significance. In the GC-MS method, citrate was also significantly enriched during $[Na]_i$ elevation (Figure 6.4). Given that citrate and isocitrate exist in equilibrium (Costello et al., 2000) this aligns with the increased enrichment of isoctrate measured by LC-MS/MS (Figure 6.7) following a period of high $[Na]_i$. Based on the simple model of carbon fluxes shown in Figure 6.1, the greater abundance of m+3 fumarate and m+4 fumarate in the high $[Na]_i$ group versus vehicle (Table 6.3) indicate that these isotopologues had been subject to more turns of the TCA cycle with high $[Na]_i$.

Table 6.2 ^{13}C Mean enrichment summary (GC-MS & LC-MS/MS)

Analyte	GC-MS		LC-MS/MS	
	% change	P-value	% change	P-value
Fumarate	↑ 25	0.006	↑ 22	0.068
Malate	↑ 21	0.020	↑ 19	0.071

% changes are for High $[Na]_i$ group vs vehicle at 80 minutes where '0 %' change represents zero fold-change. Only metabolites that were significantly altered and/or gave similar values from GC-MS and LC-MS/MS were included.

Table 6.3 ^{13}C Mass distribution vector summary (GC-MS & LC-MS/MS)

Analyte	GC-MS		LC-MS/MS	
	% change	P-value	% change	P-value
Isocitrate m+1	↓ 48	0.001	↓ 45	0.017
Fumarate m+0	↓ 18	0.015	↓ 32	0.017
Fumarate m+3	↑ 15	0.004	↑ 18	0.040
Fumarate m+4	↑ 40	0.029	↑ 25	0.045
Malate m+0	↓ 26	0.041	↓ 30	0.028

% changes are for High $[Na]_i$ group vs vehicle at 80 minutes where '0 %' change represents zero fold-change. Only isotopologues that were significantly altered and/or gave similar values from both GC-MS and LC-MS/MS were included.

Furthermore, unlabelled fumarate and malate as well as m+1 isocitrate isotopologues (which all underwent zero turns of the TCA cycle during the ^{13}C labelling period according to Figure 6.1) were more abundant in the vehicle group than in the high $[Na]_i$ group. There was a high level of agreement between the two mass spectrometry techniques with respect to these data (Table 6.3). There were also several other isotopologue differences observed by GC-MS (Figure 6.6) that were suggestive of greater TCA cycle activity in the high $[Na]_i$ group versus vehicle including m+0 citrate, m+2 citrate, m+2 succinate and m+1 fumarate (all significantly lower in high $[Na]_i$ group versus vehicle) as well as m+5 citrate, m+4 succinate, m+4 fumarate and m+4 malate (all significantly higher in the high $[Na]_i$ group versus vehicle). Overall, the mean enrichment datasets are suggestive of greater incorporation of ^{13}C label into TCA cycle intermediates during $[Na]_i$ elevation.

This finding was unanticipated. It was hypothesised that $[Na]_i$ elevation leads to decreased stimulation of the TCA cycle following a reduction in $[Ca]_m$. However, increased TCA cycle activity may be a consequence of the ATP depletion that was associated with $[Na]_i$ elevation (Figures 5.8). Direct interaction between ATP synthase and Ca^{2+} has been reported (Hubbard and McHugh, 1996) as has indirect interaction via calcium binding ATPase inhibitor (CaBI) (Yamada and Huzel, 1989), protein kinase Cδ (Nguyen et al., 2010) and S100A1 (Boerries et al., 2007), which are all postulated to have stimulatory effects on ATP synthase. It is possible that the heart would use the same entity (Ca^{2+}) to directly stimulate both the primary sites of ATP utilisation (the myofilament) and ATP production (ATP synthase). Furthermore, there has been no study thus far investigating the importance of Ca^{2+} in its regulation of PDH, αKDH and

IDH relative to its regulation of ATP synthase. It is plausible that the primary metabolic consequence of $[Na]_i$ elevation is a reduction in stimulation of ATP synthase activity by Ca^{2+}. Given the high ATP demand in the contracting heart, this would result in depletion of ATP and an increase in P_i and ADP. The latter molecule is a classic activator of the TCA cycle via allosteric binding to IDH (Vaughan and Newsholm, 1969, Nichols et al., 1994) and αKDH (Nichols et al., 1994, Ostrovtsova and Strumilo, 1990). Furthermore, Balaban (2009) has demonstrated that IDH, αKDH and MDH are stimulated by P_i. Increases in ADP and P_i would thereby lead to increased TCA cycle activity following a derangement in ATP supply-demand matching. This aligns with the work of Marin-Garcia et al (2001) and O'Brien et al (1990) which infer that TCA cycle activity is increased as a consequence of impairment of ATP generating enzymes following pacing-induced HF. Indeed, $[Na]_i$ elevation may be an important pathophysiological component of this HF model given that electrical pacing is associated with a rise in $[Na]_i$ in cardiomyocytes (Despa et al., 2008)

According to LC-MS/MS, $[Na]_i$ elevation resulted in significantly higher ^{13}C mean enrichment of isocitrate (and a trend toward increased mean enrichment of fumarate and malate) (Figure 6.7). However, the enrichment of the other targeted TCA cycle intermediates cannot be commented on from the LC-MS/MS data as several of their isotopomers were not detected due to instrumental factors. Nonetheless, it was possible to obtain the absolute LC-MS/MS counts of the unlabelled (m+0) form of all targeted metabolites for both perfusion groups (Figure 6.9). In agreement with the GC-MS measurements, $[Na]_i$ elevation did not alter the abundance of the unlabelled (m+0) forms of pyruvate, lactate, succinate and α-ketoglutarate although the m+0 citrate result

differed between the methods. The presence of unlabelled forms of the targeted metabolites in the samples could be due to multiple factors. Firstly, residual [U]-$^{12}C_6$-glucose (m+0) and/or its downstream metabolic products may have been present at the end of the perfusion protocol due to these reaching an equilibrium with their labelled counterparts. Secondly, the TCA cycle is fed not only by exogenous fuel substrates but also by endogenous fuel stores. Glycogen-derived glucose and triacylglycerol-derived fatty acids have been shown to each provide approximately 12-13% of the total ATP produced in the perfused rat heart (Henning et al., 1996) and the vast majority of this is TCA cycle-dependent. It is probable that a portion of the unlabelled m+0 isotopologues were derived from unenriched, endogenous fuel sources. The effect of $[Na]_i$ elevation on the utilisation of these fuel stores has not been studied here. Thirdly, $[Na]_i$ elevation may have increased TCA cycle activity leading to greater enrichment of TCA cycle intermediates and thus a lower concentration of m+0 isotopologues.

The GC-MS technique also permitted the assessment of ^{13}C incorporation into glycolytic and anaplerotic metabolites which are pathways known to be tightly linked to TCA cycle activity (see Section 1.3.2). M+3 DHAP was substantially increased in the high $[Na]_i$ group vs vehicle without differences in pyruvate and lactate labelling (Figure 6.5). This suggests an elevation in the overall flux of ^{13}C from hexokinase through to fructose-bisphosphate aldolase followed by a bypassing of ^{13}C around the subsequent enzymes of the glycolytic pathway, for example, via glycerol-3-phosphate dehydrogenase. It should be noted that glycolysis occurs in the cytosol and therefore, in contrast to the TCA cycle, may be affected by elevated cytosolic Na^+ rather than elevated mitochondrial Na^+. It is unclear whether this would an adaptive or maladaptive

process in the context of deranged ATP supply-demand matching. In terms of anaplerotic pathways, greater total incorporation of ^{13}C label into alanine and α-ketoglutarate occurred in the high $[Na]_i$ group versus vehicle (Figure 6.4) and the abundance of fully-labelled (m+5) glutamate was also greater in the former group (Figure 6.5F). Interestingly, all three of these molecules are involved in the alanine transaminase reaction (Figure 1.6) and may infer a potential role of this enzyme during $[Na]_i$ elevation in the isolated perfused heart. It is also plausible that an increase in TCA cycle activity (due to deranged ATP production) leads to an increased flux of carbon into glutamate from α-KG via glutamate dehydrogenase. It is currently unknown whether Ca^{2+} and/or Na^+ have any direct stimulatory or inhibitory effects on enzymes involved in glycolysis or anaplerosis in the isolated perfused heart.

The results provide evidence to support an increased activity of the TCA cycle during a steady-state of $[Na]_i$ elevation and baseline inotropy. This regulation appears to take place at several points of the TCA cycle as the ^{13}C abundance of multiple metabolites was altered to similar degrees. Independent GC-MS and LC-MS/MS experiments suggest that these points of enzyme regulation involve isocitrate, fumarate and malate. Interestingly, the total pool sizes of fumarate and malate were found to be elevated by $[Na]_i$ elevation in Chapter 5. GC-MS also pointed towards an involvement of citrate, α-ketoglutarate and succinate during $[Na]_i$ elevation thereby adding further weight to an increase in TCA cycling under these conditions. The GC-MS also revealed an increase in partial glycolytic flux from glucose to DHAP as well as possible enhancements in the activities of alanine transaminase and glutamate dehydrogenase. These alterations may

reflect the tight coupling of glycolysis and anaplerosis to TCA cycle activity which appears to increase during $[Na]_i$ elevation.

6.9 Summary

It was hypothesised based on the malate and fumarate data in Chapter 5 that TCA cycle activity is decreased as a consequence of $[Na]_i$ elevation in the isolated perfused heart. However, TCA cycle measurements by GC-MS and LC-MS/MS of normally-contracting hearts perfused with ^{13}C-labelled glucose during a period of acutely elevated $[Na]_i$ by ouabain suggested an increased TCA cycle activity during high $[Na]_i$. The underlying mechanisms remain unclear but may be a consequence of altered cardiac energetics and reduced ATP supply due to an acute rise in $[Na]_i$ and a compensatory increase in TCA cycle activity. This chapter adds weight to the overall hypothesis that $[Na]_i$ elevation gives rise to metabolic alterations in the isolated perfused heart and that the activity of the TCA cycle is implicated in this adaptation.

7 GENERAL DISCUSSION AND CONCLUSIONS.

7.1 Summary of conclusions.

The studies presented in this thesis have investigated whether $[Na]_i$ elevation alters intermediary metabolism and cardiac energetics in the isolated perfused rat heart independently of elevated inotropy. As previously discussed, inhibition of NKA by ouabain induces a rise in $[Na]_i$ by blocking the only quantitatively important efflux pathway for Na^+. However, this rise in $[Na]_i$ leads to an elevation in $[Ca]_i$ via altered sarcolemmal NCX activity and a subsequent increase in inotropy and therefore increased ATP demand. A major challenge has been to overcome this positive inotropy which confounds the interpretation of metabolic measurements.

There is an abundance of literature reporting the use of ouabain to inhibit NKA in the Langendorff model, the majority of which use a single high concentration of ouabain (>100 μM) which leads to arrest, considerably reducing the physiological relevance of the model. Initial studies (Chapter 3) showed a dose-dependent increase in $[Na]_i$ between 0 and 100 μM ouabain without inducing arrest or notable arrhythmias. Hearts perfused with 50 μM ouabain and subject to end-point metabolomics following snap freezing revealed several metabolites that were significantly altered including increased fumarate (TCA cycle) and acetylcarnitine (shuttles carbon acetyl groups into the mitochondria). These altered metabolite levels were augmented by increased contractile demand at high electrical pacing rate (500 BPM) and gave rise to additional metabolite changes including elevated succinate (TCA cycle) and lactate (glycolysis). Inhibition of

NKA with ouabain induced significant inotropy, confounding the interpretation of these results due to increased ATP demand.

Perfusion protocols were developed (Chapters 4 and 5) combining blebbistatin (to uncouple contraction) and ouabain (to elevate Na^+) to remove the inotropy-dependent metabolic consequences of ouabain and better distinguish any $[Na]_i$-dependent changes. Perfusion with 5 μM blebbistatin completely eliminated contraction after 10 minutes of perfusion thus eliminating contractile ATP demand. Electrocardiogram measurements showed that 5 μM blebbistatin had no significant effects on heart rate, QRS duration or QT90% suggesting that blebbistatin does not profoundly affect electrophysiology. The dose-response to ouabain in the presence of 5 μM blebbistatin revealed an attenuation of the ability of ouabain to elevate $[Na]_i$ as measured by TQF ^{23}Na NMR which has not been reported previously. In isolated cell experiments, blebbistatin did not alter the degree of NKA pump inhibition by ouabain measured by patch clamping. Increasing the concentration of ouabain in the presence of 5 μM blebbistatin normalised for this attenuation, allowing a sustained elevation of $[Na]_i$ in the absence of contraction. End-point metabolomics performed in non-contracting hearts perfused with blebbistatin and ouabain revealed only minor changes in fumarate, glutamate, glutamine and acetate compared to vehicle treated controls. The changes in metabolite levels observed in the contracting hearts (Chapter 3) which were subject to both elevated $[Na]_i$ and increased ATP demand were largely absent in the non-contracting situation (Chapter 4). The relevance of the non-contracting model to the beating heart is therefore questionable due to the substantially reduced ATP demand.

A contracting heart protocol was therefore developed (Chapter 5) to better elucidate $[Na]_i$-dependent from inotropy-dependent effects on metabolism and energetics while maintaining contractility at baseline levels. The first protocol involved perfusing ouabain first followed by blebbistatin to titrate the elevated LVDP back down to baseline at the end of the protocol, thereby inducing a transient positive inotropy (TPI). The second protocol involved perfusing in reverse order with blebbistatin first followed by ouabain to titrate the depressed LVDP back up to baseline at the end of the protocol, thereby inducing a transient negative inotropy (TNI). TQF ^{23}Na measurements revealed that $[Na]_i$ was significantly elevated to the same degree in both groups at the end of the protocol.

Real-time ^{31}P measurements of TPI and TNI groups showed a transient increase or decrease in both PCr and Pi that mirrored the transient increase or decrease in inotropy. PCr levels returned to baseline at the end of the protocol. However there was a strong negative correlation between $[Na]_i$ and [ATP] in both groups irrespective of inotropy induced. Although the reductions in ATP appear relatively modest they are indicative of a significant metabolic perturbation. Given the central importance of ATP to contractile function and cell survival, the heart is able to maintain its steady-state ATP levels during high levels of stress by buffering its concentration with PCr. For example, ATP levels do not appear to decline in patients with moderate HF but do so in end-stage HF (Neubauer et al., 1997). With respect to the Langendorff model, previous work showed that 30 minutes of regional ischaemia following ligation of the left ascending coronary artery reduced ATP by approximately 50% (Wilder et al., 2016). This is similar to the reduction in ATP by up to 41% due to $[Na]_i$ elevation in aerobically-perfused control

hearts described in this thesis. Therefore, $[Na]_i$ elevation in the absence of elevated ATP demand appears to substantially alter energy balance in the perfused heart. Although ADP was not measured in the TPI and TNI studies, it can be inferred that the dramatic reduction in ATP would have been mirrored by a proportional fold increase in ADP. As contractile function was at baseline levels at the end of the TPI and TNI periods in the absence of arrhythmias, it appears that the preparation was able to sustain normal EC coupling despite a substantial reduction in [ATP] (and thereby a reduction in the ATP/ADP ratio). This was surprising as [ATP] is significantly reduced in HF (Starling et al., 1998, Nascimben et al., 1995, Liao et al., 1996). It is possible that the observed increase in TCA cycle activity with $[Na]_i$ elevation (Chapter 6) is an implication of reduced [ATP]. Furthermore, there may be other metabolic pathways that were also altered due to [ATP] depletion but were not assessed in this thesis, for example, substrate utilisation. Another potential consequence of [ATP] depletion is activation of $K^+_{(ATP)}$ channels which efflux K^+ from the cardiomyocyte in the absence of ATP (Craig et al., 2008). $[Na]_i$ elevation in the TPI and TNI groups may therefore have also been associated with decreased $[K]_i$ versus vehicle which could have led to metabolic and/or electrophysiological consequences.

Given that PCr and CK are known to buffer ATP in muscle during periods of stress (Duffield et al., 2004), the finding that ATP was decreased but PCr was unaltered by elevated $[Na]_i$ in both TPI and TNI groups was unanticipated, suggesting a possible role of $[Na]_i$ in the regulation of CK or ATP supply. The explanation for the inability of CK to buffer ATP leading to metabolic compromise remains to be determined. Furthermore, the relative impact of perturbation in the CK reaction versus perturbation in ATP

synthase during $[Na]_i$ elevation is also unclear. If demand is not elevated and CK activity and PCr are unaffected by $[Na]_i$ elevation, then a possible explanation for a drop in ATP levels would be a sustained inhibition (or reduced stimulation) of ATP synthase.

Myocardial tissue metabolites were assessed at the end of the TPI and TNI protocols by high resolution ^{1}H NMR and an LC-MS/MS method for the quantification of TCA cycle intermediates and pyruvate. A transient elevation in inotropy appeared to increase acetylcarnitine shuttling as well as the concentrations of alanine (potentially due to increased alanine transaminase activity), citrate and isocitrate (suggesting increased TCA cycle activity). On the other hand, a transient reduction in inotropy was associated with decreases in glutamate:glutamine and α-ketoglutarate (potentially due to reduced glutamate anaplerosis) as well as decreases in ATP+ADP and creatine (indicative of decreased energetic reserve). Given that these metabolite changes were not recapitulated in the two groups, the observations support the existence of a "metabolic memory" for the transient elevation or depression of contractility during the experiment. That is, the immediately preceding contractile history of a heart influences the prevailing metabolic status and this effect persists for at least 10-15 mins. Despite many metabolite changes not being common to the two groups, two metabolites, malate and (more tentatively) fumarate, were increased in both groups. This may infer a link between $[Na]_m$ and malate dehydrogenase activity or more generally a change in overall TCA cycle flux in the perfused heart subject to an acute elevation of $[Na]_i$. Malate is a central component of the TCA cycle and thereby important for ATP generation but it is not clear whether a ~50% elevation would have marked effects on the bioenergetic status of the heart. Doenst et al (2013) proposed that elevated anaplerosis of pyruvate into malate via

increased malic enzyme activity is a maladaptive mechanism during HF. This is because pyruvate flux through PDH would decrease leading to energetic inefficiency of the TCA cycle. Interestingly, PDH is known to be stimulated by increases in $[Ca]_m$ in the physiological range (Denton et al., 1972, Siess, 1972) thus $[Na]_i$-induced blunting of this effect may contribute to a diversion of pyruvate away from PDH and toward malic enzyme in order to divert carbon skeletons into the TCA cycle. Furthermore, increased malic enzyme activity is known to decrease the NADPH pool size which may increase oxidative stress (Pound et al., 2009).

Elevations in malate and fumarate do not demonstrate whether activity of the TCA cycle was decreased or increased. To address this question, the TPI protocol was adapted by perfusing hearts for an additional 25 minutes at steady-state with [U]-^{13}C-glucose during which time LVDP was sustained at baseline levels and $[Na]_i$ remained significantly elevated. Assessment of ^{13}C isotopologue patterns of the TCA cycle intermediates by LC-MS/MS and GC/MS was supportive of greater incorporation of ^{13}C into TCA intermediates inferring increased TCA cycle activity in the high $[Na]_i$ group versus time-matched vehicle. This is in contrast to the thesis hypothesis that $[Na]_i$ elevation reduces TCA cycle activity leading to altered energetics.

7.2 Critical assessment of methods and results in this thesis

This thesis has made use of sophisticated experimental techniques in order to investigate an important biological question. These techniques have potential drawbacks which can confound the interpretation of the data that they generate.

7.2.1 The isolated perfused heart model

The primary limitation of the Langendorff perfused heart is that it is an *ex vivo* model that was perfused with glucose as its sole fuel supply. Indeed, it cannot be discounted that the apparent effect of $[Na]_i$ elevation on metabolism is specific to this particular model. It is a possibility that the hearts in this thesis were approaching metabolic "stress" at baseline (for example, due to lower oxygen delivery and/or substrate availability versus *in vivo*) and may therefore have been more sensitive to changes in LVDP or $[Na]_i$ compared with healthy hearts *in vivo*. Heineman and Balaban (1990) demonstrated in healthy dogs *in vivo* that an increase in workload does not alter the PCr-ATP ratio due to compensatory increases in mean arterial pressure and coronary flow. Although increases in coronary flow were observed during the TPI period in Chapter 5, this may not have been sufficient to compensate for the increased ATP demand thus giving rise to reduced [PCr]. The Langendorff preparation can be made more physiologically-relevant by the addition of insulin and reduction of glucose concentration (although insulin is known to adhere to perfusion glassware thereby increasing heart-to-heart variability). Under aerobic conditions, healthy hearts use FAs preferentially as a fuel source over carbohydrates (Gertz et al., 1988, Stanley et al., 2005). However, the preparation of FA-containing perfusion buffers is laborious, necessitates specialised gassing procedures and increases the likelihood of contamination in the perfusion rig. The effect of $[Na]_i$ on substrate selection was not a focus of this thesis but may be an important factor. Indeed, perfusion of hearts with FAs or other metabolic substrates such as glutamate may alter the metabolic response to $[Na]_i$ overload in this preparation.

To minimise heart-to-heart variability, male Wistar rats weighing approximately 300g were used for all experiments. Restricting studies to only one gender (Townsend et al., 2015), minimises experimental variability due to hormonal differences between the genders. The rat is known to have a significantly higher baseline $[Na]_i$ compared with other species including man (Table 1.1). Species-differences (particularly when comparing rodent models with the human situation) are a common issue in medical research. The relationship between $[Na]_i$ and metabolism may differ qualitatively and/or quantitatively between the rat and humans or other species. Significant metabolic differences have been reported between rats and mice (reviewed by Radermacher et al., 2013). The question remains whether the relationship between $[Na]_i$ and metabolism in the rat is similar to man and specifically whether this is important in the development of HF. Maack et al (2006) showed that $[Na]_i$ overload results in metabolic alterations *in vitro* in guinea pig myocytes. Recent work in our laboratory performed by Dr Dunja Aksentijevic has shown that $[Na]_i$ overload significantly alters metabolism in the *ex vivo* mouse heart (unpublished data) as well as in a mouse expressing a PLM mutation (PLM 3SA) which has a chronic elevation in Na^+ at baseline. *In vivo* models of $[Na]_i$ overload may provide justification to assess this in larger species (such as the dog or minipig) in the future.

Animals were weight-matched as much as possible so that variability in heart size and structure was minimised as these can particularly alter ^{23}Na NMR measurements due to the mass and geometry of the myocardium within the RF coil. However, relatively young rats were used (~8-10 weeks of age) and basal metabolism is known to alter with age (Villa et al., 2006). In addition, HF is more prominent with age (Townsend et al.,

2015) thus the age-dependence of the $[Na]_i$-metabolism relationship should be investigated in the future.

Due to a technical issue with the ventricular pressure transducer, it was not possible to measure LVEDP during NMR acquisition in Chapters 3 and 4. Therefore, the intraventricular balloon was inflated to a fixed volume of 150 µL for all hearts before the start of each perfusion experiment. Although hearts were approximately the same size, this may have induced an over-inflation for some hearts with a smaller left ventricular lumen thereby leading to regional ischemia and potentially compromised $[Na]_i$ handling. Notwithstanding this, ^{31}P NMR of Langendorff hearts from rats weighing ~300 g (the same weight as that used in this thesis) by Abe et al (1988) showed that intraventicular balloon inflation from 50 µL to 150 µL leads to a small increase in the inorganic phosphate signal although there was no observable change in either the PCr or ATP signals. On the other hand, 150 µL may have been an under-inflation and hence reduced LVDP due to less myofilament stretch (Frank-Starling effect) which may explain why the inotropic responses to 50-100 µM ouabain were lower than anticipated. Importantly, this technical issue was solved for later experiments in Chapters 5 and 6.

7.2.2 The use of ouabain and blebbistatin

The most effective way to induce $[Na]_i$ elevation in the Langendorff preparation is to inhibit NKA as it is the most quantitatively important efflux pathway of $[Na]_i$. It was not investigated whether stimulating one or more of the influx pathways is a viable

alternative. It is known that the heart is able to ramp up NKA activity to counteract any increases in influx (Bers and Despa, 2009) and has a large capacity for Na^+ efflux (~32μM $[Na]_i$ is extruded by NKA during the action potential (Bers and Despa, 2009)). Ouabain was chosen as there is a wealth of literature reporting its use in the Langendorff preparation including ^{23}Na NMR measurements in the rat (for example, Schepkin et al., 1998). However, as ouabain was the only agent used to elevate $[Na]_i$ in this thesis it should be considered that ouabain may have exerted off-target effects that may have altered the metabolic profile irrespective of $[Na]_i$. There is evidence to suggest that ouabain activates signalling cascades via interaction with NKA. For example, Mohammadi et al. (2003) showed that perfusion of rat and guinea pig hearts with 50 μM and 1 μM respectively for 10 minutes increased the expression of Src kinase and extracellular signal-regulated kinases (ERK) 1 and 2. The authors did not perform any metabolic measurements. Longer term elevations in ERK have been shown to increase flux through PDH in proliferating cancer cells (Huddleston, 2011) and in addition ouabain alters cell cycle S-phase progression in cancer cells (Xu et al., 2015). However, it is ambiguous whether this bears any relevance to the ouabain-perfused Langendorff preparation. Indeed, it was shown in Chapter 4 that ouabain appeared to have minimal effects on the metabolic profile of non-contracting hearts perfused with blebbistatin in which $[Na]_i$ was elevated by only a small extent. Nonetheless, future work employing other agents to elevate $[Na]_i$ may help to distinguish any signalling effects of ouabain from its effect on $[Na]_i$. It should also be taken into account that inhibition of NKA may decrease intracellular K^+ (Browning et al., 1981) which might have metabolic consequences in addition to those of $[Na]_i$. However, there are no data on this at present and the decrease in K^+ is likely to be relatively small compared to

basal levels. Avoiding NKA-targeted agents altogether and stimulating Na^+ influx (reviewed by Endoh, 2004), for example, using veratridine, may be a better alternative to the induction of $[Na]_i$ overload in the isolated perfused heart. Given that an elevation in the late Na^+ current is a key pathophysiological feature of HF (Gremmler and Kisters, 2013, Noble and Noble, 2006, Sossalla et al., 2008), it is also important to assess whether this can lead to alterations in ATP supply-demand matching in the intact heart. Indeed, this also applies to other mechanisms of Na^+ influx that are known to be elevated in HF, such as NCX (Reinecke et al., 1996) and NHE (Baartscheer et al., 2003b, Baartscheer et al., 2008).

The possibility of off-target effects also applies to blebbistatin although there is less data available on this compared with ouabain. Helfman et al (2005) demonstrated that blebbistatin reduces ERK activation in a dose-dependent manner and also alters cell morphology (Wilkinson et al., 2005) although high blebbistatin concentrations were used (50-200μM) in non-cardiac cells. The current consensus appears to be that its apparent signalling effects are due to its inhibition of contractile activity via myosin II ATPase rather than via other proteins. Therefore, it is unclear whether the blebbistatin-ouabain titration protocols used in this thesis (in which contraction was the same in both vehicle and high $[Na]_i$ at the end of perfusion) elicited significant signalling effects in the high $[Na]_i$ group that may have confounded metabolic measurements.

DMSO was used as a vehicle for blebbistatin in this thesis. In Chapter 4 (Section 4.4.3), TQF ^{23}Na NMR measurements in perfused hearts suggested that DMSO does not affect baseline $[Na]_i$ or the ability of ouabain to elevate $[Na]_i$. However, this experiment did not negate the possibility that DMSO may synergise or activate the inhibitory effect of

blebbistatin on ouabain-induced $[Na]_i$ elevation. Future experiments involving perfusion with blebbistatin dissolved in a different vehicle (such as dimethyl formamide) are necessary to elucidate this further.

The small inotropic responses of 75µM and 100µM ouabain, following the cessation of contraction in blebbistatin-perfused hearts demonstrates that sarcolemmal NCX is still active in these preparations. This was demonstrated further by the larger positive inotropy induced by 155µM ouabain in these hearts. For this response to be avoided in future experiments, concentrations of (±)-blebbistatin higher than 5µM should be used. However, caution should be taken as this would increase the probability of off-target effects including, for example, altered Ca^{2+} handling (Dou et al., 2007, Farman et al., 2008, Brack et al., 2013).

Despite attempts to elucidate the mechanism underlying BDM and blebbistatins' attenuation of ouabain action in Chapter 4, this was unsuccessful and thus further studies are needed.

7.2.3 NMR

A Triple Quantum Filtered ^{23}Na NMR method was adapted for use in the rat heart that allowed measurements of fold-changes in $[Na]_i$ as well as to ascertain estimates of absolute $[Na]_i$. This method removes the need to use toxic shift reagents to distinguish intra and extra cellular Na^+ in the isolated rat heart, allowing all measurements to be performed under more physiological conditions. A key limitation of the ^{23}Na NMR measurements performed is that the reliability of the derived $[Na]_i$ values rely on the

accuracy of the measurements performed in Schepkin et al (1997) in which the reported baseline $[Na]_i$ was 17.5 mM. Furthermore, the reported slope on the TQF vs $[Na]_i$ curve (0.35) and normalisation factor for 50% extracellular Na^+ contribution to the TQF signal were assumed to be correct. However, fold differences in $[Na]_i$ between treatment groups are not affected by these assumptions and are thus more reliable.

The reported 'end-point' values of $[Na]_i$ and ^{31}P energetics measurements were performed ~2-3 minutes prior to snap-freezing. This is because the heart had to be removed from the NMR apparatus to permit snap-freezing. However, the heart continued to be perfused with the end-point perfusion buffer throughout the entirety of this process and thus error was kept to a minimum.

In order to permit fair comparisons between cardiac energetics and $[Na]_i$ measurements as well as peak integration of the P_i signal by ^{31}P NMR, all KH used was phosphate-free. The presence or absence of P_i may also influence the apparent $[Na]_i$-metabolism relationship.

7.2.4 LC-MS/MS

The LC-MS/MS method adapted in this thesis gave an insight into the relationship between $[Na]_i$ and the TCA cycle. An internal standard was not included in this method and thus the recovery of analytes was not assessed. Loss of analyte is inevitable for any extraction procedure due to, for example, incomplete homogenisation, sample concentration steps and degradation. Analyte concentrations were therefore likely

underestimated, although fold differences can be trusted given that the samples were prepared in an identical fashion and all analyses were blinded and randomised.

Other than the addition of chelex and universal indicator, the dual phase metabolite extraction procedure was identical for both NMR and LC-MS/MS. This increased throughput but an additional solid-phase extraction step (for instance, using an ion-exchange column) preceding LC-MS/MS analysis would have removed extraneous matter that may have blunted detectability of the TCA cycle intermediates and pyruvate. A good example of extraneous matter is the high concentration of salt that may have been responsible for the ion suppression associated with α-ketoglutarate.

7.2.5 Whole-cell voltage clamp

In Chapter 4, it was shown that blebbistatin appears to attenuate the ability of ouabain to elevate $[Na]_i$. To assess whether NKA was directly involved in this phenomenon, voltage clamp experiments using cardiomyocytes were kindly performed by Dr Sergiy Tokar. However, work by Zak (1974) and Nag (1980) that was subsequently verified by Banerjee et al. (2007) revealed that cardiomyocytes form only ~30% of the total cell count in the adult rat heart with fibroblasts accounting for 64% and the remainder consisting of other cells including smooth muscle cells (although more recently Pinto et al. (2016) showed that endothelial cells constitute >60 % of the total cell number in the mouse heart). Therefore, the observed attenuation of ouabain by blebbistatin in the isolated perfused rat heart may reflect a phenomenon that is specific to the non-myocyte compartments in the heart although cardiomyocytes were used in the patch clamp

experiments. It is also important to consider that cells will behave differently in several ways when in isolation compared with the more physiological context of the intact heart, for example, the absence of paracrine signalling in the former as well as differences in metabolism. Nonetheless, cardiomyocytes constitute ~70-85 % of the total cell volume in the heart (Anversa et al., 1980, Dammrich and Pfeifer, 1983, Mattfeldt et al., 1986, Tang et al., 2009) so it seems likely that it is the response of these cells that are the main driving force for the blebbistatin attenuation of ouabain in the whole heart. With the data currently available, it appears that the mechanism underlying this attenuation does not involve NKA.

7.2.6 Statistics and interpetation

There is no gold-standard approach for statistical assessment of metabolomics datasets and is dependent upon the question and type of metabolomics being performed. The Bonferonni multiplicity correction is too conservative for targeted metabolomics and is susceptible to false negatives (Perneger, 1998, Rothman, 1990). In order for a metabolite to be deemed statistically significant following multiplicity correction, that metabolite would have to be profoundly different between the treatment groups with low biological and instrumental error as well as powered with large *n* numbers. Fulfilling these criteria is often very difficult to achieve due to the experimental challenges associated with Langendorff perfusions, metabolite extractions, NMR and LC-MS/MS. Therefore, raw p-values from unpaired t-tests for each metabolite were used as a guide as to whether that metabolite may be affected by $[Na]_i$ elevation. The likelihood of false positives was minimised by the experimental design of the TPI/TNI

metabolomics studies (Chapters 6 and 7). That is, the probability of a metabolite reaching statistical significance ($P<0.05$ versus vehicle counterpart) in both the TPI and TNI groups is very low as these groups were perfused in separate studies and compared with their own vehicle counterpart group. The likelihood of that metabolite reaching statistical significance and exhibiting the same fold-change across both studies (as was the case for malate; Table 5.2) is smaller still. Thus, the finding that malate is elevated in both TPI and TNI by 50%, gives confidence that this was not a false positive. However, it is more difficult to discount false negatives in the metabolomics datasets. For metabolites that, for example, reside at high concentration but change by only a small extent or where changes occur within the error of the technique false negatives may occur. This may have been the case for oxaloacetate which gave rise to small peaks by LC-MS/MS and did not appear to be altered by $[Na]_i$ elevation despite increased incorporation of ^{13}C into the TCA cycle under these conditions. Furthermore, there were metabolites that were not measured due to technical challenges such as NAD and NAD(H) as separate entities (the NAD(H) pool was measured by ^{1}H NMR).

7.2.7 ^{13}C enrichment experiments

The ^{13}C enrichment data acquired by mass spectrometry in Chapter 6 do not permit the elucidation of real-time enzyme kinetics of the TCA cycle during $[Na]_i$. Although the methodology does not exist at present, this would be best achieved in the future by quantifying all TCA cycle intermediates in the Langendorff preparation in real-time. Future measurements using real-time hyperpolarised ^{13}C NMR in conjunction with this preparation may give a time-course of changes in TCA cycle activity during $[Na]_i$

elevation. However, this technique involves perfusion with a supra-physiological concentration of pyruvate which has been shown to affect the NAD^+:NADH ratio (Mariotti et al., 2016) and may therefore confound interpretation of the metabolic data generated. Alternatively, TCA cycle kinetics during $[Na]_i$ elevation could be investigated *in vitro* using the spectrophotometric method of Goncalves et al (2010) in which the activities of all TCA cycle enzymes can be rapidly determined for multiple samples of heart homogenate.

7.2.8 Discussion

The experiments reported here suggest deranged ATP supply and increased TCA cycle activity in ouabain/blebbistatin treated hearts with elevated $[Na]_i$ in the absence of elevated inotropy. The specific mechanisms and chronology of these metabolic alterations is unclear. It is postulated that energetics are altered initially and TCA cycle activity increases as a compensatory mechanism for the reduced ATP supply. Direct interaction between ATP synthase and Ca^{2+} has been reported (Hubbard and McHugh, 1996) as has indirect interaction via calcium binding ATPase inhibitor (CaBI) (Yamada and Huzel, 1989), protein kinase Cδ (Nguyen et al., 2010) and S100A1 (Boerries et al., 2007) which are all postulated to have stimulatory effects on ATP synthase. It is possible that the heart uses the same entity (Ca^{2+}) to directly stimulate both the primary sites of ATP utilisation (the myofilament) and ATP production (ATP synthase). This hypothesis is supported by Harris et al (1991). $[Na]_i$ elevation may reduce Ca^{2+} stimulation of ATP synthase leading to reduced ATP and increased ADP and Pi. Interestingly, there was a trend towards increased P_i with $[Na]_i$ elevation in both TPI

and TNI groups. ADP was not measured but is a classic activator of the TCA cycle via allosteric binding to IDH (Vaughan and Newsholm, 1969, Nichols et al., 1994) and αKDH (Nichols et al., 1994, Ostrovtsova and Strumilo, 1990) and would thereby increase TCA cycle activity to compensate for decreased ATP supply. This aligns with the work of Marin-Garcia et al (2001) and O'Brien et al (1990) which showed increased TCA cycle activity as a consequence of impairment of ATP generating enzymes following pacing-induced HF.

The apparent discrepancy between previous work suggesting decreased TCA cycle in HF and the findings reported in this thesis is likely due to the different models used. Most of the previous HF studies involved pressure-overload giving rise to a plethora of pathophysiological events including $[Na]_i$ elevation. Whereas, the ouabain-perfused heart used in this thesis is clearly not a model of HF but of $[Na]_i$ elevation (only one aspect of HF). Other pathophysiological events during HF may outweigh the increase in TCA cycle activity due to elevated $[Na]_i$. It is also important to consider the timescale of these pathophysiological events. The duration of $[Na]_i$ overload in this thesis was approximately 30 minutes thus representing an acute situation whereas those in models of HF are likely to be chronic and therefore notably longer. Shorter periods of $[Na]_i$ elevation may lead to a transient increase of TCA cycle activity (as a compensatory mechanism for reduced ATP) but this activity may gradually wane with HF progression and lead to metabolic remodelling as a result of the more chronic $[Na]_i$ overload associated with heart failure. The TCA cycle is important for the catabolism of precursors used to generate proteins and lipids (Owen et al., 2002) and is speculated to be a causal factor of cardiac hypertrophy and HF (Doenst et al., 2013). Although

chronic alterations to metabolism as a result of $[Na]_i$ elevation were not investigated in this thesis, the data may give an insight into the early events that may be reversed therapeutically and precede irreversible longer term consequences such as transcriptional, post-translational and structural remodelling. Pharmacological reduction of myocardial $[Na]_i$ may be a novel therapeutic approach for heart failure and hence the development of novel activators of NKA is a promising avenue currently under investigation. From a diagnostic standpoint, there is currently no "gold standard" for the clinical diagnosis of HF. Plasma BNP concentration, ultrasound imaging and assessment of symptoms are the main ways in which the presence of the condition is currently confirmed in patients (Authors/Task Force et al., 2012). These alterations are observed relatively late in the aetiology of HF once irreversible structural remodelling has occurred. $[Na]_i$ might be an earlier biomarker of HF that could potentially allow therapies to be assessed earlier to mitigate the severity or progression of the disease.

The ^{23}Na NMR methods presented have the potential to be translated clinically. A recent study by Qian et al. (2015) measured total and bound Na^+ in patients with brain tumours using a 3T MRI scanner. The development of cardiac ^{23}Na MRI is an area of active research. It would be challenging to implement ^{23}Na MR routinely as a predictor of HF in a clinical setting and it is unclear whether $[Na]_i$ elevation is a cause or consequence (or both) of HF. However this could be a potential way to screen patients deemed to have increased risk of developing HF, for example, individuals with diabetes (Lambert et al., 2015) or indeed as part of clinical trials for novel therapeutics.

The relationship between $[Na]_i$ and metabolism may also be relevant in other tissues. Using TQF ^{23}Na NMR Hansen et al. (1993) showed that $[Na]_i$ is higher in cancer cells

compared with wildtype counterparts. The role of Na^+ in cancer is not well understood, however rewiring of metabolism is a classic hallmark in cancer progression (reviewed in Kee et al., 2014). Furthermore, diabetes is also associated with $[Na]_i$ elevation (Lambert et al., 2015, Scheuermann-Freestone et al., 2003). $[Na]_i$ has been found to be elevated in brain cortex biopsies from Alzheimer's Disease (AD) patients due to depressed NKA activity compared with normal individuals (Vitvitsky et al., 2012), as well as other neurodegenerative disorders, which are highly correlated with metabolic dysfunction (reviewed in Cai et al., 2012).

7.3 Final conclusion

This thesis has investigated the metabolic consequences of acute $[Na]_i$ elevation in the isolated perfused rat heart. Ouabain was used to inhibit NKA in this model in order to induce $[Na]_i$ overload and measurements of lactate efflux and myocardial metabolomics using ^1H NMR inferred several metabolic alterations with ouabain. These changes were potentiated by increased contractile demand (using high-rate electrical pacing), including altered TCA cycle intermediates. Cessation of contraction using the electromechanical uncoupler, blebbistatin (5 µM), negated these metabolite changes due to ouabain (50 µM). The dose-response relationship between ouabain and $[Na]_i$ was found to be sigmoidal between 0 and 100 µM using TQF ^{23}Na NMR. This relationship was found to be blunted by 5 µM blebbistatin which appeared to attenuate the ability of ouabain to elevate $[Na]_i$ by approximately 50%. *In vitro* and *ex vivo* investigations were carried out in order to elucidate the mechanism underlying this phenomenon. Blebbistatin did not alter NKA activity nor sequester Na^+ or alter the detectability of

Na^+ by NMR. The mechanism did not appear to be blebbistatin-specific as another electromechanical uncoupler, BDM, attenuated ouabain to the same extent.

Titrating hearts with a combination of ouabain and blebbistatin during perfusion induced a significant and sustained $[Na]_i$ elevation (~2-fold baseline) with either a transient positive inotropy or a transient negative inotropy in contracting hearts that had identical end-point contractile demand. Transient changes in contraction resulted in several metabolic alterations including acetylcarnitine shuttling, anaplerosis and the TCA cycle. In both protocols, ATP levels (measured in real-time by ^{31}P NMR) were reduced in the absence of a change in PCr and showed a strong inverse correlation with $[Na]_i$. Malate (and more tentatively fumarate) were both elevated in both protocols suggesting an inotropy independent contribution of elevated $[Na]_i$. This supports the hypothesis that $[Na]_i$ elevation alters cardiac energetics and intermediary metabolism in the isolated perfused heart. ^{13}C isotopomer analysis demonstrated that TCA cycle activity was increased by acute $[Na]_i$ elevation and may reflect ATP supply-demand mismatch following a derangement of ATP synthesis in the absence of elevated demand.

These findings add weight to the hypothesis that $[Na]_i$ elevation alters energetics and intermediary metabolism in the heart. However, this does not appear to be caused by reduced-Ca^{2+} stimulation of the TCA cycle. Therefore, more comprehensive mechanistic investigations are required to elucidate the events that occur due to $[Na]_i$ elevation leading to loss of ATP in this model. It is also important to assess this using agents that elevate $[Na]_i$ other than ouabain to strengthen the claim that these metabolic effects are truly a result of $[Na]_i$ derangement.

7.4 Future work

Taken together with the conclusions and drawbacks discussed in Sections 7.1 and 7.2, this thesis work provides a platform for a number of potential future studies related to the thesis hypothesis. In particular the following questions should be answered in future work:

Given the relationship between elevated $[Na]_i$ and decreased ATP in the absence of a change in PCr or altered contractility:

- Does high $[Na]_i$ (or high $[Na]_m$) directly inhibit ATP synthase or CK activity in the perfused heart?
- Does high $[Na]_i$ indirectly inhibit ATP synthase or CK activity via reduced stimulation by Ca_m?
- Is the $[Na]_i$ induced reduction in ATP exacerbated by increased ATP demand?
- Can the $[Na]_i$ induced reduction in ATP be reversed by inhibiting NCLX and normalise ATP levels during Na^+ overload?
- Is the metabolic phenotype of reduced ATP and elevated TCA cycle activity recapitulated in a chronic model of Na^+ overload such as hypertrophy?

8 APPENDICES

8.1 Unpaced metabolomics (Chapter 3)

Metabolite	Mean (nmol/g wet wt)		SEM		Fold Change	Propagated SEM	P-value
	Unpaced Control	Unpaced Ouabain	Unpaced Control	Unpaced Ouabain			
Acetate	67.299	71.818	3.715	5.321	1.067	0.099	0.502
Acetylcarnitine	27.972	48.699	2.713	3.552	1.741	0.211	0.001
Acetylcarnitine:Carnitine	0.053	0.100	0.005	0.006	1.888	0.205	0.000
Alanine	156.147	236.322	14.028	35.486	1.513	0.265	0.084
Aspartate	1055.974	1178.542	114.339	46.597	1.116	0.129	0.350
ATP+ADP	957.359	1078.232	34.481	48.328	1.126	0.065	0.076
Carnitine	488.063	461.165	21.933	23.021	0.945	0.063	0.422
Choline	68.261	73.100	7.422	1.448	1.071	0.118	0.619
Cr	3211.962	3129.229	139.379	166.491	0.974	0.067	0.719
Formate	43.576	41.067	4.088	2.110	0.942	0.101	0.597
Fumarate	7.423	12.190	0.421	1.472	1.642	0.219	0.034
Glutamate	1040.453	1066.148	136.246	57.275	1.025	0.145	0.875
Glutamate:Glutamine	1.504	1.343	0.091	0.086	0.893	0.079	0.234
Glutamine	690.105	762.984	113.740	35.565	1.106	0.189	0.554
Glycine	178.940	183.541	13.681	8.345	1.026	0.091	0.780
Isoleucine	24.087	22.640	1.653	1.083	0.940	0.079	0.503
Lactate	324.435	304.381	37.486	29.541	0.938	0.142	0.694
NAD(H)	195.715	197.804	23.624	12.623	1.011	0.138	0.939
PCr	1420.445	1442.956	224.808	107.293	1.016	0.178	0.930
PCR:Cr	0.518	0.464	0.068	0.034	0.896	0.134	0.471
PCr+Cr	4322.756	4131.137	266.160	113.806	0.956	0.064	0.554
Phosphocholine	173.904	179.613	10.214	7.887	1.033	0.076	0.668
Succinate	17.121	15.239	2.333	0.596	0.890	0.126	0.542
Taurine	9544.995	10102.658	584.725	211.551	1.058	0.069	0.391
Valine	9.473	10.085	1.303	0.665	1.065	0.162	0.704

8.2 Paced metabolomics (Chapter 3)

Metabolite	Mean (nmol/g wet wt)		SEM		Fold Change	Propagated SEM	P-value
	Paced Control	Paced Ouabain	Paced Control	Paced Ouabain			
Acetate	72.727	84.763	6.552	6.277	1.165	0.136	0.214
Acetylcarnitine	40.265	93.377	4.170	7.222	2.319	0.300	0.000
Acetylcarnitine:Carnitine	0.079	0.174	0.008	0.017	2.188	0.313	0.001
Alanine	317.187	340.672	59.248	18.764	1.074	0.209	0.764
Aspartate	1197.381	1170.776	50.334	77.025	0.978	0.076	0.805
ATP+ADP	1427.854	1415.684	160.420	65.196	0.991	0.120	0.949
Carnitine	469.622	493.543	64.494	34.062	1.051	0.162	0.750
Choline	93.903	138.987	10.847	10.399	1.480	0.204	0.013
Cr	2829.814	4246.493	335.490	136.499	1.501	0.184	0.003
Formate	44.066	32.443	7.934	1.014	0.736	0.135	0.177
Fumarate	3.206	9.974	1.268	1.749	3.111	1.346	0.015
Glutamate	1159.809	1277.681	118.576	76.838	1.102	0.131	0.428
Glutamate:Glutamine	2.140	2.921	0.157	0.460	1.365	0.237	0.147
Glutamine	547.577	398.057	88.085	50.369	0.727	0.149	0.198
Glycine	532.830	570.508	14.221	12.982	1.071	0.038	0.092
Isoleucine	28.804	29.889	3.062	2.367	1.038	0.138	0.785
Lactate	384.346	772.706	50.725	132.602	2.010	0.435	0.032
NAD(H)	364.445	362.017	12.538	3.780	0.993	0.036	0.873
PCr	1569.945	1679.209	269.966	120.537	1.070	0.199	0.703
PCR:Cr	0.660	0.399	0.102	0.036	0.605	0.108	0.036
PCr+Cr	4713.178	5993.180	536.436	83.835	1.272	0.146	0.061
Phosphocholine	222.208	238.752	8.342	4.240	1.074	0.045	0.095
Succinate	45.899	87.079	4.440	8.170	1.897	0.256	0.002
Taurine	10567.147	12243.694	1283.131	353.079	1.159	0.145	0.236
Valine	8.627	10.538	1.160	2.139	1.221	0.297	0.479

8.3 A ‘positive inotropy’ method using the Frank-Starling mechanism (Chapter 4)

This study was performed in order to assess the feasibility of inducing a positive inotropy in a control group of Langendorff rat hearts. This control group would have lower $[Na]_i$ but identical inotropy to its ouabain counterpart group thus permitting metabolomic comparison.

Positive inotropy can be induced mechanically via an increase in the Frank-Starling (FS) stretch mechanism (Saks et al., 2006) using intraventricular balloon inflation. This mechanism is underpinned not by calcium (Rhodes et al., 2015) but by titin (connectin) geometry and thin filament “on-off” regulation (Kobirumaki-Shimozawa et al., 2014). Experiments were performed to investigate whether the elevated inotropy in response to ouabain can be mimicked in the control group by over inflation of the intraventricular balloon.

8.3.1 Experimental methods

Rat hearts (n=6/group for all studies) were perfused in the Langendorff mode as described in Sections 2.1 and 2.2.2. Ouabain octahydrate was obtained from Sigma (UK).

Hearts were stabilised for 30 minutes with standard KH (Section 2.1.3) and then for a further 20 minutes with either ouabain or balloon over-inflation. In the FS group, increased inotropy was achieved by gradually increasing the volume of the intraventricular balloon until the maximal LVDP elevation was achieved without

exceeding 150 µL intraventricular balloon volume, to avoid the risk of inducing ischaemia due to balloon over-inflation (Abe et al., 1988). Hearts were perfused with 20 µM ouabain between 30 and 50 minutes to achieve the same LVDP profiles for the ouabain group as the FS group. ^{23}Na NMR measurements were performed with interleaved TQF and DQF measurements to elucidate the $[Na]_i$ profile associated with 20µM ouabain treatment. However it became apparent that it was not feasible to increase intraventricular balloon volume during ^{23}Na NMR data acquisition using the current NMR perfusion setup.

8.3.2 Results

LVDP, heart rate and coronary flow were constant, within predefined acceptance criteria (detailed in Section 2.1.6) and were not different between the control and 20 µM ouabain group during the stabilisation period. Baseline LVDP (Figure 8.1A) was 114±6 mmHg (average) in the control group. The maximum increase in LVDP that could be achieved using intraventricular balloon inflation in the FS group during the treatment period was 139±5 mmHg (at 40 minutes). This increase in LVDP was matched by using 20 µM ouabain in the ouabain group (144±8 mmHg at 40 minutes). Deflating the balloon slightly in the FS group after 40 minutes led to these two groups exhibiting almost identical inotropic profiles during the treatment period. FS and ouabain LVDP values were 131±3 mmHg and 137±11 mmHg at the end of perfusion respectively. Mean values of heart rate (Figure 8.1B) and coronary flow (Figure 8.1C) of the control group during stabilisation were 290±12 BPM and 12±1 mmHg respectively. There were

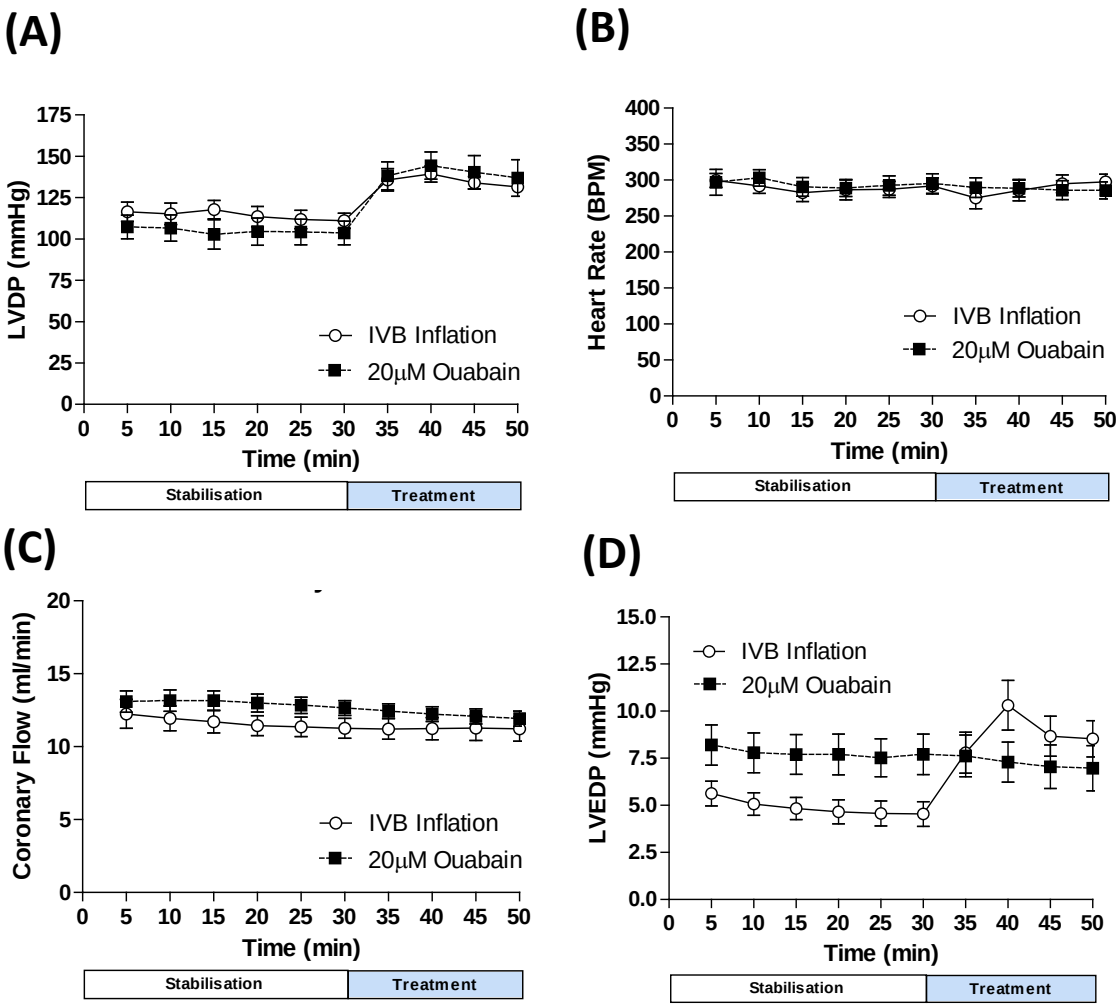

Figure 8.1 Perfusion measurements ('increased inotropy' study).

Symbols and error bars represent mean±SEM of five minute time windows (n=6/group). IVB (intraventricular balloon) inflation = Frank-Starling (FS) group.

no significant deviations from these values in either perfusion group at any point during the perfusion protocol.

LVEDP (Figure 8.1D) was constant in both groups during the stabilisation period and was set to an average of 7.8±1.1 mmHg in the ouabain group but 5.1±0.6 mmHg in the FS group. These values were significantly different ($P<0.05$). This was necessary in order to prevent LVEDP from markedly exceeding 10 mmHg (used as stabilisation exclusion criteria; Section 2.1.6) following balloon inflation in the FS group. There were no significant differences ($P>0.05$) in LVEDP between the two groups at any point during the treatment period and were highly similar at the end of perfusion (FS = 8.5±1.0 mmHg and ouabain = 7.0±1.2 mmHg).

TQF ^{23}Na NMR was used to assess whether 20 µM ouabain induces a significant and sustained $[Na]_i$ elevation. Due to technical issues, it was not possible to include an FS group in the NMR study. Figure 8.2A shows that derived $[Na]_i$ was stable throughout the stabilisation period and averaged 17.6±0.5 mM. There was a small, significant elevation in derived $[Na]_i$ at 35 min (following 5 minutes of perfusion with 20 µM ouabain) to 20.4±0.9 mM ($P<0.05$ vs baseline) but this elevation gradually decreased and was not significant at the end of perfusion (18.2±0.9 mM, $P>0.05$ vs baseline). Mean DQF (Figure 8.2B) was 1.0±0.2 during stabilisation and did not change upon perfusion with 20 µM ouabain although was associated with a higher level of noise than the TQF measurements. Since the $[Na]_i$ elevation arising from 20 µM ouabain was very modest and not sustained at the end of the experiment, metabolomic analysis was not performed in this study.

8.3.3 Discussion - Is it practical to use an 'increased inotropy' approach to eliminate inotropic differences between control and ouabain hearts?

This study explored the potential of using the Frank-Starling (FS) mechanism using intraventricular balloon inflation to mimic the inotropic profile of isolated rat hearts perfused with 20 µM ouabain. Modulation of LVEDP in the normal FS group via

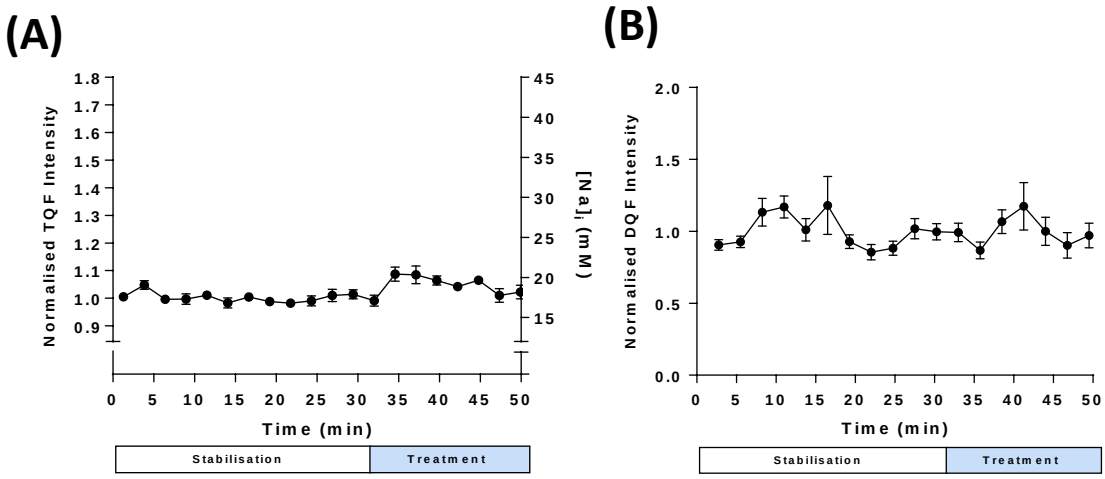

Figure 8.2 ^{23}Na NMR during 20 µM ouabain perfusion.

(A) Normalised triple quantum filtered (TQF) ^{23}Na NMR intensity (left axis) with derived intracellular [Na]i (right axis). **(B)** Normalised double quantum filtered (DQF) ^{23}Na NMR intensity. Symbols and error bars represent mean±SEM of five minute time windows (n=6/group).

intraventricular balloon inflation was a highly effective way to increase or decrease LVDP so that the LVDP profile was nearly identical to the ouabain group. However, the maximal LVDP that could be achieved via mechanical stretching was relatively low (~140 mmHg). This protocol was carried out without exceeding 150 µL intraventricular balloon volume (≤10 mmHg LVEDP) that has been reported to cause ischaemia in the

isolated rat heart (Abe et al., 1988). The low LVDP achieved in the FS group meant that the concentration of ouabain required to induce an equivalent positive inotropic effect was relatively low (20 µM). The TQF ^{23}Na NMR of hearts perfused with 20 µM ouabain showed a fairly modest elevation in derived $[Na]_i$ compared to the results in Chapter 3. Furthermore, it became apparent during the NMR study that it was not practically possible to modulate intraventricular balloon volume during NMR data acquisition. This is because the NMR perfusion rig is setup with the ventricular pressure transducer housed within the NMR probe close to the centre of the spectrometer during acquisition (Figure 2.2). Given that normalised TQF and DQF values are sensitive to the positioning of the heart within the RF coil, removal of the NMR probe to gain access to the pressure transducer during data acquisition introduces systematic error to the NMR measurements. Thus, ^{23}Na NMR measurements could not be carried out for the FS group and it remains unclear whether $[Na]_i$ was altered by increased mechanical stretch. In conclusion, practical considerations precluded the use of the 'increased inotropy' approach using enhanced FS mechanism to overcome the issue of inotropy interference by ouabain during metabolic studies. An alternative approach to induce positive inotropy is the use of a myofilament sensitizer such as levosimendan. However, it is unknown whether this drug alters $[Ca]_i$ (Todaka et al., 1996, du Toit et al., 2001, Wilson et al., 2014, Yang et al., 2016) which may give rise to metabolic alterations that would exacerbate the issue of identifying $[Na]_i$-dependent metabolic pathways in the heart. This is also the case for better understood positive inotropes such as isoprenaline, adrenaline and noradrenaline. Another alternative to increasing intraventricular balloon inflation is increasing coronary perfusion pressure (Vassallo et al., 1998). However, the key caveat would be the necessity to use coronary flows that are significantly above

those used at baseline (~10 mL/min) which may give rise to differences in perfusate temperature and pH at the aortic cannula as well as in the delivery of oxygen and fuel to the heart.

8.4 Non-contracting (blebbistatin) metabolomics (Chapter 4)

Metabolite	Mean (nmol/g wet wt)		SEM		Fold Change	Propagated SEM	P-value
	Bleb	Bleb+Oua	Bleb	Bleb+Oua			
Acetate	64.097	67.621	0.647	0.158	1.055	0.011	0.002
Acetylcarnitine	17.417	18.237	0.840	1.083	1.047	0.080	0.577
Acetylcarnitine:Carnitine	0.042	0.044	0.001	0.003	1.056	0.072	0.447
Alanine	255.972	236.152	7.948	24.772	0.923	0.101	0.502
Aspartate	799.704	875.715	59.147	41.418	1.095	0.096	0.317
ATP+ADP	1114.434	1095.347	30.736	30.585	0.983	0.039	0.673
Carnitine	445.759	412.370	29.609	18.997	0.925	0.075	0.365
Choline	50.183	56.026	1.775	5.586	1.116	0.118	0.384
Cr	2313.489	2124.984	138.548	69.291	0.919	0.063	0.252
Formate	47.882	44.792	1.170	2.309	0.935	0.053	0.260
Fumarate	5.404	3.482	0.334	0.465	0.644	0.095	0.010
Glutamate	1935.690	1515.014	83.663	74.690	0.783	0.051	0.004
Glutamate:Glutamine	2.051	2.045	0.103	0.126	0.997	0.079	0.973
Glutamine	948.464	819.354	33.579	47.149	0.864	0.058	0.048
Glycine	196.843	184.163	5.682	4.168	0.936	0.034	0.117
Isoleucine	28.973	24.967	1.720	0.912	0.862	0.060	0.067
Lactate	307.891	250.192	10.306	22.873	0.813	0.079	0.061
NAD(H)	190.106	169.848	25.103	9.602	0.893	0.128	0.468
PCr	2008.781	1994.623	130.965	45.994	0.993	0.069	0.927
PCR+Cr	4164.256	3845.399	147.892	109.444	0.923	0.042	0.114
PCr:Cr	0.812	0.956	0.066	0.041	1.177	0.108	0.103
Phosphocholine	166.932	153.116	6.880	5.462	0.917	0.050	0.147
Succinate	12.346	11.235	0.626	1.214	0.910	0.109	0.465
Taurine	9812.690	9711.723	515.550	325.285	0.990	0.062	0.878
Valine	13.023	11.777	0.693	0.459	0.904	0.060	0.165

8.5 Mass Spectra of blebbistatin and ouabain solutions (Chapter 4).

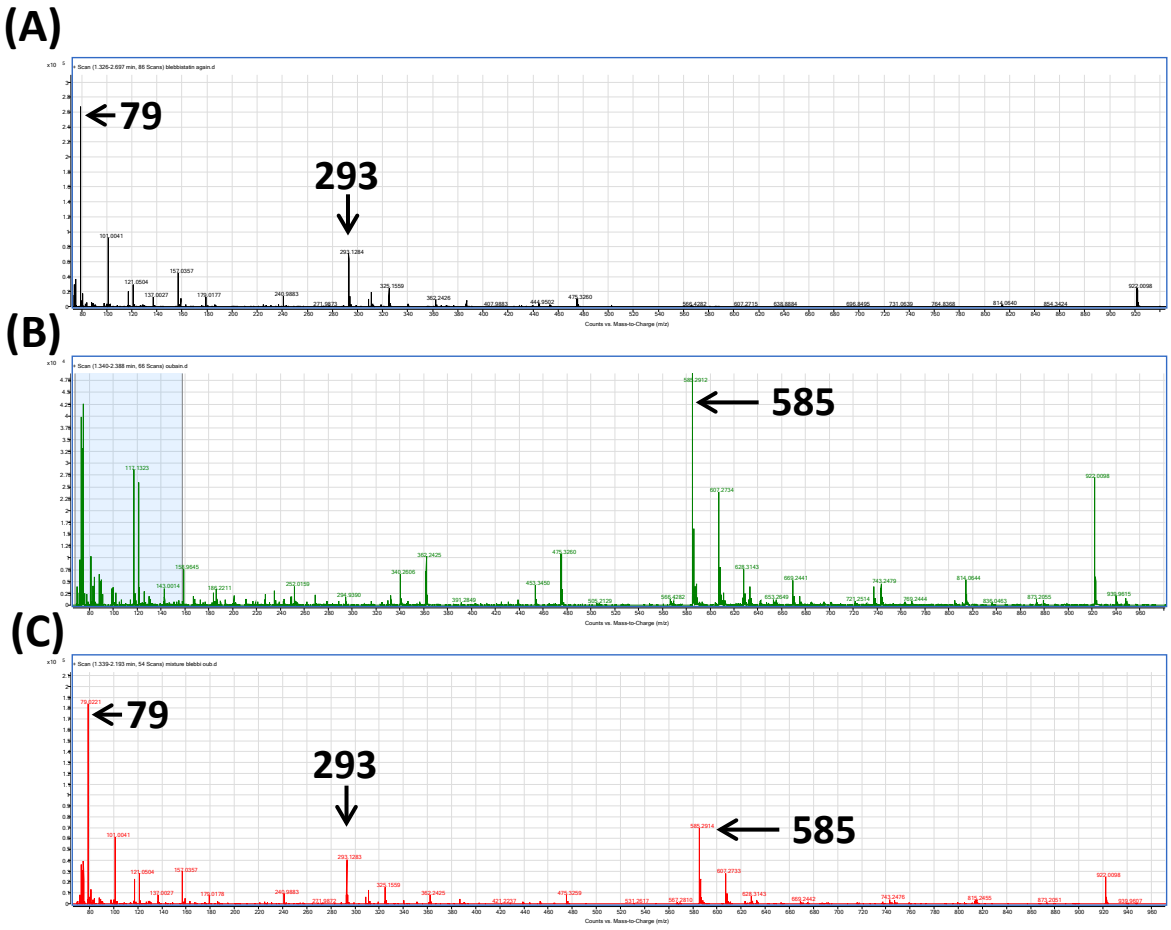

Figure 8.4 Mass spectra of blebbistatin (DMSO) and ouabain solutions.

(A) 5 µM blebbistatin (0.029 % v/v dimethylsulfoxide, DMSO) in water. **(B)** 50 µM ouabain in water. **(C)** 5µM blebbistatin (0.029 % v/v DMSO) + 50µM ouabain in water. The molecular ion signals for blebbistatin (293 m/z), dimethylsulphoxide (79 m/z) and ouabain (585 m/z) are indicated. Many of the low-level unlabelled peaks were probably due to a small extent of carryover from previous analyses or trace impurities in the solutions. Data acquisition was kindly performed by Cinzia Imberti (Imaging Chemistry & Biology, KCL on 09-Jan-2015).

8.6 Transient Negative Inotropy (TNI) method development (Chapter 4)

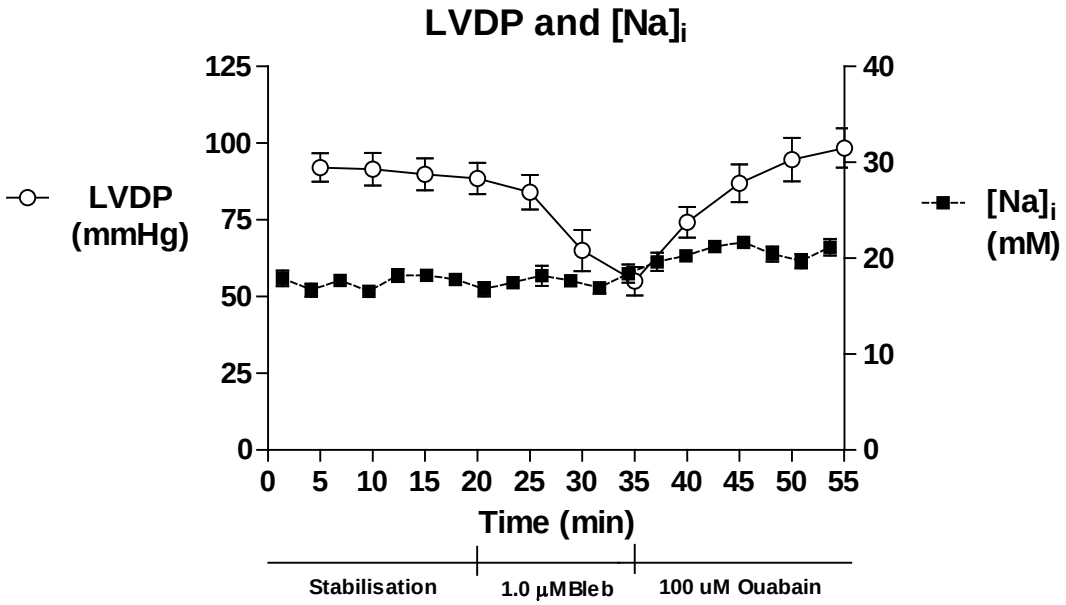

Figure 8.5 LVDP and $[Na]_i$ (preliminary TNI protocol development).

Left ventricular developed pressure (LVDP) (left axis). $[Na]_i$ derived from TQF signal (right axis). Abbreviations: Bleb (blebbistatin).

8.7 Transient Positive Inotropy (TPI) ^{1}H NMR metabolomics (Chapter 5)

Metabolite	Mean (nmol/g wet wt)		SEM		Fold Change	Propagated SEM	P-value
	Vehicle	TPI	Vehicle	TPI			
Acetate	187.692	173.074	4.173	14.138	0.922	0.078	0.387
Acetylcarnitine	57.330	93.115	5.742	11.423	1.624	0.257	0.019
Acetylcarnitine:Carnitine	0.085	0.157	0.008	0.011	1.840	0.216	0.001
Alanine	184.292	346.465	11.641	51.512	1.880	0.304	0.012
Aspartate	1579.658	1085.088	229.502	164.709	0.687	0.144	0.111
ATP:ADP	2166.666	1740.753	143.017	179.089	0.803	0.098	0.093
Carnitine	727.645	588.979	24.802	47.980	0.809	0.071	0.039
Choline	172.336	151.675	4.305	13.677	0.880	0.082	0.218
Cr	5004.638	4566.807	253.241	350.745	0.913	0.084	0.335
Formate	56.937	46.619	4.349	5.374	0.819	0.113	0.166
Glucose	3995.005	4756.707	116.177	349.346	1.191	0.094	0.065
Glutamate	1555.795	2175.553	44.649	247.960	1.398	0.164	0.082
Glutamate:Glutamine	0.939	1.553	0.316	0.175	1.654	0.586	0.102
Glutamine	1260.025	1453.667	28.830	164.807	1.154	0.133	0.378
Glycine	241.444	244.072	11.843	15.155	1.011	0.080	0.894
Isoleucine	15.024	18.150	1.968	2.567	1.208	0.233	0.357
Lactate (NMR)	258.184	474.852	8.378	102.006	1.839	0.400	0.088
NAD(H)	360.307	350.481	16.998	25.487	0.973	0.084	0.755
PCr (1-H NMR)	1439.099	1611.598	209.440	216.570	1.120	0.222	0.580
PCr+Cr	6134.592	5877.095	285.288	396.999	0.958	0.079	0.610
PCR:Cr	0.293	0.367	0.048	0.058	1.254	0.287	0.349
Phosphocholine	254.978	238.725	6.298	13.434	0.936	0.058	0.333
Succinate (NMR)	26.445	36.645	2.607	5.632	1.386	0.253	0.131
Taurine	13053.329	12473.683	547.440	649.724	0.956	0.064	0.511

8.8 Transient Positive Inotropy (TPI) LC-MS/MS TCA cycle metabolomics (Chapter 5)

Metabolite	Mean (nmol/g wet wt)		SEM		Fold Change	Propagated SEM	P-value
	Vehicle	TPI	Vehicle	TPI			
Alpha ketoglutarate	0.005	0.004	0.001	0.001	0.871	0.152	0.434
Citrate	1.265	4.354	0.496	1.228	3.442	1.664	0.065
Fumarate	1.313	3.285	0.310	0.890	2.501	0.898	0.076
Isocitrate	0.529	0.925	0.051	0.076	1.749	0.222	0.001
Lactate	69.433	75.747	12.544	8.650	1.091	0.233	0.679
Malate	8.375	12.607	1.011	1.617	1.505	0.265	0.038
Pyruvate	0.064	0.065	0.012	0.013	1.012	0.268	0.966
Succinate	24.344	31.288	5.134	10.185	1.285	0.499	0.550

8.9 Transient Negative Inotropy (TNI) ^{1}H NMR metabolomics (Chapter 5)

Metabolite	Mean (nmol/g wet wt)		SEM		Fold Change	Propagated SEM	P-Value
	Vehicle	TNI	Vehicle	TNI			
Acetate	149.617	136.789	7.806	12.237	0.914	0.095	0.422
Acetylcarnitine	43.040	43.679	1.863	2.019	1.015	0.064	0.827
Acetylcarnitine:Carnitine	0.071	0.093	0.006	0.012	1.307	0.195	0.206
Alanine	205.433	251.664	34.943	30.179	1.225	0.255	0.340
Aspartate	1549.437	1934.542	133.362	388.353	1.249	0.273	0.410
ATP:ADP	1870.044	1303.840	128.734	184.904	0.697	0.110	0.036
Carnitine	597.459	528.847	23.785	51.732	0.885	0.093	0.290
Choline	146.495	119.239	14.363	10.838	0.814	0.109	0.157
Cr	4505.913	3864.794	85.948	198.289	0.858	0.047	0.031
Formate	34.368	33.514	1.957	3.153	0.975	0.107	0.832
Glucose	3081.380	3085.647	45.803	150.871	1.001	0.051	0.984
Glutamate	1217.916	1080.350	55.042	93.210	0.887	0.086	0.260
Glutamate:Glutamine	0.984	0.795	0.071	0.044	0.808	0.073	0.044
Glutamine	1248.925	1389.602	40.395	154.220	1.113	0.129	0.441
Glycine	196.262	202.019	8.822	16.533	1.029	0.096	0.799
Isoleucine	21.220	20.829	1.395	2.499	0.982	0.134	0.900
Lactate (NMR)	291.576	358.694	27.220	65.768	1.230	0.253	0.420
NAD(H)	292.474	280.282	34.057	35.935	0.958	0.166	0.814
PCr (1-H NMR)	888.006	980.132	42.090	124.098	1.104	0.149	0.547
PCr+Cr	5437.041	4637.571	197.665	224.930	0.853	0.052	0.028
PCR:Cr	0.191	0.259	0.011	0.014	1.355	0.104	0.028
Phosphocholine	203.613	191.261	8.458	15.068	0.939	0.084	0.517
Succinate (NMR)	22.111	25.024	1.286	4.406	1.132	0.210	0.575
Taurine	11710.966	9887.421	717.111	723.480	0.844	0.081	0.111

8.10 Transient Negative Inotropy (TNI) LC-MS/MS TCA cycle metabolomics (Chapter 5)

Metabolite	Mean (nmol/g wet wt)		SEM		Fold Change	Propagated SEM	P-value
	Vehicle	TNI	Vehicle	TNI			
Alpha ketoglutarate	0.004	0.002	0.001	0.000	0.535	0.127	0.045
Citrate	1.688	1.915	0.461	0.524	1.135	0.439	0.749
Fumarate	0.886	2.021	0.054	0.314	2.280	0.381	0.013
Isocitrate	0.363	0.279	0.044	0.033	0.768	0.130	0.165
Lactate	65.310	80.923	13.365	19.538	1.239	0.392	0.517
Malate	5.730	8.799	0.531	0.643	1.535	0.181	0.002
Pyruvate	0.392	1.562	0.252	0.449	3.986	2.806	0.062
Succinate	1.573	6.142	0.268	1.503	3.905	1.164	0.037

8.11 ^{13}C isotopologue mass distribution vectors by GC-MS (Chapter 6)

Metabolite	Isotopologue	Vehicle			High [Na]i			P value
		Mean MDV	SEM	N	Mean MDV	SEM	N	
DHAP	m+0	0.063	0.003	3	0.083	0.009	6	0.198
	m+1	0.586	0.139	5	0.550	0.061	6	0.807
	m+2	0.093	0.065	4	0.145	0.040	6	0.493
	m+3	0.085	0.017	4	0.183	0.022	5	0.013
Pyruvate	m+0	0.640	0.007	4	0.575	0.027	6	0.091
	m+1	0.088	0.001	4	0.086	0.006	6	0.798
	m+2	0.076	0.005	5	0.076	0.003	6	0.969
	m+3	0.219	0.021	5	0.021	0.020	5	0.594
Lactate	m+0	0.510	0.043	5	0.453	0.016	5	0.257
	m+1	0.115	0.010	5	0.104	0.003	5	0.345
	m+2	0.076	0.002	5	0.077	0.004	6	0.865
	m+3	0.300	0.054	5	0.345	0.027	6	0.442
Alanine	m+0	0.434	0.027	5	0.314	0.012	6	0.002
	m+1	0.098	0.004	4	0.079	0.006	6	0.047
	m+2	0.062	0.005	5	0.058	0.001	6	0.390
	m+3	0.398	0.039	5	0.534	0.010	5	0.009
Aspartate	m+0	0.169	0.024	5	0.124	0.013	6	0.125
	m+1	0.188	0.005	4	0.158	0.003	4	0.001
	m+2	0.227	0.005	5	0.209	0.007	5	0.071
	m+3	0.202	0.014	5	0.221	0.014	6	0.379
	m+4	0.228	0.010	4	0.262	0.022	5	0.251
Glutamate	m+0	0.200	0.029	4	0.160	0.024	6	0.318
	m+1	0.116	0.004	3	0.090	0.007	6	0.034
	m+2	0.171	0.003	3	0.128	0.008	5	0.006
	m+3	0.173	0.008	5	0.158	0.006	4	0.209
	m+4	0.164	0.014	5	0.185	0.006	4	0.261
	m+5	0.198	0.040	5	0.304	0.015	5	0.039
Oxaloacetate	m+0	0.430	0.060	5	0.358	0.068	6	0.455
	m+1	0.126	0.057	4	0.196	0.007	4	0.268
	m+2	0.197	0.019	5	0.158	0.030	6	0.327
	m+3	0.108	0.026	5	0.148	0.027	6	0.314
	m+4	0.107	0.003	3	0.128	0.030	6	0.643

N values are post-outlier removal. Table continued overleaf.

Metabolite	Isotopologue	Vehicle			High [Na]i			P value
		Mean MDV	SEM	N	Mean MDV	SEM	N	
Citrate	m+0	0.274	0.005	3	0.2112	0.01678	6	0.039
	m+1	0.145	0.014	5	0.1151	0.008729	6	0.101
	m+2	0.139	0.004	4	0.1263	0.002416	5	0.025
	m+3	0.108	0.026	5	0.1476	0.0266	6	0.314
	m+4	0.107	0.003	3	0.1277	0.0295	6	0.643
	m+5	0.123	0.018	5	0.1696	0.008289	6	0.035
	m+6	0.092	0.016	5	0.1521	0.02465	6	0.082
Isocitrate	m+0	0.139	0.017	4	0.1425	0.02434	6	0.910
	m+1	0.107	0.008	4	0.05547	0.002841	4	0.001
	m+2	0.108	0.013	5	0.1081	0.004395	5	0.766
	m+3	0.174	0.005	3	0.1345	0.01757	6	0.176
	m+4	0.126	0.017	4	0.1799	0.01701	6	0.065
	m+5	0.201	0.028	5	0.2251	0.01745	6	0.457
	m+6	0.101	0.031	5	0.1396	0.01964	6	0.309
α-ketoglutarate	m+0	0.124	0.016	4	0.09851	0.005897	4	0.189
	m+1	0.074	0.017	5	0.05355	0.005787	5	0.294
	m+2	0.126	0.017	4	0.1799	0.01701	6	0.065
	m+3	0.152	0.005	3	0.1448	0.006011	4	0.446
	m+4	0.115	0.043	4	0.1493	0.02635	6	0.485
	m+5	0.226	0.034	4	0.2063	0.01291	6	0.551
Succinate	m+0	0.242	0.010	4	0.2629	0.01787	6	0.395
	m+1	0.113	0.006	4	0.1057	0.004632	5	0.334
	m+2	0.261	0.018	5	0.1892	0.01141	5	0.011
	m+3	0.165	0.002	3	0.1626	0.01073	6	0.873
	m+4	0.163	0.028	4	0.2691	0.03132	6	0.046
Fumarate	m+0	0.506	0.017	5	0.4165	0.02299	6	0.015
	m+1	0.163	0.004	4	0.146	0.005385	5	0.049
	m+2	0.098	0.010	5	0.08953	0.01112	6	0.593
	m+3	0.134	0.005	5	0.1591	0.004063	5	0.004
	m+4	0.102	0.002	4	0.1687	0.0214	5	0.029
Malate	m+0	0.175	0.011	5	0.1508	0.00679	5	0.110
	m+1	0.175	0.011	5	0.1508	0.00679	5	0.110
	m+2	0.191	0.007	4	0.1633	0.01511	6	0.202
	m+3	0.169	0.013	5	0.189	0.01831	6	0.402
	m+4	0.158	0.023	5	0.2549	0.02077	5	0.015

N values are post-outlier removal.

8.12 ^{13}C mean enrichment by GC-MS (Chapter 6)

Metabolite	Vehicle			High [Na]i			P value
	Mean enrichment	SEM	N	Mean enrichment	SEM	N	
DHAP	0.414	0.023	4	0.469	0.018	5	0.098
Pyruvate	0.270	0.008	4	0.311	0.020	5	0.133
Lactate	0.384	0.052	5	0.430	0.025	6	0.421
Alanine	0.467	0.038	5	0.603	0.009	5	0.008
Aspartate	0.546	0.546	4	0.583	0.018	5	0.171
Glutamate	0.560	0.038	4	0.596	0.024	5	0.430
Citrate	0.366	0.019	4	0.488	0.026	6	0.009
Isocitrate	0.514	0.028	5	0.563	0.028	6	0.258
α-ketoglutarate	0.523	0.015	3	0.559	0.007	5	0.048
Succinate	0.500	0.018	4	0.500	0.012	5	0.980
Fumarate	0.276	0.012	5	0.366	0.021	5	0.006
Malate	0.440	0.030	5	0.551	0.026	6	0.020

N values are post-outlier removal.

8.13 ^{13}C isotopologue mass distribution vectors by LC-MS/MS (Chapter 6).

Metabolite	Isotopologue	Vehicle			High [Na]i			P value
		Mean (MDV)	SEM	N	Mean	SEM	N	
Fumarate	m+0	0.3534	0.03498	5	0.2409	0.02011	6	<0.0001
	m+1	0.1317	0.01216	5	0.09444	0.01525	6	0.1232
	m+2	0.1917	0.005102	5	0.1768	0.008075	5	0.5509
	m+3	0.162	0.01204	5	0.198	0.005085	4	0.177
	m+4	0.1884	0.006703	4	0.2486	0.0212	5	0.0271
Isocitrate	m+0	0.1308	0.04298	5	0.07586	0.004017	6	0.1316
	m+1	0.04724	0.007015	4	0.02604	0.003524	6	0.5818
	m+2	0.1448	0.01933	4	0.09587	0.01349	6	0.206
	m+3	0.1526	0.01248	4	0.1214	0.01706	6	0.4185
	m+4	0.2918	0.03483	4	0.2202	0.04801	6	0.0668
	m+5	0.2621	0.03992	5	0.3322	0.02597	6	0.0557
	m+6	0.06074	0.01666	4	0.09359	0.01073	5	0.4123
Malate	m+0	0.3723	0.0389	5	0.2616	0.02112	6	0.0148
	m+1	0.1174	0.01008	5	0.168	0.04279	6	0.2516
	m+2	0.1819	0.00717	5	0.1159	0.01663	6	0.1372
	m+3	0.1701	0.009217	4	0.1899	0.01504	6	0.6715
	m+4	0.1981	0.007252	4	0.3068	0.05892	6	0.0239

N values are post-outlier removal.

8.14 ^{13}C mean enrichment by LC-MS/MS (Chapter 6).

Metabolite	Vehicle			High [Na]i			P value
	Mean	SEM	N	Mean	SEM	N	
Fumarate	0.4338	0.003799	3	0.5580	0.3939	6	0.0684
Isocitrate	0.5196	0.03949	4	0.6490	0.02229	6	0.0148
Malate	0.4451	0.01050	4	0.5489	0.03928	6	0.0706

N values are post-outlier removal.

8.15 M+0 raw LC-MS/MS counts (Chapter 6)

Metabolite	Vehicle			High [Na]i			P value
	Mean	SEM	N	Mean	SEM	N	
Pyruvate	6360	1768	5	8488.0000	1763	6	0.4202
Lactate	2.08E+06	444623	5	2462000.0000	502795	6	0.5913
Citrate	2.47E+06	397450	4	3.39E+06	527028	6	0.2454
Succinate	3.74E+06	1.34E+06	5	2.50E+06	668981	6	0.4039
α-ketoglutarate	58460	12514	5	62250	8892	6	0.8059

N values are post-outlier removal.

9 REFERENCE LIST

ABE, H., HOLT, W., WATTERS, T. A., WU, S., PARMLEY, W. W., SCHILLER, N., et al. 1988. Mechanics and energetics of overstretch: the relationship of altered left ventricular volume to the Frank-Starling mechanism and phosphorylation potential. *Am Heart J,* 116**,** 447-54.

ABRAHAM, D. M., DAVIS, R. T., WARREN, C. M., MAO, L., WOLSKA, B. M., SOLARO, R. J., et al. 2016. β-Arrestin mediates the Frank–Starling mechanism of cardiac contractility. *Proceedings of the National Academy of Sciences,* 113**,** 14426-14431.

AHMED, Z., ZEESHAN, S., HUBER, C., HENSEL, M., SCHOMBURG, D., MUENCH, R., et al. 2013. Software LS-MIDA for efficient mass isotopomer distribution analysis in metabolic modelling. *Bmc Bioinformatics,* 14.

AKKI, A., SMITH, K. & SEYMOUR, A.-M. L. 2008. Compensated cardiac hypertrophy is characterised by a decline in palmitate oxidation. *Molecular and Cellular Biochemistry,* 311**,** 215-224.

AKSENTIJEVIC, D., LEWIS, H. R. & SHATTOCK, M. J. 2016. Is rate-pressure product of any use in the isolated rat heart? Assessing cardiac "effort' and oxygen consumption in the Langendorff-perfused heart. *Experimental Physiology,* 101**,** 282-294.

ALLEN, D. G., EISNER, D. A., MORRIS, P. G., PIROLO, J. S. & SMITH, G. L. 1986. Metabolic consequences of increasing intracellular calcium and force production in perfused ferret hearts. *The Journal of Physiology,* 376**,** 121-141.

ALLEN, P. D., SCHMIDT, T. A., MARSH, J. D. & KJELDSEN, K. 1992. Na,K-ATPase expression in normal and failing human left-ventricle. *Basic Research in Cardiology,* 87**,** 87-94.

ANVERSA, P., OLIVETTI, G., MELISSARI, M. & LOUD, A. V. 1980. Stereological measurement of cellular and subcellular hypertrophy and hyperplasia in the papillary muscle of adult rat. *J Mol Cell Cardiol,* 12**,** 781-95.

ARBUSTINI, E., DIEGOLI, M., FASANI, R., GRASSO, M., MORBINI, P., BANCHIERI, N., et al. 1998. Mitochondrial DNA mutations and mitochondrial abnormalities in dilated cardiomyopathy. *American Journal of Pathology,* 153**,** 1501-1510.

ATHERTON, H. J., BAILEY, N. J., ZHANG, W., TAYLOR, J., MAJOR, H., SHOCKCOR, J., et al. 2006. A combined ^{1}H-NMR spectroscopy- and mass spectrometry-based metabolomic study of the PPAR-α null mutant mouse defines profound systemic changes in metabolism linked to the metabolic syndrome. *Physiological Genomics,* 27**,** 178-186.

ATHERTON, H. J., DODD, M. S., HEATHER, L. C., SCHROEDER, M. A., GRIFFIN, J. L., RADDA, G. K., et al. 2011. Role of Pyruvate Dehydrogenase Inhibition in the Development of Hypertrophy in the Hyperthyroid Rat Heart A Combined Magnetic Resonance Imaging and Hyperpolarized Magnetic Resonance Spectroscopy Study. *Circulation,* 123**,** 2552-U134.

AUTHORS/TASK FORCE, M., MCMURRAY, J. J. V., ADAMOPOULOS, S., ANKER, S. D., AURICCHIO, A., BÖHM, M., et al. 2012. ESC Guidelines for the diagnosis and treatment of acute and chronic heart failure 2012. *European Journal of Heart Failure,* 14**,** 803-869.

AWAN, M. M., TAUNYANE, C., AITCHISON, K. A., YELLON, D. M. & OPIE, L. H. 1999. Normothermic transfer times up to 3 min will not precondition the isolated rat heart. *Journal of Molecular and Cellular Cardiology,* 31**,** 503-511.

BAARTSCHEER, A., HARDZIYENKA, M., SCHUMACHER, C. A., BELTERMAN, C. N. W., VAN BORREN, M. M. G. J., VERKERK, A. O., et al. 2008. Chronic inhibition of the Na(+)/H(+)-exchanger causes regression of hypertrophy, heart

failure, and ionic and electrophysiological remodelling. *British Journal of Pharmacology,* 154**,** 1266-1275.

BAARTSCHEER, A., SCHUMACHER, C. A., BELTERMAN, C. N. W., CORONEL, R. & FIOLET, J. W. T. 2003a. Na^+ (i) and the driving force of the Na^+/Ca^{2+}-exchanger in heart failure. *Cardiovascular Research,* 57**,** 986-995.

BAARTSCHEER, A., SCHUMACHER, C. A., VAN BORREN, M., BELTERMAN, C. N., CORONEL, R. & FIOLET, J. W. T. 2003b. Increased Na^+/H^+-exchange activity is the cause of increased Na+ (i) and underlies disturbed calcium handling in the rabbit pressure and volume overload heart failure model. *Cardiovascular Research,* 57**,** 1015-1024.

BAKER, L. C., WOLK, R., CHOI, B. R., WATKINS, S., PLAN, P., SHAH, A., et al. 2004. Effects of mechanical uncouplers, diacetyl monoxime, and cytochalasin-D on the electrophysiology of perfused mouse hearts. *Am J Physiol Heart Circ Physiol,* 287**,** H1771-9.

BALABAN, R. S. 2009. Domestication of the cardiac mitochondrion for energy conversion. *Journal of Molecular and Cellular Cardiology,* 46**,** 832-841.

BANERJEE, I., FUSELER, J. W., PRICE, R. L., BORG, T. K. & BAUDINO, T. A. 2007. Determination of cell types and numbers during cardiac development in the neonatal and adult rat and mouse. *American Journal of Physiology - Heart and Circulatory Physiology,* 293**,** H1883-H1891.

BARRY, W. H., HASIN, Y. & SMITH, T. W. 1985. Sodium-pump inhibition, enhanced calcium influx via sodium-calcium exchange, and positive inotropic response in cultured heart-cells. *Circulation Research,* 56**,** 231-241.

BAUDET, S., NOIREAUD, J. & LEOTY, C. 1991. Intracellular Na activity measurements in the control and hypertrophied heart of the ferret: an ion-sensitive micro-electrode study. *Pflugers Arch,* 418**,** 313-8.

BECKER, T. A., DELLAVALLE, B., GESSER, H. & RODNICK, K. J. 2013. Limited effects of exogenous glucose during severe hypoxia and a lack of hypoxia-stimulated glucose uptake in isolated rainbow trout cardiac muscle. *Journal of Experimental Biology,* 216**,** 3422-3432.

BECKONERT, O., KEUN, H. C., EBBELS, T. M. D., BUNDY, J. G., HOLMES, E., LINDON, J. C., et al. 2007. Metabolic profiling, metabolomic and metabonomic procedures for NMR spectroscopy of urine, plasma, serum and tissue extracts. *Nature Protocols,* 2**,** 2692-2703.

BEER, M., LANDSCHUETZ, W., SANDSTEDE, J. J. W., KOESTLER, H., PABST, T., MEININGER, M., et al. 2000. Absolute levels of cardiac high-energy phosphate metabolites in human heart failure and left ventricular hypertrophy - Non-invasive measurements by P-31-SLOOP MRS. *Circulation,* 102**,** 804-804.

BELL, R. M., MOCANU, M. M. & YELLON, D. M. 2011. Retrograde heart perfusion: The Langendorff technique of isolated heart perfusion. *Journal of Molecular and Cellular Cardiology,* 50**,** 940-950.

BERS, D. M. 2002. Cardiac excitation-contraction coupling. *Nature,* 415**,** 198-205.

BERS, D. M. & DESPA, S. 2009. Na(+) Transport in Cardiac Myocytes; Implications for Excitation-Contraction Coupling. *IUBMB life,* 61**,** 215-221.

BERSIN, R. M. & STACPOOLE, P. W. 1997. Dichloroacetate as metabolic therapy for myocardial ischemia and failure. *American Heart Journal,* 134**,** 841-855.

BERSIN, R. M., WOLFE, C., KWASMAN, M., LAU, D., KLINSKI, C., TANAKA, K., et al. 1994. Improved hemodynamic function and mechanical efficiency in congestive-heart-failure with sodium dichloroacetate. *Journal of the American College of Cardiology,* 23**,** 1617-1624.

BLONDE, D. J., KRESACK, E. J. & KOSICKI, G. W. 1967. Effects of ions and freeze-thawing on supernatant and mitochondrial malate dehydrogenase. *Canadian Journal of Biochemistry,* 45**,** 641-&.

BOERRIES, M., MOST, P., GLEDHILL, J. R., WALKER, J. E., KATUS, H. A., KOCH, W. J., et al. 2007. Ca^{2+}-dependent interaction of S100A1 with F-1-ATPase leads to an increased ATP content in cardiomyocytes. *Molecular and Cellular Biology,* 27**,** 4365-4373.

BOGUSLAVSKYI, A., PAVLOVIC, D., AUGHTON, K., CLARK, J. E., HOWIE, J., FULLER, W., et al. 2014. Cardiac hypertrophy in mice expressing unphosphorylatable phospholemman. *Cardiovascular Research,* 104**,** 72-82.

BOSE, S., FRENCH, S., EVANS, F. J., JOUBERT, F. & BALABAN, R. S. 2003. Metabolic network control of oxidative phosphorylation - Multiple roles of inorganic phosphate. *Journal of Biological Chemistry,* 278**,** 39155-39165.

BOSSUYT, J., AI, X., MOORMAN, J. R., POGWIZD, S. M. & BERS, D. M. 2005. Expression and phosphorylation of the Na-pump regulatory subunit phospholemman in heart failure. *Circulation Research,* 97**,** 558-565.

BOSSUYT, J., DESPA, S., HAN, F., HOU, Z., ROBIA, S. L., LINGREL, J. B., et al. 2009. Isoform specificity of the Na/K-ATPase association and regulation by phospholemman. *J Biol Chem,* 284**,** 26749-57.

BRACK, K. E., NARANG, R., WINTER, J. & NG, G. A. 2013. The mechanical uncoupler blebbistatin is associated with significant electrophysiological effects in the isolated rabbit heart. *Experimental Physiology,* 98**,** 1009-1027.

BRIXIUS, K., MEHLHORN, U., BLOCH, W. & SCHWINGER, R. H. 2000. Different effect of the Ca(2+) sensitizers EMD 57033 and CGP 48506 on cross-bridge cycling in human myocardium. *J Pharmacol Exp Ther,* 295**,** 1284-90.

BROWNING, D. J., GUARNIERI, T. & STRAUSS, H. C. 1981. Ouabain effects on intracellular potassium activity and contractile force in cat papillary muscle. *Journal of Clinical Investigation,* 68**,** 942-956.

BRUHL, A., HAFNER, G. & LOFFELHOLZ, K. 2004. Release of choline in the isolated heart, an indicator of ischemic phospholipid degradation and its

protection by ischemic preconditioning: No evidence for a role of phospholipase D. *Life Sciences,* 75**,** 1609-1620.

BUCHWALD, A., TILL, H., UNTERBERG, C., OBERSCHMIDT, R., FIGULLA, H. R. & WIEGAND, V. 1990. Alterations of the mitochondrial respiratory-chain in human dilated cardiomyopathy. *European Heart Journal,* 11**,** 509-516.

BUESCHER, J. M., ANTONIEWICZ, M. R., BOROS, L. G., BURGESS, S. C., BRUNENGRABER, H., CLISH, C. B., et al. 2015. A roadmap for interpreting C-13 metabolite labeling patterns from cells. *Current Opinion in Biotechnology,* 34**,** 189-201.

BUSTER, D. C., CASTRO, M. M., GERALDES, C. F., MALLOY, C. R., SHERRY, A. D. & SIEMERS, T. C. 1990. Tm(DOTP)5-: a $^{23}Na^{+}$ shift agent for perfused rat hearts. *Magn Reson Med,* 15**,** 25-32.

BYLUND, D., NORSTROM, S. H., ESSEN, S. A. & LUNDSTROM, U. S. 2007. Analysis of low molecular mass organic acids in natural waters by ion exclusion chromatography tandem mass spectrometry. *Journal of Chromatography A,* 1176**,** 89-93.

BYRNE, N. J., LEVASSEUR, J., SUNG, M. M., MASSON, G., BOISVENUE, J., YOUNG, M. E., et al. 2016. Normalization of cardiac substrate utilization and left ventricular hypertrophy precede functional recovery in heart failure regression. *Cardiovascular Research,* 110**,** 249-257.

CAI, H., CONG, W.-N., JI, S., ROTHMAN, S., MAUDSLEY, S. & MARTIN, B. 2012. Metabolic Dysfunction in Alzheimer's Disease and Related Neurodegenerative Disorders. *Current Alzheimer research,* 9**,** 5-17.

CARLEY, A. N., TAGLIERI, D. M., BI, J., SOLARO, R. J. & LEWANDOWSKI, E. D. 2015. Metabolic Efficiency Promotes Protection From Pressure Overload in Hearts Expressing Slow Skeletal Troponin I. *Circulation-Heart Failure,* 8**,** 119-U202.

CARVALHO, R. A., ZHAO, P., WIEGERS, C. B., JEFFREY, F. M. H., MALLOY, C. R. & SHERRY, A. D. 2001. TCA cycle kinetics in the rat heart by analysis of C-13 isotopomers using indirect H-1 C-13 detection. *American Journal of Physiology-Heart and Circulatory Physiology,* 281**,** H1413-H1421.

CHANDLER, M. P., KERNER, J., HUANG, H., VAZQUEZ, E., RESZKO, A., MARTINI, W. Z., et al. 2004. Moderate severity heart failure does not involve a downregulation of myocardial fatty acid oxidation. *American Journal of Physiology-Heart and Circulatory Physiology,* 287**,** H1538-H1543.

CHENG, H., LEDERER, M. R., LEDERER, W. J. & CANNELL, M. B. 1996. Calcium sparks and Ca^{2+} (i) waves in cardiac myocytes. *American Journal of Physiology-Cell Physiology,* 270**,** C148-C159.

CHOUCHANI, E. T., PELL, V. R., GAUDE, E., AKSENTIJEVIC, D., SUNDIER, S. Y., ROBB, E. L., et al. 2014. Ischaemic accumulation of succinate controls reperfusion injury through mitochondrial ROS. *Nature,* 515**,** 431-+.

CHUNG, Y. L., LEACH, M. O. & EYKYN, T. R. 2016. Magnetic Resonance Spectroscopy to Study Glycolytic Metabolism During Autophagy. *Methods in Enzymology*. Academic Press.

CINGOLANI, H. E., PEREZ, N. G., CINGOLANI, O. H. & ENNIS, I. L. 2013. The Anrep effect: 100 years later. *Am J Physiol Heart Circ Physiol,* 304**,** H175-82.

CLEMENTS-JEWERY, H., HEARSE, D. J. & CURTIS, M. J. 2002. The isolated blood-perfused rat heart: an inappropriate model for the study of ischaemia- and infarction-related ventricular fibrillation. *British Journal of Pharmacology,* 137**,** 1089-1099.

COHEN, C. J., FOZZARD, H. A. & SHEU, S. S. 1982. Increase in intracellular sodium-ion activity during stimulation in mammalian cardiac-muscle. *Circulation Research,* 50**,** 651-662.

COMTE, B., VINCENT, G., BOUCHARD, B., JETTE, M., CORDEAU, S. & DESROSIERS, C. 1997. A C-13 mass isotopomer study of anaplerotic pyruvate carboxylation in perfused rat hearts. *Journal of Biological Chemistry,* 272**,** 26125-26131.

CONSOLINI, A. E., QUIROGA, P., YULN, G. & VOLONTE, M. G. 2004. Participation of Na/Ca-exchanger and sarcoplasmic reticulum in the high K (o)-protection against ischaemia-reperfusion dysfunction in rat hearts. *Acta Physiologica Scandinavica,* 182**,** 121-132.

CONTRERAS, L., GOMEZ-PUERTAS, P., IIJIMA, M., KOBAYASHI, K., SAHEKI, T. & SATRUSTEGUI, J. 2007. Ca2+ activation kinetics of the two aspartate-glutamate mitochondrial carriers, aralar and citrin - Role in the heart malate-aspartate NADH shuttle. *Journal of Biological Chemistry,* 282**,** 7098-7106.

COOK, S. J., CHAMUNORWA, J. P., LANCASTER, M. K. & O'NEILL, S. C. 1997. Regional differences in the regulation of intracellular sodium and in action potential configuration in rabbit left ventricle. *Pflügers Archiv,* 433**,** 515-522.

CORRELL, R. N., EDER, P., BURR, A. R., DESPA, S., DAVIS, J., BERS, D. M., et al. 2014. Overexpression of the Na^+/K^+ ATPase alpha 2 But Not a1 Isoform Attenuates Pathological Cardiac Hypertrophy and Remodeling. *Circulation Research,* 114**,** 249-256.

COSTELLO, L. C., FRANKLIN, R. B., LIU, Y. & KENNEDY, M. C. 2000. Zinc causes a shift toward citrate at equilibrium of the m-aconitase reaction of prostate mitochondria. *Journal of Inorganic Biochemistry,* 78**,** 161-165.

COX, D. A. & MATLIB, M. A. 1993. Modulation of intramitochondrial free Ca^{2+} concentration by antagonists of Na^+-Ca^{2+} exchange. *Trends in Pharmacological Sciences,* 14**,** 408-413.

CRAIG, T. J., ASHCROFT, F. M. & PROKS, P. 2008. How ATP inhibits the open K(ATP) channel. *J Gen Physiol,* 132**,** 131-44.

CUPERLOVIC-CULF, M. & CULF, A. S. 2016. Applied metabolomics in drug discovery. *Expert Opinion on Drug Discovery,* 11**,** 759-770.

DALY, M. J., ELZ, J. S. & NAYLER, W. G. 1987. Contracture and the calcium paradox in the rat heart. *Circ Res,* 61**,** 560-9.

DAMMRICH, J. & PFEIFER, U. 1983. Cardiac hypertrophy in rats after supravalvular aortic constriction. II. Inhibition of cellular autophagy in hypertrophying cardiomyocytes. *Virchows Arch B Cell Pathol Incl Mol Pathol,* 43**,** 287-307.

DARVEY, I. G. 1999. What factors are responsible for the greater yield of ATP per carbon atom when fatty acids are completely oxidised to CO2 and water compared with glucose? *Biochemical Education,* 27**,** 209-210.

DAWSON, M. J., GADIAN, D. G. & WILKIE, D. R. 1980. Studies of the biochemistry of contracting and relaxing muscle by the use of P-31 nmr in conjunction with other techniques. *Philosophical Transactions of the Royal Society of London Series B-Biological Sciences,* 289**,** 445-455.

DEL ARCO, A. & SATRUSTEGUI, J. 2004. Identification of a novel human subfamily of mitochondrial carriers with calcium-binding domains. *Journal of Biological Chemistry,* 279**,** 24701-24713.

DENTON, R. M., RANDLE, P. J. & MARTIN, B. R. 1972. Stimulation by calcium-ions of pyruvate dehydrogenase phosphate phosphatase. *Biochemical Journal,* 128**,** 161-163.

DESPA, S. & BERS, D. M. 2013. Na+ transport in the normal and failing heart — Remember the balance. *Journal of Molecular and Cellular Cardiology,* 61**,** 2-10.

DESPA, S., ISLAM, M. A., POGWIZD, S. M. & BERS, D. M. 2002a. Intracellular Na^+ and Na^+ pump rate in rat and rabbit ventricular myocytes. *Journal of Physiology-London,* 539**,** 133-143.

DESPA, S., ISLAM, M. A., WEBER, C. R., POGWIZD, S. M. & BERS, D. M. 2002b. Intracellular Na^+ concentration is elevated in heart failure but Na/K pump function is unchanged. *Circulation,* 105**,** 2543-2548.

DESPA, S., TUCKER, A. L. & BERS, D. M. 2008. Phospholemman-Mediated Activation of Na/K-ATPase Limits [Na](i) and Inotropic State During β-Adrenergic Stimulation in Mouse Ventricular Myocytes. *Circulation,* 117**,** 1849-1855.

DHANJAL, T. S., MEDINA, R. A., LEEM, J., CLARK, J. E., SOUTHWORTH, R. & CURTIS, M. J. 2013. Trapped platelets activated in ischemia initiate ventricular fibrillation. *Circ Arrhythm Electrophysiol,* 6**,** 995-1001.

DIZON, J. M., TAUSKELA, J. S., WISE, D., BURKHOFF, D., CANNON, P. J. & KATZ, J. 1996. Evaluation of triple-quantum-filtered ^{23}Na NMR in monitoring of Intracellular Na content in the perfused rat heart: comparison of intra- and extracellular transverse relaxation and spectral amplitudes. *Magn Reson Med,* 35**,** 336-45.

DOENST, T., NGUYEN, T. D. & ABEL, E. D. 2013. Cardiac Metabolism in Heart Failure. *Implications Beyond ATP Production,* 113**,** 709-724.

DONOSO, P., MILL, J. G., ONEILL, S. C. & EISNER, D. A. 1992. Fluorescence measurements of cytoplasmic and mitochondrial sodium concentration in rat ventricular myocytes. *Journal of Physiology-London,* 448**,** 493-509.

DORNER, A., GIESSEN, S., GAUB, R., SIESTRUP, H. G., SCHWIMMBECK, P. L., HETZER, R., et al. 2006. An isoform shift in the cardiac adenine nucleotide translocase expression alters the kinetic properties of the carrier in dilated cardiomyopathy. *European Journal of Heart Failure,* 8**,** 81-89.

DORNER, A., PAUSCHINGER, M., SCHWIMMBECK, P. L., KUHL, U. & SCHULTHEISS, H. P. 2000. The shift in the myocardial adenine nucleotide translocator isoform expression pattern is associated with an enteroviral

infection in the absence of an active T-cell dependent immune response in human inflammatory heart disease. *Journal of the American College of Cardiology,* 35**,** 1778-1784.

DOU, Y., ARLOCK, P. & ARNER, A. 2007. Blebbistatin specifically inhibits actin-myosin interaction in mouse cardiac muscle. *American Journal of Physiology - Cell Physiology,* 293**,** C1148-C1153.

DOUMEN, C., WAN, B. & ONDREJICKOVA, O. 1995. Effect of BDM, verapamil, and cardiac work on mitochondrial membrane potential in perfused rat hearts. *Am J Physiol,* 269**,** H515-23.

DU TOIT, E., HOFMANN, D., MCCARTHY, J. & PINEDA, C. 2001. Effect of levosimendan on myocardial contractility, coronary and peripheral blood flow, and arrhythmias during coronary artery ligation and reperfusion in the in vivo pig model. *Heart,* 86**,** 81-87.

DUFFIELD, R., DAWSON, B. & GOODMAN, C. 2004. Energy system contribution to 100-m and 200-m track running events. *J Sci Med Sport,* 7**,** 302-13.

EISNER, D. A. & LEDERER, W. J. 1980. Characterization of the electrogenic sodium pump in cardiac Purkinje fibres. *The Journal of Physiology,* 303**,** 441-474.

EISNER, D. A., LEDERER, W. J. & VAUGHAN-JONES, R. D. 1984. The quantitative relationship between twitch tension and intracellular sodium activity in sheep cardiac Purkinje fibres. *The Journal of Physiology,* 355**,** 251-266.

EL-ARMOUCHE, A., WITTKOPPER, K., FULLER, W., HOWIE, J., SHATTOCK, M. J. & PAVLOVIC, D. 2011. Phospholemman-dependent regulation of the cardiac Na/K-ATPase activity is modulated by inhibitor-1 sensitive type-1 phosphatase. *Faseb Journal,* 25**,** 4467-4475.

ENDOH, M. 2004. A Na(+) channel agonist: a potential cardiotonic agent with a novel mechanism? *British Journal of Pharmacology,* 143**,** 663-665.

EPPENBERGER, H. M., DAWSON, D. M. & KAPLAN, N. O. 1967. Comparative enzymology of creatine kinases .I. Isolation and characterization from chicken and rabbit tissues. *Journal of Biological Chemistry,* 242**,** 204-&.

EYKYN, T. R., AKSENTIJEVIC, D., AUGHTON, K. L., SOUTHWORTH, R., FULLER, W. & SHATTOCK, M. J. 2015. Multiple quantum filtered Na-23 NMR in the Langendorff perfused mouse heart: Ratio of triple/double quantum filtered signals correlates with Na (i). *Journal of Molecular and Cellular Cardiology,* 86**,** 95-101.

FARMAN, G. P., TACHAMPA, K., MATEJA, R., CAZORLA, O., LACAMPAGNE, A. & DE TOMBE, P. P. 2008. Blebbistatin: use as inhibitor of muscle contraction. *Pflügers Archiv - European Journal of Physiology,* 455**,** 995-1005.

FEDOROV, V. V., LOZINSKY, I. T., SOSUNOV, E. A., ANYUKHOVSKY, E. P., ROSEN, M. R., BALKE, C. W., et al. 2007. Application of blebbistatin as an excitation-contraction uncoupler for electrophysiologic study of rat and rabbit hearts. *Heart Rhythm,* 4**,** 619-626.

FELIG, P. & WAHREN, J. 1971. Amino acid metabolism in exercising man. *Journal of Clinical Investigation,* 50**,** 2703-&.

FERRIER, G. R. 1977. Digitalis arrhythmias - role of oscillatory afterpotentials. *Progress in Cardiovascular Diseases,* 19**,** 459-474.

FLETCHER, P. J., PFEFFER, J. M., PFEFFER, M. A. & BRAUNWALD, E. 1981. Left-ventricular diastolic pressure-volume relations in rats with healed myocardial-infarction - effects on systolic function. *Circulation Research,* 49**,** 618-626.

FORSEY, R. G. P., REID, K. & BROSNAN, J. T. 1987. Competition between fatty-acids and carbohydrate or ketone-bodies as metabolic fuels for the isolated perfused heart. *Canadian Journal of Physiology and Pharmacology,* 65**,** 401-406.

FRAGASSO, G., PALLOSHI, A., PUCCETTI, P., SILIPIGNI, C., ROSSODIVITA, A., PALA, M., et al. 2006. A randomized clinical trial of trimetazidine, a partial free fatty acid oxidation inhibitor, in patients with heart failure. *Journal of the American College of Cardiology,* 48**,** 992-998.

FULLER, W., TULLOCH, L. B., SHATTOCK, M. J., CALAGHAN, S. C., HOWIE, J. & WYPIJEWSKI, K. J. 2013. Regulation of the cardiac sodium pump. *Cellular and Molecular Life Sciences,* 70**,** 1357-1380.

GARNIER, A., FORTIN, D., DELOMENIE, C., MOMKEN, I., VEKSLER, V. & VENTURA-CLAPIER, R. 2003. Depressed mitochondrial transcription factors and oxidative capacity in rat failing cardiac and skeletal muscles. *Journal of Physiology-London,* 551**,** 491-501.

GEERING, K. 1991. The functional role of the beta-subunit in the maturation and intracellular transport of Na,K-ATPase. *FEBS Lett,* 285**,** 189-93.

GERTZ, E. W., WISNESKI, J. A., STANLEY, W. C. & NEESE, R. A. 1988. Myocardial substrate utilization during exercise in humans - dual carbon-labeled carbohydrate isotope experiments. *Journal of Clinical Investigation,* 82**,** 2017-2025.

GIBBS, C. L. 2003. Cardiac energetics: Sense and nonsense. *Clinical and Experimental Pharmacology and Physiology,* 30**,** 598-603.

GIBBS, C. L. & LOISELLE, D. S. 2001. Cardiac basal metabolism. *Jpn J Physiol,* 51**,** 399-426.

GLANCY, B. & BALABAN, R. S. 2012. Role of Mitochondrial Ca^{2+} in the Regulation of Cellular Energetics. *Biochemistry,* 51**,** 2959-2973.

GLITSCH, H. G. 2001. Electrophysiology of the sodium-potassium-ATPase in cardiac cells. *Physiol Rev,* 81**,** 1791-826.

GONANO, L. A., SEPULVEDA, M., RICO, Y., KAETZEL, M., VALVERDE, C. A., DEDMAN, J., et al. 2011. Calcium-Calmodulin Kinase II Mediates Digitalis-Induced Arrhythmias. *Circulation-Arrhythmia and Electrophysiology,* 4**,** 947-U276.

GONCALVES, S., PAUPE, V., DASSA, E. P., BRIERE, J. J., FAVIER, J., GIMENEZ-ROQUEPLO, A. P., et al. 2010. Rapid determination of tricarboxylic acid cycle enzyme activities in biological samples. *Bmc Biochemistry,* 11.

GONG, G. R., LIU, J. B., LIANG, P. H., GUO, T., HU, Q. S., OCHIAI, K., et al. 2003. Oxidative capacity in failing hearts. *American Journal of Physiology-Heart and Circulatory Physiology,* 285**,** H541-H548.

GOODWIN, G. W., TAYLOR, C. S. & TAEGTMEYER, H. 1998. Regulation of energy metabolism of the heart during acute increase in heart work. *Journal of Biological Chemistry,* 273**,** 29530-29539.

GOTTWALD, E., NEUBAUER, A. & SCHAD, L. R. 2016. Tracking Cellular Functions by Exploiting the Paramagnetic Properties of X-Nuclei. *In:* CONSTANTINIDES, C. (ed.) *Assessment of Cellular and Organ Function and Dysfunction using Direct and Derived MRI Methodologies.*

GRAY, R. P., MCINTYRE, H., SHERIDAN, D. S. & FRY, C. H. 2001. Intracellular sodium and contractile function in hypertrophied human and guinea-pig myocardium. *Pflugers Archiv-European Journal of Physiology,* 442**,** 117-123.

GREMMLER, B. & KISTERS, K. 2013. Reduction of hypertension induced diastolic relaxation disorder by Ranolazine - role of late sodium influx inhibition. *Trace Elements and Electrolytes,* 30**,** 66-69.

GRIFFITHS, E. R., FRIEHS, I., SCHERR, E., POUTIAS, D., MCGOWAN, F. X. & DEL NIDO, P. J. 2010. Electron transport chain dysfunction in neonatal pressure-overload hypertrophy precedes cardiomyocyte apoptosis independent

of oxidative stress. *Journal of Thoracic and Cardiovascular Surgery,* 139**,** 1609-1617.

GRUPP, I., IM, W. B., LEE, C. O., LEE, S. W., PECKER, M. S. & SCHWARTZ, A. 1985. Relation of sodium pump inhibition to positive inotropy at low concentrations of ouabain in rat heart muscle. *J Physiol,* 360**,** 149-60.

GUO, J., YONG, Y., AA, J., CAO, B., SUN, R., YU, X., et al. 2016. Compound danshen dripping pills modulate the perturbed energy metabolism in a rat model of acute myocardial ischemia. *Scientific Reports,* 6**,** 37919.

GUZUN, R., KAAMBRE, T., BAGUR, R., GRICHINE, A., USSON, Y., VARIKMAA, M., et al. 2015. Modular organization of cardiac energy metabolism: energy conversion, transfer and feedback regulation. *Acta Physiologica,* 213**,** 84-106.

HAIKALA, H., NISSINEN, E., ETEMADZADEH, E., LEVIJOKI, J. & LINDEN, I. B. 1995. Troponin C-mediated calcium sensitization induced by levosimendan does not impair relaxation. *J Cardiovasc Pharmacol,* 25**,** 794-801.

HAJJAR, R. J., SCHWINGER, R. H. G., SCHMIDT, U., KIM, C. S., LEBECHE, D., DOYE, A. A., et al. 2000. Myofilament calcium regulation in human myocardium. *Circulation,* 101**,** 1679-1685.

HANSEN, L. L., RASMUSSEN, J., FRICHE, E. & JAROSZEWSKI, J. W. 1993. Method for determination of intracellular sodium in perfused cancer cells by 23Na nuclear magnetic resonance spectroscopy. *Anal Biochem,* 214**,** 506-10.

HANSFORD, R. G. 1972. Some properties of pyruvate and 2-oxoglutarate oxidation by blowfly flight-muscle mitochondria. *Biochemical Journal,* 127**,** 271-&.

HARRIS, D. A. & DAS, A. M. 1991. Control of mitochondrial ATP synthesis in the heart. *Biochemical Journal,* 280**,** 561-573.

HARRISON, S. M., MCCALL, E. & BOYETT, M. R. 1992. The relationship between contraction and intracellular sodium in rat and guinea-pig ventricular myocytes. *Journal of Physiology-London,* 449**,** 517-550.

HEBISCH, S., BISCHOFF, E. & SOBOLL, S. 1993. Influence of 2,3-butanedione monoxime on heart energy metabolism. *Basic Research in Cardiology,* 88**,** 566-575.

HEINEMAN, F. W. & BALABAN, R. S. 1990. Phosphorus-31 nuclear magnetic resonance analysis of transient changes of canine myocardial metabolism in vivo. *Journal of Clinical Investigation,* 85**,** 843-852.

HELFMAN, D. M. & PAWLAK, G. 2005. Myosin light chain kinase and acto-myosin contractility modulate activation of the ERK cascade downstream of oncogenic Ras. *Journal of Cellular Biochemistry,* 95**,** 1069-1080.

HEMMER, W., ZANOLLA, E., FURTERGRAVES, E. M., EPPENBERGER, H. M. & WALLIMANN, T. 1994. Creatine-kinase isoenzymes in chicken cerebellum - specific localization of brain-type creatine-kinase in bergmann glial-cells and muscle-type creatine-kinase in purkinje neurons. *European Journal of Neuroscience,* 6**,** 538-549.

HENNING, S. L., WAMBOLT, R. B., SCHONEKESS, B. O., LOPASCHUK, G. D. & ALLARD, M. F. 1996. Contribution of glycogen to aerobic myocardial glucose utilization. *Circulation,* 93**,** 1549-1555.

HENSLEY, C. B., AZUMA, K. K., TANG, M. J. & MCDONOUGH, A. A. 1992. Thyroid-hormone induction of rat myocardial Na+-N+-ATPase - alpha-1-messenger RNA, alpha-2-messenger RNA, and beta-1-messenger RNA and alpha-1-protein, alpha-2-protein, and beta-1-protein levels at steady-state. *American Journal of Physiology,* 262**,** C484-C492.

HERRMANN, C., WRAY, J., TRAVERS, F. & BARMAN, T. 1992. Effect of 2,3-butanedione monoxime on myosin and myofibrillar ATPases. An example of an uncompetitive inhibitor. *Biochemistry,* 31**,** 12227-32.

HERRMANN, G. & DECHERD, G. M. 1939. The chemical nature of heart failure. *Annals of Internal Medicine,* 12**,** 1233-1244.

HONDA, H., TANAKA, K., AKITA, N. & HANEDA, T. 2002. Cyclical Changes in High-Energy Phosphates During the Cardiac Cycle by Pacing-Gated ^{31}P Nuclear Magnetic Resonance. *Circulation Journal,* 66**,** 80-86.

HUBBARD, M. J. & MCHUGH, N. J. 1996. Mitochondrial ATP synthase F-1-beta-subunit is a calcium-binding protein. *Febs Letters,* 391**,** 323-329.

HUDDLESTON, J. E. 2011. Metabolism: Metabolic regulation by ERK. *Nat Rev Mol Cell Biol,* 12**,** 546-546.

HUE, L. & TAEGTMEYER, H. 2009. The Randle cycle revisited: a new head for an old hat. *American Journal of Physiology-Endocrinology and Metabolism,* 297**,** E578-E591.

HUSER, J., BLATTER, L. A. & SHEU, S. S. 2000. Mitochondrial calcium in heart cells: Beat-to-beat oscillations or slow integration of cytosolic transients? *Journal of Bioenergetics and Biomembranes,* 32**,** 27-33.

HUXLEY, A. F. & NIEDERGERKE, R. 1954. Structural Changes in Muscle During Contraction: Interference Microscopy of Living Muscle Fibres. *Nature,* 173**,** 971-973.

HUXLEY, H. & HANSON, J. 1954. Changes in the Cross-Striations of Muscle during Contraction and Stretch and their Structural Interpretation. *Nature,* 173**,** 973-976.

IDE, T., TSUTSUI, H., KINUGAWA, S., UTSUMI, H., KANG, D. C., HATTORI, N., et al. 1999. Mitochondrial electron transport complex I is a potential source of

oxygen free radicals in the failing myocardium. *Circulation Research,* 85**,** 357-363.

ISENBERG, G. & TRAUTWEIN, W. 1975. Temperature sensitivity of outward current in cardiac Purkinje fibers. Evidence of electrogenicity of active transport. *Pflugers Arch,* 358**,** 225-34.

IWAI, T., TANONAKA, K., INOUE, R., KASAHARA, S., MOTEGI, K., NAGAYA, S., et al. 2002. Sodium accumulation during ischemia induces mitochondrial damage in perfused rat hearts. *Cardiovascular Research,* 55**,** 141-149.

JACOB, S. W. & DE LA TORRE, J. C. 2009. Pharmacology of dimethyl sulfoxide in cardiac and CNS damage. *Pharmacol Rep,* 61**,** 225-35.

JACOBUS, W. E. & LEHNINGE.AL 1973. Creatine kinase of rat-heart mitochondria - coupling of creatine phosphorylation to electron-transport. *Journal of Biological Chemistry,* 248**,** 4803-4810.

JANSEN, M., BADLOU, B., ECHTELD, C. & RUIGROK, T. 2000. Cytosolic Ca2+ concentration during Ca2+ depletion of isolated rat hearts. *Molecular and Cellular Biochemistry,* 203**,** 169-175.

JARRETA, D., ORUS, J., BARRIENTOS, A., MIRO, O., ROIG, E., HERAS, M., et al. 2000. Mitochondrial function in heart muscle from patients with idiopathic dilated cardiomyopathy. *Cardiovascular Research,* 45**,** 860-865.

JEFFREY, F. M. H., DICZKU, V., SHERRY, A. D. & MALLOY, C. R. 1995. Substrate selection in the isolated working rat heart: effects of reperfusion, afterload, and concentration. *Basic Research in Cardiology,* 90**,** 388-396.

JELICKS, J. A. & SIRI, F. M. 1995. Effects of hypertrophy and heart-failure on na+ (i) in pressure-overloaded guinea-pig heart. *American Journal of Hypertension,* 8**,** 934-943.

KAPLAN, J. H. 2002. Biochemistry of Na,K-ATPase. *Annual Review of Biochemistry,* 71**,** 511-535.

KEE, H. J. & CHEONG, J.-H. 2014. Tumor bioenergetics: An emerging avenue for cancer metabolism targeted therapy. *BMB Reports,* 47**,** 158-166.

KELAVKAR, U. P. & CHHATPAR, H. S. 1993. Relations of enzymes in aspergillus-repens grown under sodium-chloride stress. *Current Microbiology,* 27**,** 157-162.

KENNEDY, D. J., SHRESTHA, K., SHEEHEY, B., LI, X. S., GUGGILAM, A., WU, Y., et al. 2015. Elevated Plasma Marinobufagenin, An Endogenous Cardiotonic Steroid, Is Associated With Right Ventricular Dysfunction and Nitrative Stress in Heart Failure. *Circ Heart Fail,* 8**,** 1068-76.

KETTLEWELL, S., WALKER, N. L., COBBE, S. M., BURTON, F. L. & SMITH, G. L. 2004. The electrophysiological and mechanical effects of 2,3-butane-dione monoxime and cytochalasin-D in the Langendorff perfused rabbit heart. *Exp Physiol,* 89**,** 163-72.

KHAN, M. A. 1976. Effect of calcium on creatine-kinase activity of cerebellum. *Histochemistry,* 48**,** 29-32.

KOBAYASHI, K. & NEELY, J. R. 1983. Mechanism of pyruvate-dehydrogenase activation by increased cardiac work. *Journal of Molecular and Cellular Cardiology,* 15**,** 369-382.

KOBIRUMAKI-SHIMOZAWA, F., INOUE, T., SHINTANI, S. A., OYAMA, K., TERUI, T., MINAMISAWA, S., et al. 2014. Cardiac thin filament regulation and the Frank-Starling mechanism. *Journal of Physiological Sciences,* 64**,** 221-232.

KOLMAKOVA, E. V., HALLER, S. T., KENNEDY, D. J., ISACHKINA, A. N., BUDNY, G. V., FROLOVA, E. V., et al. 2011. Endogenous cardiotonic steroids in chronic renal failure. *Nephrol Dial Transplant,* 26**,** 2912-9.

KOLWICZ, S. C., JR., PUROHIT, S. & TIAN, R. 2013. Cardiac Metabolism and its Interactions With Contraction, Growth, and Survival of Cardiomyocytes. *Circulation Research,* 113**,** 603-616.

KOOMEN, J. M., VAN GILST, W. H., SCHEVERS, J. A. & WILTING, J. 1984. Biphasic positive inotropic actions of ouabain on rat, guinea-pig and cat heart: a mathematical description. *Basic Res Cardiol,* 79 Suppl**,** 102-9.

KOVÁCS, M., TÓTH, J., HETÉNYI, C., MÁLNÁSI-CSIZMADIA, A. & SELLERS, J. R. 2004. Mechanism of Blebbistatin Inhibition of Myosin II. *Journal of Biological Chemistry,* 279**,** 35557-35563.

LAI, L., LEONE, T. C., KELLER, M. P., MARTIN, O. J., BROMAN, A. T., NIGRO, J., et al. 2014. Energy Metabolic Reprogramming in the Hypertrophied and Early Stage Failing Heart A Multisystems Approach. *Circulation-Heart Failure,* 7**,** 1022-U287.

LAMBERT, R., SRODULSKI, S., PENG, X., MARGULIES, K. B., DESPA, F. & DESPA, S. 2015. Intracellular Na^+ concentration ($[Na]_i$) is elevated in diabetic hearts due to enhanced Na^+–glucose cotransport. *Journal of the American Heart Association,* 4.

LANG, D., SULKIN, M., LOU, Q. & EFIMOV, I. R. 2011. Optical Mapping of Action Potentials and Calcium Transients in the Mouse Heart. e3275.

LANGER, G. A. & BRADY, A. J. 1974. *The mammalian myocardium,* New York ; London, Wiley.

LEE, C. O. & DAGOSTINO, M. 1982. Effect of strophanthidin on intracellular Na ion activity and twitch tension of constantly driven canine cardiac Purkinje fibers. *Biophysical Journal,* 40**,** 185-198.

LEE, C. O., KANG, D. H., SOKOL, J. H. & LEE, K. S. 1980. Relation between intracellular Na ion activity and tension of sheep cardiac Purkinje fibers exposed to dihydro-ouabain. *Biophysical Journal,* 29**,** 315-330.

LEE, W. N. P., BYERLEY, L. O., BERGNER, E. A. & EDMOND, J. 1991. Mass isotopomer analysis - theoretical and practical considerations. *Biological Mass Spectrometry,* 20**,** 451-458.

LEMIEUX, H., SEMSROTH, S., ANTRETTER, H., HOFER, D. & GNAIGER, E. 2011. Mitochondrial respiratory control and early defects of oxidative phosphorylation in the failing human heart. *International Journal of Biochemistry & Cell Biology,* 43**,** 1729-1738.

LEVI, A. J., LEE, C. O. & BROOKSBY, P. 1994. Properties of the fluorescent sodium indicator sbfi in rat and rabbit cardiac myocytes. *Journal of Cardiovascular Electrophysiology,* 5**,** 241-257.

LEWANDOWSKI, E. D. 1992. Nuclear-magnetic-resonance evaluation of metabolic and respiratory support of work load in intact rabbit hearts. *Circulation Research,* 70**,** 576-582.

LEYS, C., LEY, C., KLEIN, O., BERNARD, P. & LICATA, L. 2013. Detecting outliers: Do not use standard deviation around the mean, use absolute deviation around the median. *Journal of Experimental Social Psychology,* 49**,** 764-766.

LI, Q., DENG, S., IBARRA, R. A., ANDERSON, V. E., BRUNENGRABER, H. & ZHANG, G.-F. 2015. Multiple mass isotopomer tracing of acetyl-coa metabolism in langendorff-perfused rat hearts: Channeling of acetyl-coa from pyruvate dehydrogenase to carnitine acetyltransferase. *The Journal of Biological Chemistry,* 290**,** 8121-8132.

LIAO, R. L., NASCIMBEN, L., FRIEDRICH, J., GWATHMEY, J. K. & INGWALL, J. S. 1996. Decreased energy reserve in an animal model of dilated cardiomyopathy - Relationship to contractile performance. *Circulation Research,* 78**,** 893-902.

LIMOUZE, J., STRAIGHT, A. F., MITCHISON, T. & SELLERS, J. E. 2004. Specificity of blebbistatin, an inhibitor of myosin II. *Journal of Muscle Research and Cell Motility,* 25**,** 337-341.

LIPSKAYA, T. Y. 2001. The physiological role of the creatine kinase system: Evolution of views. *Biochemistry-Moscow,* 66**,** 115-129.

LIU, T. & O'ROURKE, B. 2008. Enhancing mitochondrial Ca($^{2+}$) uptake in myocytes from failing hearts restores energy supply and demand matching. *Circulation Research,* 103**,** 279-288.

LIU, Y., CABO, C., SALOMONSZ, R., DELMAR, M., DAVIDENKO, J. & JALIFE, J. 1993. Effects of diacetyl monoxime on the electrical properties of sheep and guinea pig ventricular muscle. *Cardiovasc Res,* 27**,** 1991-7.

LOPASCHUK, G. D. & KELLY, D. P. 2008. Signalling in cardiac metabolism. *Cardiovascular Research,* 79**,** 205-207.

LOTAN, C. S., MILLER, S. K., POHOST, G. M. & ELGAVISH, G. A. 1992. Amiloride in ouabain-induced acidification, inotropy and arrhythmia: ^{23}Na & 31P NMR in perfused hearts. *Journal of Molecular and Cellular Cardiology,* 24**,** 243-257.

LOUCH, W. E., HOUGEN, K., MORK, H. K., SWIFT, F., ARONSEN, J. M., SJAASTAD, I., et al. 2010. Sodium accumulation promotes diastolic dysfunction in end-stage heart failure following Serca2 knockout. *Journal of Physiology-London,* 588**,** 465-478.

LU, S. B., SUN, X. M., SHI, C. O. & ZHANG, Y. X. 2003. Determination of tricarboxylic acid cycle acids and other related substances in cultured mammalian cells by gradient ion-exchange chromatography with suppressed conductivity detection. *Journal of Chromatography A,* 1012**,** 161-168.

LYMN, R. W. & TAYLOR, E. W. 1971. Mechanism of adenosine triphosphate hydrolysis by actomyosin. *Biochemistry,* 10**,** 4617-&.

MAACK, C., CORTASSA, S., AON, M. A., GANESAN, A. N., LIU, T. & O'ROURKE, B. 2006. Elevated cytosolic Na^+ decreases mitochondrial Ca^{2+} uptake during excitation-contraction coupling and impairs energetic adaptation in cardiac myocytes. *Circulation Research,* 99**,** 172-182.

MAIXENT, J. M., LELIEVRE, L. & BERREBI-BERTRAND, I. 1998. Mechanism underlying the strong positive inotropic effects of LND-623: Specific inhibition of Na, K-ATPase isoforms and exclusion of cellular sites of contractile control. *Cardiovascular Drugs and Therapy,* 12**,** 585-594.

MAMER, O., GRAVEL, S. P., CHOINIERE, L., CHENARD, V., ST-PIERRE, J. & AVIZONIS, D. 2013. The complete targeted profile of the organic acid intermediates of the citric acid cycle using a single stable isotope dilution analysis, sodium borodeuteride reduction and selected ion monitoring GC/MS. *Metabolomics,* 9**,** 1019-1030.

MANSOR, L. S., MEHTA, K., AKSENTIJEVIC, D., CARR, C. A., LUND, T., COLE, M. A., et al. 2016. Increased oxidative metabolism following hypoxia in the type 2 diabetic heart, despite normal hypoxia signalling and metabolic adaptation. *Journal of Physiology-London,* 594**,** 307-320.

MARCINKIEWICZ-SIEMION, M., CIBOROWSKI, M., KRETOWSKI, A., MUSIAL, W. J. & KAMINSKI, K. A. 2016. Metabolomics - A wide-open door to personalized treatment in chronic heart failure? *International Journal of Cardiology,* 219**,** 156-163.

MARIN-GARCIA, J., GOLDENTHAL, M. J. & MOE, G. W. 2001a. Abnormal cardiac and skeletal muscle mitochondrial function in pacing-induced cardiac failure. *Cardiovascular Research,* 52**,** 103-110.

MARIN-GARCIA, J., GOLDENTHAL, M. J. & MOE, G. W. 2001b. Mitochondrial pathology in cardiac failure. *Cardiovascular Research,* 49**,** 17-26.

MARIOTTI, E., ORTON, M. R., EERBEEK, O., ASHRUF, J. F., ZUURBIER, C. J., SOUTHWORTH, R., et al. 2016. Modeling non-linear kinetics of hyperpolarized [1-(13)C] pyruvate in the crystalloid-perfused rat heart. *Nmr in Biomedicine,* 29**,** 377-386.

MARMOL, P., PARDO, B., WIEDERKEHR, A., DEL ARCO, A., WOLLHEIM, C. B. & SATRUSTEGUI, J. 2009. Requirement for Aralar and Its Ca^{2+}-binding Sites in Ca^{2+} Signal Transduction in Mitochondria from INS-1 Clonal beta-Cells. *Journal of Biological Chemistry,* 284**,** 515-524.

MATSUI, S., SUGITA, T., MATOBA, M., MURAKAMI, E., TAKEKOSHI, N., SHINKA, T., et al. 1994. Urinary carnitine excretion in patients with heart failure. *Clin Cardiol,* 17**,** 301-5.

MATTFELDT, T., KRAMER, K. L., ZEITZ, R. & MALL, G. 1986. Stereology of myocardial hypertrophy induced by physical exercise. *Virchows Arch A Pathol Anat Histopathol,* 409**,** 473-84.

MATTIAZZI, A., MUNDINA-WEILENMANN, C., CHU, G. X., VITTONE, L. & KRANIAS, E. 2005. Role of phospholamban phosphorylation on Thr(17) in cardiac physiological and pathological conditions. *Cardiovascular Research,* 68**,** 366-375.

MCCORMACK, J. G. & DENTON, R. M. 1979. Effects of calcium-ions and adenine-nucleotides on the activity of pig-heart 2-oxoglutarate dehydrogenase complex. *Biochemical Journal,* 180**,** 533-544.

MCCUTCHEON, L. J., CORY, C. R., NOWACK, L., SHEN, H., MIRSALAMI, M., LAHUCKY, R., et al. 1992. Respiratory-chain defect of myocardial mitochondria in idiopathic dilated cardiomyopathy of doberman-pinscher dogs. *Canadian Journal of Physiology and Pharmacology,* 70**,** 1529-1533.

MCNAUGHT, A. D. & WILKINSON, A. 2000. *International Union of Pure and Applied Chemistry (Great Britain).* Cambridge, UK., Royal Society of Chemistry.

MELENOVSKY, V., BENES, J., SKAROUPKOVA, P., SEDMERA, D., STRNAD, H., KOLAR, M., et al. 2011. Metabolic characterization of volume overload heart failure due to aorto-caval fistula in rats. *Molecular and Cellular Biochemistry,* 354**,** 83-96.

MIKKONEN, J. J. W., SINGH, S. P., HERRALA, M., LAPPALAINEN, R., MYLLYMAA, S. & KULLAA, A. M. 2016. Salivary metabolomics in the diagnosis of oral cancer and periodontal diseases. *Journal of Periodontal Research,* 51**,** 431-437.

MILLARD, P., LETISSE, F., SOKOL, S. & PORTAIS, J. C. 2012. IsoCor: correcting MS data in isotope labeling experiments. *Bioinformatics,* 28**,** 1294-1296.

MIRZA, M. A., LANE, S., YANG, Z. Q., KARAOLI, T., AKOSAH, K., HOSSACK, J., et al. 2012. Phospholemman Deficiency in Postinfarct Hearts: Enhanced Contractility but Increased Mortality. *Cts-Clinical and Translational Science,* 5**,** 235-242.

MJOS, O. D. 1971. Effect of free fatty acids on myocardial function and oxygen consumption in intact dogs. *J Clin Invest,* 50**,** 1386-9.

MOE, G. W., MARIN-GARCIA, J., KONIG, A., GOLDENTHAL, M., LU, X. R. & FENG, Q. P. 2004. In vivo TNF-alpha inhibition ameliorates cardiac mitochondrial dysfunction, oxidative stress, and apoptosis in experimental heart failure. *American Journal of Physiology-Heart and Circulatory Physiology,* 287**,** H1813-H1820.

MOHAMMADI, K., LIU, L., TIAN, J., KOMETIANI, P., XIE, Z. & ASKARI, A. 2003. Positive Inotropic Effect of Ouabain on Isolated Heart Is Accompanied by

Activation of Signal Pathways that Link Na^+/K^+-ATPase to ERK1/2. *Journal of Cardiovascular Pharmacology,* 41**,** 609-614.

MORENO-SANCHEZ, R. 1983. Inhibition of oxidative-phosphorylation by a Ca^{-2+}-induced diminution of the adenine-nucleotide translocator. *Biochimica Et Biophysica Acta,* 724**,** 278-285.

MORENO-SANCHEZ, R. 1985. Regulation of oxidative-phosphorylation in mitochondria by external free Ca^{-2+} concentrations. *Journal of Biological Chemistry,* 260**,** 4028-4034.

MOSELEY, H. N. B. 2010. Correcting for the effects of natural abundance in stable isotope resolved metabolomics experiments involving ultra-high resolution mass spectrometry. *Bmc Bioinformatics,* 11.

MURPHY, A. N., KELLEHER, J. K. & FISKUM, G. 1990. Submicromolar Ca-2+ regulates phosphorylating respiration by normal rat-liver and as-30d hepatoma mitochondria by different mechanisms. *Journal of Biological Chemistry,* 265**,** 10527-10534.

MURPHY, E. & ALLEN, D. G. 2009. Why did the NHE inhibitor clinical trials fail? *Journal of molecular and cellular cardiology,* 46**,** 137-141.

MURPHY, E. & EISNER, D. A. 2009. Regulation of Intracellular and Mitochondrial Sodium in Health and Disease. *Circulation Research,* 104**,** 292-303.

NAG, A. C. 1980. Study of non-muscle cells of the adult mammalian heart: a fine structural analysis and distribution. *Cytobios,* 28**,** 41-61.

NASCIMBEN, L., FRIEDRICH, J., LIAO, R., PAULETTO, P., PESSINA, A. C. & INGWALL, J. S. 1995. Enalapril Treatment Increases Cardiac Performance and Energy Reserve Via the Creatine Kinase Reaction in Myocardium of Syrian Myopathic Hamsters With Advanced Heart Failure. *Circulation,* 91**,** 1824-1833.

NASCIMBEN, L., INGWALL, J. S., PAULETTO, P., FRIEDRICH, J., GWATHMEY, J. K., SAKS, V., et al. 1996. Creatine kinase system in failing and nonfailing human myocardium. *Circulation,* 94**,** 1894-1901.

NAUMOVA, A. V., CHACKO, V. P., OUWERKERK, R., STULL, L., MARBAN, E. & WEISS, R. G. 2006. Xanthine oxidase inhibitors improve energetics and function after infarction in failing mouse hearts. *American Journal of Physiology-Heart and Circulatory Physiology,* 290**,** H837-H843.

NEMUTLU, E., ZHANG, S., XU, Y. Z., TERZIC, A., ZHONG, L., DZEJA, P. D., et al. 2015. Cardiac Resynchronization Therapy Induces Adaptive Metabolic Transitions in the Metabolomic Profile of Heart Failure. *Journal of Cardiac Failure,* 21**,** 460-469.

NEUBAUER, S. 2007. Mechanisms of disease - The failing heart - An engine out of fuel. *New England Journal of Medicine,* 356**,** 1140-1151.

NEUBAUER, S., HORN, M., CRAMER, M., HARRE, K., NEWELL, J. B., PETERS, W., et al. 1997. Myocardial phosphocreatine-to-ATP ratio is a predictor of mortality in patients with dilated cardiomyopathy. *Circulation,* 96**,** 2190-2196.

NEUBAUER, S., REMKES, H., SPINDLER, M., HORN, M., WIESMANN, F., PRESTLE, J., et al. 1999. Downregulation of the Na+-creatine cotransporter in failing human myocardium and in experimental heart failure. *Circulation,* 100**,** 1847-1850.

NGUYEN, T. D., SHINGU, Y., AMORIM, P. A., SCHWARZER, M. & DOENST, T. 2015. Triheptanoin Alleviates Ventricular Hypertrophy and Improves Myocardial Glucose Oxidation in Rats With Pressure Overload. *Journal of Cardiac Failure,* 21**,** 906-915.

NGUYEN, T. T., OGBI, M., YU, Q. L., FISHMAN, J. B., THOMAS, W., HARVEY, B. J., et al. 2010. Modulation of the protein kinase C delta interaction with the "D" subunit of F1F0-ATP synthase in neonatal cardiac myocytes development

of cell-permeable, mitochondrially targeted inhibitor and facilitator peptides. *Journal of Biological Chemistry,* 285**,** 22164-22173.

NICHOLS, B. J., RIGOULET, M. & DENTON, R. M. 1994. Comparison of the effects of Ca^{2+}, adenine-nucleotides and pH on the kinetic-properties of mitochondrial NAD(+)-isocitrate dehydrogenase and oxoglutarate dehydrogenase from the yeast saccharomyces-cerevisiae and rat-heart. *Biochemical Journal,* 303**,** 461-465.

NOBLE, D. & NOBLE, P. J. 2006. Late sodium current in the pathophysiology of cardiovascular disease: consequences of sodium-calcium overload. *Heart,* 92**,** 1-5.

NOSEK, M. T., DRANSFIELD, D. T. & APRILLE, J. R. 1990. Calcium stimulates ATP-Mg/Pi carrier activity in rat-liver mitochondria. *Journal of Biological Chemistry,* 265**,** 8444-8450.

O'BRIEN, P. J., IANUZZO, C. D., MOE, G. W., STOPPS, T. P. & ARMSTRONG, P. W. 1990. Rapid ventricular pacing of dogs to heart-failure - biochemical and physiological-studies. *Canadian Journal of Physiology and Pharmacology,* 68**,** 34-39.

OSORIO, J. C., STANLEY, W. C., LINKE, A., CASTELLARI, M., DIEP, Q. N., PANCHAL, A. R., et al. 2002. Impaired myocardial fatty acid oxidation and reduced protein expression of retinoid X receptor-alpha in pacing-induced heart failure. *Circulation,* 106**,** 606-612.

OSTROVTSOVA, S. A. & STRUMILO, S. A. 1990. Participation of adenosine-diphosphate in regulation of the 2-oxoglutarate dehydrogenase complex from human heart. *Biomedica Biochimica Acta,* 49**,** 515-517.

OWEN, O. E., KALHAN, S. C. & HANSON, R. W. 2002. The Key Role of Anaplerosis and Cataplerosis for Citric Acid Cycle Function. *Journal of Biological Chemistry,* 277**,** 30409-30412.

PALMER, C. J., SCOTT, B. T. & JONES, L. R. 1991. Purification and complete sequence determination of the major plasma membrane substrate for cAMP-dependent protein kinase and protein kinase C in myocardium. *J Biol Chem,* 266**,** 11126-30.

PALMIERI, L., PARDO, B., LASORSA, F. M., DEL ARCO, A., KOBAYASHI, K., IIJIMA, M., et al. 2001. Citrin and aralar1 are Ca^{2+}-stimulated aspartate/glutamate transporters in mitochondria. *Embo Journal,* 20**,** 5060-5069.

PAVLOVIC, D., FULLER, W. & SHATTOCK, M. J. Novel regulation of cardiac Na pump via phospholemman. *Journal of Molecular and Cellular Cardiology,* 61**,** 83-93.

PAVLOVIC, D., FULLER, W. & SHATTOCK, M. J. 2007. The intracellular region of FXYD1 is sufficient to regulate cardiac Na/K ATPase. *Faseb Journal,* 21**,** 1539-1546.

PAVLOVIC, D., FULLER, W. & SHATTOCK, M. J. 2013a. Novel regulation of cardiac Na pump via phospholemman. *Journal of Molecular and Cellular Cardiology,* 61**,** 83-93.

PAVLOVIC, D., HALL, A. R., KENNINGTON, E. J., AUGHTON, K., BOGUSLAVSKYI, A., FULLER, W., et al. 2013b. Nitric oxide regulates cardiac intracellular Na(+) and Ca(2)(+) by modulating Na/K ATPase via PKCepsilon and phospholemman-dependent mechanism. *J Mol Cell Cardiol,* 61**,** 164-71.

PAYNE, G. S., SEYMOUR, A. M., STYLES, P. & RADDA, G. K. 1990. Multiple quantum filtered 23Na NMR spectroscopy in the perfused heart. *NMR Biomed,* 3**,** 139-46.

PENG, M., HUANG, L., XIE, Z., HUANG, W.-H. & ASKARI, A. 1996. Partial Inhibition of Na/K-ATPase by Ouabain Induces the Ca-dependent Expressions

of Early-response Genes in Cardiac Myocytes. *Journal of Biological Chemistry,* 271**,** 10372-10378.

PERINGS, S. M., SCHULZE, K., DECKING, U., KELM, M. & STRAUER, B. E. 2000. Age-related decline of PCr/ATP-ratio in progressively hypertrophied hearts of spontaneously hypertensive rats. *Heart and Vessels,* 15**,** 197-202.

PERNEGER, T. V. 1998. What's wrong with Bonferroni adjustments. *BMJ : British Medical Journal,* 316**,** 1236-1238.

PERRY, C. G. R., KANE, D. A., HERBST, E. A. F., MUKAI, K., LARK, D. S., WRIGHT, D. C., et al. 2012. Mitochondrial creatine kinase activity and phosphate shuttling are acutely regulated by exercise in human skeletal muscle. *Journal of Physiology-London,* 590**,** 5475-5486.

PEUHKURINEN, K. J., NUUTINEN, E. M., PIETILAINEN, E. P., HILTUNEN, J. K. & HASSINEN, I. E. 1982. Role of pyruvate carboxylation in the energy-linked regulation of pool sizes of tricarboxylic acid-cycle intermediates in the myocardium. *Biochem J,* 208**,** 577-81.

PIESKE, B., MAIER, L. S., PIACENTINO, V., WEISSER, J., HASENFUSS, G. & HOUSER, S. 2002. Rate dependence of Na^+ (i) and contractility in nonfailing and failing human myocardium. *Circulation,* 106**,** 447-453.

PINTO, A. R., ILINYKH, A., IVEY, M. J., KUWABARA, J. T., D'ANTONI, M. L., DEBUQUE, R., et al. 2016. Revisiting Cardiac Cellular Composition. *Circulation Research,* 118**,** 400-409.

PISARENKO, S. I., MINKOVSKII, E. B. & STUDNEVA, I. M. 1980. Urea synthesis in heart muscle. *Bulletin of Experimental Biology and Medicine,* 89**,** 138-141.

POUND, K. M., SOROKINA, N., BALLAL, K., BERKICH, D. A., FASANO, M., LANOUE, K. F., et al. 2009. Substrate-Enzyme Competition Attenuates Upregulated Anaplerotic Flux Through Malic Enzyme in Hypertrophied Rat

Heart and Restores Triacylglyceride Content Attenuating Upregulated Anaplerosis in Hypertrophy. *Circulation Research,* 104**,** 805-812.

PUCAR, D., JANSSEN, E., DZEJA, P. P., JURANIC, N., MACURA, S., WIERINGA, B., et al. 2000. Compromised energetics in the adenylate kinase AK1 gene knockout heart under metabolic stress. *Journal of Biological Chemistry,* 275**,** 41424-41429.

QIAN, Y. X., PANIGRAHY, A., LAYMON, C. M., LEE, V. K., DRAPPATZ, J., LIEBERMAN, F. S., et al. 2015. Short-T-2 imaging for quantifying concentration of sodium (Na-23) of bi-exponential T-2 relaxation. *Magnetic Resonance in Medicine,* 74**,** 162-174.

QUIGLEY, A. F., KAPSA, R. M. I., ESMORE, D., HALE, G. & BYRNE, E. 2000. Mitochondrial respiratory chain activity in idiopathic dilated cardiomyopathy. *Journal of Cardiac Failure,* 6**,** 47-55.

RADERMACHER, P. & HAOUZI, P. 2013. A mouse is not a rat is not a man: species-specific metabolic responses to sepsis - a nail in the coffin of murine models for critical care research? *Intensive Care Medicine Experimental,* 1**,** 7.

RADFORD, N. B., MAKOS, J. D., RAMASAMY, R., SHERRY, A. D. & MALLOY, C. R. 1998. Dissociation of intracellular sodium from contractile state in guinea-pig hearts treated with ouabain. *Journal of Molecular and Cellular Cardiology,* 30**,** 639-647.

REES, S. A. & CURTIS, M. J. 1993. Specific IK1 blockade: a new antiarrhythmic mechanism? Effect of RP58866 on ventricular arrhythmias in rat, rabbit, and primate. *Circulation,* 87**,** 1979-89.

REINECKE, H., STUDER, R., VETTER, R., HOLTZ, J. & DREXLER, H. 1996. Cardiac Na^{+}/Ca^{2+} exchange activity in patients with end-stage heart failure. *Cardiovascular Research,* 31**,** 48-54.

RHODES, S. S., CAMARA, A. K. S., ALDAKKAK, M., HEISNER, J. S. & STOWE, D. F. 2015. Stretch-induced increase in cardiac contractility is independent of myocyte Ca^{2+} while block of stretch channels by streptomycin improves contractility after ischemic stunning. *Physiological Reports*, 3.

RITCHIE, R. H. & DELBRIDGE, L. M. D. 2006. Cardiac hypertrophy, substrate utilization and metabolic remodelling: Cause or effect? *Clinical and Experimental Pharmacology and Physiology,* 33**,** 159-166.

ROBINSON, A. 2015. *Modelling Mitochondrial Metabolism* [Online]. Mitochondrial Biology Unit. Available: http://www.mrc-mbu.cam.ac.uk/projects/61/modelling-mitochondrial-metabolism [Accessed 11 September 2016].

RODRIGUEZ-ZAVALA, J. S., PARDO, J. P. & MORENO-SANCHEZ, R. 2000. Modulation of 2-oxoglutarate dehydrogenase complex by inorganic phosphate, Mg2+, and other effectors. *Archives of Biochemistry and Biophysics,* 379**,** 78-84.

ROSCA, M. G., TANDLER, B. & HOPPEL, C. L. 2013. Mitochondria in cardiac hypertrophy and heart failure. *Journal of Molecular and Cellular Cardiology,* 55**,** 31-41.

ROSSI, A. M., VOLPE, P., EPPENBERGER, H. M. & WALLIMANN, T. 1989. Functional coupling of creatine-kinase with SR-Ca-2+-Mg-2+-ATPase. *Journal of Muscle Research and Cell Motility,* 10**,** 178-178.

ROTHMAN, K. J. 1990. No adjustments are needed for multiple comparisons. *Epidemiology,* 1**,** 43-6.

ROVETTO, M. J., LAMBERTON, W. F. & NEELY, J. R. 1975. Mechanisms of glycolytic inhibition in ischemic rat hearts. *Circulation Research,* 37**,** 742-751.

RUSSELL, R. R. & TAEGTMEYER, H. 1991. Pyruvate carboxylation prevents the decline in contractile function of rat hearts oxidizing acetoacetate. *American Journal of Physiology,* 261**,** H1756-H1762.

SAHLIN, K., KATZ, A. & BROBERG, S. 1990. Tricarboxylic-acid cycle intermediates in human muscle during prolonged exercise. *American Journal of Physiology,* 259**,** C834-C841.

SAKS, V., DZEJA, P., SCHLATTNER, U., VENDELIN, M., TERZIC, A. & WALLIMANN, T. 2006. Cardiac system bioenergetics: metabolic basis of the Frank-Starling law. *Journal of Physiology-London,* 571**,** 253-273.

SAKS, V. A., LIPINA, N. V., SHAROV, V. G., SMIRNOV, V. N., CHAZOV, E. & GROSSE, R. 1977. Localization of MM isoenzyme of creatine-phosphokinase on surface-membrane of myocardial-cells and its functional coupling to ouabain-inhibited (Na^+,K^+)-ATPase. *Biochimica Et Biophysica Acta,* 465**,** 550-558.

SANBE, A., TANONAKA, K., NIWANO, Y. & TAKEO, S. 1994. Improvement of cardiac-function and myocardial energy-metabolism of rats with chronic heart-failure by long-term coenzyme Q(10) treatment. *Journal of Pharmacology and Experimental Therapeutics,* 269**,** 51-56.

SCADUTO, R. C. & GROTYOHANN, L. W. 2000. 2,3-Butanedione monoxime unmasks Ca^{2+}-induced NADH formation and inhibits electron transport in rat hearts. *American Journal of Physiology - Heart and Circulatory Physiology,* 279**,** H1839-H1848.

SCHEPKIN, V. D., CHOY, I. O., BUDINGER, T. F., OBAYASHI, D. Y., TAYLOR, S. E., DECAMPLI, W. M., et al. 1998. Sodium TQF NMR and intracellular sodium in isolated crystalloid perfused rat heart. *Magnetic Resonance in Medicine,* 39**,** 557-563.

SCHEUBEL, R. J., TOSTLEBE, M., ROHRBACH, S., DARMER, D., GELLERICH, F. N., SILBER, R. E., et al. 2002. Dysfunction of mitochondrial respiratory chain complex I in human failing myocardium is not based on disturbed mitochondrial gene expression. *European Heart Journal,* 23**,** 126-126.

SCHEUERMANN-FREESTONE, M., MADSEN, P. L., MANNERS, D., BLAMIRE, A. M., BUCKINGHAM, R. E., STYLES, P., et al. 2003. Abnormal Cardiac and Skeletal Muscle Energy Metabolism in Patients With Type 2 Diabetes. *Circulation,* 107**,** 3040-3046.

SCHISLER, J. C., GREVENGOED, T. J., PASCUAL, F., COOPER, D. E., ELLIS, J. M., PAUL, D. S., et al. 2015. Cardiac Energy Dependence on Glucose Increases Metabolites Related to Glutathione and Activates Metabolic Genes Controlled by Mechanistic Target of Rapamycin. *Journal of the American Heart Association,* 4.

SCHMIED, R., WANG, G. X. & KORTH, M. 1991. Intracellular Na^+ activity and positive inotropic effect of sulmazole in guinea pig ventricular myocardium. Comparison with a cardioactive steroid. *Circ Res,* 68**,** 597-604.

SCHONER, W. 2001. Endogenous cardiotonic steroids. *Cellular and Molecular Biology,* 47**,** 273-280.

SCHOUTEN, V. J. A. & TER KEURS, H. E. D. J. 1991. Role of I_{ca} and Na^+/Ca^{2+} exchange in the force-frequency relationship of rat heart muscle. *Journal of Molecular and Cellular Cardiology,* 23**,** 1039-1050.

SCHRAMM, M., KLIEBER, H. G. & DAUT, J. 1994. The energy expenditure of actomyosin-ATPase, Ca(2+)-ATPase and Na+,K(+)-ATPase in guinea-pig cardiac ventricular muscle. *The Journal of Physiology,* 481**,** 647-662.

SCHULTHEISS, H. P. & BOLTE, H. D. 1985. Immunological analysis of autoantibodies against the adenine-nucleotide translocator in dilated cardiomyopathy. *Journal of Molecular and Cellular Cardiology,* 17**,** 603-617.

SCHWINGER, R. H. G., WANG, J. N., FRANK, K., MULLER-EHMSEN, J., BRIXIUS, K., MCDONOUGH, A. A., et al. 1999. Reduced sodium pump alpha(1), alpha(3), and beta(1)-isoform protein levels and Na+,K+-ATPase

activity but unchanged Na+-Ca2+ exchanger protein levels in human heart failure. *Circulation,* 99**,** 2105-2112.

SCOTCHER, J., PRYSYAZHNA, O., BOGUSLAVSKYI, A., KISTAMAS, K., HADGRAFT, N., MARTIN, E. D., et al. 2016. Disulfide-activated protein kinase G Ialpha regulates cardiac diastolic relaxation and fine-tunes the Frank-Starling response. *Nat Commun,* 7**,** 13187.

SEMB, S. O., LUNDE, P. K., HOLT, E., TONNESSEN, T., CHRISTENSEN, G. & SEJERSTED, O. M. 1998. Reduced myocardial Na^+, K^+-pump capacity in congestive heart failure following myocardial infarction in rats. *Journal of Molecular and Cellular Cardiology,* 30**,** 1311-1328.

SEPP, M., SOKOLOVA, N., JUGAI, S., MANDEL, M., PETERSON, P. & VENDELIN, M. 2014. Tight Coupling of Na+/K+-ATPase with Glycolysis Demonstrated in Permeabilized Rat Cardiomyocytes. *Plos One,* 9.

SHARMA, N., OKERE, I. C., BRUNENGRABER, D. Z., MCELFRESH, T. A., KING, K. L., STERK, J. P., et al. 2005. Regulation of pyruvate clehydrogenase activity and citric acid cycle intermediates during high cardiac power generation. *Journal of Physiology-London,* 562**,** 593-603.

SHAROV, V. G., TODOR, A. V., SILVERMAN, N., GOLDSTEIN, S. & SABBAH, H. N. 2000. Abnormal mitochondrial respiration in failed human myocardium. *Journal of Molecular and Cellular Cardiology,* 32**,** 2361-2367.

SHATTOCK, M. J. 1984. *Studies on the Isolated Papillary Muscle Preparation With Particular Emphasis on the Effects of Hypothermia.* PhD thesis., University of London.

SHATTOCK, M. J. 2009. Phospholemman: its role in normal cardiac physiology and potential as a drugable target in disease. *Current Opinion in Pharmacology,* 9**,** 160-166.

SHATTOCK, M. J. & BERS, D. M. 1989. Rat vs. rabbit ventricle: Ca flux and intracellular Na assessed by ion-selective microelectrodes. *Am J Physiol,* 256**,** C813-22.

SHATTOCK, M. J. & MATSUURA, H. 1993. Measurement of Na(+)-K+ pump current in isolated rabbit ventricular myocytes using the whole-cell voltage-clamp technique. Inhibition of the pump by oxidant stress. *Circulation Research,* 72**,** 91-101.

SHATTOCK, M. J., MILLER, J. I. A., BRAY, D. G. & WALDRON, C. B. 1997. An electronic feedback circuit to control peristaltic pump for constant-pressure perfusion of isolated hearts or other organs. *Journal of Physiology-London,* 505P**,** 4P-5P.

SHEN, A. C. & JENNINGS, R. B. 1972. Myocardial calcium and magnesium in acute ischemic injury. *American Journal of Pathology,* 67**,** 417-&.

SHIBAYAMA, J., YUZYUK, T. N., COX, J., MAKAJU, A., MILLER, M., LICHTER, J., et al. 2015. Metabolic Remodeling in Moderate Synchronous versus Dyssynchronous Pacing-Induced Heart Failure: Integrated Metabolomics and Proteomics Study. *PLoS ONE,* 10**,** e0118974.

SHU, S., LIU, X. & KORN, E. D. 2005. Blebbistatin and blebbistatin-inactivated myosin II inhibit myosin II-independent processes in Dictyostelium. *Proceedings of the National Academy of Sciences of the United States of America,* 102**,** 1472-1477.

SIDELL, R. J., COLE, M. A., DRAPER, N. J., DESROIS, M., BUCKINGHAM, R. E. & CLARKE, K. 2002. Thiazolidinedione treatment normalizes insulin resistance and ischemic injury in the Zucker fatty rat heart. *Diabetes,* 51**,** 1110-1117.

SIESS, E. A. 1972. Purification and characterization of pyruvate-dehydrogenase phosphatase from pig-heart muscle. *European Journal of Biochemistry,* 26**,** 96-&.

SILL, B., HAMMER, P. E. & COWAN, D. B. 2009. Optical Mapping of Langendorff-perfused Rat Hearts. *Journal of Visualized Experiments : JoVE***,** 1138.

SILVERMAN, B. D. Z., FULLER, W., EATON, P., DENG, J., MOORMAN, J. R., CHEUNG, J. Y., et al. 2005. Serine 68 phosphorylation of phospholemman: acute isoform-specific activation of cardiac Na/K ATPase. *Cardiovascular Research,* 65**,** 93-103.

SIMOR, T., LÓRÁND, T., GASZNER, B. & ELGAVISH, G. A. 1997. The modulation of pacing-induced changes in intracellular sodium levels by extracellular Ca2+in isolated perfused rat hearts. *Journal of Molecular and Cellular Cardiology,* 29**,** 1225-1235.

SINGHAL, A., SHIVKUMAR, K., HUDA, A. & THOMAS, M. A. 2009. Current status of cardiac MR spectroscopy. *Progress in Nuclear Magnetic Resonance Spectroscopy,* 54**,** 255-277.

SOROKINA, N., O'DONNELL, J. M., MCKINNEY, R. D., POUND, K. M., WOLDEGIORGIS, G., LANOUE, K. F., et al. 2007. Recruitment of compensatory pathways to sustain oxidative flux with reduced carnitine palmitoyltransferase I activity characterizes inefficiency in energy metabolism in hypertrophied hearts. *Circulation,* 115**,** 2033-2041.

SOSSALLA, S., WAGNER, S., RASENACK, E. C. L., RUFF, H., WEBER, S. L., SCHOENDUBE, F. A., et al. 2008. Ranolazine improves diastolic dysfunction in isolated myocardium from failing human hearts - Role of late sodium current and intracellular ion accumulation. *Journal of Molecular and Cellular Cardiology,* 45**,** 32-43.

SPARAGNA, G. C., CHICCO, A. J., MURPHY, R. C., BRISTOW, M. R., JOHNSON, C. A., REES, M. L., et al. 2007. Loss of cardiac tetralinoleoyl cardiolipin in human and experimental heart failure. *Journal of Lipid Research,* 48**,** 1559-1570.

STANLEY, W. C., LOPASCHUK, G. D., HALL, J. L. & MCCORMACK, J. G. 1997. Regulation of myocardial carbohydrate metabolism under normal and ischaemic conditions - Potential for pharmacological interventions. *Cardiovascular Research,* 33**,** 243-257.

STANLEY, W. C., RECCHIA, F. A. & LOPASCHUK, G. D. 2005. Myocardial substrate metabolism in the normal and failing heart. *Physiological Reviews,* 85**,** 1093-1129.

STARLING, R. C., HAMMER, D. F. & ALTSCHULD, R. A. 1998. Human myocardial ATP content and in vivo contractile function. *Molecular and Cellular Biochemistry,* 180**,** 171-177.

STRILAKOU, A. A., LAZARIS, A. C., PERELAS, A. I., MOUROUZIS, I. S., DOUZIS, I. C., KARKALOUSOS, P. L., et al. 2013. Heart dysfunction induced by choline-deficiency in adult rats: The protective role of L-carnitine. *European Journal of Pharmacology,* 709**,** 20-27.

STUEWE, S. R., GWIRTZ, P. A., AGARWAL, N. & MALLET, R. T. 2000. Exercise training enhances glycolytic and oxidative enzymes in canine ventricular myocardium. *Journal of Molecular and Cellular Cardiology,* 32**,** 903-913.

SUZUKI, J., TSUBONE, H. & SUGANO, S. 1991. Characteristics of electrocardiographic changes with some representative antiarrhythmic drugs in adult rats. *J Vet Med Sci,* 53**,** 779-87.

SWEADNER, K. J. 1989. Isozymes of the Na^+/K^+-ATPase. *Biochimica et Biophysica Acta (BBA) - Reviews on Biomembranes,* 988**,** 185-220.

SWEADNER, K. J., HERRERA, V. L. M., AMATO, S., MOELLMANN, A., GIBBONS, D. K. & REPKE, K. R. H. 1994. Immunological identification of Na+,K+-ATPase isoforms in myocardium - isoform change in deoxycorticosterone acetate salt hypertension. *Circulation Research,* 74**,** 669-678.

SWEADNER, K. J. & RAEL, E. 2000. The FXYD Gene Family of Small Ion Transport Regulators or Channels: cDNA Sequence, Protein Signature Sequence, and Expression. *Genomics,* 68**,** 41-56.

SWIFT, L. M., ASFOUR, H., POSNACK, N. G., ARUTUNYAN, A., KAY, M. W. & SARVAZYAN, N. 2012. Properties of blebbistatin for cardiac optical mapping and other imaging applications. *Pflugers Archiv : European journal of physiology,* 464**,** 503-512.

SYLVEN, C., LIN, L., JANSSON, E., SOTONYI, P., FU, L. X., WAAGSTEIN, F., et al. 1993. Ventricular adenine-nucleotide translocator messenger-rna is up-regulated in dilated cardiomyopathy. *Cardiovascular Research,* 27**,** 1295-1299.

SZABO, B. & ARMSTRONG, W. M. 1984. Double-barreled Na-selective microelectrodes (DMB) for measuring Na activity (ANa_i) in resting and stimulated heart-cells. *Federation Proceedings,* 43**,** 1022-1022.

SZASZ, G., GRUBER, W. & BERNT, E. 1976. Creatine kinase in serum: 1. Determination of optimum reaction conditions. *Clin Chem,* 22**,** 650-6.

TAEGTMEYER, H., HEMS, R. & KREBS, H. A. 1980. Utilization of energy-providing substrates in the isolated working rat heart. *Biochem J,* 186**,** 701-11.

TAEGTMEYER, H., YOUNG, M. E., LOPASCHUK, G. D., ABEL, E. D., BRUNENGRABER, H., DARLEY-USMAR, V., et al. 2016. Assessing Cardiac Metabolism A Scientific Statement From the American Heart Association. *Circulation Research,* 118**,** 1659-U485.

TANG, Y., NYENGAARD, J. R., ANDERSEN, J. B., BAANDRUP, U. & GUNDERSEN, H. J. 2009. The application of stereological methods for estimating structural parameters in the human heart. *Anat Rec (Hoboken),* 292**,** 1630-47.

TAUSKELA, J. S., DIZON, J. M., WHANG, J. & KATZ, J. 1997. Evaluation of multiple-quantum-filtered 23Na NMR in monitoring intracellular Na content in

the isolated perfused rat heart in the absence of a chemical-shift reagent. *J Magn Reson,* 127**,** 115-27.

TEN HOVE, M., CHAN, S., LYGATE, C., MONFARED, M., BOEHM, E., HULBERT, K., et al. 2005. Mechanisms of creatine depletion in chronically failing rat heart. *Journal of Molecular and Cellular Cardiology,* 38**,** 309-313.

TODAKA, K., WANG, J., YI, G. H., STENNETT, R., KNECHT, M., PACKER, M., et al. 1996. Effects of levosimendan on myocardial contractility and oxygen consumption. *J Pharmacol Exp Ther,* 279**,** 120-7.

TOWNSEND, N., BHATNAGAR, P., WILKINS, E., WICKRAMASINGHE, K. & RAYNER, M. 2015. Cardiovascular Disease Statistics 2015. London: British Heart Foundation.

TRAUTWEIN, W. & HESCHELER, J. 1990. Regulation of cardiac L-type calcium current by phosphorylation and G-proteins. *Annual Review of Physiology,* 52**,** 257-274.

TRUEBLOOD, N. A., RAMASAMY, R., WANG, L. F. & SCHAEFER, S. 2000. Niacin protects the isolated heart from ischemia-reperfusion injury. *American Journal of Physiology-Heart and Circulatory Physiology,* 279**,** H764-H771.

TURER, A. T., STEVENS, R. D., BAIN, J. R., MUEHLBAUER, M. J., VAN DER WESTHUIZEN, J., MATHEW, J. P., et al. 2009. Metabolomic profiling reveals distinct patterns of myocardial substrate use in humans with coronary artery disease or left ventricular dysfunction during surgical ischemia/reperfusion. *Circulation,* 119**,** 1736-46.

TUUNANEN, H., ENGBLOM, E., NAUM, A., NAGREN, K., SCHEININ, M., HESSE, B., et al. 2008. Trimetazidine, a metabolic modulator, has cardiac and extracardiac benefits in idiopathic dilated cardiomyopathy. *Circulation,* 118**,** 1250-1258.

UNITT, J. F., MCCORMACK, J. G., REID, D., MACLACHLAN, L. K. & ENGLAND, P. J. 1989. Direct evidence for a role of intramitochondrial Ca^{2+} in the regulation of oxidative phosphorylation in the stimulated rat heart. Studies using ^{31}P n.m.r. and ruthenium red. *Biochem J,* 262**,** 293-301.

UNVERFERTH, D. V., LEE, S. W. & WALLICK, E. T. 1988. Human myocardial adenosine-triphosphatase activities in health and heart-failure. *American Heart Journal,* 115**,** 139-146.

VASSALLO, P. F., STEFANON, I., ROSSONI, L. V., TUCCI, P. J. & VASSALLO, D. V. 1998. The left ventricular contractility of the rat heart is modulated by changes in flow and alpha 1-adrenoceptor stimulation. *Braz J Med Biol Res,* 31**,** 1353-9.

VAUGHAN, H. & NEWSHOLM, E. 1969. Effects of Ca^{2+} and ADP on activity of NAD-linked isocitrate dehydrogenase of muscle. *Febs Letters,* 5**,** 124-&.

VENTURA-CLAPIER, R., GARNIER, A. & VEKSLER, V. 2008. Transcriptional control of mitochondrial biogenesis: the central role of PGC-1 alpha. *Cardiovascular Research,* 79**,** 208-217.

VERDONCK, F., VOLDERS, P. G. A., VOS, M. A. & SIPIDO, K. R. 2003. Intracellular Na^+ and altered Na^+ transport mechanisms in cardiac hypertrophy and failure. *Journal of Molecular and Cellular Cardiology,* 35**,** 5-25.

VILLA, R. F., GORINI, A. & HOYER, S. 2006. Differentiated effect of ageing on the enzymes of Krebs' cycle, electron transfer complexes and glutamate metabolism of non-synaptic and intra-synaptic mitochondria from cerebral cortex. *Journal of Neural Transmission,* 113**,** 1659-1670.

VIOLA, H. M. & HOOL, L. C. 2011. Targeting Calcium and the Mitochondria in Prevention of Pathology in the Heart. *Current Drug Targets,* 12**,** 748-760.

VITVITSKY, V. M., GARG, S. K., KEEP, R. F., ALBIN, R. L. & BANERJEE, R. 2012. Na(+) and K(+) ion imbalances in Alzheimer's disease. *Biochimica et biophysica acta,* 1822**,** 1671-1681.

WANG, G. X., SCHMIED, R., EBNER, F. & KORTH, M. 1993. Intracellular sodium activity and its regulation in guinea-pig atrial myocardium. *The Journal of Physiology,* 465**,** 73-84.

WANG, Y., LI, C., CHUO, W. J., LIU, Z. Y., OUYANG, Y. L., LI, D., et al. 2013. Integrated proteomic and metabolomic analysis reveals the NADH-mediated TCA cycle and energy metabolism disorders based on a new model of chronic progressive heart failure. *Molecular Biosystems,* 9**,** 3135-3145.

WASSERSTROM, J. A. 1983. Intracellular sodium-ion activity in rat ventricular myocardium. *Federation Proceedings,* 42**,** 1113-1113.

WATANABE, Y., IWAMOTO, T., MATSUOKA, I., OHKUBO, S., ONO, T., WATANO, T., et al. 2001. Inhibitory effect of 2,3-butanedione monoxime (BDM) on Na(+)/Ca(2+) exchange current in guinea-pig cardiac ventricular myocytes. *British Journal of Pharmacology,* 132**,** 1317-1325.

WEBER, C. R., PIACENTINO, V., HOUSER, S. R. & BERS, D. M. 2003. Dynamic regulation of sodium/calcium exchange function in human heart failure. *Circulation,* 108**,** 2224-2229.

WEGMANN, G., HUBER, R., ZANOLLA, E., EPPENBERGER, H. M. & WALLIMANN, T. 1991. Differential expression and localization of brain-type and mitochondrial creatine-kinase isoenzymes during development of the chicken retina - MI-CK as a marker for differentiation of photoreceptor cells. *Differentiation,* 46**,** 77-87.

WEISS, R. G., CHATHAM, J. C., CHARRON, M. J., GEORGAKOPOLOUS, D., WALLIMANN, T., KAY, L., et al. 2002. An increase in the myocardial PCr/ATP ratio in GLUT4 null mice. *Faseb Journal,* 16**,** 613-+.

WENGROWSKI, A. M., KUZMIAK-GLANCY, S., JAIMES, R. & KAY, M. W. 2014. NADH changes during hypoxia, ischemia, and increased work differ between isolated heart preparations. *American Journal of Physiology-Heart and Circulatory Physiology,* 306**,** H529-H537.

WILDE, A. A. & KLEBER, A. G. 1986. The combined effects of hypoxia, high K^+, and acidosis on the intracellular sodium activity and resting potential in guinea pig papillary muscle. *Circ Res,* 58**,** 249-56.

WILDER, C. D. E., MASOUD, R., YAZAR, D., O'BRIEN, B. A., EYKYN, T. R. & CURTIS, M. J. 2016. Contractile function assessment by intraventricular balloon alters the ability of regional ischaemia to evoke ventricular fibrillation. *British Journal of Pharmacology,* 173**,** 39-52.

WILKINSON, S., PATERSON, H. F. & MARSHALL, C. J. 2005. Cdc42-MRCK and Rho-ROCK signalling cooperate in myosin phosphorylation and cell invasion. *Nat Cell Biol,* 7**,** 255-261.

WILSON, K., GUGGILAM, A., WEST, T. A., ZHANG, X., TRASK, A. J., CISMOWSKI, M. J., et al. 2014. Effects of a myofilament calcium sensitizer on left ventricular systolic and diastolic function in rats with volume overload heart failure. *Am J Physiol Heart Circ Physiol,* 307**,** H1605-17.

WISHART, D. S. 2016. Emerging applications of metabolomics in drug discovery and precision medicine. *Nature Reviews Drug Discovery,* 15**,** 473-484.

WISNESKI, J. A., GERTZ, E. W., NEESE, R. A., GRUENKE, L. D. & CRAIG, J. C. 1985a. Dual carbon-labelled isotope experiments using D- 6-C-14 glucose and L- 1,2,3-C-3(C-13) lactate - a new approach for investigating human myocardial-metabolism during ischemia. *Journal of the American College of Cardiology,* 5**,** 1138-1146.

WISNESKI, J. A., GERTZ, E. W., NEESE, R. A., GRUENKE, L. D., MORRIS, D. L. & CRAIG, J. C. 1985b. Metabolic-fate of extracted glucose in normal human myocardium. *Journal of Clinical Investigation,* 76**,** 1819-1827.

WISNESKI, J. A., STANLEY, W. C., NEESE, R. A. & GERTZ, E. W. 1990. Effects of acute hyperglycemia on myocardial glycolytic activity in humans. *Journal of Clinical Investigation,* 85**,** 1648-1656.

WU, F. & BEARD, D. A. 2009. Roles of the creatine kinase system and myoglobin in maintaining energetic state in the working heart. *Bmc Systems Biology,* 3.

WU, S. T., KOJIMA, S., PARMLEY, W. W. & WIKMANCOFFELT, J. 1992. Relationship between cytosolic calcium and oxygen-consumption in isolated rat hearts. *Cell Calcium,* 13**,** 235-247.

WYSS, M., SMEITINK, J., WEVERS, R. A. & WALLIMANN, T. 1992. Mitochondrial creatine-kinase - a key enzyme of aerobic energy-metabolism. *Biochimica Et Biophysica Acta,* 1102**,** 119-166.

XU, K. Y., ZWEIER, J. L. & BECKER, L. C. 1995. Functional coupling between glycolysis and sarcoplasmic-reticulum Ca^{2+} transport. *Circulation Research,* 77**,** 88-97.

XU, Z., WANG, F., FAN, F., GU, Y., SHAN, N., MENG, X., et al. 2015. Quantitative proteomics reveals that the inhibition of Na^{+}/K^{+}-ATPase activity affects S-phase progression leading to a chromosome segregation disorder by attenuating the aurora a function in hepatocellular carcinoma cells. *Journal of Proteome Research,* 14**,** 4594-4602.

YAKU, H., SLINKER, B. K., MOCHIZUKI, T., LORELL, B. H. & LEWINTER, M. M. 1993. Use of 2,3-butanedione monoxime to estimate nonmechanical VO_2 in rabbit hearts. *Am J Physiol,* 265**,** H834-42.

YAMADA, E. W. & HUZEL, N. J. 1989. Calcium-binding ATPase inhibitor protein of bovine heart-mitochondria - role in ATP synthesis and effect of Ca-2+. *Biochemistry,* 28**,** 9714-9718.

YANG, Y.-Q., CAO, J.-L., ZOU, H.-Y.-Y., HAN, Z.-L., SUN, H.-W., HOU, M.-H., et al. 2016. Effects of levosimendan on calcium transient in norepinephrine-cultured neonatal rat ventricular myocytes. *European Heart Journal Supplements,* 18**,** A13-A20.

YAO, A., SU, Z., NONAKA, A., ZUBAIR, I., LU, L., PHILIPSON, K. D., et al. 1998. Effects of overexpression of the Na^{+}-Ca^{2+} exchanger on $[Ca^{2+}]_i$ transients in murine ventricular myocytes. *Circulation Research,* 82**,** 657-665.

ZAHLER, R., GILMOREHEBERT, M., BALDWIN, J. C., FRANCO, K. & BENZ, E. J. 1992. Expression of alpha-isoforms of the Na,K-ATPase in human heart. *Clinical Research,* 40**,** A220-A220.

ZAK, R. 1974. Development and proliferative capacity of cardiac muscle cells. *Circ Res,* 35**,** suppl II:17-26.

ZHANG, B., DAVIS, J. P. & ZIOLO, M. T. 2015. Cardiac Catheterization in Mice to Measure the Pressure Volume Relationship: Investigating the Bowditch Effect. *Jove-Journal of Visualized Experiments*.

ZHANG, X.-Q., MOORMAN, J. R., AHLERS, B. A., CARL, L. L., LAKE, D. E., SONG, J., et al. 2006. Phospholemman Overexpression Inhibits Na(+)-K(+)-ATPase in Adult Rat Cardiac Myocytes: Relevance to Decreased Na(+) pump Activity in Post-Infarction Myocytes. *Journal of applied physiology (Bethesda, Md. : 1985),* 100**,** 212-220.

ZHU, Y., WU, J. & YUAN, S. Y. 2013. MCT1 and MCT4 Expression During Myocardial Ischemic-Reperfusion Injury in the Isolated Rat Heart. *Cellular Physiology and Biochemistry,* 32**,** 663-674.

ZIMMER, H. G. 1998. The isolated perfused heart and its pioneers. *News in Physiological Sciences,* 13**,** 203-210.